



**Universidade do Minho**

Escola de Ciências

André Filipe Gomes Soares Fontes

**DOTA-based Ga(III) and Gd(III)  
chelates for medical imaging  
(PET, SPECT and MRI)**

PhD Thesis in Sciences

Specialization in Chemistry

Supervisors

**Doctor João Paulo R. F. André**

**Doctor Paula Margarida V. S. T. Ferreira**

February 2015

***Autor:***

André Filipe Gomes Soares Fontes

e-mail: andre.fontes@quimica.uminho.pt

***Título:*** DOTA-based Ga(III) and Gd(III) chelates for medical imaging (PET, SPECT and MRI)

***Orientadores:***

Doutor João Paulo R. F. André

e-mail: jandre@quimica.uminho.pt

Doutora Paula Margarida V. S. T. Ferreira

e-mail: pmf@quimica.uminho.pt

***Ano de Publicação:*** 2015

Tese de Doutoramento em Ciências, especialidade em Química

É autorizada a reprodução integral desta tese apenas para efeitos de investigação, mediante declaração escrita do interessado, que a tal se compromete.

Universidade do Minho, 27 de Fevereiro de 2015

---

André Fontes

## DECLARAÇÃO DE INTEGRIDADE

Declaro ter atuado com integridade na elaboração da presente tese. Confirmando que em todo o trabalho conducente à sua elaboração não recorri à prática de plágio ou a qualquer forma de falsificação de resultados.

Mais declaro que tomei conhecimento integral do Código de Conduta Ética da Universidade do Minho.

Universidade do Minho, 27 de Fevereiro de 2015

Nome Completo:

André Filipe Gomes Soares Fontes

Assinatura:

---



## Acknowledgments

The work presented in this thesis would never have been possible without the support and help of many people. First, I would like to thank my family and friends. Without their support, friendship and fun, life as I know would be impossible. A special thank to my wife, who always is at my side.

I would like to thank my supervisors, Professor João Paulo André and Professor Paula Margarida Ferreira for the guidance and advice that allowed me to conclude this thesis.

Many thanks to Professor Lothar Helm for having received me in his research group in the Federal Polytechnic School in Lausanne. He supervised my work during my stay and was responsible for the data analysis. Thanks to Shima Karimi for having helped me to conduct the relaxometric experiments during my stay at Lausanne.

I would like to express my gratitude to Doctor Isabel Prata from Coimbra University for the studies with  $^{67}\text{Ga}$ . I want to thank Professor Carlos Geraldés for making available the equipment at the Center of Science and Cell Biology of Coimbra University, where the relaxometric studies at 20 MHz were conducted. I also thank Doctor Maxim Yulikov for conducting the DEER tests in the laboratory of physical-chemistry of the Swiss Federal Institute of Technology in Zurich.

A big thank to all my colleagues Arsénio Sá, Miguel Ferreira, Helena Vilaça, Sandra Barros, Rui Fernandes, Nuno Ribeiro and Joana Malheiro. Thank you for all the good times that I have spent with you. A special thanks to Elisa Pinto and Vânia Azevedo for the NMR and MS spectra.

I thank the Chemistry Research Center and the Chemistry Department of the Minho University for offering the necessary resources for the development of this project. I also thank the NMR Portuguese network (PTNMR, Bruker Avance III 400-Universidade do Minho).

I would like to thank Fundação para a Ciência e Tecnologia and the European Fund for Regional Development-COMPETE-QREN-EU for providing the funding for the project through the PhD grant (reference SFRH /BD/63676/2009).





*DOTA-based Ga(III) and Gd(III) chelates for medical imaging (PET, SPECT and MRI)***Abstract**

The work developed aimed at the design, synthesis and characterization of new Gd(III) and Ga(III) chelates with potential application as imaging probes for magnetic resonance imaging (MRI), positron emission tomography (PET) and single-photon emission computed tomography (SPECT).

The initial part of the work is focused on the synthesis of new DOTA-based bifunctional ligands. Through the development of an efficient synthetic route, the chelator **DOTA-AHA** (1,4,7,10-tetraazacyclododecane-1-[(6-amino)hexanoic]-4,7,10-triacetic acid) was successfully synthesized and characterized. This ligand was the starting point for the development of three sets of molecular constructs, which include dimeric ligands, PEGylated chelators and c(RGDWK) peptide bioconjugates.

The Gd(III) chelates of **DOTA-AHA**, dimeric ligands and **DOTA-AHA** PEGylated ligands were obtained. The kinetic stability of **Gd(DOTA-AHA)** was evaluated in the presence of Zn(II) and as a function of pH. All Gd(III) chelates were studied by variable temperature <sup>1</sup>H NMRD (nuclear magnetic relaxation dispersion) and <sup>17</sup>O NMR (nuclear magnetic resonance) spectroscopy in order to measure the relaxivity and the parameters that govern it. The exchange of inner-sphere water from the monomeric chelate **Gd(DOTA-AHA)** and from the two binuclear chelates [**Gd<sub>2</sub>(Bis(DOTA-AHA)adipate)]<sup>2-</sup> and [**Gd<sub>2</sub>(Bis(DOTA-AHA)1,3-phenyldiacetate)]<sup>2-</sup> is similar (<sup>298</sup>k<sub>ex</sub> ≈ 6.5 x 10<sup>6</sup> s<sup>-1</sup>) and slightly faster than that of [**Gd(DOTA)]<sup>-</sup> (<sup>298</sup>k<sub>ex</sub> = 4.1 x 10<sup>6</sup> s<sup>-1</sup>). All three compounds form weakly bound aggregates with equilibrium constants <sup>298</sup>K of 2.9, 15.6 and 14.6 for **Gd(DOTA-AHA)**, [**Gd<sub>2</sub>(Bis(DOTA-AHA)adipate)]<sup>2-</sup> and [**Gd<sub>2</sub>(Bis(DOTA-AHA)1,3-phenyldiacetate)]<sup>2-</sup>, respectively. Even if the aggregates contain only 10 to 15% of the total amount of Gd(III) ions a marked increase in relaxivity between 30 and 100 MHz is observed.**********

PEGylation did not show to be a very efficient process for relaxivity improvement. Despite the moderate water exchange rates (<sup>298</sup>k<sub>ex</sub> ≈ 4.9x10<sup>6</sup> s<sup>-1</sup>) of the PEGylated Gd(III) chelates and the high global rotational correlation times (τ<sub>g</sub> ≈ 6900 ps), these chelates present lower relaxivity values than the binuclear chelates. Although the increased weight, the elevated PEG flexibility and fast isotropic local movements

may prevent higher relaxivity improvements. Similarly to what happens with the binuclear chelates, the global rotational correlation time suggests the presence of aggregation in solution.

The distance between the two Gd(III) centers in the binuclear compounds has been determined by double electron-electron resonance (DEER) experiments and by molecular modelling studies giving comparable distances. The linkers between the chelating moieties allow Gd(III)-Gd(III) distances of *circa* 3.0 nm for completely stretched linker conformation and  $\leq 1.9$  nm for the conformation with the metal centers at closer distance.

$^1\text{H}$  NMR spectra of paramagnetic lanthanide chelates of **DOTA-A(PEG<sub>750</sub>)HA** were recorded at different temperatures. The data obtained gave information on the structure and dynamics of the chelates in solution, showing throughout the lanthanide series *M/m* isomeric ratios with the same trend as those obtained for Ln(III) chelates of other DOTA-based ligands but with a strong predominance of the *M* form in the case of the Gd(III) chelate, which in part might account for its low relaxivity.

*In vitro* studies with  $^{67}\text{Ga}$ -radiolabeled **DOTA-AHA** and **DOTA-A(PEG<sub>750</sub>)HA** showed that both chelates are extremely hydrophilic.  $[\text{}^{67}\text{Ga}(\text{DOTA-A(PEG}_{750}\text{)HA})]^-$  chelate presents kinetic stability despite its considerable interaction with blood serum proteins. The lack of biospecificity of  $^{67}\text{Ga}(\text{DOTA-AHA})$  and  $[\text{}^{67}\text{Ga}(\text{DOTA-A(PEG}_{750}\text{)HA})]^-$  is revealed by their biodistribution profiles, which show that both radiolabeled chelates have significant uptake in major tissues. The fast elimination of  $^{67}\text{Ga}(\text{DOTA-AHA})$  from blood and tissues seems not to be altered by the presence of PEG moieties, as  $[\text{}^{67}\text{Ga}(\text{DOTA-A(PEG}_{750}\text{)HA})]^-$  presents a similar excretion rate.



*Quelatos do tipo DOTA de Ga(III) e Gd(III) para imagem médica (TEP, cintigrafia gama e IRM)*

## Resumo

O trabalho desenvolvido teve como objectivo o desenho, síntese e caracterização de novos quelatos de Gd(III) e Ga(III) com potencial aplicação como agentes de imagem para imagiologia de ressonância magnética (IRM), tomografia por emissão de positrões (TEP) e tomografia computadorizada por emissão de fóton único (cintigrafia gama).

A parte inicial do trabalho focou-se na síntese de novos ligandos bifuncionais do tipo **DOTA**. O ligando **DOTA-AHA** (ácido 1,4,7,10-tetraazaciclododecano-1-[(6-amino)hexanóico]-4,7,10-triacético) foi sintetizado e caracterizado utilizando uma estratégia de síntese particularmente eficaz. Este ligando foi o ponto de partida para o desenvolvimento de ligandos diméricos, ligandos PEGuilados e bioconjugados com o péptido c(RGDWK).

Preparam-se os quelatos de Gd(III) do ligando **DOTA-AHA**, dos ligandos diméricos e dos ligandos PEGuilados. A estabilidade cinética do quelato **Gd(DOTA-AHA)** foi avaliada na presença de Zn(II) e em função do pH. Todos os quelatos de Gd(III) foram estudados por DRMN (dispersão de relaxação magnética nuclear) e RMN (ressonância magnética nuclear) de  $^{17}\text{O}$ , de modo a obter os valores de relaxividade e os parâmetros que a afectam. Os valores das constantes de troca de água do quelato monomérico **Gd(DOTA-AHA)** e dos dois quelatos binucleares [**Gd<sub>2</sub>(Bis(DOTA-AHA)adipate)]<sup>2-</sup>** e [**Gd<sub>2</sub>(Bis(DOTA-AHA)1,3-phenyldiacetate)]<sup>2-</sup>** são semelhantes ( $^{298}k_{\text{ex}} \approx 6,5 \times 10^6 \text{ s}^{-1}$ ) e ligeiramente superiores aos do [**Gd(DOTA)]<sup>-</sup>** ( $^{298}k_{\text{ex}} = 4,1 \times 10^6 \text{ s}^{-1}$ ). Os três compostos formam agregados fracamente ligados, com constantes de equilíbrio  $^{298}K$  de 2,9, 15,6 e 14,6 para **Gd(DOTA-AHA)**, [**Gd<sub>2</sub>(Bis(DOTA-AHA)adipate)]<sup>2-</sup>** e [**Gd<sub>2</sub>(Bis(DOTA-AHA)1,3-phenyldiacetate)]<sup>2-</sup>**, respectivamente. Apesar de os agregados só conterem 10 a 15% da quantidade total de iões Gd(III) verifica-se um aumento acentuado na relaxividade para frequências entre 30 e 100 MHz.

A PEGuilação mostrou ser um processo pouco eficiente para melhorar a relaxividade. Apesar das constantes de troca de água dos respectivos complexos de

Gd(III) se mostrarem consideráveis ( $^{298}k_{\text{ex}} \approx 4,9 \times 10^6 \text{ s}^{-1}$ ) e dos seus elevados tempos de correlação rotacional globais ( $\tau_g \approx 6900 \text{ ps}$ ), estes quelatos apresentam valores de relaxividade inferior à dos quelatos binucleares. Mesmo considerando o seu peso molecular superior, a elevada flexibilidade do PEG e os rápidos movimentos isotrópicos locais podem impedir grandes ganhos de relaxividade. Tal como acontece com os quelatos binucleares, o tempo rotacional global sugere a presença da formação de agregados em solução.

A distância entre os dois centros de Gd(III) nos compostos binucleares foi determinada por ressonância dupla electrão-electrão (RDEE) e por estudos de modelação molecular, tendo sido obtidos resultados comparáveis. Os espaçadores entre as unidades quelantes permitem distâncias Gd(III)-Gd(III) de cerca de 3,0 nm para a conformação com o espaçador completamente esticado e  $\leq 1,9 \text{ nm}$  para a conformação com os centros metálicos à menor distância de aproximação.

Estudos de  $^1\text{H}$  RMN dos quelatos de **DOTA-A(PEG<sub>750</sub>)HA** com lantanídeos paramagnéticos foram efectuados a diferentes temperaturas. Os dados obtidos forneceram informação sobre a estrutura e dinâmica destes quelatos em solução, mostrando que ao longo da série dos lantanídeos, a proporção dos isómeros *M/m* segue a mesma tendência de outros quelatos de Ln(III) de ligandos do tipo DOTA mas com uma predominância acentuada do isómero *M* no caso do complexo de Gd(III), o que em parte explicará a sua baixa relaxividade.

Estudos *in vitro* com os ligandos **DOTA-AHA** e **DOTA-A(PEG<sub>750</sub>)HA** marcados com  $^{67}\text{Ga}$  mostraram que ambos os quelatos são extremamente hidrofílicos. O radiocomplexo [ $^{67}\text{Ga}(\text{DOTA-A}(\text{PEG}_{750})\text{HA})$ ]<sup>-</sup> apresenta estabilidade cinética apesar da sua interacção ser considerável com as proteínas do soro sanguíneo. A falta de bioespecificidade de  $^{67}\text{Ga}(\text{DOTA-AHA})$  e [ $^{67}\text{Ga}(\text{DOTA-A}(\text{PEG}_{750})\text{HA})$ ]<sup>-</sup> é evidenciada através dos perfis de biodistribuição destes radiocomplexos, para os quais se verifica uma acumulação significativa nos principais tecidos. A rápida eliminação de  $^{67}\text{Ga}(\text{DOTA-AHA})$  do sangue e tecidos não parece ser alterada pela presença de PEG, pois o radiocomplexo [ $^{67}\text{Ga}(\text{DOTA-A}(\text{PEG}_{750})\text{HA})$ ]<sup>-</sup> apresenta uma taxa de eliminação semelhante.

---

**Table of Contents**

<b>List of abbreviations</b> .....	<b>xv</b>
<b>List of symbols</b> .....	<b>xxi</b>
<b>List of figures</b> .....	<b>xxv</b>
<b>List of schemes</b> .....	<b>xxix</b>
<b>List of tables</b> .....	<b>xxxii</b>
<b>1 Introduction</b> .....	<b>1</b>
1.1 Metals in biology and medicine .....	3
1.2 Metal ions used in this work .....	5
1.2.1 Gallium.....	5
1.2.1.1 Coordination chemistry .....	5
1.2.1.2 Aqueous chemistry .....	8
1.2.1.3 Comparison with iron .....	9
1.2.1.4 <i>In vivo</i> behavior .....	10
1.2.1.5 Radioisotopes and uses .....	12
1.2.2 Lanthanides .....	15
1.2.2.1 Coordination chemistry .....	17
1.2.2.2 Radioisotopes and uses .....	18
1.2.2.3 Spectroscopic properties.....	20
1.2.2.4 Magnetic properties .....	21
1.2.2.5 Lanthanides as relaxation and chemical shift probes .....	22
1.3 Nuclear magnetic relaxation .....	23
1.3.1 Nuclear relaxation induced by Gd(III) .....	25
1.3.1.1 Inner Sphere Relaxivity .....	27
1.3.1.1.1 Number of water molecules ( $q$ ) .....	30
1.3.1.1.2 Gadolinium-proton distance ( $r_{\text{GdH}}$ ) .....	31
1.3.1.1.3 Residence time of coordinated water ( $\tau_m$ ) .....	32

1.3.1.1.4 Rotational correlation time ( $\tau_R$ ) .....	33
1.3.1.1.5 Electronic spin relaxation times ( $T_{1,2e}$ ) .....	35
1.3.1.2 Second sphere relaxivity .....	35
1.3.1.3 Outer sphere relaxivity .....	36
1.4 Ligands .....	37
1.4.1 Macrocyclic ligands .....	37
1.4.1.1 DOTA .....	39
1.4.1.2 DOTA-based bioconjugates and coupling strategies .....	41
1.4.1.3 DOTA-based bioconjugates with RGD peptide analogues .....	45
1.5 Medical imaging modalities .....	51
1.5.1 Magnetic resonance imaging .....	52
1.5.1.1 Contrast agents .....	54
1.5.1.1.1 Extracellular contrast agents .....	55
1.5.1.1.2 Blood pool contrast agents .....	58
1.5.1.1.3 Targeted contrast agents .....	59
1.5.2 Positron emission tomography .....	60
1.5.3 Single photon emission computed tomography .....	63
1.6 Objective of the thesis .....	65
<b>2 Results and Discussion .....</b>	<b>67</b>
2.1 Synthesis .....	69
2.1.1 Synthesis of the bifunctional chelators .....	69
2.1.2 Synthesis of DOTA-AHA conjugates .....	74
2.2 Temperature dependence and kinetic stability studies of Gd(DOTA-AHA) and [Gd(DOTA-A(PEG <sub>750</sub> )HA)] <sup>-</sup> chelates .....	79
2.3 <sup>1</sup> H NMRD and <sup>17</sup> O NMR relaxometric studies .....	81
2.3.1 DOTA-AHA and binuclear Gd(III) chelates .....	81
2.3.2 PEGylated Gd(III) chelates .....	91

---

2.4 DEER and modelling studies of Gd(III) binuclear chelates .....	95
2.5 $^1\text{H}$ NMR studies of paramagnetic lanthanide DOTA-A(PEG <sub>750</sub> )HA chelates .....	97
2.6 <i>In vitro</i> and <i>in vivo</i> studies of $^{67}\text{Ga}$ (DOTA-AHA) and $[\text{}^{67}\text{Ga}(\text{DOTA-A}(\text{PEG}_{750})\text{HA})]^-$ .....	102
<b>3 Conclusion and Perspectives .....</b>	<b>107</b>
3.1 Conclusion .....	109
3.2 Perspectives .....	111
<b>4 Experimental Part .....</b>	<b>113</b>
4.1 Chemicals and materials .....	115
4.2 Instruments.....	115
4.3 Synthesis .....	117
4.4 Temperature dependence and kinetic stability studies of Gd(DOTA-AHA) and $[\text{Gd}(\text{DOTA-A}(\text{PEG}_{750})\text{HA})]^-$ chelates .....	141
4.4.1 Samples preparation .....	141
4.4.2 Measurements.....	141
4.5 $^1\text{H}$ NMRD and $^{17}\text{O}$ NMR relaxometric studies .....	142
4.5.1 Samples preparation .....	142
4.5.2 $^1\text{H}$ NMRD.....	142
4.5.3 $^{17}\text{O}$ NMR .....	143
4.5.4 Data analysis .....	143
4.6 DEER and modelling studies of Gd(III) binuclear chelates .....	144
4.6.1 Samples preparation .....	144
4.6.2 Measurements.....	144
4.6.3 Data analysis .....	144
4.6.4 Molecular modelling .....	145
4.7 $^1\text{H}$ NMR studies of paramagnetic lanthanide DOTA-A(PEG <sub>750</sub> )HA chelates ...	145
4.7.1 Samples preparation .....	145
4.7.2 Measurements.....	145

4.8 <i>In vitro</i> and <i>in vivo</i> studies of $^{67}\text{Ga}(\text{DOTA-AHA})$ and $[\text{}^{67}\text{Ga}(\text{DOTA-A}(\text{PEG}_{750})\text{HA})]^-$ .....	146
4.8.1 Samples preparation .....	146
4.8.2 Determination of LogP .....	146
4.8.3 Stability studies in blood serum .....	147
4.8.4 Biodistribution and blood clearance studies.....	147
4.9 Ligand titrations.....	148
<b>5 Bibliography.....</b>	<b>149</b>
<b>6 Appendix .....</b>	<b>169</b>
6.1 General equations for the analysis of $^1\text{H}$ NMRD and $^{17}\text{O}$ NMR experimental data <sup>293</sup> .....	171
6.1.1 Electron spin relaxation <sup>351</sup> .....	172
6.1.2 $^1\text{H}$ NMRD.....	173
6.1.3 $^{17}\text{O}$ NMR .....	174
6.1.4 Simultaneous fits of $^{17}\text{O}$ NMR and $^1\text{H}$ NMRD experiments .....	176
6.1.5 Rotational correlation time of dimers.....	183
6.1.6 Experimental data of temperature dependence and kinetic stability studies.....	184
6.2 Experimental data of DEER studies .....	185
6.3 Experimental data of <i>in vitro</i> and <i>in vivo</i> studies.....	186

---

**List of abbreviations**

<b>aa</b>	Amino acid
<b>Ac</b>	Acetate
<b>AcOH</b>	Acetic acid
<b>Alloc</b>	Allyloxycarbonyl
<b>Be</b>	Benzhydryl
<b>BFC</b>	Bifunctional chelator
<b>BM</b>	Targeting biomolecule
<b>Boc</b>	<i>tert</i> -Butyloxycarbonyl
<b>Boc<sub>2</sub>O</b>	Di- <i>tert</i> -butyl dicarbonate
<b>BPA</b>	Blood pool agents
<b>CA</b>	Contrast agent
<b>Cbz</b>	Carboxybenzyl
<b>cit</b>	Citrate
<b>CT</b>	Computed tomography
<b>Cyclen</b>	1,4,7,10-tetraazacyclododecane
<b>d</b>	Doublet
<b>d<sub>b</sub></b>	Broad doublet
<b>DCC</b>	<i>N,N'</i> -Dicyclohexylcarbodiimide
<b>DCM</b>	Dichloromethane
<b>dd</b>	Double doublet
<b>DDM</b>	Diphenyldiazomethane
<b>DEER</b>	Double electron-electron resonance
<b>DEPT</b>	Distortionless enhancement by polarization transfer
<b>DFO-B</b>	Desferrioxamine-B
<b>DIC</b>	<i>N,N'</i> -Diisopropylcarbodiimide
<b>DIPEA</b>	<i>N,N</i> -Diisopropylethylamine
<b>DMAP</b>	4-Dimethylaminopyridine
<b>DMF</b>	<i>N,N</i> -Dimethylformamide
<b>DMSO</b>	Dimethyl sulfoxide
<b>DNA</b>	Deoxyribonucleic acid
<b>DOTA</b>	1,4,7,10-Tetraazacyclododecane-1,4,7,10-tetraacetic acid

<b>DOTA-AHA</b>	1,4,7,10-Tetraazacyclododecane-1-[(6-amino)hexanoic]-4,7,10-triacetic acid
<b>DOTA-A(PEG<sub>350</sub>)HA</b>	1,4,7,10-Tetraazacyclododecane-1-[6-amino(MeO-PEG <sub>350</sub> -succinate)]hexanoic-4,7,10-triacetic acid
<b>DOTA-A(PEG<sub>550</sub>)HA</b>	1,4,7,10-Tetraazacyclododecane-1-[6-amino(MeO-PEG <sub>550</sub> -succinate)]hexanoic-4,7,10-triacetic acid
<b>DOTA-A(PEG<sub>750</sub>)HA</b>	1,4,7,10-Tetraazacyclododecane-1-[6-amino(MeO-PEG <sub>750</sub> -succinate)]hexanoic-4,7,10-triacetic acid
<b>DOTA-APPA</b>	1,4,7,10-Tetraazacyclododecane-1- {[3-(4-aminophenyl)]propanoic} -4,7,10-triacetic acid
<b>DOTAGA</b>	1,4,7,10-Tetraazacyclododecane-1-glutamic acid-4,7,10-triacetic acid
<b>DOTASA</b>	1,4,7,10-Tetraazacyclododecane-1-succinic acid-4,7,10-triacetic acid
<b>DOTPM</b>	1,1'-Bis(di-o-tolylphosphino)methane
<b>DO3A</b>	1,4,7,10-Tetraazacyclododecane-1,4,7-triacetic acid
<b>DO3(<i>t</i>-Bu)A</b>	1,4,7,10-Tetraazacyclododecane-1,4,7-triacetate <i>tert</i> -butyl ester
<b>DO3A-<math>\beta</math>ABA</b>	1,4,7,10-Tetraazacyclododecane-1-[ $\beta$ -(4-amino)butanoic]-4,7,10-triacetic acid
<b>dt</b>	Double triplet
<b>DTPA</b>	Diethylenetriamine- <i>N,N,N',N'',N'''</i> -pentaacetic acid
<b>EC</b>	<i>N,N'</i> -Ethylene-di-cysteine
<b>ECF</b>	Extracellular fluid agents
<b>EDTA</b>	Ethylenediamine- <i>N,N,N',N''</i> -tetraacetic acid
<b>EDTPM</b>	Ethylenediamine- <i>N,N,N',N''</i> -tetra(methylene phosphonic acid)
<b>EPR</b>	Electron paramagnetic resonance
<b>ESEEM</b>	Electron spin echo envelope modulation
<b>ESI</b>	Electrospray ionization
<b>Et<sub>3</sub>N</b>	<i>N,N,N</i> -Triethylamine
<b>EtOH</b>	Ethanol
<b>FHMA</b>	Ferric hydroxymacroaggregates



---

<b>Fmoc</b>	9-Fluorenylmethoxycarbonyl
<b>GABOB</b>	4-Amino-3-hydroxybutanoic acid
<b>HATU</b>	1-[Bis(dimethylamino)methylene]-1 <i>H</i> -1,2,3-triazolo[4,5- <i>b</i> ]pyridinium 3-oxid hexafluorophosphate
<b>HBED</b>	<i>N,N'</i> -bis(2-hydroxybenzyl)ethylenediamine- <i>N,N'</i> -diacetic acid
<b>HBTU</b>	<i>O</i> -(Benzotriazol-1-yl)- <i>N,N,N',N'</i> -tetramethyluronium hexafluorophosphate
<b>HDI</b>	1,6-Diisocyanatohexane
<b>HEPES</b>	2-[4-(2-hydroxyethyl)piperazin-1-yl]ethanesulfonic acid
<b>HMBC</b>	Heteronuclear multiple bond correlation
<b>HOBt</b>	1-Hydroxybenzotriazole
<b>HOPO</b>	Hetero-tripodal hydroxypyridonate
<b>HPLC</b>	High performance liquid chromatography
<b>HRMS</b>	High resolution mass spectrometry
<b>HSA</b>	Human serum albumin
<b>HSQC</b>	Heteronuclear Single Quantum Coherence
<b>ID</b>	Injected dose
<b>IR</b>	Infra-red
<b>ITLC</b>	Instant thin layer chromatography
<b>L</b>	Ligand
<b>LF</b>	Lactoferrin
<b>LFSE</b>	Ligand field stabilization energies
<b>Ln</b>	Lanthanide
<b>LogP</b>	Octanol/water coefficient partition
<b>Lys</b>	Lysine
<b>m</b>	Multiplet
<b>m<sub>b</sub></b>	Broad multiplet
<b>MeCN</b>	Acetonitrile
<b>MeO</b>	Methoxy
<b>MeOH</b>	Methanol
<b>Mn</b>	Average molecular weight
<b>MRI</b>	Magnetic resonance imaging

<b>Mw</b>	Molecular weight
<b>NDMBA</b>	<i>N,N'</i> -Dimethyl barbituric acid
<b>NMR</b>	Nuclear magnetic resonance
<b>NMRD</b>	Nuclear magnetic relaxation dispersion
<b>NODASA</b>	1,4,7-Triazacyclononane-1-succinic acid-4,7-diacetic acid
<b>NOTA</b>	1,4,7-Triazacyclononane-1,4,7-triacetic acid
<b>PA-DOTA</b>	$\alpha$ -[2-(4-aminophenyl)-ethyl]-1,4,7,10-tetraazacyclododecane-1,4,7,10-tetraacetic acid
<b>Pbf</b>	2,2,4,6,7-Pentamethyldihydrobenzofuran-5-sulfonyl
<b>PBS</b>	Phosphate buffered saline
<b>Pd/C</b>	Palladium on carbon
<b>PEG</b>	Poly(ethylene glycol)
<b>PET</b>	Positron emission tomography
<b>PKM</b>	Pharmacokinetic Modifier
<b>PPM</b>	Parts per million
<b>Rf</b>	Retention factor
<b>RNA</b>	Ribonucleic acid
<b>rRNA</b>	Ribosomal ribonucleic acid
<b>s</b>	Singlet
<b>s<sub>b</sub></b>	Broad singlet
<b>SBAD</b>	1,10-bis(2-hydroxy-5-sulfonybenzyl)-1,4,7,10-tetraazadecane
<b>SD</b>	Standard deviation
<b>SDSL</b>	Site directed spin labelling
<b>SPECT</b>	Single-photon emission computed tomography
<b>SPIOs</b>	Supermagnetic iron oxides
<b>SPPS</b>	Solid phase peptide synthesis
<b>sulfo-NHS</b>	<i>N</i> -hydroxysulfosuccinimide
<b>t</b>	Triplet
<b>TACN-TM</b>	1,4,7-Triazacyclononane-1,4,7-tri(2-mercaptoethyl)
<b>t<sub>b</sub></b>	Broad triplet
<b>TETA</b>	1,4,8,11-Tetraazacyclotetradecane-1,4,8,11-tetraacetic acid
<b>TF</b>	Transferrin

<b>TFA</b>	Trifluoroacetic acid
<b>TFE</b>	2,2,2-Trifluoroethanol
<b>THF</b>	Tetrahydrofuran
<b>TLC</b>	Thin layer chromatography
<b>TMG</b>	<i>1,1,3,3</i> -Tetramethylguanidine
<b>TMS</b>	Tetramethylsilane
<b>TNBS</b>	2,4,6-Trinitrobenzenesulfonic acid
<b>TTHA</b>	Triethylenetetramine- <i>N,N,N',N'',N''',N''''</i> -hexaacetic acid
<b>tRNA</b>	Transfer ribonucleic acid
<b>TSP</b>	3-(Trimethylsilyl)propionic-2,2,3,3- $d_4$ acid sodium salt
<b><i>t</i>-Bu</b>	<i>tert</i> -Butyl
<b>UV</b>	Ultra violet
<b>XAFS</b>	X-ray absorption fine structure
<b>XRD</b>	X-ray diffraction
<b>ZFS</b>	Zero field splitting



---

**List of symbols**

$\hbar$	Reduced Planck's constant or Dirac's constant
$A/\hbar$	Hyperfine or scalar coupling constant
$\beta^+$	Positron
$\beta^-$	Electron
$\delta$	Chemical shift
$\Delta$	Lanthanide induced shift
$\Delta_d$	Diamagnetic shift
$\Delta_c$	Contact shift
$\Delta_{pc}$	Pseudo-contact shift
$\Delta\omega_m$	Chemical shift difference between bound and bulk water
$\Delta^2$	Mean square ZFS energy
$\Delta H^\ddagger$	Enthalpy of activation for the water exchange process
$\Delta S^\ddagger$	Entropy of activation for the water exchange process
$\varepsilon$	Electron capture
$\eta$	Microviscosity
$\mu$	Magnetic dipole moment
$\mu_{eff}$	Magnetic moment
$\mu_B$	Bohr magneton
$\tau_m$	Lifetime of a water molecule in the inner sphere
$\tau_R$	Rotational correlation time
$\tau_g$	Rotational correlation time of the slow global motion
$\tau_l$	Rotational correlation time of the rapid local motion
$\tau_c$	Effective correlation time of proton relaxation
$\tau_v$	Correlation time for the modulation of ZFS interaction
$\tau_D$	Diffusional correlation time
$\nu$	Frequency
$\nu_0$	Larmor frequency
$\gamma$	Gyromagnetic ratio
$\gamma_I$	Nuclear gyromagnetic ratio

## List of Symbols

---

$\gamma_S$	Electronic gyromagnetic ratio
$\omega_I$	Nuclear Larmor frequency
$\omega_S$	Electron Larmor frequency
$\omega_r$	Reduced chemical shift
$\omega_A$	Reduced chemical shift of acidified water reference
$\zeta$	Spin-orbit coupling constant
$B_0$	Magnetic field
$c$	Molal concentration
$d$	Closest distance of approach of spins $I$ and $S$
$D_{GdH}$	Diffusion constant for relative diffusion of water proton from Gd(III) center
$E_v$ or $E_{GdH}$	Activation energy
$f(v)$	Flow factor
$g$	Landé g-factor
$h$	Planck constant
$[H]$	Proton density
$I$	Nuclear spin
$J$	Angular momentum quantum number
$j(\omega)$	Spectral densities
K	Kelvin
$K$	Thermodynamic stability constant
$k_B$	Boltzmann constant
$k_{ex}$	Water exchange rate
$L$	Orbital angular momentum quantum number
$[M]$	Molar concentration of the metal bearing spin $S$
$N_A$	Avogadro's constant
$P_m$	Mole fraction of the bound water molecules
$q$	Number of bound water molecules per Gd
$r_{eff}$	Effective radius
$r_{GdH}$	Electron spin-proton distance
$r_{GdO}$	Electron spin-oxygen distance
$r_{1(2)}$	Longitudinal (transverse) proton relaxivity
$R_{1(2)}$	Longitudinal (transverse) proton relaxation rate

$R$	Gas Constant
$S$	Spin angular momentum quantum number
$S^2$	degree of spatial restriction of the local motion
$S_{\text{spin-echo}}$	Spin-echo pulse sequence
$t_e$	Echo time
$t_r$	Repetition time
$T$	Temperature or Tesla
$T_{1(2)obs}$	Observed solvent longitudinal (transverse) relaxation rate
$T_{1(2)d}$	Diamagnetic solvent longitudinal (transverse) relaxation rate
$T_{1(2)p}$	Paramagnetic solvent longitudinal (transverse) relaxation rate
$T_{1(2)m}$	Longitudinal (transverse) relaxation rate of a bound water molecule
$T_{1(2)e}$	Longitudinal (transverse) electron spin relaxation time of metal
$Z$	Atomic number





---

**List of figures**

<b>Figure 1.1:</b> Production of $^{68}\text{Ge}$ by the ( $p, 2n$ ) reaction of $^{69}\text{Ga}$ . .....	13
<b>Figure 1.2:</b> Macrocyclic ligands of $\text{N}_3\text{R}_3$ and $\text{N}_4\text{R}_4$ type. ....	15
<b>Figure 1.3:</b> A) Precession of magnetic moment of protons in the presence of an external magnetic field; B) Proton spin energy in the presence of a magnetic field; C) Change in proton spin energy with increasing radiofrequency at the Larmor frequency. ....	24
<b>Figure 1.4:</b> Schematic representation of the paramagnetic interactions that contribute to water proton relaxivity. ....	26
<b>Figure 1.5:</b> Schematic representation of Gd(III) chelate solvent environment. ....	29
<b>Figure 1.6:</b> Chelators 2,3,2-tet and meso-1,7-CTH. ....	38
<b>Figure 1.7:</b> Schematic representation of a bioconjugate. ....	41
<b>Figure 1.8:</b> DOTA-based bifunctional ligands. ....	43
<b>Figure 1.9:</b> The integrin group: RGD receptors, laminin receptors, leukocyte receptors and collagen receptors. ....	46
<b>Figure 1.10:</b> The $\alpha\text{v}\beta 3$ integrin structure: a) bent image; b) straightened image. ...	47
<b>Figure 1.11:</b> Structure of DOTA-c(RGDfK). ....	48
<b>Figure 1.12:</b> DOTA-cyclic RGD derivatives as $\alpha\text{v}\beta 3$ agonists. ....	51
<b>Figure 1.13:</b> Representation of the MR imaging system. ....	52
<b>Figure 1.14:</b> $T_1$ weighted MRI of brain before (A) and after (B) gadolinium complex contrast enhancement, showing a metastatic deposit involving the right frontal bon with a large extracranial soft tissue component and meningeal invasion. ....	53
<b>Figure 1.15:</b> DO3A-based dimeric ligands for Gd(III). ....	57
<b>Figure 1.16:</b> Representation of the PET imaging system. ....	61
<b>Figure 2.1:</b> $^1\text{H}$ NMR spectrum at 400 MHz of compound 9 in $\text{CDCl}_3$ . ....	72
<b>Figure 2.2:</b> $^1\text{H}$ NMR spectrum at 400 MHz of compound 12 in $\text{CDCl}_3$ . ....	73
<b>Figure 2.3:</b> $^1\text{H}$ NMR spectrum at 400 MHz of compound 14 in $\text{CDCl}_3$ . ....	75
<b>Figure 2.4:</b> $^1\text{H}$ NMR spectrum at 400 MHz of compound 27 in DMSO. ....	77
<b>Figure 2.5:</b> Dependency of longitudinal proton paramagnetic relaxation rate ( $R_{1\text{Obs}}$ ) at 20 MHz and $\text{pH} = 7.0$ on the temperature for Gd(DOTA-AHA) and $[\text{Gd}(\text{DOTA-A}(\text{PEG}_{750})\text{HA})]^-$ solutions. ....	79

---

<b>Figure 2.6:</b> Dependency of longitudinal proton paramagnetic relaxation rate ( $R_{1p}$ ) at 20 MHz and 25 °C on the pH for Gd(DOTA-AHA) and [Gd(DOTA-A(PEG <sub>750</sub> )HA)] <sup>-</sup> solutions. ....	80
<b>Figure 2.7:</b> Time evolution of the relative longitudinal proton paramagnetic relaxation rate ( $R_{1p}(t)/R_{1p}(0)$ ) at 20 MHz and 37 °C for Gd(DOTA-AHA) + PBS solution and Gd(DOTA-AHA) + PBS + Zn(II) solution. ....	80
<b>Figure 2.8:</b> Reduced transverse and longitudinal <sup>17</sup> O NMR relaxation rates; reduced <sup>17</sup> O chemical shifts; and <sup>1</sup> H NMRD profiles for Gd(DOTA-AHA), [Gd <sub>2</sub> (Bis(DOTA-AHA)adipate)] <sup>2-</sup> and [Gd <sub>2</sub> (Bis(DOTA-AHA)1,3-phenyldiacetate)] <sup>2-</sup> . ....	82
<b>Figure 2.9:</b> Concentration dependent relaxivity of the binuclear [Gd <sub>2</sub> (Bis(DOTA-AHA)adipate)] <sup>2-</sup> and [Gd <sub>2</sub> (Bis(DOTA-AHA)1,3-phenyldiacetate)] <sup>2-</sup> measured at 1.41 T (60 MHz) and 37 °C. ....	84
<b>Figure 2.10:</b> Anisotropic rotation of binuclear compounds. ....	89
<b>Figure 2.11:</b> Influence of [Gd <sub>2</sub> (Bis(DOTA-AHA)1,3-phenyldiacetate)] <sup>2-</sup> aggregation on <sup>17</sup> O NMR and <sup>1</sup> H NMRD. ....	90
<b>Figure 2.12:</b> <sup>1</sup> H NMRD profile of [Gd(DOTA-A(PEG <sub>350</sub> )HA)] <sup>-</sup> , [Gd(DOTA-A(PEG <sub>550</sub> )HA)] <sup>-</sup> and [Gd(DOTA-A(PEG <sub>750</sub> )HA)] <sup>-</sup> chelates at 25°C and 37°C. ....	92
<b>Figure 2.13:</b> Reduced <sup>17</sup> O transverse and longitudinal relaxation rates and reduced chemical shifts ( $B = 9.4$ T) for the [Gd(DOTA-A(PEG <sub>750</sub> )HA)] <sup>-</sup> chelate. ....	92
<b>Figure 2.14:</b> Molecular mechanics structures (MM3 force field) illustrating possible conformations of a) [Gd <sub>2</sub> (Bis(DOTA-AHA)adipate)] <sup>2-</sup> and b) [Gd <sub>2</sub> (Bis(DOTA-AHA)1,3-phenyldiacetate)] <sup>2-</sup> with Gd-Gd distances. ....	96
<b>Figure 2.15:</b> <sup>1</sup> H NMR resonances of the ax <sub>1</sub> protons of the <i>M</i> and <i>m</i> isomers of the paramagnetic lanthanide DOTA-A(PEG <sub>750</sub> )HA chelates at pH=7 and 25 °C. ....	100
<b>Figure 2.16:</b> <sup>1</sup> H NMR resonances of the ax <sub>1</sub> protons of the <i>M</i> and <i>m</i> isomers of the paramagnetic lanthanide DOTA-A(PEG <sub>750</sub> )HA chelates at pH=7 and 40 °C. ....	101

<b>Figure 2.17:</b> Biodistribution results of $^{67}\text{Ga}(\text{DOTA-AHA})$ and $[\text{}^{67}\text{Ga}(\text{DOTA-A}(\text{PEG}_{750})\text{HA})]^-$ . Percentage of injected dose per gram of organ (%ID/g) 1 hour after injection on Wistar rats. ....	105
<b>Figure 2.18:</b> Biodistribution results of $^{67}\text{Ga}(\text{DOTA-AHA})$ and $[\text{}^{67}\text{Ga}(\text{DOTA-A}(\text{PEG}_{750})\text{HA})]^-$ . Percentage of injected dose per gram of organ (%ID/g) 24 hours after injection on Wistar rats. ....	105
<b>Figure 2.19:</b> Blood clearance results of $^{67}\text{Ga}(\text{DOTA-AHA})$ and $[\text{}^{67}\text{Ga}(\text{DOTA-A}(\text{PEG}_{750})\text{HA})]^-$ . Percentage of injected dose per gram of organ (%ID/g) 5, 30, 60 and 1440 minutes after injection on Wistar rats. ...	106
<b>Figure 6.1:</b> Reduced transverse and longitudinal $^{17}\text{O}$ NMR relaxation rates; reduced $^{17}\text{O}$ chemical shifts; and $^1\text{H}$ NMRD profiles for $\text{Gd}(\text{DOTA-AHA})$ and $[\text{Gd}_2(\text{Bis}(\text{DOTA-AHA})1,3\text{-phenyldiacetate})]^{2-}$ . ....	177
<b>Figure 6.2:</b> Simultaneous fits of $[\text{Gd}_2(\text{Bis}(\text{DOTA-AHA})1,3\text{-phenyldiacetate})]^{2-}$ NMR data using Lipari-Szabo approach and formation of weak aggregates. ....	179
<b>Figure 6.3:</b> Simple molecular mechanics model of a $[\text{Gd}_2(\text{Bis}(\text{DOTA-AHA})\text{adipate})]^{2-}$ dimer. ....	183
<b>Figure 6.4:</b> Hydrodynamic model of $[\text{Gd}_2(\text{Bis}(\text{DOTA-AHA})\text{adipate})]^{2-}$ dimer created by HYDRONMR using 2.2 Å as effective radius of the atomic elements. ....	183
<b>Figure 6.5:</b> DEER measurements of $[\text{Gd}_2(\text{Bis}(\text{DOTA-AHA})1,3\text{-phenyldiacetate})]^{2-}$ and $[\text{Gd}_2(\text{Bis}(\text{DOTA-AHA})\text{adipate})]^{2-}$ samples. ...	185



## List of schemes

<b>Scheme 2.1:</b> Structures of the bifunctional chelators DOTA-APPA, DOTA- $\beta$ ABA and DOTA-AHA. ....	69
<b>Scheme 2.2:</b> Synthetic methodologies proposed for the preparation of the bifunctional residues 3, 6 and 9. ....	70
<b>Scheme 2.3:</b> Synthesis of DOTA-AHA, 13. ....	73
<b>Scheme 2.4:</b> Synthesis of DOTA-AHA dimmers, 15 and 17. ....	74
<b>Scheme 2.5:</b> Synthesis of DOTA-AHA PEGylated conjugates. ....	75
<b>Scheme 2.6:</b> Synthesis of c(R(Pbf)GD( <i>t</i> -Bu)WK) peptide. ....	76
<b>Scheme 2.7:</b> Synthesis of DOTA-AHA bioconjugates with c(RGDWK). ....	78



## List of tables

<b>Table 1.1:</b>	Metal-based compounds and their applications in medicine. ....	4
<b>Table 1.2:</b>	Stability constants of gallium complexes at 25 °C. ....	6
<b>Table 1.3:</b>	Some chemical parameters for trivalent gallium and iron. ....	9
<b>Table 1.4:</b>	Radioisotopes of gallium. ....	12
<b>Table 1.5:</b>	Some properties of lanthanides. ....	16
<b>Table 1.6:</b>	Isotopes of some lanthanides. ....	19
<b>Table 1.7:</b>	Lanthanide compounds for diagnostic and therapeutic applications. ...	19
<b>Table 1.8:</b>	Trivalent lanthanide magnetic moments at room temperature. ....	22
<b>Table 1.9:</b>	Crystallographic and structural data of some DOTA chelates. ....	40
<b>Table 1.10:</b>	Values of stability constant, bond length, bond angle and distance between metal and N <sub>4</sub> plan of some DOTA chelates. ....	40
<b>Table 1.11:</b>	Names and structures of commercially Gd-DOTA-based contrast agents. ....	56
<b>Table 1.12:</b>	Nuclear parameters of useful PET radionuclides. ....	63
<b>Table 1.13:</b>	Nuclear parameters of useful SPECT radionuclides. ....	63
<b>Table 2.1:</b>	Water exchange parameters, $^{298}k_{ex}$ , $\Delta H^\ddagger$ , $\Delta S^\ddagger$ , rotational correlation times, $^{298}\tau_R^{mono}$ , $^{298}\tau_R^{agg}$ , and equilibrium constants, $K^{298}$ , $\Delta H^0$ , $\Delta S^0$ , for aggregation Gd(DOTA-AHA), [Gd <sub>2</sub> (Bis(DOTA-AHA)adipate)] <sup>2-</sup> and [Gd <sub>2</sub> (Bis(DOTA-AHA)1,3-phenyldiacetate)] <sup>2-</sup> . ....	87
<b>Table 2.2:</b>	Distribution of gadolinium in monomers, dimers and trimers calculated from $K^{298}$ and equation 2.3 at 298K. ....	87
<b>Table 2.3:</b>	Relaxometric parameters for [Gd(DOTA-A(PEG <sub>350</sub> )HA)] <sup>-</sup> , [Gd(DOTA-A(PEG <sub>550</sub> )HA)] <sup>-</sup> and [Gd(DOTA-A(PEG <sub>750</sub> )HA)] <sup>-</sup> . The [Gd(DOTA-A(PEG <sub>350</sub> )HA)] <sup>-</sup> , [Gd(DOTA-A(PEG <sub>550</sub> )HA)] <sup>-</sup> and [Gd(DOTA-A(PEG <sub>750</sub> )HA)] <sup>-</sup> parameters were obtained from the simultaneous analysis of <sup>17</sup> O NMR and <sup>1</sup> H NMRD data, using the Solomon-Bloembergen-Morgan approach. ....	94
<b>Table 2.4:</b>	<sup>1</sup> H NMR chemical shifts (ppm) of the ax <sub>1</sub> protons of the paramagnetic lanthanide DOTA-A(PEG <sub>750</sub> )HA chelates in <i>M</i> and <i>m</i> isomeric forms at 25 °C and pH=7. ....	99

---

<b>Table 2.5:</b>	Measured activity of $[\text{}^{67}\text{Ga}(\text{DOTA-A}(\text{PEG}_{750})\text{HA})]^-$ in aqueous and proteins phase of human serum solution. ....	104
<b>Table 6.1:</b>	Comparison of parameters from simultaneous fits of $[\text{Gd}_2(\text{Bis}(\text{DOTA-AHA})1,3\text{-phenyldiacetate})]^{2-}$ $^{17}\text{O}$ NMR and $^1\text{H}$ NMRD using SBM theory with Lipari-Szabo and self-aggregation of compounds. ....	180
<b>Table 6.2:</b>	Parameters from simultaneous fits of $^{17}\text{O}$ NMR and $^1\text{H}$ NMRD using SBM theory and self-aggregation of compounds. ....	182
<b>Table 6.3:</b>	Longitudinal proton paramagnetic relaxation rate ( $R_{1\text{Obs}}$ ) of $\text{Gd}(\text{DOTA-AHA})$ (1.25 mM) and $[\text{Gd}(\text{DOTA-A}(\text{PEG}_{750})\text{HA})]^-$ (1.25 mM) at 20 MHz and pH = 7. ....	184
<b>Table 6.4:</b>	Longitudinal proton paramagnetic relaxation rates ( $R_{1\text{p}}$ ) of $\text{Gd}(\text{DOTA-AHA})$ (1.25 mM) and $[\text{Gd}(\text{DOTA-A}(\text{PEG}_{750})\text{HA})]^-$ (1.25 mM) at 20 MHz and 25 °C. ....	184
<b>Table 6.5:</b>	Biodistribution results of $^{67}\text{Ga}(\text{DOTA-AHA})$ and $[\text{}^{67}\text{Ga}(\text{DOTA-A}(\text{PEG}_{750})\text{HA})]^-$ . Percentage of injected dose per gram of organ (%ID/g) 1 hour and 24 hours after injection on Wistar rats. ....	186
<b>Table 6.6:</b>	Blood clearance results of $^{67}\text{Ga}(\text{DOTA-AHA})$ and $[\text{}^{67}\text{Ga}(\text{DOTA-A}(\text{PEG}_{750})\text{HA})]^-$ . Percentage of injected dose per gram of organ (%ID/g) 5, 30, 60 and 1440 minutes after injection on Wistar rats. ....	186
<b>Table 6.7:</b>	Activities of 1-octanol and water phases of the $^{67}\text{Ga}(\text{DOTA-AHA})$ and $[\text{}^{67}\text{Ga}(\text{DOTA-A}(\text{PEG}_{750})\text{HA})]^-$ solutions. ....	186



# **1 Introduction**



## 1.1 Metals in biology and medicine

Since early times, mankind used metals for making tools and accessories. The use of metals in medicine is recognized and documented for more than 3000 years, when early oriental civilizations used gold amalgams to treat sick noble men, zinc to heal wounds or copper to disinfect water. Still, in the early 20<sup>th</sup> century, the knowledge of the chemical processes in the human body was very limited and the role of metal ions on those processes was practically unknown. Due to this lack of information, the use of metal compounds in medicine was very restricted and performed through an empirical approach.

Throughout the 20<sup>th</sup> century, the scientific development allowed identifying and understanding the importance and the role of metallic elements on living systems. It is now known that some metal ions are essential to biological processes, and these can be divided in two major classes, the bulk and the trace metals.

Bulk metals such as sodium, potassium or calcium have an elevated concentration in human body. The main roles of sodium ions are related to the management of concentration gradients across the membranes and conservation of pH, through  $\text{Na}^+/\text{H}^+$  transport.<sup>1</sup> Potassium ions control osmotic pressure, equilibrium of cellular electrolytes and are involved in the control of transmembrane potentials.<sup>1</sup> Due to the high concentration of calcium in bones and teeth, this element is very important at the structural level, playing also an important role in nerve impulse transmission, muscle action, cell permeability and blood pressure regulation.<sup>2</sup>

Oppositely, metals such as iron, magnesium, zinc or copper are considered trace metals due to their low concentration in human body, being mostly responsible for cell metabolism. Every eukaryote cell contains iron, making it one of the most important metals in biological systems. In humans, about two thirds of iron ions are confined in hemoglobin, which is responsible for oxygen transport, the remaining third is stored in bone marrow, spleen, liver and muscles.<sup>1</sup> With a standard concentration of 30 mM, magnesium is one of the major intracellular ions (together with potassium), and approximately 90% is localized in ribosomes. Magnesium has an important role in protein synthesis and cell division since it is a crucial cofactor for many DNA and RNA processing enzymes<sup>3</sup> and it is vital in the regulation of rRNA and tRNA structures.<sup>4</sup> Present in more than 3000 human proteins, specifically in more than 200

metalloenzymes, zinc is an essential element with a wide range of biological applications. As part of prosthetic groups, zinc can play a catalytic, structural, metabolic or regulatory role. The structural role in human proteins is quite relevant, because zinc ions directly contribute for “zinc fingers” formation, which are crucial for the integrity of biological membranes.<sup>1</sup>

Despite the fact many metal elements do not present any metabolic role in biological systems, some are potentially useful for medical applications. Nowadays, medicinal inorganic chemistry is an important domain in chemistry, and the number of metal-based compounds used for both therapeutic and diagnostic purposes does not stop increasing. Cisplatin, a divalent platinum compound discovered in 1965 by Barnett Rosenberg is one of the most extensively used anticancer drug, mostly to treat ovarian and testicular cancer.<sup>5</sup> Elements such as gadolinium, gallium or technetium, which are non-existent in living systems, are examples of metals that can be useful for diagnosis through medical imaging techniques. Table 1.1 presents some examples of metal-based compounds used for medicinal purposes.

**Table 1.1:** Metal-based compounds and their applications in medicine. Adapted from reference 5.

<b>Metal</b>	<b>Active Compound</b>	<b>Medicinal Application</b>
Pt	Cis-[Pt(NH <sub>3</sub> ) <sub>2</sub> Cl <sub>2</sub> ]	Anticancer Agent
Tc	<sup>99m</sup> Tc-pyrophosphate	Bone scan by SPECT technique
Ga	<sup>68</sup> Ga-DOTA-TOC	Tumor scan by PET technique
Gd	[Gd(DOTA)] <sup>-</sup>	MRI contrast agent
Au	Au(I)(Pet <sub>3</sub> )(acetylthioglucose)	Antiarthritic
Fe	Fe(II) fumarate or succinate	Dietary supplement
Mg	MgO	Antacid
Li	Li <sub>2</sub> CO <sub>3</sub>	Bipolar dysfunctions
Co	Coenzyme vitamin B <sub>12</sub>	Dietary supplement
Mn	[Mn(DPDP)] <sup>4-</sup>	MRI contrast agent
Zn	Zn undecanoate	Antifungal
Ba	BaSO <sub>4</sub>	X-ray contrast agent
Bi	K <sub>3</sub> [Bi(III)(citrate) <sub>2</sub> ]	Antacid and antiulcer
Sb	NaSb(V) gluconate	Antileishmanial

## 1.2 Metal ions used in this work

This work is focused on the development of gadolinium complexes as potential contrast agents for magnetic resonance imaging (MRI) and gallium complexes as potential imaging probes for single-photon emission computed tomography (SPECT) and positron emission tomography (PET). Throughout the work, new ligands with Gd(III) and Ga(III) chelating capability were synthesized, characterized and its complexes were studied *in vitro* and *in vivo*.

### 1.2.1 Gallium

Gallium is a chemical element discovered in 1875 by the French chemist Paul Emile Lecoq de Boisbaudran. Nevertheless, in 1871 the Russian chemist Dmitri Mendeleev had predicted its existence based on its position in the periodic table, naming it “eka-aluminium”. This element belongs to group 13 (IIIa) and period 4 of the periodic table and has an atomic number of 31. Gallium does not exist in the free form in nature and its abundance on earth’s crust is very low, just proximately 16.9 ppm.<sup>6</sup> It can be found and extracted as a trace component from the minerals bauxite and sphalerite, associated to aluminum and iron.

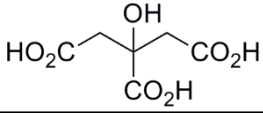
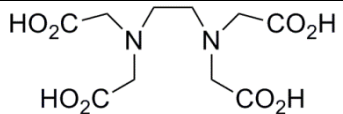
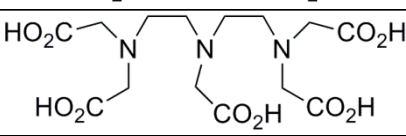
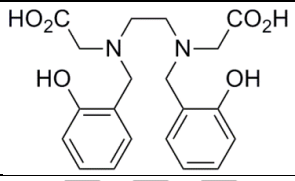
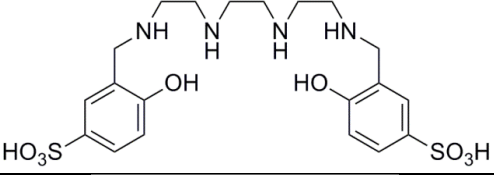
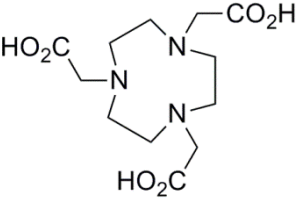
Gallium has no known role in biological systems, but it can be absorbed in small portions by the intestinal tract. *In vivo* studies using subnanomolar concentrations of <sup>67</sup>Ga showed that practically all gallium in the blood stream is present in the plasma, with some traces in the leukocytes.<sup>7, 8</sup> Neutron activation studies also showed that there is only 10<sup>-4</sup> ppm of gallium present in human tissues.<sup>9</sup>

#### 1.2.1.1 Coordination chemistry

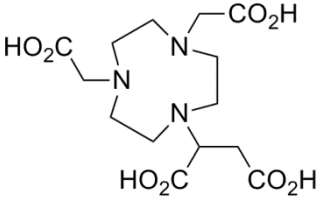
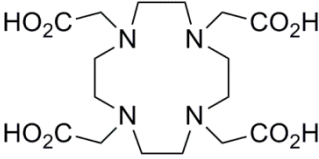
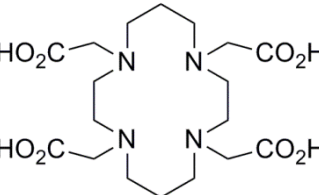
Besides the elemental gallium, this metal has two more oxidation states, Ga(I) and Ga(III). However, the monovalent cation can just be found in some compounds in solid state or dissolved in a few non-aqueous solvents, since it tends to dismutate into Ga(0) and Ga(III). In aqueous solution, just the trivalent cation is stable enough due to the 3d<sup>10</sup> electron configuration.<sup>10</sup> According to the classification of Pearson,<sup>11</sup> trivalent gallium is a hard acid and it binds most strongly to hard Lewis bases, particularly the

HO<sup>-</sup> anion. Therefore, gallium ion has a strong tendency to form chelates with oxygen containing ligands and in a lesser extent, with nitrogen containing ligands. In contrast, this metal does not tend to form chelates with ligands containing sulfur atoms, which behave as soft Lewis bases. Desferrioxamine-B (**DFO-B**) is a siderophore produced by the actinobacteria *Streptomyces pilosus* which has been used in medical applications as a chelating agent to remove iron excess in humans.<sup>12</sup> This molecule has three hydroxamate groups as metal coordinating sites and was one of the first ligands to be labeled with gallium.<sup>13</sup> Although Ga(III) can be quickly and easily chelated by **DFO-B**, this molecule is not an adequate ligand for gallium at nanomolar concentrations, because Ga(III) can be rapidly displaced by biomolecular ligands.<sup>14</sup> Since the first report of gallium chelation by **DFO-B**, several other ligands have been synthesized over the years in order to efficiently chelate Ga(III) at different concentrations and form stable chelates in biological conditions. Table 1.2 shows the stability constants of some gallium chelates.

**Table 1.2:** Stability constants of gallium complexes at 25 °C.

Chelator	Structure	Donor Set	logK
Citric Acid		O <sub>6</sub>	10.0 <sup>15</sup>
EDTA		N <sub>2</sub> O <sub>4</sub>	22.0 <sup>15</sup>
DTPA		N <sub>3</sub> O <sub>3</sub>	23.3 <sup>16</sup>
HBED		N <sub>2</sub> O <sub>4</sub>	38.5 <sup>17</sup>
SBAD		N <sub>4</sub> O <sub>2</sub>	28.3 <sup>18</sup>
NOTA		N <sub>3</sub> O <sub>3</sub>	31.0 <sup>19</sup>

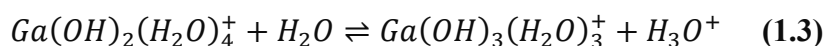
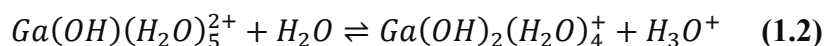
Continuation of Table 1.2

NODASA		$N_3O_3$	30.9 <sup>20</sup>
DOTA		$N_4O_2$	21.3 <sup>19</sup>
TETA		$N_4O_2$	19.7 <sup>19</sup>

Trivalent gallium can form chelates with tri, tetra, penta and hexadentate ligands or even with higher denticity.<sup>21</sup> Ga(III) coordination number is six and the metal environment has a more or less distorted octahedral geometry, which can result in excellent chelate stability with hexadentate ligands.<sup>22</sup> Chelates with vacant coordination positions that occur in four-coordinate (tetrahedral geometry) and five-coordinate (trigonal bipyramidal or square pyramidal) species are more sensitive to nucleophilic attack due to electronic and steric factors, especially in physiological media.<sup>22</sup> Nevertheless, these unsaturated Ga(III) chelates can give origin to thermodynamically stable complexes in which their biodistribution pattern is determined by the gallium complex itself and not by the gallium exchange with proteins.<sup>23</sup> Among suitable gallium chelators, macrocyclic triaza ligands present appropriate size and conformational selectivity towards gallium ions, which may explain the elevated thermodynamic stability for **Ga(NOTA)** complex ( $\log K = 31.0$ ).<sup>19</sup> This high thermodynamic stability is related to the good adjustment of the metal ion to the cyclic cavity. Although triaza ligands are among the most suitable chelators for Ga(III), one of the best known ligands used for trivalent metal ions is the macrocyclic polyaminopolycarboxylate **DOTA** (1,4,7,10-tetraazacyclododecane-1,4,7,10-tetraacetic acid). Although neutral chelates are less sensitive to metal displacement than the charged ones,  $[\text{Ga}(\text{DOTA})]^-$  is sufficiently stable to be used in medical practice despite its lower thermodynamical stability ( $\log K = 21.3$ ).<sup>19</sup>

### 1.2.1.2 Aqueous chemistry

In aqueous solution, the Ga(III) ion is octahedrally coordinated with six water molecules and it hydrolyzes almost completely at neutral pH value, originating highly insoluble Ga(OH)<sub>3</sub>.<sup>10</sup> In the pH range from 3 to 7, the water molecules are gradually replaced by hydroxyl ions, which produce hydronium ions (equations 1.1, 1.2 and 1.3). Through time, the gallium(III) hydroxide is converted to apparently stable crystalline GaO(OH), which is slightly less soluble in neutral solutions than Ga(OH)<sub>3</sub>. However, is considerably soluble in basic solutions, allowing the formation of gallate ion if the pH is above 7 (equation 1.4).<sup>10</sup>



The aqueous solubility of trivalent gallium is just 1 μM at physiological pH values (7.4) and 25 °C, where the dissolved forms of gallium (98.4% is gallate) are in equilibrium with the solid state (GaO(OH)).<sup>24</sup> The minimum solubility of gallium occurs at pH approximately 5.2 (10<sup>-7.2</sup> M) and even at pH 2 or at pH 10, the total solubility of the species is very low, 10<sup>-2</sup> and 10<sup>-3</sup> M respectively.<sup>10</sup> The quick formation of GaO(OH) and Ga(OH)<sub>3</sub> species, allied with its low solubility over a wide pH range and the formation of highly insoluble phosphate complexes at neutral pH values are the main reasons for the low bioavailability of gallium.<sup>15,25</sup>



### 1.2.1.3 Comparison with iron

Although gallium and iron do not belong to the same periodic table category, these elements display many similarities. At the biological level, the behavior of Ga(III) and Fe(III) is in fact comparable, particularly in terms of protein binding, which is responsible for most of gallium's physiological activity. The high degree of similarities between the two cations can be endorsed to some physical and chemical parameters like electronegativity, ionic radius, ionization potential and others (Table 1.3).

**Table 1.3:** Some chemical parameters for trivalent gallium and iron. Adapted from reference 26.

Parameter	Unit	Ga(III)	Fe(III) high spin
<b>Ionic Radius (Octahedral)</b> <sup>27</sup>	Å	0.620	0.645
<b>Ionic Radius (Tetrahedral)</b> <sup>27</sup>	Å	0.470	0.490
<b>Ionization Potential (4<sup>th</sup> Ionization)</b> <sup>28</sup>	eV	64.0	54.8
<b>Electron Affinity (3<sup>rd</sup> ionization)</b> <sup>28</sup>	eV	30.71	30.65
<b>Absolute Hardness (Pearson)</b> <sup>28</sup>	eV	17.00	12.08
<b>Electronegativity (Pauling)</b> <sup>29</sup>	Pauling Units	1.81	1.83
<b>Metal-Oxygen Bond Dissociation Energy</b> <sup>30</sup>	kJ.mol <sup>-1</sup>	353.5	390.4
<b>Metal-Hydroxide Formation Constant</b> <sup>15</sup>	logK <sub>1</sub>	11.40	11.81
<b>Tendency to Ionic Bonding (H<sub>A</sub>)</b> <sup>31</sup>	None	7.69	7.22

Despite the resemblances between Ga(III) and Fe(III) ions, there are also some significant differences between them, which are responsible for their different biochemical behavior. The most significant difference lies on the fact that Ga(III) is impossible to be reduced under physiological conditions, whereas Fe(III) can be easily reduced to Fe(II) and posteriorly reoxidized. The impossibility of Ga(III) to be reduced prevents it to be incorporated in metalloenzymes as part of prosthetic groups and to participate on redox reactions. This metal ion can also block the access of iron ions to binding molecules, such the heme group in hemoglobin.<sup>32</sup> In contrast to gallium, iron can only exist in physiological conditions associated to binding molecules. At pH 7.4, unbound Fe(III) precipitates as polymerized FeO(OH) (similar to the precipitated form of GaO(OH)), limiting the solubility to only 10<sup>-18</sup> M.<sup>33</sup> Alternatively, significant amounts of gallium (in the gallate form) can exist in blood plasma allowing its transport and metabolization, thus hindering plasma iron to participate on its standard functions.<sup>33</sup>

#### **1.2.1.4 *In vivo* behavior**

Since the late 1940s, studies with radioactive trivalent gallium (essentially  $^{67}\text{Ga}$  and  $^{72}\text{Ga}$ ) showed that this metal ion has a strong tendency to accumulate in certain tissues, particularly on growing or rehabbing bone,<sup>34</sup> different types of tumors<sup>35</sup> and also at inflammation and infection sites.<sup>36, 37</sup> However, it is the blood that plays a major role in the transport and distribution of gallium. *In vivo* studies using  $^{67}\text{Ga}$  demonstrated that virtually all gallium in blood is present in plasma proteins, bound to the iron transport protein transferrin (TF), with traces detected in leukocytes.<sup>7, 8</sup>

Transferrin is a blood protein responsible for the control and transport of iron in blood stream.<sup>38</sup> With 79.57 kDa, this protein is constituted by two homologous domains. Each domain can independently bind one Fe(III) (or Ga(III)) ion together with one carbonate or one bicarbonate anion per metal ion.<sup>39</sup> The total amount of TF in human body is approximately 240 mg.kg<sup>-1</sup>, divided between blood plasma and extravascular fluids.<sup>40</sup> The binding capacity of iron to TF is approximately 3.3 mg.mL<sup>-1</sup>, stressing that just 33.0% of the total TF binding sites are occupied by Fe(III) at any time.<sup>39</sup>

The iron bound to TF is transported to cells via a TF receptor, which is a surface protein that can bind two TF molecules. This receptor binds most strongly to diferric TF, less strongly to monoferric TF and weakly to apotransferrin (no metal bound).<sup>26</sup> When TF is attached to its receptor, both receptor and protein are taken into the cell by endocytosis and then the endosome is acidified (pH values inferior to 5.5) to release the metal.<sup>39</sup>

In humans, all nucleated cells seem to express TF receptors, but in different concentrations, depending on the amount of necessary iron for cell metabolism. For example, the receptor expression is distinctly elevated in placenta cells, Kupffer cells, basal epidermis, endocrine pancreas and on bone marrow cells.<sup>41</sup> However, it is on cancer cells that TF receptors are extremely high expressed,<sup>40, 41</sup> because the fast division and proliferation of these cells requires elevated amounts of iron.

As previously stated, TF possess two binding sites that can chelate both Fe(III) or Ga(III) ions. At normal plasma bicarbonate concentrations, the binding constants of TF-gallium complex are 20.3 (log $K_1$ ) and 19.3 (log $K_2$ ), and the binding constants of TF-iron complex are 22.8 (log $K_1$ ) and 21.5 (log $K_2$ ).<sup>24</sup> Despite the fact that the affinity of TF for iron ions is approximately 400 times higher than for gallium ions, the replacement of

Fe(III) by Ga(III) occurs at a slow rate, with an exchange half-time of 4 hours and 30 minutes at 310 K.<sup>42</sup> This slow rate reflects the high energy required to “open up” the metal sites once they are occupied.

Besides transferrin, gallium can also bind strongly to two other blood proteins: lactoferrin (LF) and ferritin. LF is very similar in size (80 kDa) and in structure (has two homologous domains) to TF and it can also bind a total of two Fe(III) (or Ga(III)) ions.<sup>43</sup> LF is a multifunctional protein, which seems to play an important role in the immunologic system due to its antimicrobial activity.<sup>44</sup> This protein can accumulate at inflammation and infection sites, particularly in leukocytes and neutrophils.<sup>45, 46</sup> Unlike TF and LF, ferritin is a very large and nearly spherical protein with 450 kDa and 24 subunits that can bind up to 4500 Fe(III) ions.<sup>47</sup> This protein has the function of storing iron in a non-toxic form (ferric oxide-hydroxide form)<sup>38</sup> and it is present in most cells with variable concentrations, but particularly concentrated in Kupffer cells and macrophages.

Although the mechanisms for gallium cell uptake are still not fully understood, it appears reasonable to expect that gallium accumulates in tissues with high levels of ferric proteins. Some studies with carcinogenic cells showed a direct correlation between the TF receptor expression and the gallium uptake by those cells.<sup>33, 48-50</sup> In the majority of cases it is clear that gallium enters in tumor cells through TF receptors. Nevertheless, gallium uptake by the bones does not appear to involve the TF receptor and the internalization mechanisms are largely unknown. Humans lacking TF absorb gallium into skeletal tissue at the same or greater rate than people with normal TF concentration.<sup>51</sup> People who received repeated blood transfusions, resulting in iron saturated TF, also showed high bone activity after the administration of <sup>67</sup>Ga-citrate.<sup>52</sup>

### 1.2.1.5 Radioisotopes and uses

Gallium has two naturally occurring isotopes,  $^{69}\text{Ga}$  (60.1 %) and  $^{71}\text{Ga}$  (39.9 %), but several radioisotopes can be prepared. Table 1.4 shows some gallium radioisotopes with relevant properties for medical applications.

**Table 1.4:** Radioisotopes of gallium. Adapted from references 53, 54.

Isotope	Half-Life	Type of Decay
$^{66}\text{Ga}$	9.49 h	$\beta^+$ (100.0%)
$^{67}\text{Ga}$	3.26 d	$\gamma$ (100.0%)
$^{68}\text{Ga}$	67.71 min	$\beta^+$ (89.0%); $\gamma$ (11.0%)
$^{70}\text{Ga}$	21.14 min	$\beta^-$ (99.6%); $\gamma$ (0.4%)
$^{72}\text{Ga}$	14.10 h	$\beta^-$ (100.0%)

The first use of cold gallium for medical purposes was reported in 1931 by Levaditi *et al.*,<sup>55</sup> for the treatment of syphilis in rats. This element has been investigated for the treatment of bone tumor, hyperkalemia<sup>56</sup> and Paget's disease,<sup>57</sup> since gallium has the capacity to inhibit the absorption of calcium by the bones.<sup>56</sup> Gallium has also shown some efficiency against osteolysis and pain suppression related to multiple myelomas and metastasis,<sup>58</sup> and it has been suggested for osteoporosis treatment.<sup>59</sup>

Besides natural and non-radioactive gallium isotopes, gallium radionuclides have been used for medical purposes over the last 60 decades. In the early 1950s, the  $\beta^-$  emitter  $^{72}\text{Ga}$  was the first gallium radioisotope to be used in the treatment of bone cancer metastases.<sup>60</sup> In the following decade,  $^{67}\text{Ga}$  was used for the first time in medical imaging in order to scan leukemia, melanoma and lung cancer.<sup>61</sup> Despite the potentiality of  $^{72}\text{Ga}$  for the treatment of different diseases,  $^{67}\text{Ga}$  and  $^{68}\text{Ga}$  have received bigger attention as diagnostic radionuclides. Both isotopes have suitable characteristics for scanning, such as: a) appropriate half-lives for medical usage, long enough for patient administration and carry out the scans, but short enough to avoid complications related to radiation exposure; b) proper decay and energetic characteristics:  $^{67}\text{Ga}$  is a  $\gamma$  emitter with three disintegration energies ( $E_\gamma = 92, 185$  and  $298$  keV)<sup>53, 54</sup> suitable for SPECT, whereas  $^{68}\text{Ga}$  is a  $\beta^+$  emitter with an average positron energy per disintegration of 740 keV ( $E_{\beta_{\text{max}}}^+ = 1899$  keV),<sup>53, 54</sup> c) being produced through fast and efficient methods, in particular  $^{68}\text{Ga}$ .

$^{67}\text{Ga}$  is a cyclotron produced isotope, usually by the nuclear reaction  $^{68}\text{Zn}(p, 2n)^{67}\text{Ga}$  on enriched  $^{68}\text{Zn}$  and it was prepared for the first time for human usage in 1953.<sup>62, 63</sup> Although the production cost of  $^{67}\text{Ga}$  is not particularly high, the access to a cyclotron is very limited and restricts the amount of effective radionuclide administered to patients, because the isotope will lose its activity during the transportation. On the other hand,  $^{68}\text{Ga}$  can be produced from a generator system, which involves an organic or inorganic matrix with the parent radionuclide  $^{68}\text{Ge}$  immobilized.<sup>64</sup> Germanium-68 has a lengthy half-life ( $t_{1/2} = 270.95$  days),<sup>53, 54</sup> allowing the manufacturing of long-lived and economically desirable generator systems. The combination of the parent long half-life  $^{68}\text{Ge}$  and the half-life of its daughter  $^{68}\text{Ga}$  makes this pair nearly perfect for the generator strategy. In the majority of cases, the production of  $^{68}\text{Ge}$  is made via the  $(p, 2n)$  reaction on gallium targets (Figure 1.1), providing only 0.74 MBq/ $\mu\text{Ah}$ ,<sup>65</sup> and therefore high current accelerators are needed for sufficient batch yields.

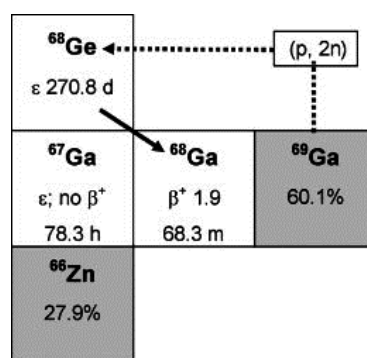


**Figure 1.1:** Production of  $^{68}\text{Ge}$  by the  $(p, 2n)$  reaction of  $^{69}\text{Ga}$ . Adapted from reference 64.

The generator systems enable a fast and routine production of  $^{68}\text{Ga}$ , while the chemical properties of Ge(IV) and Ga(III) are sufficiently different to allow the application of different purification methods. In the first generators,  $^{68}\text{Ge}$  was fixed on the column with inorganic matrices of  $\text{Al}_2\text{O}_3$  and  $\text{ZrO}_2$ , and  $^{68}\text{Ga}$  was eluted with **EDTA** solution (5 mm) to produce  $^{68}\text{Ga}(\text{EDTA})^-$ .<sup>66</sup> In this process, the  $^{68}\text{Ga}$  yield was relatively good ( $70\% \pm 10\%$ ) but decreased considerably over time. The replacement of **EDTA** solution and  $\text{Al}_2\text{O}_3$  by sodium oxalate solution (2%) and  $\text{Sb}_2\text{O}_5$  matrices, resulted in an increased total yield ( $80\% \pm 10\%$ ).<sup>67</sup> Despite good yields,  $^{68}\text{Ga}$  was still obtained in a chelated form, which must be dissociated before the radionuclide can be used in the radiopharmaceutical production. Several systems giving  $^{68}\text{Ga}$  in a directly operational form have been proposed, such as  $\text{Al}_2\text{O}_3$  or  $\text{Fe}(\text{OH})_3$  and  $\text{HCl}$ ,<sup>68</sup>  $\text{ZrO}_2$  or

SiO<sub>2</sub> and HNO<sub>3</sub>,<sup>69</sup> SnO<sub>2</sub> and HCl,<sup>70</sup> or CeO<sub>2</sub> and HCl.<sup>71</sup> However, in all those systems small amounts of the oxide matrices were found in the eluent, which make these systems inadequate for medical use. Since phenolic groups can form stable Ge(IV) chelates, Schuhmacher and Maier-Borst<sup>72</sup> proposed an alternative organic matrix composed by pyrogallol-formaldehyde polymer resin, from which gallium is obtained in a chloride form (GaCl<sub>4</sub><sup>-</sup>) after the elution with HCl solution (5.5 M). Other organic matrices to obtain <sup>68</sup>Ga have been proposed, such as a macroporous polymer based on *N*-methylglucamine reported by Nakayama and co-workers.<sup>73</sup> Nowadays, a TiO-based generator developed by the Cyclotron Company (Obninsk, Russia) has been used around the world as a <sup>68</sup>Ga provider. <sup>68</sup>Ga can be obtained with yields superior to 60% in the first year of operation using an HCl solution (0.1 M), decreasing to 25% after three years or 200 elutions. Despite being used over the world, this system presents some negative features such as metallic impurities like Zn(II) generated from the <sup>68</sup>Ga decay or Ti(IV) from the matrix, and because of that further purification is required.

Despite their attractive properties, the use of gallium radionuclides as imaging probes is relatively recent. One of the first chelators used for radioactive gallium chelation was the citrate anion, where two units of this chelator act as a tripodal ligand to afford an octahedral complex.<sup>74</sup> In early studies, <sup>67</sup>Ga- and <sup>68</sup>Ga-citrate chelates were evaluated for bone, prostate, testicles or lymphoma tumor imaging.<sup>75-78</sup> However, like many small ligands with denticity inferior to six, the chelate [Ga(cit)<sub>2</sub>]<sup>3-</sup> has low stability and the trivalent gallium can be easily sequestered by blood serum proteins like transferrin, lactoferrin or ferritin. The radionuclide accumulates mainly in sites where the iron concentration is higher, such as liver, spleen, kidneys and tumors, becoming toxic since it is unable to suffer redox reactions in physiological conditions.<sup>26</sup> In order to be used for medical purposes, gallium must be chelated by ligands that form complexes thermodynamically stable toward hydrolysis and kinetically inert to avoid ligand exchange with iron-binding proteins. Several suitable chelators with different denticities have been proposed for gallium labeling. For example, ligands having the N<sub>3</sub>O<sub>3</sub> and N<sub>2</sub>O<sub>4</sub> donor set, which provide a full gallium coordination sphere, were evaluated for gallium chelation showing that the resultant complexes have good thermodynamic and kinetic stability.<sup>17, 79</sup> Nevertheless, the thermodynamic and kinetic stability can be significantly increased due to the macrocyclic effect provided by some ligands of N<sub>3</sub>R<sub>3</sub> and N<sub>4</sub>R<sub>4</sub> type (Figure 1.2). These ligands can encapsulate gallium, isolating and shielding it from competing ligands present in biological systems. **DOTA**

( $N_4O_4$ ,  $R = CO_2H$ ), **NOTA** ( $N_3O_3$ ,  $R = CO_2H$ ) and **TACN-TM** ( $N_3O_3$ ,  $R = CH_2SH$ ) are macrocyclic ligands that may offer elevated thermodynamic stability, and have been broadly used as basis for the development of new gallium imaging agents. Despite the fact that **NOTA** and **TACN-TM** can provide gallium chelates thermodynamically more stable, **DOTA** is also a very attractive ligand for gallium chelation. The  $[Ga(DOTA)]^-$  chelate also possesses kinetic inertness<sup>80, 81</sup> and this chelate offers two non-chelated side arms available for the coupling of targeting biomolecules.

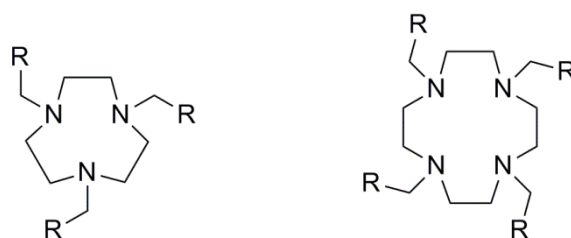


**Figure 1.2:** Macrocyclic ligands of  $N_3R_3$  and  $N_4R_4$  type.  $R = CO_2H$ ,  $PO_3H$ ,  $CH_2SH$ ,  $Ph-OH$ .

### 1.2.2 Lanthanides

The study of the lanthanide elements started in 1787 when the Finnish chemist Johan Gadolin isolated the yttrium oxide from a black mineral (ytterbite) that had recently been discovered by Carl Axel Arrhenius in Ytterby, a village near Stockholm. In 1803, another new oxide (ceria) was isolated from the mineral bastnäsite by Berzelius and Hisinger. Contrary to what was thought in the beginning, these new oxides were not of one single metallic element, but a combination of several elements, later on called lanthanides. It was posteriorly reported that yttria consisted of at least ten new elements: gadolinium, terbium, dysprosium, holmium, erbium, thulium, ytterbium, lutetium, yttrium and scandium. In present days, the lanthanides are mainly extracted from three minerals: a) bastnäsite, a red-brown carbonate mineral that contains cerium lanthanum and yttrium; b) xenotime, a brown phosphate mineral that contains yttrium, dysprosium, erbium, terbium and ytterbium; and c) monazite, a red-brown phosphate mineral that contains yttrium and the majority of lanthanides, found in mines located in China, United States, Brazil, India and Australia.

The lanthanides correspond to a series of fifteen adjacent elements in the periodic table with related electronic structure. The term lanthanide was given because the first and the lighter element in the series is the lanthanum. The lanthanide series is

covered by elements from lanthanum ( $Z = 57$ ) to lutetium ( $Z = 71$ ). All lanthanides, with the exception of lanthanum, are  $f$ -block elements since the  $4f$  electron shell is being occupied (Table 1.5). Lu is a  $d$ -block element, but is also generally considered to be a lanthanide due to its chemical similarities with the other fourteen metals.

**Table 1.5:** Some properties of lanthanides. Adapted from reference 82.

Atomic Number	Name	Symbol	Electronic Configuration	$E^\circ$ (V)	Radius $M^{3+}$ (Å)
57	Lanthanum	La	[Xe] $5d^1 6s^2$	-2.37	1.17
58	Cerium	Ce	[Xe] $4f^1 5d^1 6s^2$	-2.34	1.15
59	Praseodymium	Pr	[Xe] $4f^3 6s^2$	-2.35	1.13
60	Neodymium	Nd	[Xe] $4f^4 6s^2$	-2.32	1.12
61	Promethium	Pm	[Xe] $4f^5 6s^2$	-2.29	1.11
62	Samarium	Sm	[Xe] $4f^6 6s^2$	-2.30	1.10
63	Europium	Eu	[Xe] $4f^7 6s^2$	-1.99	1.09
64	Gadolinium	Gd	[Xe] $4f^7 5d^1 6s^2$	-2.29	1.08
65	Terbium	Tb	[Xe] $4f^9 6s^2$	-2.30	1.06
66	Dysprosium	Dy	[Xe] $4f^{10} 6s^2$	-2.29	1.05
67	Holmium	Ho	[Xe] $4f^{11} 6s^2$	-2.33	1.04
68	Erbium	Er	[Xe] $4f^{12} 6s^2$	-2.31	1.03
69	Thulium	Tm	[Xe] $4f^{13} 6s^2$	-2.31	1.02
70	Ytterbium	Yb	[Xe] $4f^{14} 6s^2$	-2.22	1.01
71	Lutetium	Lu	[Xe] $4f^{14} 5d^1 6s^2$	-2.30	1.00

Together with scandium ( $Z = 21$ ) and yttrium ( $Z = 39$ ), the lanthanides are commonly known as “rare earths”. This name arises from the minerals from which they were isolated, since they were uncommon oxide-type minerals. However, these elements are neither rare in abundance nor “earths” (an obsolete term used in the 18<sup>th</sup> century for water-insoluble strongly basic oxides of metals incapable of being melted into usable metals). For example, cerium is the 26<sup>th</sup> most abundant element in the Earth's crust, being half abundant as chlorine and five times more abundant than lead.<sup>83</sup> Neodymium is the least common naturally occurring lanthanide and is more abundant than thulium, iodine and even gold.<sup>83</sup>



In addition to their chemical similarities, the lanthanides possess interesting magnetic and spectroscopic properties, which resulted in their extensive use in chemical research and industrial application. Many compounds containing these elements have been developed for production of: a) contrast agents (CA) for MRI;<sup>84-89</sup> b) catalysts for organic synthesis;<sup>90-92</sup> c) magnets and superconductors for technological device manufacture;<sup>93-96</sup> or d) luminescent compounds for biological probes.<sup>97-100</sup>

### 1.2.2.1 Coordination chemistry

Along the lanthanide, the  $4f$  orbitals are progressively occupied from La ( $4f^0$ ) to Lu ( $4f^{14}$ ). Since the first three ionization energies are reasonably low, these elements are highly electropositive and their compounds are essentially ionic in nature. The most common oxidation state for lanthanides elements is III and in aqueous solution they readily form aqua ions with the formula  $[M(H_2O)_n]^{3+}$ . However, there are some exceptions, such as cerium, samarium, europium and ytterbium. Both in aqueous solution or in solid state, these metals can have stable divalent (Sm(II), Eu(II) and Yb(II)) or tetravalent forms (Ce(IV)). Contrary to the electrons in the  $d$  orbitals of the  $d$ -block transition elements, the electrons in the lanthanides  $f$  orbitals are much more internalized and therefore they are almost unavailable to form covalent bonds with ligands. This phenomenon contributes for the lanthanides classification as hard acids according to Pearson's classification.<sup>11</sup> They tend to bond more strongly to strong Lewis bases with oxygen and fluorine coordinating atoms, although they can also bind to chelators containing nitrogen atoms.

The lanthanides electronic configuration and consequent formation of trivalent ions give to these elements very similar chemical and physical properties along the series, contrasting with the  $d$ -block transition metals. These trivalent cations have higher coordination numbers, which can go from 7 to 12, but the typical lanthanide coordination number varies between 8 and 9.<sup>101</sup> In aqueous solution, the ions display coordination numbers from 9 in the lightest members of the series to 8 for the heaviest ones, which can be ascribed to the "lanthanide contraction".<sup>102</sup> This phenomenon refers to a continuous decrease in atomic and ionic size with increasing atomic number. A major cause of the lanthanide contraction is the electrostatic effect provided by an increasing nuclear charge very imperfectly shielded by the  $4f$  electrons.<sup>82</sup>

The geometries of lanthanide complexes are very diverse, being determined mainly by ligand conformation, ligand donor groups, competition between ligand donor groups and solvent molecules, crystal packing forces and in some cases by the size of the Ln(III) ion. The nine-coordinated aqua complexes usually display tricapped trigonal prismatic geometry while eight-coordinated aqua complexes usually display square antiprismatic geometry.

The ionic radius of the trivalent lanthanide ions range from 1.1 Å for La(III) to 0.85 Å for Lu(III).<sup>103</sup> Located nearly in the center of the lanthanide series, gadolinium has an ionic radius of 0.99 Å, which is very close to the value of the divalent calcium ion. Gd(III) can compete with Ca(II) in all biological systems that require calcium for proper function. The trivalent ion can bind with much higher affinity to calcium requiring proteins.<sup>104</sup> When bound to a calcium binding enzyme, the lanthanide ion replacement often modifies the structure and thus, the catalytic mechanism.<sup>105</sup>

#### **1.2.2.2 Radioisotopes and uses**

The use of radioisotopes of the lanthanide series for imaging and therapeutic purposes in nuclear medicine has been increasing over the past decades.<sup>106, 107</sup> Like other radioisotopes (ex: <sup>67/68</sup>Ga), the radioactive lanthanides must have suitable properties to be used in nuclear medicine, such as appropriate half-lives, proper decay energies and the possibility of rapid and efficient production. These radionuclides can be obtained from different methods, such as generator (ex: <sup>134</sup>La, <sup>140</sup>Pr, <sup>166</sup>Ho, <sup>177</sup>Lu), cyclotron (ex: <sup>153</sup>Sm, <sup>161</sup>Tb, <sup>157/165</sup>Dy, <sup>166</sup>Ho, <sup>167</sup>Tm) or nuclear reactor (ex: <sup>141</sup>Ce, <sup>153</sup>Gd, <sup>169</sup>Yb). Table 1.6 shows some lanthanide radioisotopes with relevant properties for medical applications.

**Table 1.6:** Isotopes of some lanthanides. Adapted from references 53, 54.

Isotope	Half-Life	Type of Decay
$^{153}\text{Sm}$	46.28 h	$\beta^-$ (100%)
$^{161}\text{Tb}$	6.91 d	$\beta^-$ (100%)
$^{153}\text{Dy}$	6.41 h	$\beta^+$ (100%)
$^{157}\text{Dy}$	8.14 h	$\beta^+$ (100%)
$^{165}\text{Dy}$	2.33 h	$\beta^-$ (100%)
$^{166}\text{Ho}$	26.83 h	$\beta^-$ (100%)
$^{169}\text{Er}$	9.40 d	$\beta^-$ (100%)
$^{171}\text{Er}$	7.52 h	$\beta^-$ (100%)
$^{167}\text{Tm}$	9.25 d	$\gamma$ (100%)
$^{177}\text{Lu}$	6.65 d	$\beta^-$ (100%)

Many lanthanide chelates have been prepared and evaluated to be used as diagnostic probes or therapeutic pharmaceuticals (Table 1.7).

**Table 1.7:** Lanthanide compounds for diagnostic or therapeutic applications.

Isotope	Chemical Form	Application
$^{153}\text{Sm}$	EDTPM	Palliative treatment of bone cancer metastasis <sup>108</sup>
$^{153}\text{Sm}$	DTPA	Palliative treatment of bone cancer metastasis <sup>109</sup>
$^{161}\text{Tb}$	DTPA	Intraoperative scanning <sup>110</sup>
$^{165}\text{Dy}$	FHMA	Radiation synovectomy <sup>111, 112</sup>
$^{166}\text{Ho}$	FHMA	Radiation synovectomy <sup>111</sup>
$^{166}\text{Ho}$	DTPA	Endovascular brachytherapy <sup>113</sup>
$^{166}\text{Ho}$	DOTPM	Bone-seeking radioisotope for therapy <sup>114</sup>
$^{169}\text{Er}$	Colloid	Radiation synovectomy <sup>115</sup>
$^{177}\text{Lu}$	DTPA	Palliative treatment of bone cancer metastasis <sup>109</sup>
$^{177}\text{Lu}$	Antibody	Radioimmunotherapy of ovarian cancer <sup>116</sup>

### **1.2.2.3 Spectroscopic properties**

One important characteristic of most of the lanthanide ions is their luminescence. The electronic terms of the various  $4f^n$  configurations give rise in most of the cases to excited states of low energy, absorbing in the visible region. Some of the excited states of the lanthanides might relax with emission of luminescence, even in solution, in spite of the non-radioactive deactivation pathways which are likely to arise, especially in water (O-H oscillator).<sup>117</sup>

The transitions between the electronic states of the  $4f^n$  configurations are partly forbidden, according to the selection rule of Laporte, which means that the probability of these transitions to occur is very low, and their molar absorption coefficients are also very low (typically  $\epsilon < 10 \text{ M}^{-1} \cdot \text{cm}^{-1}$  in aqueous solution).<sup>118</sup>

Lanthanides can just afford low intensity luminescence in solution, but this problem can be circumvented by chelating the metal ion with an adequate chromophore ligand. The chromophore must absorb energy at a suitable wavelength, acting like an “antenna”, transferring the energy from an excited state (normally via triplet states) to the lanthanide ion, which becomes excited to the emitting state.<sup>119</sup> Among the lanthanide ions, europium and terbium are the most extensively studied in solution and their luminescence properties make these ions evident candidates to be used as luminescent probes in biomolecular systems.<sup>120</sup> The design of efficient chromophore ligands is also an important research goal, in order to optimize the lanthanide spectroscopic properties and to obtain adequate luminescent coordination compounds.

### 1.2.2.4 Magnetic properties

Another important feature of the trivalent lanthanide ions is their paramagnetism, due to the existence of unpaired electrons (the exceptions are La(III) and Lu(III)).

The majority of lanthanide ions only have a  $^{2S+1}L_J$  state occupied at room temperature and their ground state can be determined by the Hund's rules, which are:

a) for a given electronic configuration, the spin multiplicity ( $2S+1$ ) is as high as possible since maximum multiplicity has the lowest energy; b) for a given multiplicity, the term with the largest value of  $L$  has the lowest energy ; and c) for a shell less than half-filled ( $n < 7$ ),  $J$  for the ground state takes the lowest possible value, and for a shell more than half-filled ( $n > 7$ ),  $J$  for the ground state has the highest possible value.

Since the lanthanide magnetic properties are determined mainly by the ground state, the magnetic moment ( $\mu_{eff}$ ) of the trivalent lanthanides is fundamentally independent of the surroundings and is given by equation 1.5.<sup>121</sup> Nevertheless, this expression is only valid for the electronic occupation of the ground state.

$$\mu_{eff} = g_J \sqrt{J(J+1)} \quad (1.5)$$

where  $g_J$  is the Landé g-factor defined by equation 1.6.

$$g_J = \frac{3}{2} + \frac{[S(S+1) - L(L+1)]}{2J(J+1)} \quad (1.6)$$

As  $J = L + S$  for  $n > 7$  and  $J = L - S$  for  $n < 7$ , it can be immediately recognized that the magnetic moments in the series second half are greater than the magnetic moments in the series first half. Due to the strength of the spin-orbit coupling, the ground state is well separated from the excited states with the exception of Eu(III) and Sm(III). Despite trivalent samarium and europium ions have very small or inexistent predicted magnetic moments for the ground state (Table 1.8), contributions from excited states are evident and represent a huge contribution for the overall magnetic moment. If the magnetic properties of these elements were only determined by the ground state, the Eu(III) chelates would be diamagnetic ( $\mu_{eff} = 0.0$ ) and the Sm(III) chelates would have small magnetic moments ( $\mu_{eff} = 0.85$  instead of  $\mu_{eff} = 1.64$ ).

**Table 1.8:** Trivalent lanthanide magnetic moments at room temperature. Adapted from reference 121.

M	$f^n$	Ground Term	Predicted $\mu_{eff} (\mu_B)$	$\mu_{eff}$ M(phen) <sub>2</sub> (NO <sub>3</sub> ) <sub>3</sub> ( $\mu_B$ )
La	0	<sup>1</sup> S <sub>0</sub>	0.00	0.00
Ce	1	<sup>2</sup> F <sub>5/2</sub>	2.54	2.46
Pr	2	<sup>3</sup> H <sub>4</sub>	3.58	3.48
Nd	3	<sup>4</sup> I <sub>9/2</sub>	3.68	3.44
Pm	4	<sup>5</sup> I <sub>4</sub>	2.83	Not Available
Sm	5	<sup>6</sup> H <sub>5/2</sub>	0.85	1.64
Eu	6	<sup>7</sup> F <sub>0</sub>	0.00	3.36
Gd	7	<sup>8</sup> S <sub>7/2</sub>	7.94	7.97
Tb	8	<sup>7</sup> F <sub>6</sub>	9.72	9.81
Dy	9	<sup>6</sup> H <sub>15/2</sub>	10.63	10.60
Ho	10	<sup>5</sup> I <sub>8</sub>	10.60	10.70
Er	11	<sup>4</sup> I <sub>15/2</sub>	9.59	9.46
Tm	12	<sup>3</sup> H <sub>6</sub>	7.57	7.51
Yb	13	<sup>2</sup> F <sub>7/2</sub>	4.53	4.47
Lu	14	<sup>1</sup> S <sub>0</sub>	0.00	0.00

### 1.2.2.5 Lanthanides as relaxation and chemical shift probes

Paramagnetic species can shorten the solvent longitudinal and transverse nuclear relaxation times ( $T_1$  and  $T_2$  respectively) and can also shift and resolve NMR signals.<sup>122</sup> Due to this feature, paramagnetic lanthanide-based compounds can be used as relaxation probes to improve the MRI signal and to obtain enhanced scans. Lanthanide complexes can also be used as useful complementary compounds in NMR spectroscopy as they can spread and resolve the signals by a mechanism defined as the lanthanide-induced shift (LIS).

Paramagnetic species like the lanthanide trivalent ions affect both the nuclear relaxation times and the chemical shifts based on two types of interaction between the nuclear spins ( $I$ ) and the unpaired electronic spins ( $S$ ): a) Contact interaction (scalar) and b) Pseudo-contact interaction (dipolar). The contact interaction comprehends the delocalization and/or spin polarization of the unpaired electrons via the ligand molecular orbital. Due to this interaction, the unpaired electron spin density is extended over a number of ligand atomic sites and therefore will induce a contact shift. The

pseudo-contact interaction (dipolar) results from the space dipole-dipole interaction between the unpaired electronic spins and the nuclear spins. This term directly depends on the structure, on the ion magnetic anisotropy, and is the type of interaction which dominates in most trivalent lanthanide chelates.

Lanthanide induced chemical shifts usually occur in systems with short electronic spin relaxation, for instance in lanthanide ions such as Pr(III), Eu(III) or Yb(III). These cations have short electronic spin relaxation times (shorter than  $10^{-12}$  seconds)<sup>123</sup> and due to this, their chelates are useful NMR shift reagents, helping in the assignment and interpretation of NMR spectra signals. Opposite to the previous ions, Gd(III) and Eu(II) have long electronic spin relaxation times (higher than  $10^{-10}$  seconds),<sup>123</sup> which does not cause substantial NMR signal shifting, but can increase the nuclear relaxation rates.

The induced shift ( $\Delta$ ) for a nucleus of a ligand upon coordination to a trivalent lanthanide is given by equation 1.7 and arises via three mechanisms: the diamagnetic, the contact and the pseudo-contact mechanism.<sup>122</sup> Diamagnetic shifts ( $\Delta_d$ ) arise from the chelation of the paramagnetic ion with a given ligand and are usually small, except for the donor atoms. They are originated from effects such as conformational changes, inductive effects, direct field effects, and can be determined directly or by interpolation from the shifts induced by the diamagnetic members of the series (ex: La(III) or Lu(III)).<sup>124</sup>

$$\Delta = \Delta_d + \Delta_c + \Delta_{pc} \quad (1.7)$$

### 1.3 Nuclear magnetic relaxation

MRI is a powerful and useful technique very used in medical imaging to visualize soft tissues, based on the NMR spectroscopy principles. Nuclides such as  $^1\text{H}$  and  $^{13}\text{C}$  possess an overall nuclear spin, due to the unpaired spins of their nuclear particles, which makes them detectable by NMR. Since hydrogen-1 nuclei, containing a single proton, have almost 100% natural abundance (around 99.985%) and the body is constituted majority by water, this nucleus is used in MRI to obtain body images.

The rotation of an atom nucleus creates a magnetic moment ( $\mu$ ), as the corresponding nucleus can be seen has a charged sphere rotating on its axis. In the

presence of a strong magnetic field ( $B_0$ ), the nuclear magnetic moment precesses about  $B_0$  with a frequency, frequently denominated the Larmor frequency ( $\nu_0$ ) (Figure 1.3A). The resonance frequency or Larmor frequency is directly proportional to the applied magnetic field (equation 1.8) and depends on the atom type, since the gyromagnetic ratio ( $\gamma$ ) is a constant characteristic of each nuclear species.<sup>125</sup>

$$\nu_0 = \gamma B_0 \quad (1.8)$$

The nuclear spins of hydrogen atoms can adopt only two possible orientations relative to the field direction, parallel or antiparallel (Figure 1.3B). The nuclear spins in the two orientations have different energies and since the parallel one is the lower energy state, more spins exist in this configuration. This is sufficient to endow the sample as a whole with a small bulk magnetization, lying along the positive  $z$ -axis and because of the random phases of the moments, there is no net magnetization in the  $xy$  plane. When a radiofrequency pulse is applied at the Larmor frequency, the nuclear spins are excited and rise from the lower state to the high state energy (Figure 1.3C). This phenomenon can be represented by a rotation of the net magnetization away from equilibrium state (from  $z$ -axis to the  $xy$  plane). When the radiofrequency is turned off, the magnetization once more freely precesses about the  $B_0$  direction and during the free precession, the magnetization returns to its original state (lower energy state) by a process denominated relaxation.

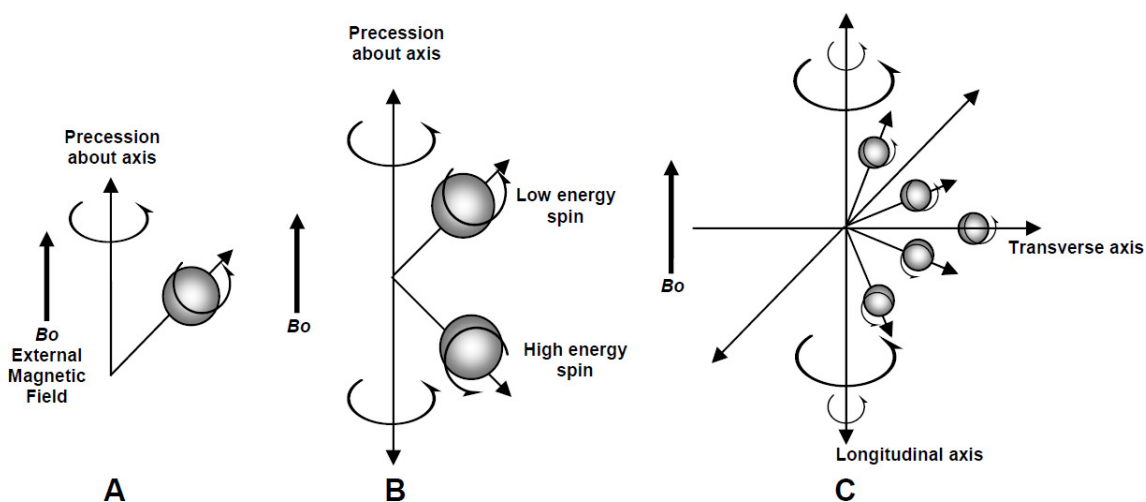


**Figure 1.3:** A) Precession of the magnetic moment of protons in the presence of an external magnetic field; B) Proton spin energy in the presence of a magnetic field; C) Change in proton spin energy with increasing radiofrequency at the Larmor frequency. Adapted from reference 126.



The nuclear relaxation times  $T_1$  (longitudinal) and  $T_2$  (transverse) are the time constants of the mechanisms through which the nuclear spins return from their excited state to their equilibrium state. In the longitudinal (spin-lattice) relaxation process, the nuclei in their excited state return to the ground state by dispersing their excess of energy to the magnetic nuclei environment (lattice). In this case, the longitudinal magnetization (along z-axis) returns to its equilibrium state as energy is released to the lattice, and for this process to be efficient, the magnetic nuclei environment must fluctuate at a rate that matches the precessional frequency of the excited spins (Larmor frequency). In the transverse (spin-spin) relaxation process, the nuclei exchange energy with each other. The magnetic moments in the same phase begin to stretch in the transverse plane and lose their phase coherence. This phenomenon will result in an exponential decrease of the net transverse magnetization to zero.<sup>127</sup>

### 1.3.1 Nuclear relaxation induced by Gd(III)

The relaxation of solvent nuclei can be enhanced by the presence of paramagnetic species, like trivalent gadolinium compounds. Gd(III) ion presents unique features for relaxation agents due to its seven unpaired electrons and a long electronic relaxation time. The presence of a gadolinium complex will increase the longitudinal and transverse relaxation rates of solvent nuclei (water).<sup>85</sup> The observed solvent relaxation rate ( $1/T_{i,obs}$ ) is the sum of a diamagnetic term ( $1/T_{i,d}$ ), corresponding to the solvent nuclei relaxation rate without a paramagnetic species, and a paramagnetic term ( $1/T_{i,p}$ ), which is the relaxation rate enhancement caused by the presence of the paramagnetic species in the solvent (equation 1.9).<sup>86</sup>

$$\frac{1}{T_{i,obs}} = \frac{1}{T_{i,d}} + \frac{1}{T_{i,p}}, \text{ where } i = 1, 2 \quad (1.9)$$

Since the paramagnetic contribution is linearly proportional to the concentration of the paramagnetic species, the observed solvent relaxation rate can be expressed by equation 1.10, where  $r_i$  corresponds to the proton relaxivity induced by the paramagnetic agent. Proton relaxivity ( $r_i$ ) can be defined as the efficiency of a 1 mM paramagnetic compound solution to enhance the water protons relaxation and it is usually expressed by the units  $\text{mM}^{-1} \cdot \text{s}^{-1}$ .<sup>86</sup>

$$\frac{1}{T_{i,\text{obs}}} = \frac{1}{T_{i,\text{d}}} + r_i[\text{Gd}], \text{ where } i = 1, 2 \quad (1.10)$$

The water proton relaxation is originated by scalar and dipolar interactions between the proton spins and the fluctuating magnetic fields that result from the unpaired electrons of the paramagnetic center.<sup>87</sup> The water molecules that are coordinated with the metal center make a direct contribution, and the bulk solvent molecules experience the paramagnetic effect when they diffuse around the metal center. Since the magnetic fields fall rapidly with increasing distance, random translational diffusion of water and complex molecules, as specific chemical interactions that bring the solvent molecules into the proximity of the metal ion are important in the paramagnetic effect transmission.<sup>128</sup> The metal-water interactions can be divided in three different types (Figure 1.4) and all are relevant for the water proton relaxation.

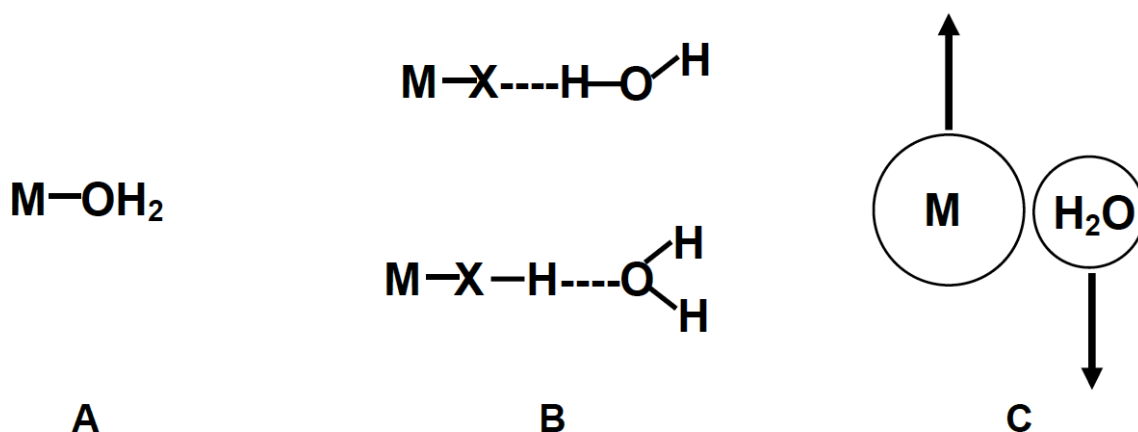


**Figure 1.4:** Schematic representation of the paramagnetic interactions that contribute to water proton relaxivity. Adapted from reference 128.

In case A, a water molecule binds in the primary coordination sphere of the metal ion and exchanges with the bulk solvent. This type of relaxation mechanism is often called inner sphere relaxation and is analyzed using the Solomon-Bloembergen theory. In case B, the water molecules are hydrogen-bound in the second coordination sphere of the complex. If the water molecules can be retained in the periphery of the metal center through hydrogen binding to the metal, this type of relaxation mechanism can be described by the Solomon-Bloembergen theory and is often called “second sphere relaxation”. This contribution plays a significant role in chelates containing phosphonate groups.<sup>129</sup> Nevertheless, since it is difficult to separate the second

coordination sphere interactions, this relaxation mechanism is not distinguished from the relaxivity that arises from the translational diffusion of the water molecules past the chelate (case C), referred to as “outer sphere relaxation”. The separation of the inner and outer sphere relaxation terms is based on the intra and intermolecular nature of the interaction, respectively.<sup>86</sup> The total relaxivity of a paramagnetic agent is therefore given by equations 1.11 and 1.12, where IS and OS refer to inner sphere and outer sphere, respectively. It is believed that for currently used Gd(III)-based contrast agents, the outer and inner-sphere relaxation mechanisms contribute approximately in the same extent to the observed proton relaxivity at the imaging fields.

$$\left(\frac{1}{T_{i,p}}\right) = \left(\frac{1}{T_{i,p}}\right)^{IS} + \left(\frac{1}{T_{i,p}}\right)^{OS} + \left(\frac{1}{T_{i,p}}\right)^{SS}, \text{ where } i = 1, 2 \quad (1.11)$$

$$r_i = r_i^{IS} + r_i^{OS} + r_i^{SS}, \text{ where } i = 1, 2 \quad (1.12)$$

### 1.3.1.1 Inner Sphere Relaxivity

The interactions between the metal electronic spin and the inner sphere water protons are responsible for the proton inner sphere relaxivity, and these interactions result from the exchange of coordinated water protons with the bulk.<sup>86</sup> This mechanism is governed by the scalar and dipolar mechanisms. Both processes are dependent on the magnetic field and the scalar mechanism takes place through the bonds while the dipolar mechanism takes place through the space. The longitudinal and transverse inner sphere relaxation rates are given by equations 1.13 and 1.4, where  $c$  is the molal concentration,  $q$  is the number of bound water molecules per gadolinium,  $P_m$  is the mole fraction of the bound water molecules,  $\tau_m$  is the lifetime of the solvent (water) molecule in the inner sphere of the complex,  $1/T_{1m}$  and  $1/T_{2m}$  are the longitudinal and transverse proton relaxation rates of the bound water, and  $\Delta\omega_m$  is the chemical shift difference between bound and bulk solvent.<sup>86</sup>

$$\left(\frac{1}{T_1}\right)^{IS} = \frac{cq}{55.5} \frac{1}{T_{1m} + \tau_m} = P_m \frac{1}{T_{1m} + \tau_m} \quad (1.13)$$

$$\left(\frac{1}{T_2}\right)^{\text{IS}} = \frac{P_m}{\tau_m} \frac{T_{2m}^{-2} + \tau_m^{-1} T_{2m}^{-1} + \Delta\omega_m^2}{(\tau_m^{-1} + T_{2m}^{-1}) + \Delta\omega_m^2} \quad (1.14)$$

The relaxation rate is generally expressed by the modified Solomon-Bloembergen equations (equations 1.15-1.19).<sup>85</sup>

$$\frac{1}{T_{\text{im}}} = \frac{1}{T_{\text{i}}^{\text{DD}}} + \frac{1}{T_{\text{i}}^{\text{SD}}}, \text{ where } i = 1, 2 \quad (1.15)$$

$$\frac{1}{T_1^{\text{DD}}} = \frac{2}{15} \frac{\gamma_I^2 g^2 \mu_B^2}{r_{\text{GDH}}^6} S(S+1) \left(\frac{\mu_0}{4\pi}\right)^2 \left[ 7 \frac{\tau_{c2}}{1 + \omega_S^2 \tau_{c2}^2} + 3 \frac{\tau_{c1}}{1 + \omega_I^2 \tau_{c1}^2} \right] \quad (1.16)$$

$$\frac{1}{T_1^{\text{SD}}} = \frac{2S(S+1)}{3} \left(\frac{A}{\hbar}\right)^2 \left(\frac{\tau_{e2}}{1 + \omega_S^2 \tau_{e2}^2}\right) \quad (1.17)$$

$$\frac{1}{T_2^{\text{DD}}} = \frac{1}{15} \frac{\gamma_I^2 g^2 \mu_B^2}{r_{\text{GDH}}^6} S(S+1) \left(\frac{\mu_0}{4\pi}\right)^2 \left[ 13 \frac{\tau_{c2}}{1 + \omega_S^2 \tau_{c2}^2} + 3 \frac{\tau_{c1}}{1 + \omega_I^2 \tau_{c1}^2} + 4\tau_{c1} \right] \quad (1.18)$$

$$\frac{1}{T_2^{\text{SD}}} = \frac{S(S+1)}{3} \left(\frac{A}{\hbar}\right)^2 \left(\frac{\tau_{e2}}{1 + \omega_S^2 \tau_{e2}^2} + \tau_{e1}\right) \quad (1.19)$$

In the previous equations,  $\gamma_I$  is the nuclear gyromagnetic ratio,  $g$  is the electron  $g$ -factor,  $\mu_B$  is the Bohr magneton,  $r_{\text{GDH}}$  is the electron spin-proton distance,  $\omega_I$  and  $\omega_S$  are the nuclear and electron Larmor frequencies respectively,  $A/\hbar$  is the hyperfine or scalar coupling constant between the electron of the paramagnetic center and the proton of the coordinated water. The correlation times that are characteristic of the relaxation process are given by equations 1.20 and 1.21, where  $\tau_R$  is the rotational correlation time and  $T_{1e}$  and  $T_{2e}$  are the longitudinal and transverse electron spin relaxation times of the metal ion.

$$\frac{1}{\tau_{ci}} = \frac{1}{\tau_R} + \frac{1}{T_{ie}} + \frac{1}{\tau_m}, \text{ where } i = 1, 2 \quad (1.20)$$

$$\frac{1}{\tau_{ie}} = \frac{1}{\tau_{ie}} + \frac{1}{\tau_m}, \text{ where } i = 1, 2 \quad (1.21)$$

Since electronic relaxation rates also depend on the magnetic field, trivalent gadolinium complexes are usually interpreted in terms of zero field splitting interactions (ZFS). The electronic relaxation rates can be described by the Bloembergen-Morgan theory of paramagnetic electron spin relaxation (equations 1.22-1.23).<sup>86</sup>

$$\left(\frac{1}{T_{1e}}\right)^{ZFS} = 2C \left( \frac{1}{1+\omega_S^2\tau_v^2} + \frac{4}{1+4\omega_S^2\tau_v^2} \right) \quad (1.22)$$

$$\left(\frac{1}{T_{2e}}\right)^{ZFS} = C \left( \frac{5}{1+\omega_S^2\tau_v^2} + \frac{4}{1+4\omega_S^2\tau_v^2} + 3 \right) \quad (1.23)$$

$$C = \frac{1}{50} \Delta^2 \tau_v [4S(S+1) - 3] \quad (1.24)$$

In the previous equations,  $\Delta^2$  represents the mean square zero field splitting energy and  $\tau_v$  represents the correlation time for the modulation of the zero field splitting interaction. The Solomon-Bloembergen-Morgan (SBM) theory is the most complete model that explains the observed paramagnetic relaxation rate enhancement and results from the combination of the modified Solomon-Bloembergen equations (equations 1.15-1.19) with the electron spin relaxation equations (equations 1.22-1.24).

According to SBM equations, a large number of parameters influence the inner sphere proton relaxivity, such as: number of solvent molecules ( $q$ ), gadolinium-proton distance ( $r_{GdH}$ ), residence time of coordinated solvent ( $\tau_m$ ), rotational correlation time ( $\tau_R$ ) and electronic spin relaxation times ( $T_{1,2e}$ ), which is depicted in Figure 1.5.

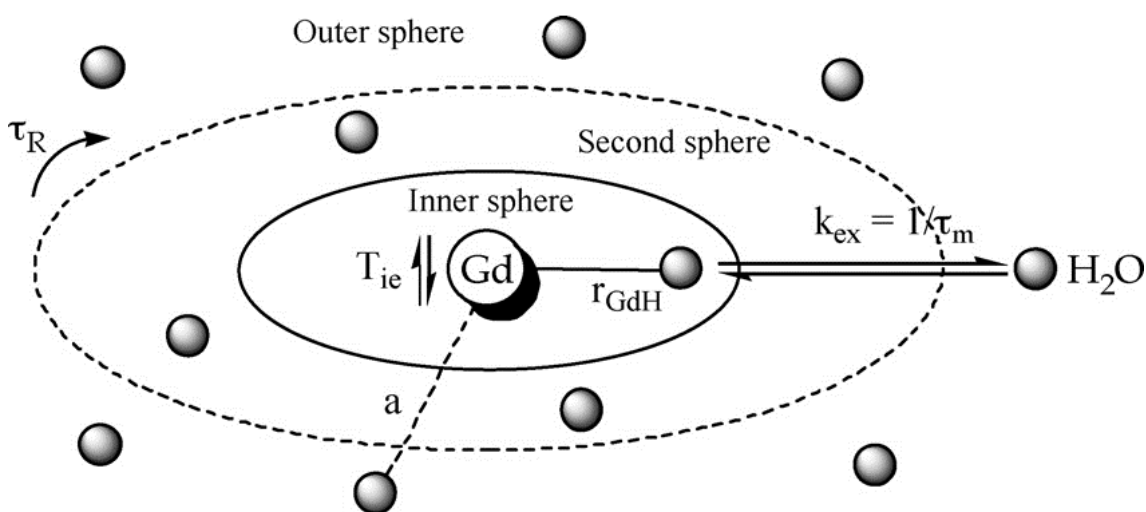


**Figure 1.5:** Schematic representation of Gd(III) chelate solvent environment. Adapted from reference 87.

### 1.3.1.1.1 Number of water molecules ( $q$ )

From equation 1.13, it is clear that the inner sphere proton relaxivity is linearly proportional to the hydration number  $q$ , therefore a higher  $q$  value results in increased relaxivities. Since all approved Gd(III)-based contrast agents display a low hydration number ( $q = 1$ ), several attempts have been made to increase this parameter. However, it is well known that free trivalent gadolinium is toxic and can deposit in the internal organs of patients with impaired renal function and nephrogenic systemic fibrosis.<sup>130</sup> Since ligands that allow the presence of more than one water molecule in the inner coordination sphere give rise to chelates with reduced kinetic and thermodynamic stability, this apparently obvious strategy of increasing the proton relaxivity is not applicable due to toxicity reasons.

The determination of the gadolinium complex  $q$  value is crucial to understand its efficiency as a contrast agent. However, this value is not measured directly and extrapolations are necessary to access the chelate hydration degree, where the  $q$  value is determined using other lanthanides, such as Eu(III), Tb(III) or Dy(III). Eu(III) and Tb(III) fluorescence is more efficiently quenched in H<sub>2</sub>O than in D<sub>2</sub>O due to a better coupling of the metal ion electronic excited states to the O–H oscillators than to the O–D oscillators. Measuring fluorescent lifetimes in H<sub>2</sub>O and D<sub>2</sub>O and further calculation of the fluorescence decay constants ratio in both solvents will provide the  $q$  value.<sup>131</sup> Since Dy(III) induced <sup>17</sup>O chemical shift of the bulk water is proportional to the hydration number, the lanthanide-induced shifts (LIS) method can also be used to determinate  $q$ .<sup>132</sup> In this method, measurements just take a few minutes and there is no need for isotopic enrichment, since <sup>17</sup>O natural abundance is sufficient. Despite useful, these techniques do not give information about the equilibrium between differently hydrated species, because the same chelate may also coexist in solution with different  $q$  values. An answer to this question can be provided by UV-Vis spectrophotometric measurements on the Eu(III)-chelates.<sup>133, 134</sup>

### 1.3.1.1.2 Gadolinium-proton distance ( $r_{\text{GdH}}$ )

According to equation 1.16, the distance between the coordinated water proton and the Gd(III) electronic spin ( $r_{\text{GdH}}$ ) has a six-order dependence on the dipole-dipole relaxation value. By chemically inducing an orientation of bound water molecules such that the protons are closer to the metal unpaired spin, it is possible to improve the inner sphere relaxivity value.<sup>128</sup> The inner sphere relaxivity can also be improved by delocalizing the unpaired spin density towards the water molecules through atomic or molecular orbitals of the metal ion, of the chelating ligand, or of the bound water itself.<sup>128</sup> However, this process may become difficult to achieve, since  $r_{\text{GdH}}$  is a difficult parameter to obtain experimentally and difficult to control. However, its optimization would be very profitable because a decrease of just 0.2 Å would result in a 50% increase in the relaxivity.<sup>85</sup> The  $r_{\text{GdH}}$  value cannot be directly obtained and it is generally deduced from the distance between gadolinium and the coordinated water oxygen. Although Gd-O distances are relatively well defined, Gd-H distances are not, since the angle between the plane of the water molecule and the Gd-O vector is unknown.<sup>130</sup> Several techniques have been applied in order to calculate  $r_{\text{GdH}}$ , such as neutron diffraction in solid and solution state,<sup>135, 136</sup> electron spin echo envelope modulation (ESEEM);<sup>137</sup> X-ray absorption fine structure (XAFS);<sup>138</sup> or X-ray diffraction (XRD).<sup>139</sup> The values obtained by the different techniques are not consistent among themselves, primarily because the angle between hydrogen and oxygen atoms in the water molecule tends to be different in several aqua complexes.<sup>85</sup>

### 1.3.1.1.3 Residence time of coordinated water ( $\tau_m$ )

The residence lifetime of coordinated solvent ( $\tau_m$ ) has a dual importance in relaxivity, since it can a) contribute to the overall correlation time ( $\tau_c$ ) that governs the dipole-dipole interaction between the electronic and nuclear spin (equations 1.16 and 1.20); and b) modulate the efficiency of the chemical exchange of the water molecules sampling the paramagnetic center (equation 1.13).<sup>128</sup> For the gadolinium-based contrast agents being used nowadays, the proton exchange rate is generally equal to the water exchange rate at physiological pH. However, when the solution acidity or basicity is increased, the proton exchange on the Gd(III) complex may become considerably faster than the water exchange due to acid- or base-catalyzed pathways.<sup>140, 141</sup> The rate of water exchange between an inner sphere water molecule and the bulk can usually be determined by <sup>17</sup>O NMR by measuring the transverse relaxation rate in the presence and absence of Gd(III) complex.<sup>142</sup>

Current Gd(III)-based contrast agents possess water exchange rate ( $k_{ex} = 1/\tau_m$ ) values two orders of magnitude lower than the theoretical optimal value ( $k_{ex} = 10^8 \text{ s}^{-1}$ )<sup>85</sup> and several attempts have been made in order to reduce the inner sphere water residence time and therefore, optimize the contrast agent relaxivity. For the polyaminocarboxylate chelators it is important to avoid the amide bond formation of one or more carboxylate arms, as their replacement by amide groups may result in a decrease in the exchange rate by a factor of 3 or 4,<sup>86</sup> which has been found for macrocyclic DOTA-type gadolinium chelates.<sup>143, 144</sup> The binding of a metal chelate to a biomolecule, such as a protein, can influence directly the water exchange time via hydrogen bonding interactions with the bound water or by sterically blocking the water exchange pathway to the bulk, or indirectly, via alteration of the multidentate ligand structure of the primary coordination sphere.<sup>128</sup> Non-covalent binding to a protein can also influence the water exchange rate due to the direct interaction between the Gd(III) chelate and the protein access to the water binding site. This interaction may limit the water diffusion, and consequently reduce the exchange rate, as in the case of the **Gd(PCTP-[13])** chelate.<sup>145, 146</sup> Charge effects have also to be considered when comparing amide and carboxylate derivatives. A higher negative overall charge favors the leaving of the water molecule in a dissociative process, and therefore accelerates the exchange. This phenomenon can be observed for the pentacarboxylate **DOTA** derivate



$[\text{Gd}(\text{DOTASA})]^{2-}$ , which has about a 50% higher water exchange rate than  $[\text{Gd}(\text{DOTA})]^-$ .<sup>147</sup> One way to increase the exchange rate is to increase the stereochemical compression by replacing one or more acetate arms by propionate arms. This phenomenon was described for the DOTA-based chelate  $[\text{Gd}(\text{DO3A-}N\text{-prop})]^-$ , where the increase of the water exchange rate was attributed to steric crowding around the water binding site due to the formation of a six-membered chelate by the propionate arm.<sup>148</sup> In a dissociative water exchange mechanism, steric compression around the water binding site facilitates the departure of the water molecule in the rate determining step, thus accelerating the exchange. This increase in the water exchange value was also observed in chelates of linear ligands, for instance  $\text{EPTPA}^{5-}$  and  $\text{DPTPA}^{5-}$ .<sup>149</sup> These DTPA-based ligands were obtained by replacing one ( $\text{EPTPA}^{5-}$ ) or two ( $\text{DPTPA}^{5-}$ ) ethylene bridges of the backbone by propylene bridges.

#### 1.3.1.1.4 Rotational correlation time ( $\tau_R$ )

The rotational correlation time is perhaps the most crucial variable in SBM equations. For metal ions with long  $T_{1e}$  values, like Gd(III), modification of the rotational correlation time is the most important source of relaxivity enhancement.<sup>128</sup> According to equation 1.20, for small molecular weight Gd(III)-chelates, it is  $\tau_R$  that mainly determines the effective correlation time of proton relaxation,  $\tau_c$ . This means that the fast rotation is the limiting factor for proton relaxivity in magnetic fields relevant to MRI, and this impelled the development of a wide variety of macromolecular agents.

There are four main strategies to reduce the metal chelates rotation and mobility *in vivo*: a) distribution of the agent into a tissue or tissue compartment with high microviscosity; b) covalent or non-covalent binding of metal chelates to biomolecules, such as proteins or antibodies; c) synthesis of high molecular weight conjugates, as polymers or dendrimers; and d) formation of supramolecular aggregates (micelles, liposomes) using amphiphilic conjugates. However, the increase observed in the relaxation rate in macromolecular agents is usually much lower than expected, due to the internal flexibility of these agents. Although rotation is often assumed to be isotropic, for larger molecules this may not be valid. Anisotropic rotation or internal motion within a molecule will reduce the correlation time from that predicted by an

isotropic model based on molecular weight.<sup>150</sup> For certain linear polymers, the proton relaxivity was found to be independent of the molecular weight, since their relaxivity is limited by fast rotation.<sup>151, 152</sup> The rotational correlation time of these polymers is dominated by segmental motions which are independent of the molecular weight. To account for the different motions that occur during molecular rotation, Lipari and Szabo presented the “model-free” (equations 1.25 and 1.26),<sup>153, 154</sup> which describes the rotational motion of macromolecular chelates. It is pointed out that for most complex models, there are two kinds of motions that affect relaxation: a) a rapid, local motion which lies in the extreme narrowing limit ( $\tau_l$ ); and b) a slower, global motion ( $\tau_g$ ). Equations 1.25 and 1.26 apply this dipolar relaxation for the gadolinium case, where  $\tau_g$  is a correlation time for the global motion, common to the whole molecule,  $\tau_l$  is the correlation time for the fast local motion, specific for the individual relaxation axis, which is related to the motion of the chelate unit,  $S^2$  is a model-independent measure of the degree of spatial restriction of local motion and its value ranges from 0 (internal motion is isotropic) to 1 (motion is completely restricted).

$$J(\omega) = \left( \frac{S^2\tau_g}{1+\omega^2\tau_g^2} + \frac{(1-S^2)\tau_l}{1+\omega^2\tau_l^2} \right) \quad (1.25)$$

$$\tau^{-1} = \tau_g^{-1} + \tau_l^{-1} \quad (1.26)$$

Rotational correlation time can be estimated from different physical methods, such as NMR relaxation or EPR and most of the reported  $\tau_R$  values for the Gd(III) complexes in literature have been obtained from proton relaxation measurements, but also from  $^{17}\text{O}$  relaxation measurements. For spherical molecules,  $\tau_R$  can be calculated from the Stokes-Einstein equation (equation 1.27), where  $r_{eff}^3$  is the effective radius and  $\eta$  is the microviscosity. Although usually it is impossible to know the exact microviscosity and effective radius values, this equation allows the comparison of two similar systems with different molecular weight, supposing that the values are the same for both systems.

$$\tau_R = \frac{4\pi\eta r_{eff}^3}{3k_B T} \quad (1.27)$$

### 1.3.1.1.5 Electronic spin relaxation times ( $T_{1,2e}$ )

To obtain a good reduction of the proton relaxation time, it is crucial to choose paramagnetic metal ions with slow spin relaxation times. Gd(III), Mn(III) and Fe(III) are optimal relaxation agents due to their long  $T_{1e}$  values and large magnetic moments. The influence of the electron spin relaxation on the gadolinium contrast agents relaxivity is essentially ruled by the decay of the electron spin magnetization parallel to the external magnetic field, described by  $T_{1e}$ .<sup>86</sup>  $T_{1e}$  and  $T_{2e}$  are the most difficult parameters to determine independently because of their field dependence. Nevertheless, the  $T_{2e}$  investigation may allow the  $T_{1e}$  estimation, within the framework of a given model.<sup>86</sup>

The zero field splitting (ZFS) of the spin a level is induced as a consequence of collisions between the chelate and the solvent molecules. The electronic relaxation rate is related to induced ZFS and although this approach cannot be directly extended to more asymmetrical metal chelates, an increase in ZFS will lead to shorter  $T_{1e}$  values and reduced relaxivity, limited by the values of  $\tau_m$ ,  $\tau_R$  or the correlation time of internal motions.<sup>128</sup> To achieve longer  $T_{1e}$  values, and therefore better relaxivities, it is necessary to minimize the ZFS in the metal chelates. Transverse electronic relaxation rates can be directly determined from EPR measurements. It may be possible to tune this parameter through changes in ligand field strength and/or symmetry,<sup>128</sup> however it has been a challenging and difficult task.

### 1.3.1.2 Second sphere relaxivity

The second sphere relaxation occurs when the protons of water molecules in the second coordination shell relax via dipolar mechanism. A thoughtful choice of groups that are good hydrogen bond acceptors may promote the formation of a strong interaction between the chelate functional group and the water molecules, resulting in a decrease of their average distance from the gadolinium center and offering a well-defined coordination sphere with several water molecules bound in the proximity of the paramagnetic center. For example, in ligands with phosphonate groups, the water molecules can be retained long enough in the periphery of the metal center through hydrogen binding to the metal and thus contribute to the overall relaxivity.<sup>145, 155</sup> When the residence lifetime of the structured water in the second shell is longer than the

diffusional correlation time  $\tau_D$  ( $\tau_D = a^2/D$ ), this process has to be distinguished from the typical diffusion-controlled outer-sphere relaxivity.<sup>129</sup> If this requirement is fulfilled, the quantitative effects on the relaxivity are equivalent of the inner sphere water molecules and the value can be calculated from equation 1.13.<sup>128</sup> However, concrete experimental evidence for the existence of this interaction is difficult to obtain and in the majority of cases its consideration may only represent a negligible correction to the inner and/or outer sphere relaxivities.

### 1.3.1.3 Outer sphere relaxivity

The outer sphere relaxation arises from the translational diffusion of water molecules near the metal complex. The interaction between the gadolinium electronic spin  $S$  and the water proton spin  $I$  is supposed to be a dipolar intermolecular interaction whose fluctuations are governed by random translational motion. The relaxation rate for unlike spins is given by equation 1.28<sup>156</sup>, where  $N_A$  is the Avogadro's constant,  $d$  is the closest distance of approach of spins  $I$  and  $S$ ,  $D$  is the diffusion constant for relative diffusion,  $[M]$  is the molar concentration of the metal bearing spin  $S$  and  $\hbar$  is the reduced Planck's constant or Dirac's constant. The spectral densities ( $j(\omega)$ ) are obtained from equation 1.29.<sup>157, 158</sup>

$$\frac{1}{T_1} = \frac{32\pi}{405} \left(\frac{\mu_0}{4\pi}\right)^2 \frac{N_A[M]}{dD} \gamma_I^2 \gamma_S^2 \hbar^2 S(S+1) [j_2(\omega_I - \omega_S) + 3j_1(\omega_I) + 6j_2(\omega_I + \omega_S)] \quad (1.28)$$

$$j_k(\omega) = Re \left( \frac{1 + \frac{z}{4}}{1 + z + \frac{4z^2}{9} + \frac{4z^3}{9}} \right), \text{ where } (1.29)$$

$$z = \sqrt{i\omega\tau + \frac{\tau}{T_{ke}}}; \tau = \frac{d^2}{D}; \text{ and } k = 1, 2$$

The relaxation enhancement provided by the gadolinium chelates can only be directly measured for complexes with inner sphere water. Chelates with no inner sphere water are generally uninteresting as contrast agents, since their relaxivity is too low, but they can be useful to separate the inner and outer sphere contribution. An approach often taken to estimate the outer sphere contribution on a chelate with  $q \neq 0$  is to

subtract the relaxivity of a similar  $q = 0$  complex, such as  $[\text{Gd}(\text{TTHA})]^{3-}$  or  $[\text{Gd}(\text{TETA})]^-$  from the observed  $r_1$ .<sup>159, 160</sup> However, this method can give rise to incorrect results because the observed relaxivity could result from the sum of outer and second sphere (chapter below) coordinated water. In most studies, the outer sphere contribution is estimated using equations 1.28 and 1.29, using a “reasonable value” (3.6 Å) for the closest distance of approach.<sup>86</sup>

At the magnetic fields of interest, the outer sphere contribution depends primarily on the distance of the closest approach, related to the molecular dimension, the charge distribution of the complex and the relative diffusion coefficient of solute and solvent. For the currently used Gd(III)-based contrast agents with a single coordinated water molecule, the inner-sphere relaxation mechanism has the major contribution to the observed proton relaxivity at the imaging fields.

## 1.4 Ligands

Due to the extensive variety of metals available and its isotopes with different properties, huge efforts have been made in order to synthesize metal-based pharmaceuticals to be used in medical diagnosis and therapy. Depending on their concentration and availability, metal ions can have an high *in vivo* toxicity in their free form, so it is imperative to obtain ligands that can: a) efficiently chelate the metal, to afford complexes with elevated thermodynamic and kinetic stability; b) selectively chelate a single or a group of metal ions, to prevent the essential metals chelation; c) provide biospecific chelates, to allow the treatment or diagnosis of a specific tissue, avoiding an excessive pharmaceutical dosage.

### 1.4.1 Macrocyclic ligands

Among existing chelators, macrocyclic ligands have been extensively evaluated over the past decades due to their similarity and relationship with natural compounds that can be found in biological systems, such as heme groups of erythrocyte or porphyrins existing in photosynthetic systems. These compounds can be defined as cyclic molecules with nine or more members, and three or more donor atoms.<sup>161</sup> Despite the instigated interest and the possible applications for these compounds, until the

1960's the information available was reduced, mainly due to the complications associated to isolation processes or limited synthetic procedures. Nowadays, a wide variety of such compounds can be commercially found or synthesized using relatively simple methods, in which the macrocyclic size, number and type of donor atoms can be modified, providing ligands with different specificities.

The considerable difference in the stability constant values obtained for similar open and closed-chain ligands cannot be explained solely by the chelate effect. Cabiness and Margerum<sup>162</sup> used two analogue ligands, the **2,3,2-tet** (open-chain) and the **meso-1,7-CTH** (closed-chain) (Figure 1.6) for Cu(II) chelation and verified that the cyclic complex was  $10^4$  times more stable than the acyclic one. They concluded that this large increase in the stability constant could not be attributed exclusively to the chelate effect (dominated by the entropic factor), since both complexes had the same number and bond types. Other factors would have a high influence in the general complex stability, which is entitled the "macrocyclic effect".

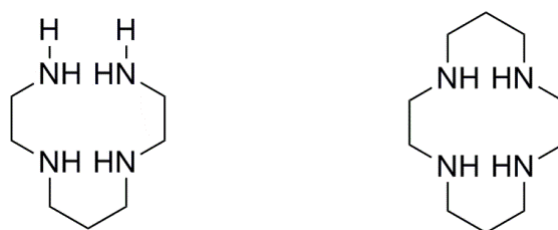


**Figure 1.6:** Chelators 2,3,2-tet and meso-1,7-CTH.

It is generally accepted that this effect is the result of the combination of enthalpic and entropic factors, as well as a higher orbital overlap between the metal ion and the donor atoms.<sup>163</sup> Since macrocyclic ligands have a more or less rigid and pre-organized geometry, the chelator structure is very similar to the chelates they will originate, so no drastic variations are required in the ligand conformation when the metal ion chelation occurs. Thus, enthalpic variation associated to the coordination reaction will be smaller in the case of macrocyclic chelators, making it a more favorable reaction. Besides the pre-organization of the cyclic chelators, the fact that they possess a smaller number of inter-molecular bonds with the solvent than the acyclic chelators, allows the cyclic chelator desolvation to occur with less energy expenditure. Therefore, the poor solvation of the donor atoms in the restrict cavities of the free macrocyclic ligands facilitates the metal complexation.<sup>162</sup> Due to the low flexibility of macrocyclic

ligands in comparison with open-chain analogues, they may impose particular coordination geometry to a given metal ion, while the open chain chelators can easily adapt to the metal geometric requirements. Nevertheless, the kinetic and thermodynamic stability of the complex formation is indeed affected by several factors, such as: the metal ion, the ring cavity size; the binding sites location in the cavity; the solvent type, the solvation degree of metal and chelator; the chelator denticity and type of donor atoms; the flexibility and the steric hindrance in the macrocycle; and the metal and chelator electric charge.

Nowadays, macrocyclic ligands and their complexes find a variety of applications across several areas particularly in the medical field. They have the potential to be directly used in chelation therapy to remove excessive amounts of a certain metal in the body. However, their main uses are in radioisotope complexation for the diagnosis and treatment of certain diseases<sup>164</sup> and in paramagnetic ions complexation (Gd(III) or Mn(II)) used in MRI.<sup>85, 87, 165</sup> The use of macrocyclic chelates also extends to areas such as electrochemistry, in which they can be used as photochemical agents capable of convert solar energy into chemical energy;<sup>166, 167</sup> or in environmental sciences, where ligands can be used for extraction, separation and recovery of toxic and costly metals present in waste sites.<sup>168</sup>

#### 1.4.1.1 DOTA

The macrocyclic chelator **DOTA** has an elevated affinity for metal ions such as In(III), Fe(III), Ga(III), Cu(II), Co(II) and the majority of lanthanides, providing complexes with distinct geometries (Table 1.9) and elevated thermodynamic stability<sup>19, 169-171</sup> (Table 1.10). Most of the mentioned metal ions possess characteristics that allow them to be used in medical imaging techniques. a) The trivalent gadolinium is a paramagnetic metal with seven unpaired electrons that is suitable for MRI; b) Ga(III) and In(III) have  $\gamma$ -emitter isotopes (<sup>67</sup>Ga and <sup>111</sup>In) that can be used in SPECT; and c) Ga(III) and Cu(II) have  $\beta^+$ -emitter isotopes (<sup>68</sup>Ga and <sup>61/62/64</sup>Cu) that can be used in PET. However, to achieve a thermodynamically stable chelate, the ion must have the appropriate features in size and charge for steady **DOTA** chelation. The type, number, lengths and bond angles between the metal ion and the donor atoms influence the resulting chelate stability.

**Table 1.9:** Crystallographic and structural data of some DOTA chelates.

Ion	Crystallographic System	Ionic Radius (Å)	Coordination Number	Geometry	Donor Atoms
Gd(III) <sup>172</sup>	Triclinic	0.938	9	Square Antiprismatic	N <sub>4</sub> O <sub>4</sub>
Sc(III) <sup>173</sup>	Tetragonal	0.745	8	Square Prismatic	N <sub>4</sub> O <sub>4</sub>
Fe(III) <sup>172</sup>	Orthorhombic	0.645	7	Not Available	N <sub>4</sub> O <sub>3</sub>
Ga(III) <sup>174</sup>	Monoclinic	0.620	6	Octahedral	N <sub>4</sub> O <sub>2</sub>

**Table 1.10:** Values of stability constant, bond length, bond angle and distance between metal and N<sub>4</sub> plan of some DOTA chelates.

Metal	logK	Bond Length M-N <sub>eq</sub> (Å)	M-O Angle (°)	Distance M-N <sub>4</sub> plan (Å)
Fe(III)	29.40 <sup>170</sup> ; 24.48 <sup>175</sup>	2.280	2.050	1.058
Cu(II)	22.25 <sup>170</sup> ; 22.72 <sup>171</sup>	2.107	1.966	0.916
Ga(III)	21.33 <sup>170</sup>	2.112	1.934	0.840
Co(II)	19.30 <sup>171</sup> ; 20.27 <sup>175</sup>	2.166	2.034	0.888
Zn(II)	18.70 <sup>171</sup> ; 21.10 <sup>175</sup>	2.171	2.037	0.891

The iron complex of **DOTA** possesses the highest stability value, due to the three carboxylate groups used in the coordination, unlike the remaining complexes that are coordinated with only two carboxylates. This complex is also the one with greater distance between the metal and the equatorial nitrogen, probably because it is a hard acid and it rather complexes hard atoms like oxygen. The remaining complexes have an octahedral geometry. If the bond lengths between the metal and the nitrogen in the equatorial plan were compared, it appears that the decrease in bond length results in increased stability. This trend can be explained by a stronger electrostatic interaction between the metal and the nitrogen electrons. In turn, the zinc complex is the less stable due to a  $d^{10}$  electronic configuration which prevents the zinc to accept charge transfers from donor atoms, decreasing the stability of its complexes.



### 1.4.1.2 DOTA-based bioconjugates and coupling strategies

The majority of contrast agents and radiopharmaceuticals used in imaging techniques are small organic compounds that chelate a metal ion with the appropriate property for the scan.<sup>63, 87, 176</sup> These imaging agents can be divided into two main classes: a) those whose biodistribution is determined entirely by their chemical and physical properties; and b) those whose final biodistribution is determined by their biological interactions resulting from the receptor binding, often called receptor-based or target-specific agents.<sup>177</sup> Target specific imaging agents allow the delivery of the imaging agent to a specific tissue. Instead of being disseminated within the body, the probe is taken up in a desired region of interest.

To design target-specific probes, the bifunctional approach is the most commonly used.<sup>178</sup> This approach is a simple and versatile methodology, which uses a bifunctional chelator (BFC) that is able to chelate the metal ion, and at the same time, possesses the functional groups required to couple a biomolecule with high affinity for the receptor ligand, which is called the targeting biomolecule (BM).<sup>179</sup> This whole molecular construct can be designated by bioconjugate (Figure 1.7). To modify the bioconjugate, chemical properties and ensure that both its affinity for the receptor and the chelating properties are not affected, a linker (or spacer) between the BFC and the BM may be introduced. The linker may act as a possible pharmacokinetic modifier (PKM), adjusting the *in vivo* behavior and the final biodistribution. Hydrocarbon chains, poly(ethylene glycol) (PEG) derivatives and polypeptide chains are the most common linkers.<sup>180-182</sup> For example, PEG linkers are very useful to modify the target-specific agent lifetime. Due to a phenomenon attributed to its molecular conformation in aqueous solution and due to steric shielding of hydrophobic patches on the protein's surface, PEG is known to be resistant to protein adsorption.<sup>183, 184</sup> Other benefits are reduced *in vivo* immunogenicity and/or increased *in vivo* plasma half-life of the PEG containing molecules. The combination of these factors can lead to a superior lifetime of the chelate in body, by decreasing the liver and kidneys excretion rate.<sup>185-187</sup>

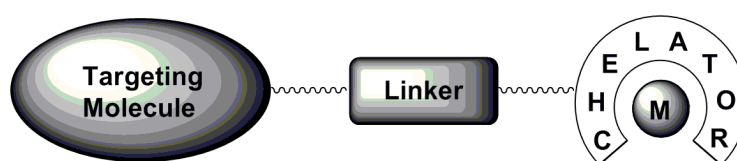


Figure 1.7: Schematic representation of a bioconjugate.

Targeting biomolecules can be small peptides, non-peptide receptor ligands and macromolecules such as antibodies, antibody fragments or proteins. Those molecules act as “carriers” for a specific delivery of the imaging agent to the diseased tissue. The choice of the BFC and PKM are equally fundamental, since the different metals used in medical imaging have distinct coordination chemistry and labeling conditions, and the metal adduct should be far enough from the biomolecule moiety to minimize possible interference with the receptor binding. As ultimate goal, a good receptor-based agent should be tissue-specific and selective, have a proper pharmacokinetic profile and may be developed into a product for routine clinical use.

There are two fundamental approaches for **DOTA** conjugation with biomolecules. In the first approach one of the four carboxylate groups in **DOTA** can be used to bind to an amine function in the biomolecule and form a stable amide bond linkage. In the second approach, **DOTA** derivatives with additional side chains on the pendant arms or on the cyclen backbone can be employed and the biomolecule will be attached to the side chain functional group. The use of **DOTA**'s carboxylic acid is somewhat restricted in the chemical point of view. Besides the amide bond formation, which in many cases can lead to tedious and unprofitable synthetic procedures, the number of possible chemical reactions between a carboxylic acid and the biomolecule functional groups is limited. Nevertheless, the carboxylic acid can be functionalized into a different conjugation group through the introduction of a linker, which may or may not be also introduced to modify the properties of the resultant bioconjugate. For example, functional groups like maleimides, alkynes or thiols can be introduced into **DOTA**, diversifying the possible conjugation reactions. Lewis and Shively<sup>188</sup> reported the synthesis of a **DOTA**-based chelator with a maleimide group for biomolecules conjugation. Using sulfo-NHS chemistry (*N*-hydroxysulfosuccinimide), L-cysteine was coupled to **DOTA**, and the 1,6-bis(maleimide)hexane was posteriorly used to introduce the maleimide functionality via a sulfide linkage to the **DOTA** derivative. Alternatively, the sulfide group of the side chain was oxidized to a sulfone with potassium monopersulfate to afford a similar bifunctional chelator. The monoclonal antibody cT84.66 was posteriorly attached with both ligands also via sulfide group to afford two bioconjugates with different **DOTA**-antibody ratios.<sup>188</sup>

Despite the fact that **DOTA** can itself act as a bifunctional chelator, several derivatives with additional side chains on the pendant arms or on the cyclen backbone have been synthesized over the last years (Figure 1.8). These bifunctional derivatives

can have different conjugation groups, like the isothiocyanate or the amine functional group, or just have an “extra” carboxylic acid. In all cases, the introduction of a new group allows all four **DOTA** carboxylic groups to be involved in the metal complexation, which is crucial when a eight or higher coordinated metal ion is necessary.

(2-(4-isothiocyanatobenzyl)-1,4,7,10-tetraazacyclododecane-1,4,7,10-tetraacetic acid (***p*-NCS-Bz-DOTA**) (Figure 1.8a), a **DOTA** derivative with a *p*-isothiocyanatobenzyl group was one of the first **DOTA** bifunctional chelators developed for biomolecule coupling<sup>189, 190</sup> and continues to be the most widely used for antibody conjugation. This BFC is water soluble and can easily react with primary amines in somewhat basic conditions, specifically with the lysine side chain.<sup>191</sup> Grunberg *et al*<sup>192</sup> successfully conjugated the ***p*-NCS-Bz-DOTA** with two truncated forms of the surface protein L1-CAM, the monovalent chCE7 and the divalent antibody fragments chCE7F(ab')<sub>2</sub>. The coupling reaction was made in aqueous solution, affording a bioconjugate with a BFC-BM ratio of 2:1. Mohsin *et al*<sup>193</sup> has also used the ***p*-NCS-Bz-DOTA** for antibody coupling, but in this report it was used the monoclonal antibody B72.3 as the targeting molecule. In this case, it afforded a 5:1 BFC-BM ratio bioconjugate. Encouraged by the coupling success of ***p*-NCS-Bz-DOTA**, other **DOTA** derivatives with an isothiocyanate group have been synthesized (Figure 1.8b to 1.8f),<sup>194</sup> but no significant improvements were observed in biomolecule coupling or *in vivo* stability.<sup>193-195</sup>

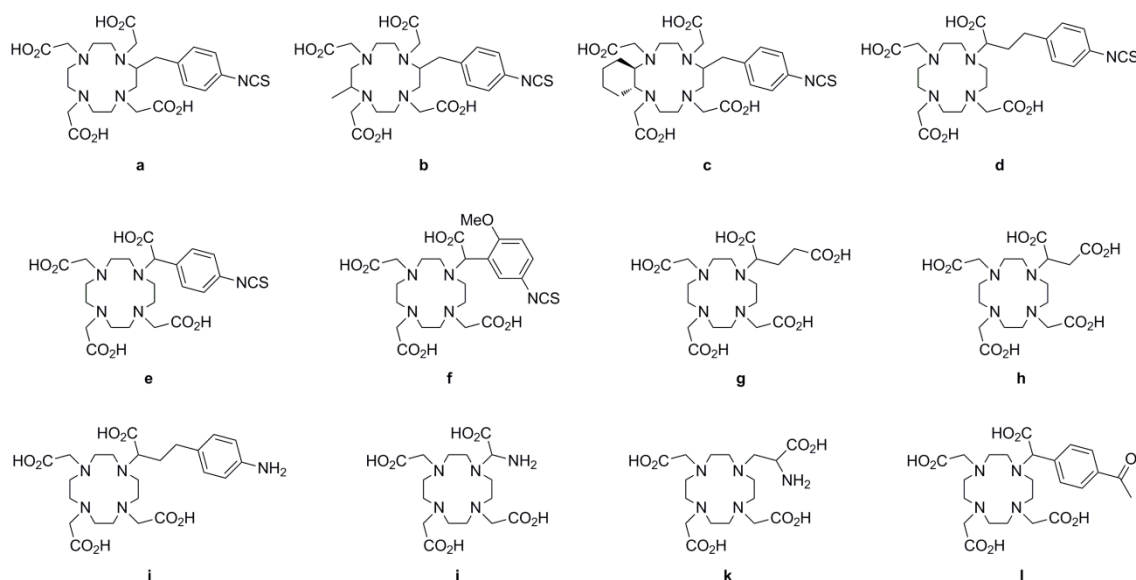


**Figure 1.8:** DOTA-based bifunctional ligands.

Some **DOTA** derivatives with an additional carboxylic acid function have been developed, such as **DOTAGA** (Figure 1.8g)<sup>196</sup> and **DOTASA** (Figure 1.8h).<sup>147</sup> The supplementary carboxylic acid allows the conjugation with biomolecules without compromise the chelating ability of the BFC, although in these cases, it is required an orthogonal protection synthetic strategy to remove the protecting groups at different stages. The advantages of using bifunctional chelators with an additional carboxylic acid were demonstrated by Eisenwiener *et al.*,<sup>196</sup> through the **DOTAGA** conjugation with the peptide D-Asp-Tyr-Nle-Gly-Trp-Nle-Asp-Phe-NH<sub>2</sub>. The biomolecule was attached to the carboxylic acid using HATU as coupling agent and the remaining protecting groups were cleaved with TFA/thioanisole/phenol/H<sub>2</sub>O (85:5:5:5) to afford the conjugate 95% pure. The **DOTAGA** conjugate structure allows the production of stable labelled chelates with different radiometals for both diagnostic (<sup>111</sup>In, <sup>67/68</sup>Ga) and internal radiotherapeutic applications (<sup>90</sup>Y, <sup>177</sup>Lu). In order to conjugate DOTA-derivatives with functional groups other than amines, some derivatives with an amine function have been developed. In the late 1990s, Chappel *et al.*<sup>194</sup> reported the synthesis of  $\alpha$ -(2-(4-aminophenyl)-ethyl)-1,4,7,10-tetraazacyclododecane-1,4,7,10-tetraacetic acid (**PA-DOTA**) (Figure 1.8i), a derivative with an aromatic amine attached to one of the sidearms. Despite having a free amine group, **PA-DOTA** was never widely used in bioconjugate chemistry primarily due to the lack of reactivity of the amine, since the electron pair is delocalized by the aromatic ring. More recently, two other amine-DOTA chelators, **DO3A-N- $\alpha$ -aminoacetate** (Figure 1.8j)<sup>197</sup> and **DO3A-N- $\alpha$ -aminopropionate** (Figure 1.8k)<sup>148</sup> have been reported for targeted-specific imaging agent production. The ligand **DO3A-N- $\alpha$ -aminoacetate** was successfully conjugated to the C-terminus of a matrix metalloproteinase enzyme (MMP-2) with 71% yield.<sup>198</sup> The peptide was synthesized by solid-phase peptide synthesis (SPPS) and the conjugation reaction was prepared in the presence of HATU, HOBt and *N*-Methyl-2-pyrrolidone. An alternative to the mentioned coupling groups was provided by the coupling of a bifunctional DOTA-derivative with a ketone functional group (Figure 1.8l) to aminoxy groups.<sup>199</sup> This BFC was coupled by oxime bond formation to the aminoxy functionalized somatostatin analogue Tyr<sup>3</sup>-octreotate to afford the desired conjugate.

### 1.4.1.3 DOTA-based bioconjugates with RGD peptide analogues

Despite the fact that numerous biomolecules can be used to introduce biospecificity to an imaging agent, the choice of these targeting moieties should be made with carefulness. The ideal targeted-imaging agent should have a high and specific affinity for the target site, which for example may be a receptor over-expressed on tumor cells or existing in high concentrations on a particular tissue. These compounds must also be efficiently internalized by target cells to achieve rapid uptake and acquire appropriate concentrations. Furthermore, the agents should be rapidly eliminated from blood stream and display low uptake in the liver and kidneys, because elevated residence time can increase the overall toxicity inherent to the metal ion.<sup>200</sup>

In recent years, integrins have been one of the most used biomolecules for design and development of targeted imaging agents. These molecules are heterodimeric transmembrane glycoproteins, which play a significant role in cell-cell and cell-matrix interactions.<sup>201</sup> Integrins are constituted by two noncovalently bound transmembrane subunits with large extracellular segments that bind to create heterodimers with distinct adhesive capabilities.<sup>202</sup> Until 2002, eighteen  $\alpha$  and eight  $\beta$  subunits have been described, which can bind up to 24 different receptors<sup>201</sup> (Figure 1.9). These proteins play a crucial role in angiogenesis and tumor metastasis,<sup>203</sup> since angiogenic processes depend on vascular endothelial cell migration and invasion, which are regulated by the cell adhesion molecules.<sup>204, 205</sup> They are routinely over-expressed in tumor cells and their function ranges from mediating migration of endothelial cells into the membrane basement to the regulation of growth, differentiation and survival of the endothelial cells during angiogenesis.<sup>206</sup>

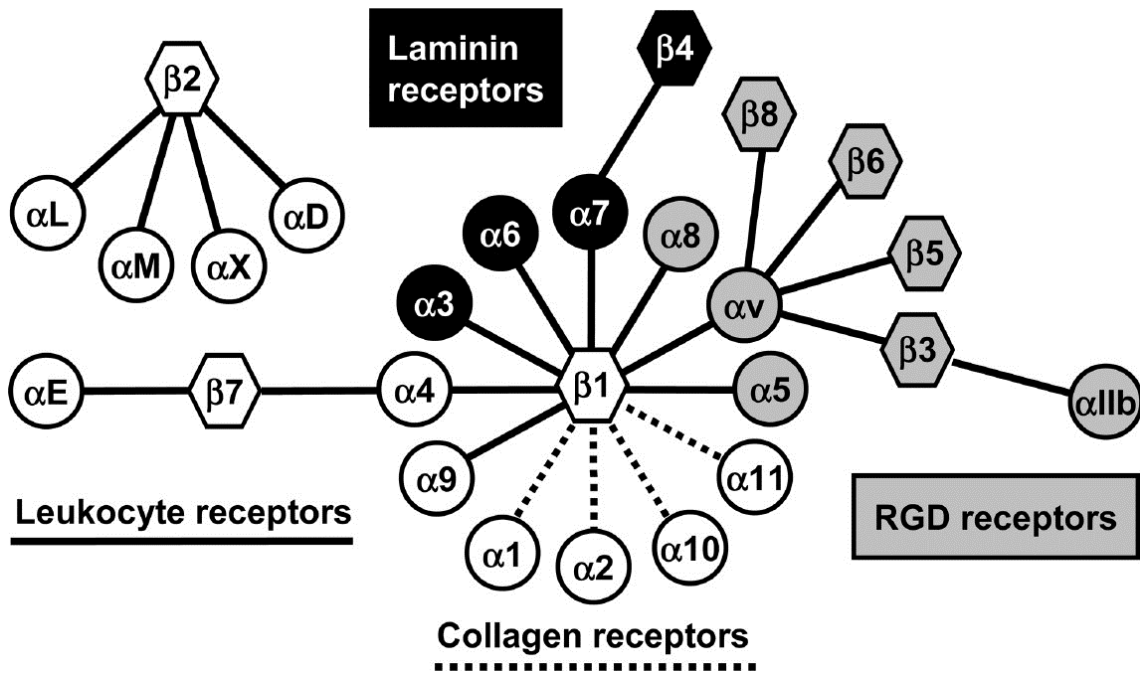


**Figure 1.9:** The integrin group: RGD receptors, laminin receptors, leukocyte receptors and collagen receptors. Adapted from reference 207.

A common feature of many integrins like  $\alpha_v\beta_3$  (Figure 1.10) is that they bind to extracellular matrix proteins such as vitronectin or fibronectin with exposed arginine-glycine-aspartic acid (RGD) amino acid sequence.<sup>207</sup> Inhibition of  $\alpha_v\beta_3$  integrin activity by RGD peptides, peptidomimetics and monoclonal antibodies can induce endothelial cell apoptosis and inhibit angiogenesis, which further supports the role of the integrin in angiogenesis.<sup>208</sup> These biomolecules act as antagonists, since they have great affinity for the receptors, obstructing other molecules (agonists) to bind to the receptors and produce a biological response. Among all 24 integrins discovered to date, the  $\alpha_v\beta_3$  is still the most extensively studied and it is assumed to have a positive and negative regulatory role in angiogenesis depending on the respective biological context. Since  $\alpha_v\beta_3$  integrin is over-expressed in melanoma, glioblastoma, ovarian and breast cancer tumor cells, and is significantly up-regulated on activated endothelial cells during angiogenesis but not on dormant endothelial cells,<sup>203</sup> this integrin represents an attractive target for cancer imaging and therapy.<sup>209</sup> Because of these features, it is the most extensively examined biomolecule concerning imaging of the angiogenic evolution in tumors.

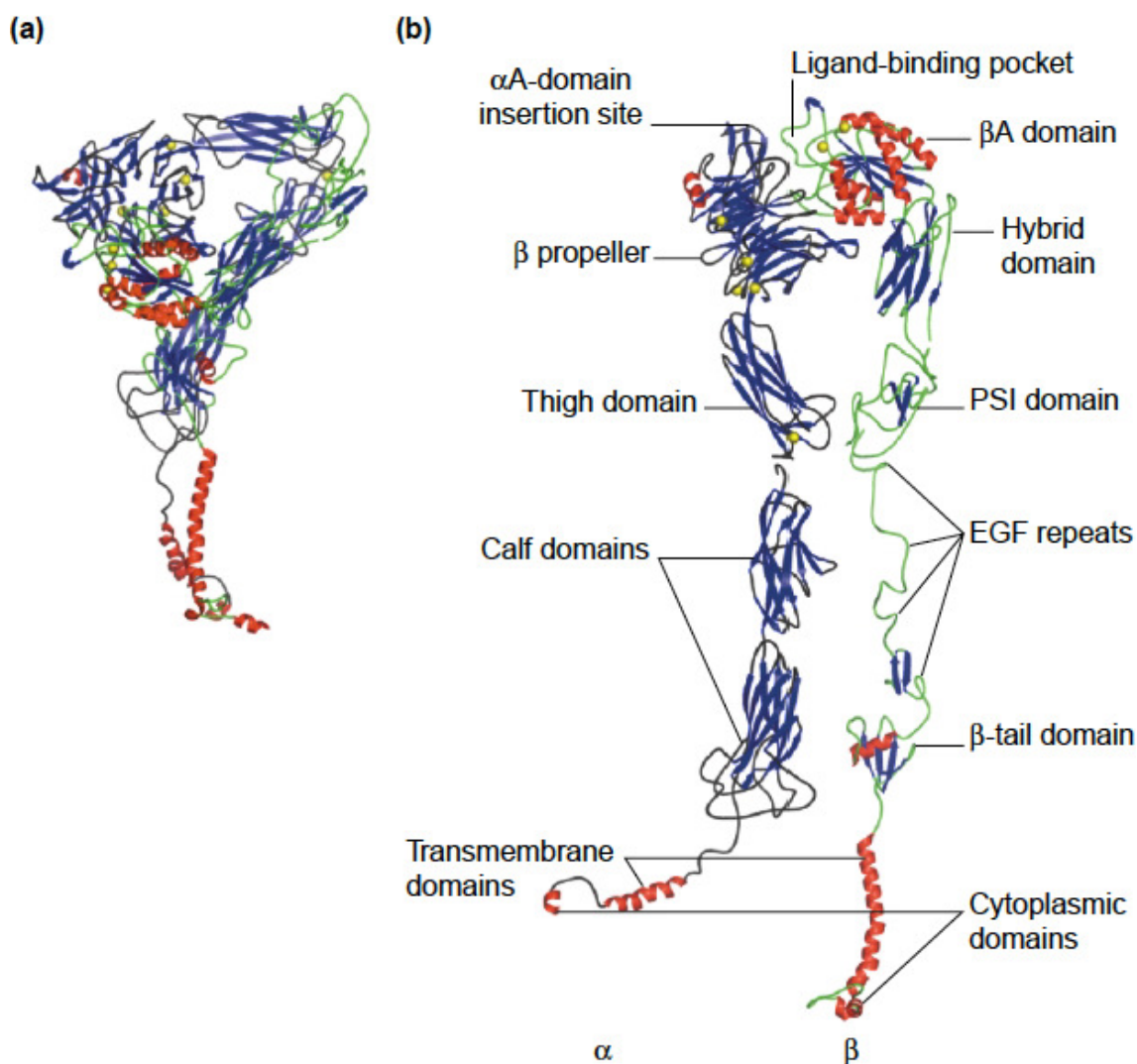


**Figure 1.10:** The  $\alpha_v\beta_3$  integrin structure: **a)** bent image;<sup>210</sup> **b)** straightened image.<sup>211</sup>

The first generation of linear peptides containing the RGD sequence or cyclic RGD peptides with disulfide bridges, such as RGD-4C suffered from low subtype selectivity and from metabolic stability or both.<sup>212</sup> The cyclic pentapeptides containing the RGD sequence, such as cyclo(RGDfV), which was developed by computational screening for the best spatial orientation of the RGD sequence,<sup>213</sup> can have an increased selectivity ( $\alpha_v\beta_3 \gg \alpha_{IIb}\beta_3$ ) and sufficient metabolic stability. The additional optimization via *N*-methylation to afford the cyclic peptide cyclo(RGDf(NMe)V) resulted in a subnanomolar- $\alpha_v\beta_3$ -affinity and low nanomolar  $\alpha_v\beta_1$ - and  $\alpha_v\beta_5$ -affinity.<sup>214</sup> Unfortunately these cyclic pentapeptides do not possess functional groups that allow efficient conjugation with signaling units to be used on medical imaging. Nonetheless, [<sup>123</sup>I]cyclo(RGDyK) was one of the first radiolabeled  $\alpha_v\beta_3$ -agents evaluated *in vivo*.<sup>215</sup> The valine substitution by a lysine residue allowed the chelators and prosthetic groups

conjugation without significantly affecting the binding affinity.<sup>216</sup> The use of cyclo pentapeptides containing amino acid residues with functional groups in their side chains will facilitate pharmacokinetics optimization via PKM attachment (ex: carbohydrates<sup>217, 218</sup> or PEG analogues<sup>181, 185, 219</sup>) or will improve binding characteristics via multimerization.<sup>220-222</sup>

Several bioconjugates with cyclo RGD peptides have been synthesized and evaluated for molecular imaging over the past years.<sup>223</sup> Decristoforo *et al*<sup>224</sup> reported the synthesis of the **DOTA-c(RGDfK)** bioconjugate (Figure 1.11) and its evaluation with <sup>68</sup>Ga for PET imaging. This bioconjugate was prepared by the amide bond formation between one of **DOTA**'s carboxylates and the lysine' amine side chain, while D-phenylalanine was used as the amino acid responsible for the peptide cyclization. Human serum stability studies showed high resistance to proteinases, since over 95% of both chelates were intact 120 minutes after incubation. Some internalization studies with <sup>68</sup>Ga and <sup>111</sup>In chelates were performed with human melanoma cancer cells M21 ( $\alpha_v\beta_3$  integrin positive) and M21-L ( $\alpha_v\beta_3$  integrin negative). It was found that labeled bioconjugates can be internalized by both cancer cells. However, due to the  $\alpha_v\beta_3$  integrin absence, the internalization process was smaller for the M21-L cell line. In the assays in which the c(RGDfK) peptide was administrated simultaneously with the radionuclide conjugates, the internalization level for radio-labeled conjugates decreased significantly. Despite the low internalization in absolute terms, it was proved that this process is receptor mediated. The microPET images obtained with <sup>68</sup>Ga-**DOTA-c(RGDfK)** showed a high uptake in tumor 60 minutes after administration. However, high activities were also found in other organs showing an initial high blood concentration and consequent low elimination rate.

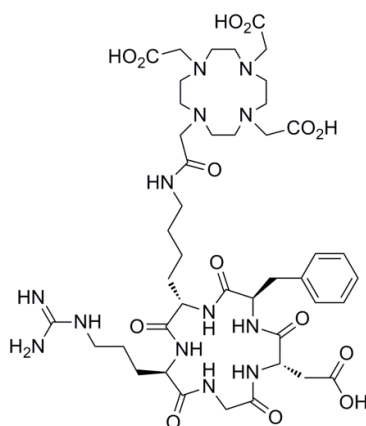


**Figure 1.11:** Structure of DOTA-c(RGDfK).



Despite small and simple DOTA-c(RGD) bioconjugates like **DOTA-c(RGDfK)** have shown interesting features, these agents have low internalization values and unsuitable pharmacokinetics properties to be used as efficient imaging probes. Several DOTA-RGD conjugates have been reported over the recent years,<sup>225</sup> in particular with the (c(RGDyK)) peptide (Figure 1.12). Similarly to <sup>68</sup>Ga-DOTA-c(RGDfK), <sup>64</sup>Cu-DOTA-c(RGDyK) conjugate (1.12a) possess an elevated affinity for cancer cells over-expressing  $\alpha_v\beta_3$  integrin receptors. The <sup>64</sup>Cu-DOTA-c(RGDyK) was tested on an orthotopic MDA-MB-435 breast cancer cell model and showed extended tumor retention compared to the <sup>18</sup>F-benzoate derivative, which showed fast tumor washout rate and elevated hepatobiliary excretion.<sup>226</sup> These results demonstrate that the introduction of the **DOTA** moiety results in profound effects on tumor accumulation and pharmacokinetics, possibly due to changes in the agent overall charge. Despite having better *in vivo* properties compared to the benzoate derivative, <sup>64</sup>Cu-DOTA-c(RGDyK) still suffers from fast tumor washout to be an efficient PET agent. In order to improve the pharmacokinetics, <sup>64</sup>Cu-DOTA-PEG-c(RGDyK) (1.12b) was designed by introducing the poly(ethylene glycol) linker (Mw = 3400) between DOTA and the peptide, since PEGylation is a powerful way to improve many properties of peptides and proteins, such as pharmacokinetics and immunogenicity.<sup>227</sup> The PEG derivative 1.12b was tested on both orthotopic and subcutaneous brain tumor models, and it demonstrated better properties, inducing fast and high tumor accumulation, rapid blood clearance and improved liver and renal accumulation.<sup>219</sup> Chen *et al.*<sup>228</sup> conjugated several RGD-containing peptides with PEG moieties with different sizes, concluding that PEGylation acts differently on the pharmacokinetics, tumor uptake, and retention of RGD peptides, which seems to depend strongly on the nature and size of the PEG moiety. Despite improved liver and renal accumulation, the monomeric agent 1.12b still had somewhat lower tumor uptake and in order to improve the tumor uptake and reduce the liver and kidney uptake, the dimeric agents <sup>64</sup>Cu-DOTA-E[c(RGDyK)]<sub>2</sub> (1.12c) and <sup>64</sup>Cu-DOTA-E[c(RGDfK)]<sub>2</sub> (1.12d) were synthesized and investigated, also by Chen *et al.*<sup>229</sup> As expected, the dimeric peptide 1.12c showed high and specific tumor uptake and better tumor retention than monomeric agents 1.12a and 1.12b, presumably due to the bivalency and increase in molecular size. It is unlikely that two RGD moieties would bind to two adjacent integrin simultaneously. However the binding of one RGD moiety to the integrin will significantly increase the “local concentration” of a second RGD moiety in the surrounding area of the integrin sites.<sup>230</sup> Interestingly,

$^{64}\text{Cu-DOTA-E}[\text{c(RGDyK)}]_2$  showed better *in vivo* kinetics than the phenylalanine derivative,  $^{64}\text{Cu-DOTA-E}[\text{c(RGDfK)}]_2$ , apparently due to the increased hydrophobicity. The introduction of the PEG moiety into the dimeric agent 1.13c, afforded  $^{64}\text{Cu-DOTA-PEG-E}[\text{c(RGDyK)}]_2$  (1.12e), which as expected, showed better pharmacokinetic properties.<sup>231</sup> The two PEG derivatives 1.12b and 1.12e led to PET images of high quality for orthotopic lung cancer tumors, both for primary tumors and small metastatic lesions since their accumulation on normal lung and heart tissue was much reduced. In contrast, with the  $^{18}\text{F-FDG}$  it was only possible to obtain an imaging of the main tumor, whereas metastatic lesions were masked by intense lung and heart uptake.

Since the natural interaction mode between  $\alpha_v\beta_3$  integrins and RGD-containing proteins, such as vitronectin, fibronectin, fibrinogen or lamin can involve multivalent binding sites, the idea of using multivalent cyclic RGD peptides to improve the  $\alpha_v\beta_3$  binding affinity could offer more efficient antagonists with better targeting capability and higher cellular uptake through the integrin-dependent endocytosis pathway.<sup>232</sup> The advantage of the multivalency effect was demonstrated using the tetrameric  $^{64}\text{Cu-DOTA-E}[\text{E}[\text{c(RGDfK)}]_2]_2$  (1.12f), as its receptor binding affinity significantly increased in comparison to the monomeric and dimeric agents 1.12a and 1.12b.<sup>233</sup> This agent also showed excellent properties in female athymic nude mice bearing subcutaneous UG87MG glioma xenografts, with fast blood clearance mainly by renal pathway, together with fast and high tumor uptake and slow washout from cancer cells. Multivalency interactions can be used in such way that weak ligand-receptor interactions may become biologically relevant.<sup>234</sup>

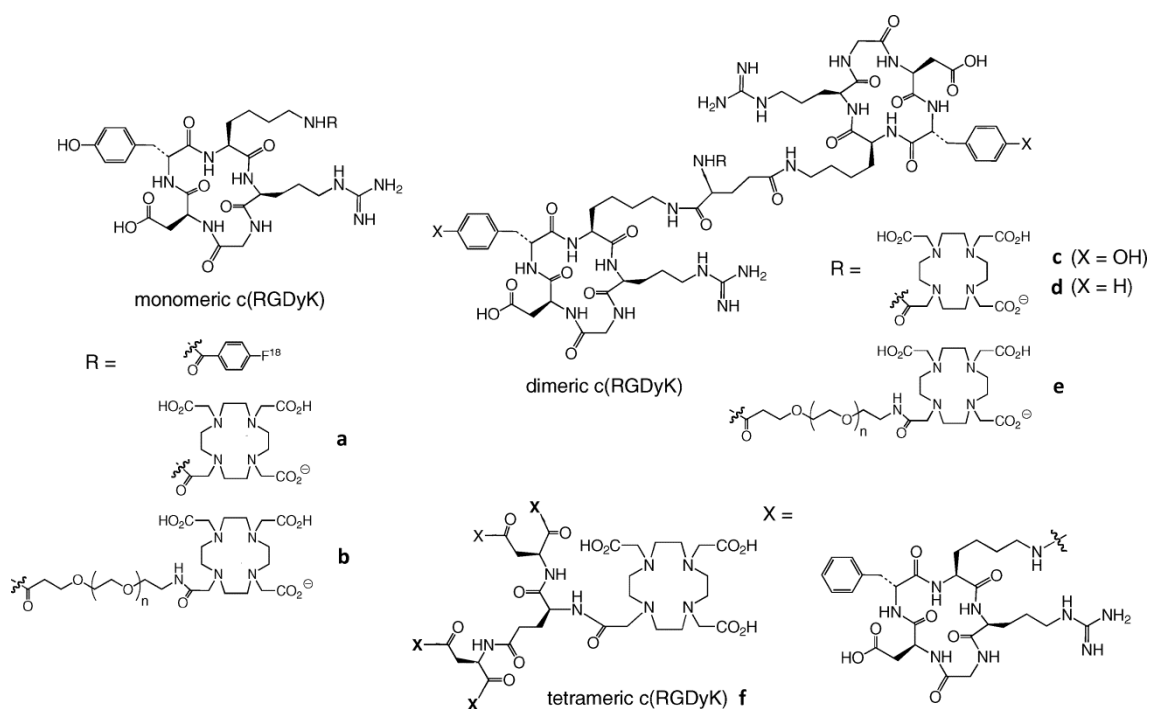


**Figure 1.12:** DOTA-cyclic RGD derivatives as  $\alpha_v\beta_3$  agonists. Adapted from reference 225.

## 1.5 Medical imaging modalities

Over the past decades medical imaging has expanded its role in medical diagnosis. Imaging approaches include both single modality, such as magnetic resonance imaging (MRI), positron emission tomography (PET), single photon emission computed tomography (SPECT) or computed tomography (CT), and also multimodalities such as PET/CT, SPECT/CT or PET/MRI. Among these approaches, MRI and the radionuclide-based PET have been particularly developed and widely used in biomedical research and diagnosis. These molecular imaging modalities are suitable to support personalized medicine by using molecules that can reveal individual biology when coupled with an appropriate imaging approach.<sup>235</sup>

### 1.5.1 Magnetic resonance imaging

Magnetic resonance imaging has become one of the most powerful and used techniques in medicine for soft tissue imaging. In the 1940's, Felix Bloch and Edward Purcell discovered the magnetic resonance phenomenon. For several decades magnetic resonance has been used mainly for studying the chemical structure of compounds. It took more than twenty years for its potential as a diagnostic imaging tool to be shown, when Raymond Damadian observed differences in nuclear magnetic relaxation times of healthy and cancerous tissues. Since then, new technical improvements have been made which make MRI an impressively growing scientific field. Huge advances have been made since the creation of the first images in 1973 to the current state of providing detailed information about both anatomy and function.

This imaging technique is based on the interaction of magnetic fields and radiofrequency waves with water hydrogen nuclei in the human body, relying on their relaxation properties.<sup>126</sup> The intensity of a MRI scan depends on biological tissue properties, such as the density  $[H]$  of the hydrogen nuclei, the blood flow and additionally, on the proton relaxation times ( $T_1$  and  $T_2$ ).

During a MRI scan, the patient is placed in a MR imaging system (Figure 1.13), and subjected to a magnetic field typically in the range of 0.5 to 3 T, which is ten to sixty thousand times the strength of the Earth's magnetic field.

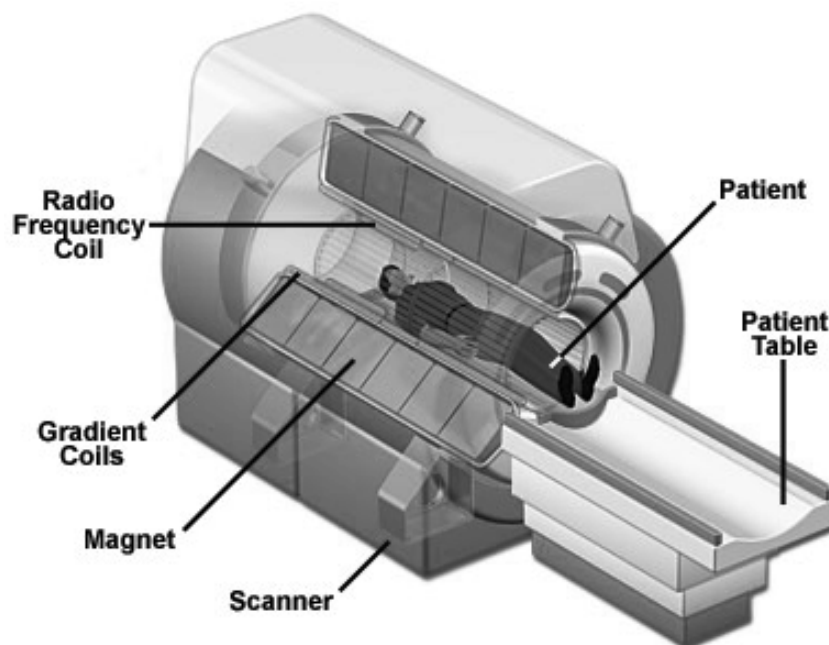


**Figure 1.13:** Representation of a MR imaging system. Adapted from reference 236.

The most common MRI pulse sequence used is the spin-echo sequence and in this case the intensity  $S_{\text{spin-echo}}$  of the signal is given by equation 1.30,<sup>237</sup> where  $[H]$  is the proton density,  $f(v)$  is a flow factor  $t_e$  is the echo time and  $t_r$  is the repetition time.  $t_e$  and  $t_r$  are experimental parameters that can be varied by the operator in order to increase the images' contrast.

$$S_{\text{spin-echo}} = [H]f(v) \left( 1 - 2e^{-\frac{t_r - t_e}{T_1}} + e^{-\frac{t_r}{T_1}} \right) e^{-\frac{t_e}{T_2}} \quad (1.30)$$

MRI allows soft tissue imaging without any predictable hazardous consequences for the patient because this technique does not require the use of nuclear isotopes or ionizing radiation like CT, PET or SPECT. So far neither the radiation employed nor the magnetic fields have been proven to be harmful to living organisms. However, soft tissues have little difference in proton density (not more than 10%) and consequently image intensity weighted with respect to proton density displays low contrast.<sup>126</sup> Sometimes there is the need to administer exogenous chemical paramagnetic substances (contrast agents) to further enhance the contrast between healthy and diseased tissue (Figure 1.14). These contrast agents are paramagnetic compounds, used to shorten the relaxation times of local nuclear spins and according to equation 1.30, they can increase in signal on  $T_1$  weighted images and decrease in signal on  $T_2$  weighted images.

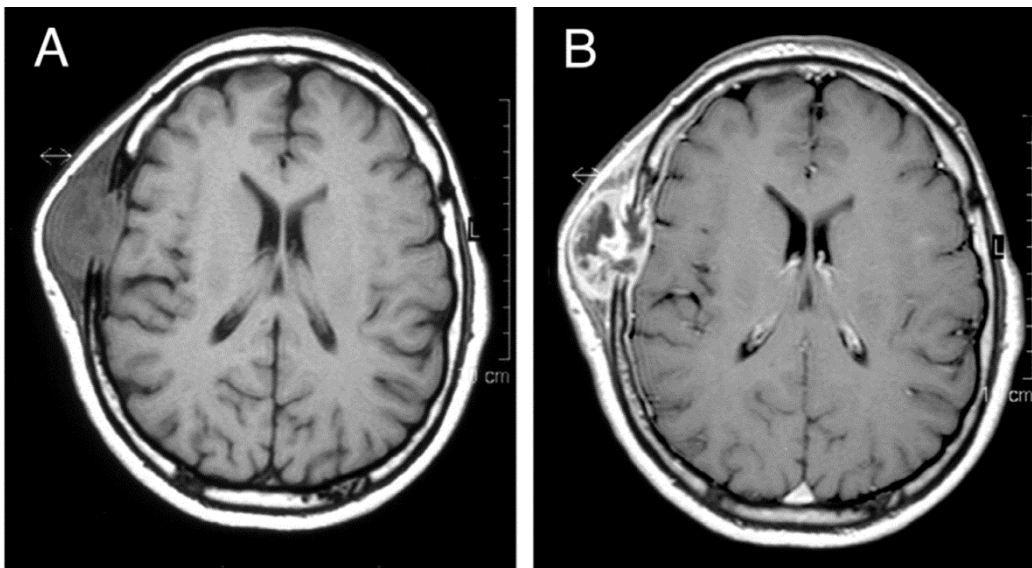


**Figure 1.14:**  $T_1$  weighted MRI of brain before (A) and after (B) gadolinium complex contrast enhancement, showing a metastatic deposit involving the right frontal bon with a large extracranial soft tissue component and meningeal invasion. Adapted from reference 238.

### 1.5.1.1 Contrast agents

Contrast agents (CA) can be divided into two classes, which are the positive enhancers and the susceptibility-effect negative enhancers. Positive enhancers can be metal ions with an elevated magnetic moment, such as Gd(III), Fe(III) or Mn(II), or stable free radicals containing unpaired electrons. At low concentrations, these positive enhancers will affect both  $T_1$  and  $T_2$  in equal manner. However, at high concentrations the  $T_2$  shortening effect of paramagnetic agents predominates over the  $T_1$  shortening effect, and the signal intensity decreases.<sup>239</sup> Negative enhancers are superparamagnetic particles, such as ferromagnetic particles or metal ions (ex: Dy(III)) that induce very large paramagnetic NMR shifts. These compounds can strongly reduce  $T_2$  and thus lead to decreased signal intensity, providing images with “negative contrast”. The effects of superparamagnetic particles on  $T_1$  are comparatively lower compared with the  $T_2$  effects.<sup>239</sup>

Among all paramagnetic relaxivity enhancers, trivalent gadolinium is one of the most effective and the most used for CA production. As stated before, trivalent gadolinium and other metal ions exhibit substantial toxicity in the free form and their administration must be done under the chelate form. The first approved contrast agent for clinical usage was  $[\text{Gd}(\text{DTPA})]^{2-}$  (Magnevist®) in 1983 and since then, the majority of the approved contrast agents are gadolinium chelates. Since almost half of the MRI scans include the use of contrast agents, new agents and applications need to be developed in order to satisfy the increasing market need. To obtain an efficient and safe MRI contrast agent, gadolinium chelates need to fulfill some requirements, such as: a) high kinetic and thermodynamic stability in order to avoid toxicity issues related to possible transmetalation by natural chelators; b) excellent water solubility and low osmolality, providing concentrated solutions in order to reduce the discomfort from injection of high osmolality solutions; c) high relaxivity to avoid the administration of large amounts of contrast agent. This property is an intrinsic characteristic of a paramagnetic complex and it is directly related to the efficiency of the contrast agent; d) specific *in vivo* distribution to provide a strong and localized image of the desired tissue and avoid background image enhancement; and e) the paramagnetic agent should also be excreted within hours of administration.

Nowadays, all gadolinium chelates used clinically are derivatives of either the macrocycle tetraamine **DOTA** or the open chain triamine **DTPA**. In terms of synthesis, the choice of **DOTA** could be less obvious because of the time consuming preparation of 1,4,7,10-tetraazacyclododecane (cyclen). However, more efficient and direct synthetic methods appeared and thus cyclen is now available at a more reasonable price.<sup>240, 241</sup> The tetraaza ring is able to adopt a more stable configuration (square conformation) in which all the lone electronic pairs of the nitrogen are directed towards the metal ion, providing more stable gadolinium complexes than **DTPA**. New low weight DOTA-based macrocycles substituted in the tetraaza cycle or on the acetate arms have been prepared over the past decades in order to effectively chelate trivalent gadolinium and achieve new contrast agents. These chelates have been evaluated *in vitro* and *in vivo* and can be classified according to their biodistribution and tissue specificity.

#### 1.5.1.1.1 Extracellular contrast agents

This class of contrast agents is constituted by low molecular weight nonspecific chelates (Mw < 1 kDa) as they were part of the first generation of MRI contrast agents. These chelates are extracellular fluid (ECF) agents since they equilibrate rapidly between the intravascular and interstitial space, and they do not interact specifically with any type of cells.<sup>242</sup> After intravascular injection, ECF agents are rapidly dispersed between plasma and interstitial spaces with a half-life distribution of about 5 minutes and they are cleared mainly by the kidneys with a half-life elimination of about 80 minutes.<sup>243, 244</sup> Despite some Gd(III) ECF agents have shown utility for angiographic scans, these chelates clear rapidly from the vasculature into the interstitial space which makes the vessel-to-background contrast very limited because of the low relaxivity of the currently available ECF agents. However, these agents are associated with an altered capillary permeability, which allows the selective accumulation of the administered CAs in these regions, such as a brain with a damaged blood brain barrier. Since ECFs have fast renal excretion, they are also useful for evaluating physiological parameters of this organ. Most of the currently available extracellular contrast agents are gadolinium chelates, being some of them DOTA-based compounds (Table 1.11).

**Table 1.11:** Names and structures of commercially Gd-DOTA-based contrast agents. Adapted from reference 242.

Chelate	Commercial Name	Structure	Relaxivity at 37 °C ( $B_0 = 1.0$ T)
[Gd(DOTA)] <sup>-</sup>	Dotarem®		$r_1 = 3.4 \text{ mM}^{-1} \cdot \text{s}^{-1}$
Gd(HP-DO3A)	Prohance®		$r_1 = 3.7 \text{ mM}^{-1} \cdot \text{s}^{-1}$
Gd(BT-DO3A)	Gadovist®		$r_1 = 3.6 \text{ mM}^{-1} \cdot \text{s}^{-1}$

Due to their limited relaxivity values and low imaging enhancement, the development of these low molecular weight CAs with improved relaxivities is highly desirable and several small Gd(III) chelates have been reported over the past years.<sup>87, 245, 246</sup> As stated before, there are several approaches to increase the relaxivity through the optimization of its molecular parameters. The development of molecular constructs containing several gadolinium units is a strategy that has been applied often. It relies on the formation of multinuclear assemblies, either through covalently bound chelates such as multimeric structures,<sup>247-252</sup> linear polymeric structures<sup>250, 253-255</sup> or spherical dendrimers;<sup>256-258</sup> or non-covalently bound chelates such as micelles,<sup>259-262</sup> liposomes,<sup>261, 263-265</sup> or even metal ion-assisted aggregation of gadolinium chelates.<sup>266</sup> To tune this parameter seems to be the most simple and straightforward choice, since  $\tau_R$  values have a direct correlation with the weight and size of the chelate.<sup>267</sup>



Despite showing improvement in relaxivity, large Gd(III)-containing molecular constructs also show some drawbacks. Their elevated size is responsible for the slow leakage from blood vessels to interstitial space through the normal endothelium of vascular systems.<sup>242</sup> This phenomenon provides long imaging windows, but limits their applicability. Their pharmacokinetic profile is also a concern, since these molecules may also be important “targets” for enzymatic systems, which may result in undesired metabolization. Moreover, problems with the excretion of these macromolecular Gd(III) agents are recurrent, since the glomerular filtration can decrease drastically.<sup>268</sup> Alternatively, dimerization can be a straightforward way to obtain CAs with improved relaxivity, without drastically increasing the molecular weight and size.<sup>267, 269, 270</sup> Several DO3A-based binuclear Gd(III)<sup>143, 144, 271</sup> (Figure 1.15) and other Ln(III)<sup>272, 273</sup> chelates are found in the literature. Overall, they present improved relaxivity per metal ion in comparison to  $[\text{Gd}(\text{DOTA})]^-$ , due to optimization of the rotational correlational time. Simultaneously, the dimerization of these Gd(DO3A)-based chelates leads to a decrease of the water exchange rate, limiting the relaxivity values potentially achievable by chelates displaying relatively long  $\tau_R$  values.

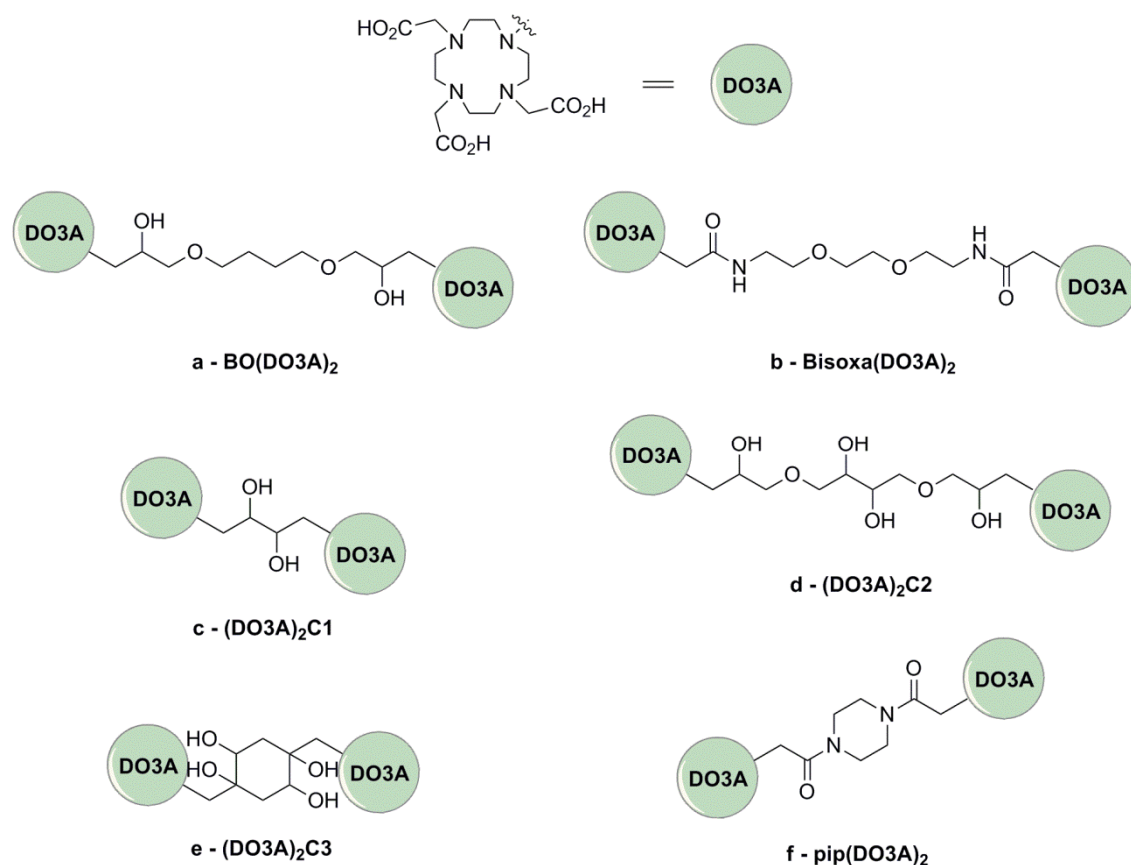


**Figure 1.15:** DO3A-based dimeric ligands for Gd(III).

### **1.5.1.1.2 Blood pool contrast agents**

Magnetic resonance angiography is useful for imaging vascular structures (arteries, arterioles, veins and venules) and angiogenesis diagnosis, which is a pathological state found in development of several diseases, including cancer, hypertension, rheumatoid arthritis and diabetic retinopathy.<sup>274</sup> Intravascular agents, more commonly known blood pool agents (BPA), are designed to image blood vessels in order to detect modifications in the vasculature associated with injuries or diseases like abnormal angiogenesis, embolism, atherosclerosis and hemorrhage.<sup>275</sup> BPA are significantly greater in size and weight than ECF and have higher  $r_1$  relaxivities due to their greater  $\tau_R$  values. Their molecular weight ( $M_w > 20$  kDa) prevents the flow into the interstitium and they remain in the intravascular system for prolonged times compared with conventional ECF. The long intravascular half-life and the elevated  $r_1$  allow vasculature imaging with higher vessel-to-background imaging ratio.<sup>276</sup>

BPA can be divided into different classes, according to their mechanism of action: a) low molecular weight Gd(III) complexes non-covalently bound to human serum albumin (which is the most abundant plasma protein with 4.5% concentration in the blood) prevent the flow into the interstitial space. In this class, several chelates have been synthesized by attaching a hydrophobic moiety to a chelating agent, such as **[Gd(DOTA-BOM<sub>3</sub>)]**,<sup>277</sup> b) macromolecular Gd(III) systems containing polymers with elevated  $M_w$ , able to slow down the CA flow through endothelial pores. Large polymeric agents (15-5000 kDa) based on dextran and polylysine derivatives were evaluated, but they did not pass beyond preclinical trials principally due to the large size, which difficult their excretion,<sup>268</sup> c) systems based on particles involve a change in the elimination route. Supermagnetic iron oxides (SPIOs) are nanoparticles made of stabilized iron oxides with very high  $T_1$  and  $T_2$  relaxivities<sup>278</sup> and very slow flow from the intravascular space due to their large size. However, unlike polymeric Gd(III) chelates, SPIOs are eliminated from body by liver, spleen and lymph nodes uptake and subsequent incorporation into the body's iron pool. This process takes much longer than kidney excretion which results in a long plasma half-life.<sup>279</sup>

### 1.5.1.1.3 Targeted contrast agents

The development of contrast agents with targeting ability for a specific organ or tissue is highly desirable and has been an important goal in recent years. Targeted contrast agents are compounds able to concentrate on specific body compartments, tissues or cells and they are crucial to improve diagnosis accuracy. To achieve tissue specific CAs, these agents can be designed to possess structural properties that will influence their *in vivo* distribution or be able to recognize specific molecular sites, such as cell receptors or transport proteins on cellular membrane.

Several organ-specific contrast agents have been designed and developed over the years, and they can be divided according to the target tissue: a) hepatobiliary agents like  $[\text{Gd}(\text{EOB-DTPA})]\text{Na}_2$  (Primovist®) or  $[\text{Gd}(\text{BOPTA})(\text{MEG})_2]$  (Multihance®) which are small water-soluble paramagnetic chelates for hepatobiliary imaging through hepatocytes uptake.<sup>87</sup> SPIOs can also be used for liver imaging, since after intravenous administration these particles are not retained in hepatocytes, but they are sequestered by normal reticuloendothelial system phagocytic Kupffer cells in liver and spleen;<sup>242</sup> b) lymph nodes and bone marrow like Gadofluorine 8®, which is a lipophilic gadolinium complex that accumulates in normal lymph nodes, but not in metastatic nodes;<sup>280</sup> c) brain agents like  $[\text{Gd}(\text{DTPA})]^{2-}$  coupled with  $A\beta_{1-40}$  peptides (PUTGdA $\beta$ ) that specifically target amyloid deposits responsible for the Alzheimer's disease.<sup>281, 282</sup> Since many brain pathologies result in an altered capillary permeability and blood brain barrier disruption, ECF agents can flow into those brain regions and allow selective accumulation; and d) contrast agents that specifically target cancerous cells through the development of high affinity bioconjugates as targeting vectors and further chelation with trivalent gadolinium. However, the main problem of this approach using Gd(III)-based contrast agents is the MRI's low sensitivity, so that to reach 50% of contrast enhancement it is necessary to have a 0.5 mM local concentration of CA.<sup>242</sup> An example of a possible targeting cell receptor is the endothelial integrin  $\alpha_v\beta_3$ . Detection of tumor angiogenesis *in vivo* using a Gd(III) bioconjugate targeted to  $\alpha_v\beta_3$  has been evaluated.<sup>283</sup> This approach provided enhanced and detailed imaging of rabbit carcinomas by directly targeting paramagnetic agents containing the LM609 monoclonal antibody to the angiogenic vasculature.

### **1.5.2 Positron emission tomography**

Positron emission tomography (PET) is a nuclear medical imaging technique that allows the visualization of locations and levels of radiotracer accumulation, providing three dimensional images of body processes with elevated definition and precision. The concept of emission and transmission tomography was introduced by David Kuhl, Luke Chapman and Roy Edwards in the 1950s. In the same decade, Brownell and Sweet<sup>284</sup> developed the first device to obtain images using the detection of  $\gamma$ -rays emitted from positron-electron annihilation events. However, it was only in the 1970s that the technique took a major leap with the introduction of tomographic systems and computer analysis, which paved the way for widespread clinical use of the modality.

In PET, the image acquisition is based on  $\gamma$ -ray acquisition from positron-electron annihilation. The process starts when a positron ( $\beta^+$ ) released by a decaying radionuclide travels in a tissue until it has exhausted its kinetic energy. At this point, it will encounter its antiparticle (electron –  $\beta^-$ ) and the two will mutually annihilate completely, converting their mass into two 511 keV  $\gamma$ -rays that travel 180° relative to each other. The  $\gamma$ -rays originated by the particle-antiparticle annihilation will travel until strike the PET detectors. The continuous emission of  $\beta^+$  particles by the radioisotope allows a constant  $\gamma$ -rays flow, which after being detected and analyzed will provide a 3D image. Depending on the scan and tissue specificity, the radioisotope can be injected intravenously, inhaled in the form of gas or taken orally in form of solution or pills. The PET imaging system (Figure 1.16) consists in two main sections, the patient table and the  $\gamma$ -ray chamber. The patient table is a movable part and allows the technician to move the patient on the horizontal to place the body at the site of interest. The  $\gamma$ -ray detector in the  $\gamma$ -ray chamber is composed by Na(Tl), BaF<sub>2</sub>, LaBr<sub>3</sub> or CsI(Tl) salts, where the detected  $\gamma$ -rays are transformed in electrical pulses by photomultipliers.<sup>285</sup> Then, the data are collected and processed, providing the final image.

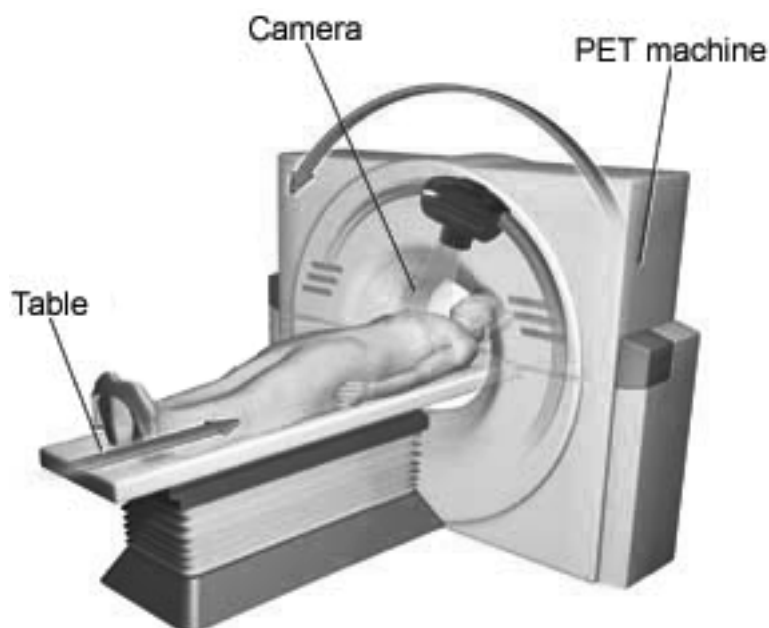


**Figure 1.16:** Representation of the PET imaging system. Adapted from reference 286.

As main advantages of this technique it can be stressed: a) the ability to obtain images with elevated quantification potential and high spatial resolution (2-3 mm); b) the elevated sensibility (requires tracer concentrations of  $10^{-8}$  M); and c) it is a non-invasive technique, not requiring any explorative procedure. Unlike other imaging techniques such as MRI, PET scans are less directed to the anatomical and structural observation and focus more on physiological description of biological processes, such as metabolic rates. High intensity areas are designated “hot spots” and indicate tissues where high amounts of isotope are accumulated, which may result in a higher metabolic activity. In contrast, low intensity areas are designated “cold spots” and indicate lower concentrations of radioisotope and therefore less chemical activity.

As main disadvantages of this technique it can be stressed: a) the administration of a radioactive agent, which despite being in very small doses can affect normal cell metabolism; b) in some cases patients can suffer excessive exposure to the  $\gamma$  radiation due to the elevated half-lifetime of the radioisotopes used; c) oppositely, when the radioisotopes have a low half-lifetime compatible for PET scans it may be difficult to obtain quality images, because when the probe reaches and accumulates in the desired tissue, the radioisotope has already decayed significantly; d) intravenously administration of the radioisotope probe can cause pain, skin irritation and in extreme cases can even cause severe allergic reactions; e) these scans can also give false results if the chemical balance in the body is out of the normal, especially in cases of patients

with diabetes or in patients who may have ingested food hours before examination, changing the concentration of blood sugar and insulin. This type of complications are usually associated with the use of radiopharmaceutical agents based on glucose and labeled with  $^{11}\text{C}$  or  $^{18}\text{F}$ , like [ $^{18}\text{F}$ ]-fluorodeoxyglucose; and f) in some situations, PET scans may be too expensive because certain isotopes used in the PET imaging must be generated in nuclear reactors or cyclotrons.

Since the advent of PET in clinic and medical research, a number of positron-emitting isotopes have been developed for application as radiopharmaceuticals. For years, this field was dominated by small molecule tracers, whose short biological half-lives favor the use of non-metallic radionuclides such as  $^{11}\text{C}$ ,  $^{18}\text{F}$  or  $^{124}\text{I}$  (Table 1.12). [ $^{18}\text{F}$ ]-fluorodeoxyglucose is one of the few FDA-approved PET radiopharmaceuticals employed in oncology, commonly used for myocardial perfusion scans.<sup>164</sup> Despite significant success, these small molecule probes labeled with non-metallic isotopes possess some limitations such as: a) short half-lives of the most common non-metallic radionuclides ( $^{11}\text{C}$  and  $^{18}\text{F}$ ) allow only the imaging of biological processes in the order of minutes using tracers with fast pharmacokinetic profiles; b) these short half-life radioisotopes often require demanding and complex synthetic procedures in order to incorporate the isotope into the tracers core, rather than in an appended chelator; and c) most short-life isotopes require a facility with a cyclotron facility for its production, because on its absence, the radionuclide will undergo many half-lives of decay while in circulation. This is simply not an option for many research and medical facilities, given the resources required for construction and operation of medical cyclotrons.

These limitations have been brought into focus by the increasing development of biomolecular targeting agents for different tissues. Given the enormous potential of biomolecular imaging agents, significant effort has been made in to the production, purification and radiochemistry of positron-emitting metal radioisotopes, such as  $^{68}\text{Ga}$ ,  $^{64}\text{Cu}$  or  $^{89}\text{Zr}$  (Table 1.12). These radioisotopes have appropriate radioactive half-lives to the PET scan timescale and all may form stable chelates that may be employed for radiolabelling biomolecules.

**Table 1.12:** Nuclear parameters of useful PET radionuclides. Adapted from reference 164.

Radionuclide	Half-Lifetime	Decay Mode	Production	E( $\beta^+$ ) (keV)	E( $\gamma$ ) (keV)
$^{11}\text{C}$	1223.1 s	$\beta^+$ (100.0)	$^{14}\text{N}(p,a)$	385.6	511.0
$^{18}\text{F}$	109.77 min	$\beta^+$ (100.0)	$^{18}\text{O}(p,n)$ $^{20}\text{Ne}(d,a)$	249.8	511.0
$^{124}\text{I}$	4.1760 d	$\beta^+$ (22.7) $\gamma$ (77.3)	$^{124}\text{Te}(p,n)$	687.04 974.74	511.0; 602.7; 722.8; 1691.0
$^{64}\text{Cu}$	12.701 h	$\gamma + \beta^+$ (61.5) $\beta^-$ (38.5)	$^{64}\text{Ni}(p,n)$	278.21	511.0
$^{68}\text{Ga}$	67.71 min	$\beta^+$ (89.14) $\gamma$ (10.86)	$^{68}\text{Ge}/^{68}\text{Ga}$	836.02	511.0
$^{89}\text{Zr}$	78.4 h	$\beta^+$ (22.74) $\gamma$ (77.26)	$^{89}\text{Y}(p,n)$	395.5	511.0 909.2

### 1.5.3 Single photon emission computed tomography

Single photon emission computed tomography (SPECT), like the PET technique, is based on the detection of  $\gamma$  radiation to produce body images. However, contrary to PET, in this technique, the  $\gamma$  radiation is directly detected from a  $\gamma$ -ray emitting radionuclide. The radioisotopes used in SPECT possess different emission energies ranging between 90 keV and 300 keV (Table 1.13). The most used radionuclide in this technique is  $^{99\text{m}}\text{Tc}$  that decays by isomeric transition. However, isotopes that decay by electron capture, such as  $^{67}\text{Ga}$ ,  $^{111}\text{In}$  or  $^{201}\text{Tl}$  also possess suitable energetic features to be used in SPECT scans. This technique was developed in the 1950s and served as the starting point for the PET development, since the latter has appeared in subsequent decades as a technique more detailed and accurate than SPECT.

**Table 1.13:** Nuclear parameters of useful SPECT radionuclides. Adapted from reference 287.

Radionuclide	Half-Lifetime	Decay Mode	Production	E( $\gamma$ ) (keV)
$^{67}\text{Ga}$	78.3 h	Electron Capture	Generator	93 (10%); 185 (24%); 296 (22%)
$^{99\text{m}}\text{Tc}$	6.02 h	Isomeric Transition	Generator	141 (89%)
$^{111}\text{In}$	2.83 d	Electron Capture	Cyclotron	171 (88%); 247 (94%);

In instrumental terms, the principles and methods applied to SPECT are quite similar to PET. However, SPECT has some limitations with respect to PET, since its  $\gamma$ -chambers have detection systems more advanced and can detect radiation simultaneously in an angle of  $360^\circ$ , while the SPECT  $\gamma$ -chambers need to rotate around the body to obtain 3D images. Although both techniques are very useful, SPECT has some limitations because it is less sensible (requires tracer concentrations of  $10^{-6}$  M), and has limited quantification potential and spatial resolution (6-8 mm) compared to PET, requiring greater isotope amounts in order to achieve high quality images. The disadvantages of this technique are essentially the same mentioned above for PET, from which it can be stressed the use of a radioactive isotope, potentially harmful to health and sometimes with low viability in economic terms.



## 1.6 Objective of the thesis

Over the past decades, medical imaging has expanded its role in medicine. Its modalities, such as MRI and the radionuclide-based imaging techniques (PET and SPECT) have become essential tools for the diagnosis of several pathologies. Contrary to nuclear imaging modalities, the MRI technique does not require the administration of external radiopharmaceutical agents for imaging acquisition. However, almost half of the MRI scans are performed with paramagnetic contrast agents in order to obtain images with improved contrast and definition. Nowadays, there is a strong need to obtain new effectiveness imaging probes (contrast agents and radiopharmaceuticals) with targeting ability that may be able to produce enhanced images. The work developed during this thesis aimed to address some of these objectives, namely the synthesis and evaluation of imaging probes for MRI, PET and SPECT modalities. To reach those objectives, we proposed to:

- a) Synthesize new DOTA and DO3A-based bifunctional chelators able to chelate different metal ions (Ga(III) and Gd(III)) with high kinetic and thermodynamic stability;
- b) Obtain new Gd(III) contrast agents with improved relaxivity through the dimerization and PEGylation reactions with the bifunctional prochelators;
- c) Synthesize cyclic RGD peptides using a combined solution and solid phase strategy;
- d) Develop a general strategy for the cyclic RGD peptide-prochelator coupling in order to obtain bioconjugates for peptide receptor mediated imaging;
- e) Study the structure and solution dynamics of the Ln(III) (Ln = Pr, Nd, Eu, Sm, and Yb) chelates by NMR spectroscopy;
- f) Study the Gd(III) chelates in aqueous solution, which includes the determination of the relaxivity ruling parameters through NMRD and  $^{17}\text{O}$  NMR spectroscopy;
- g) *In vitro* and *in vivo* studies of  $^{67}\text{Ga}$ (III)-labelled conjugates, including determination of LogP of conjugates, protein association studies and biodistribution studies in animal models.



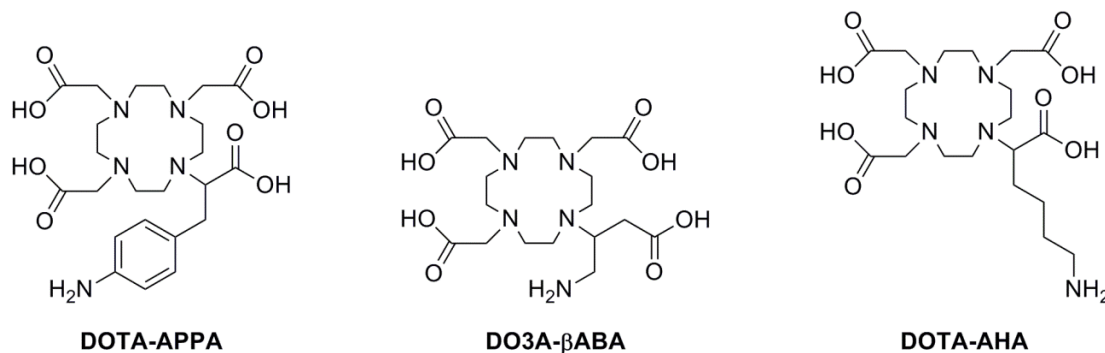
# **2 Results and Discussion**



## 2.1 Synthesis

### 2.1.1 Synthesis of the bifunctional chelators

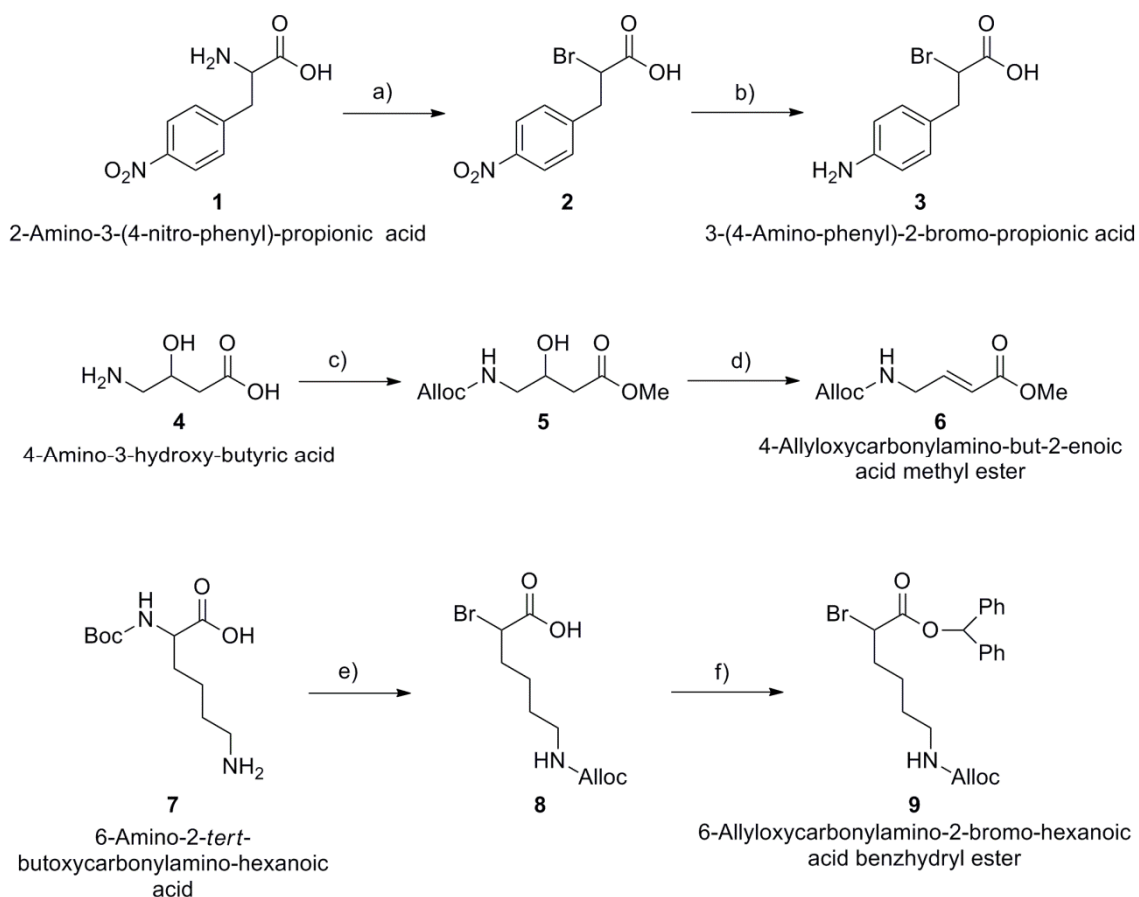
Three bifunctional chelators were designed and their synthesis attempted (Scheme 2.1).



**Scheme 2.1:** Structures of the bifunctional chelators DOTA-APPA, DOTA-βABA and DOTA-AHA.

The synthetic strategy planned for the preparation of these compounds from 1,4,7,10-tetraazacyclododecane (cyclen) involved two alkylation reactions: a mono-alkylation between the cyclen and a bifunctional moiety (2-bromo-3-(4-aminophenyl)propanoic acid – **DOTA-APPA**; 4-amino-3-butenic acid – **DO3A-βABA** and 6-amino-2-bromohexanoic acid – **DOTA-AHA**) and the alkylation of the other three cyclen amines with *tert*-butyl bromoacetate.

The methodologies proposed for the synthesis of the bifunctional residues from 3-(4-nitrophenyl)propanoic acid, 4-amino-3-hydroxybutyric acid (GABOB) and 6-amino-*tert*-butoxycarbonylamino-hexanoic acid are shown in Scheme 2.2.



**Scheme 2.2:** Synthetic methodologies proposed for the preparation of the bifunctional residues **3**, **6** and **9**.  
**a)** NaBr, NaNO<sub>2</sub>, HBr; **b)** reduction; **c)** 1. allyl chloroformate, Na<sub>2</sub>CO<sub>3</sub>; 2. SOCl<sub>2</sub>, MeOH; **d)** 1. Boc<sub>2</sub>O, DMAP, 2. TMG; **e)** 1. allyl chloroformate, Na<sub>2</sub>CO<sub>3</sub>, 2. TFA, 3. NaBr, NaNO<sub>2</sub>, HBr; **f)** DDM, Me<sub>2</sub>CO.

The synthesis of 3-(4-amino-phenyl)-2-bromo-propionic acid, **3** started with the reaction of 2-amino-3-(4-nitrophenyl)propionic acid with sodium bromide and sodium nitrite in HBr. Compound **2** was isolated as an oil in a 73 % yield. The reduction of the nitro group of compound **2** was attempted using several methods (hydrogen in the presence of a catalyst, ammonium formate and 1,4-cyclohexadiene in Pd/C), however in all cases the only product isolated was the 3-(4-aminophenyl)propionic acid. Since it was impossible to obtain compound **3**, the synthesis of the **DOTA-APPA** chelator was unfeasible.

In the case of **DO3A-βABA** the bifunctional arm was prepared from 4-amino-3-hydroxybutyric acid (GABOB), **4**. The amine and carboxylic acid functions of this non-natural amino acid were protected with the allyloxycarbonyl group (Alloc) and as a methyl ester, respectively. The methyl ester of 4-amino(Alloc)-3-hydroxybutanoic acid, **5** was dehydrated using a methodology developed in our research group with di-*tert*-

butyl dicarbonate (Boc<sub>2</sub>O) and 4-dimethylaminopyridine (DMAP) followed by 1,1,3,3-tetramethylguanidine (TMG).<sup>288</sup> In this reaction the hydroxyl group is converted into a good leaving group in the presence of Boc<sub>2</sub>O and using DMAP as catalyst and then a base (TMG) is added to promote elimination. <sup>1</sup>H NMR spectra of the reaction mixture showed the formation of two isomers, the major isomer was the methyl ester of 4-amino(Alloc)but-3(*E*)-enoate and the minor isomer was the desired product, compound **6**. Thus, the reaction conditions were optimized (amount of TMG and reaction time) in order to obtain as the major isomer, the methyl ester of 4-amino(Alloc)but-2(*E*)-enoate. It was also found that using an excess of Boc<sub>2</sub>O, the only isomer isolated was the methyl ester of 4-amino(Alloc, Boc)but-2(*E*)-enoate in a 90% yield. The latter and compound **6** were used as substrates in a Michael addition reaction with the cyclen and although several bases were tested it was impossible to isolate the mono-alkylated cyclen.

The synthesis of the bifunctional arm of **DOTA-AHA** started with the *tert*-butoxycarbonyl lysine (Boc-Lys-OH). The first step was the protection of the amino function in the side chain of lysine with Alloc. After cleavage of Boc, bromination afforded the 6-allyloxycarbonylamino-2-bromo-hexanoic acid, **8**. The carboxylic acid function of this last compound was protected as a benzhydryl ester giving compound **9** (Scheme 2.2). Figure 2.1 shows the <sup>1</sup>H NMR spectrum of compound **9**. It is possible to observe the signals of the benzhydryl and alloc protecting groups as well the α-C proton as a triplet at 4.69 ppm.

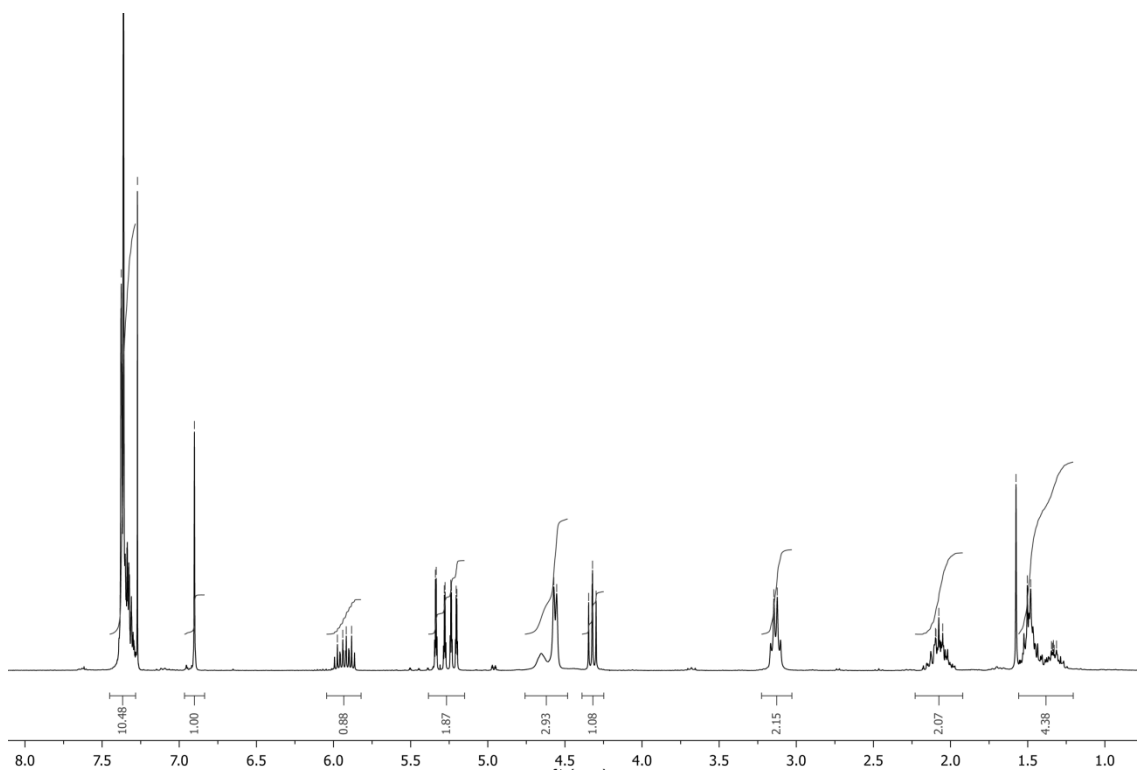
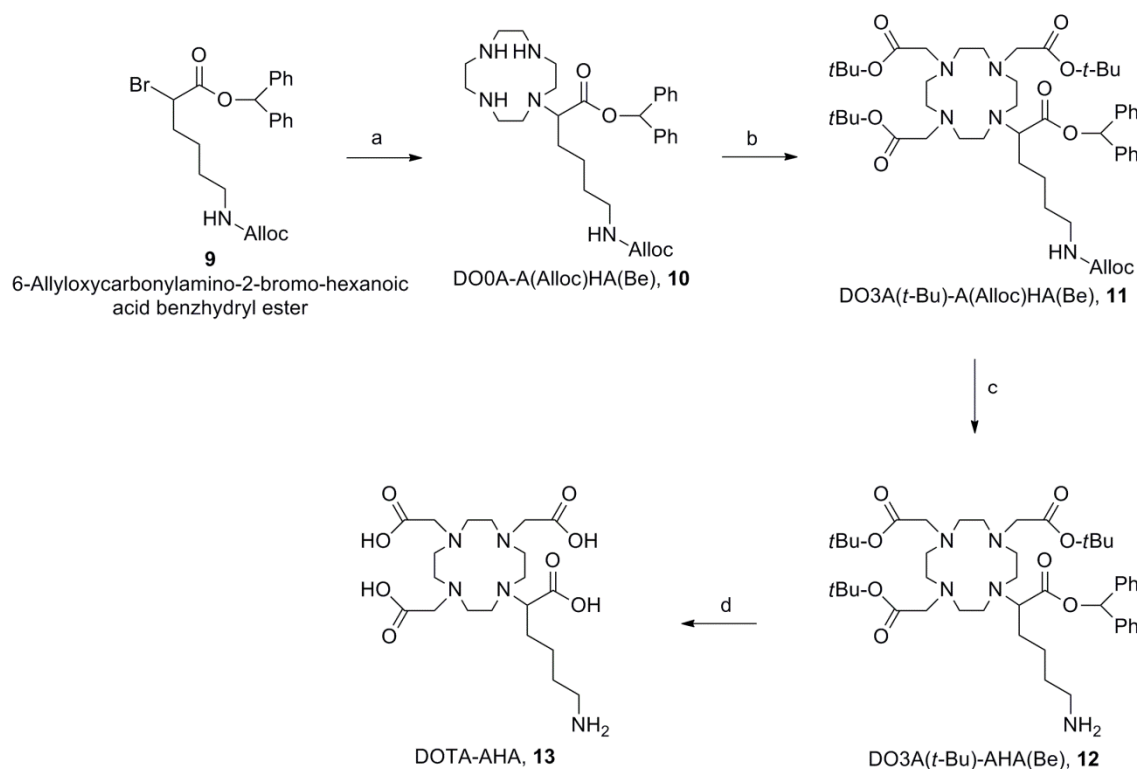


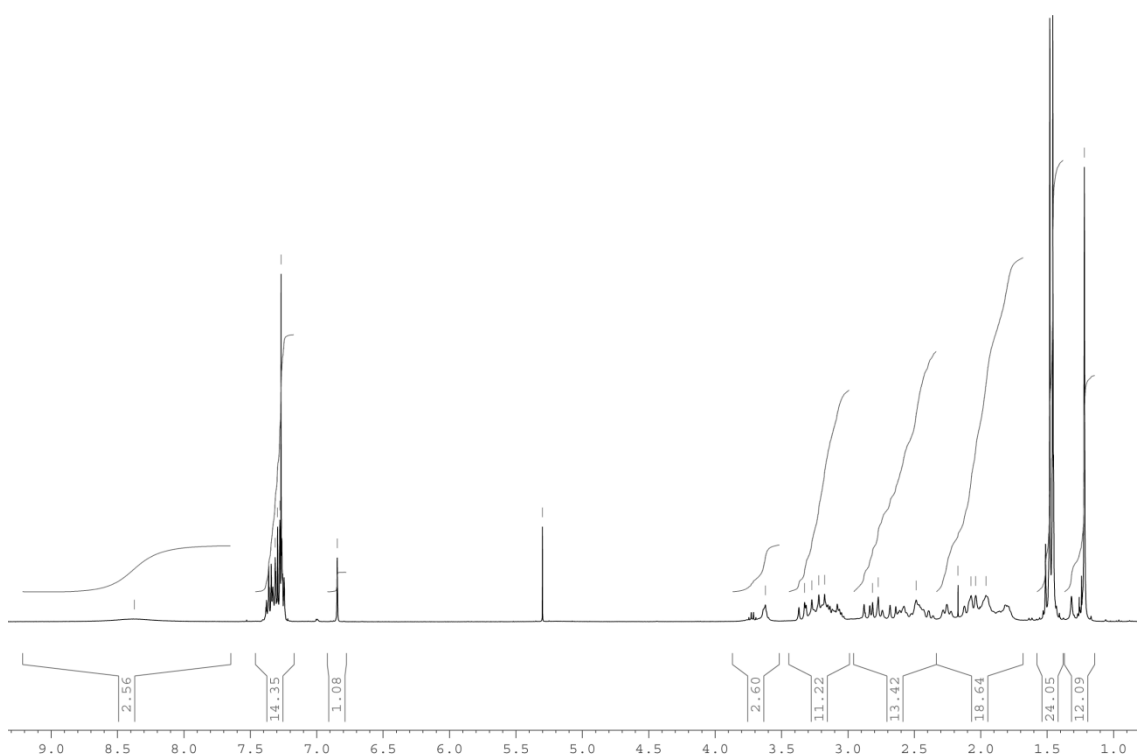
**Figure 2.1:**  $^1\text{H}$  NMR spectrum at 400 MHz of compound **9** in  $\text{CDCl}_3$ .

The cyclen was mono-alkylated with compound **9** and tri-alkylated with *tert*-butyl bromoacetate to give the pro-ligand  $\text{DO3A}(t\text{-Bu})\text{-A}(\text{Alloc})\text{HA}(\text{Be})$  (Scheme 2.3). In order to link this compound to a vectorizing agent it was necessary to remove the Alloc group using tetrakis(triphenylphosphine)palladium(0) in the presence of a scavenger (borane complex) (Scheme 2.3). Figure 2.2 shows the  $^1\text{H}$  NMR spectrum of compound **12**. It is possible to observe the signal from the benzhydryl proton as a singlet with a chemical shift of 6.81 ppm. The aromatic protons from the benzhydryl protecting group appear as a multiplet between 7.25 and 7.45 ppm. After cleavage of the benzhydryl ester, the chelator **DOTA-AHA** was obtained in good yield.



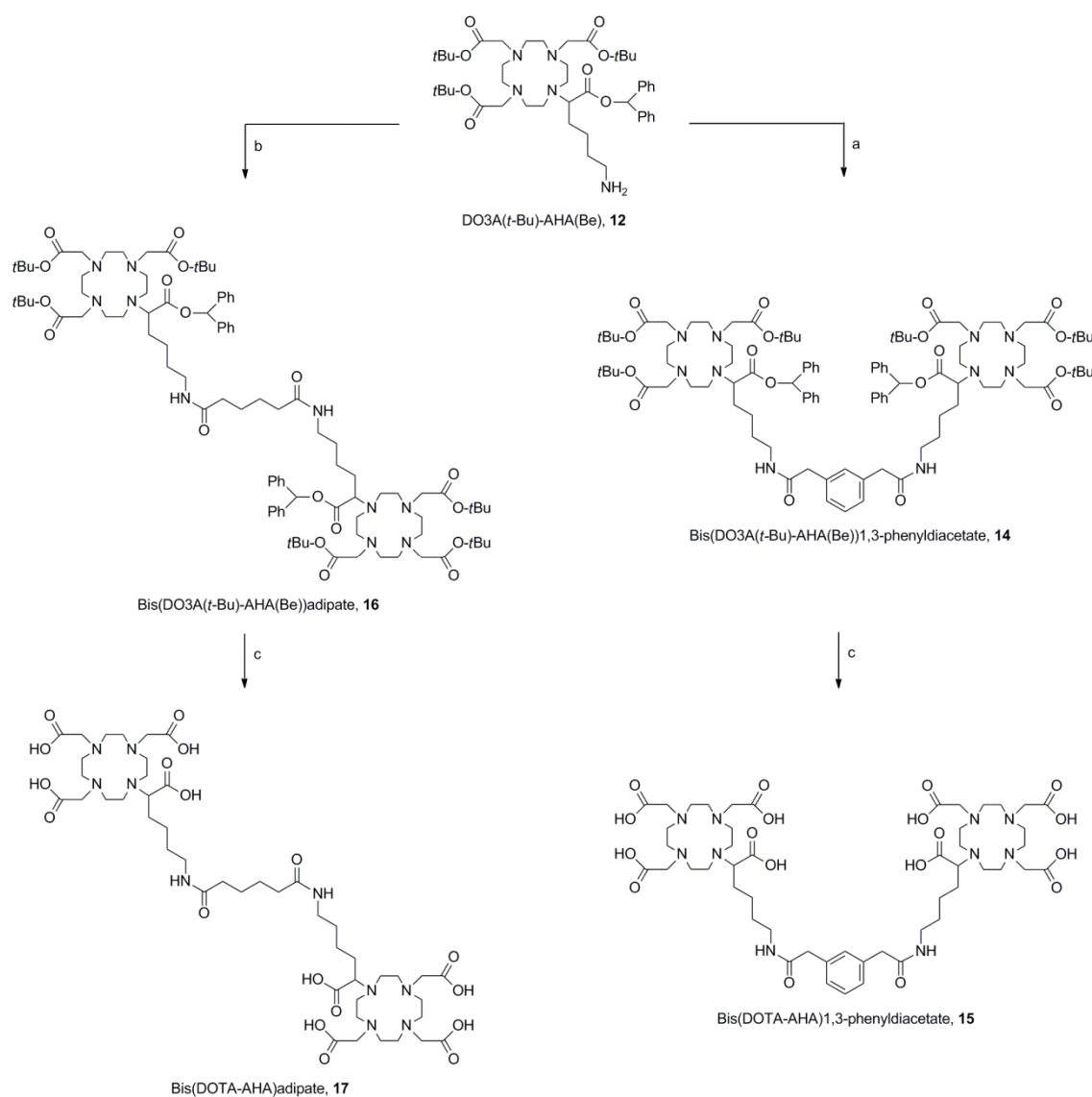


**Scheme 2.3:** Synthesis of DOTA-AHA, 13. **a)** cyclen,  $K_2CO_3$ , MeCN; **b)** *tert*-butyl bromoacetate,  $K_2CO_3$ , MeCN; **c)**  $Pd(PPh_3)_4$ ,  $Me_2NH \cdot BH_3$ ; **d)** TFA, DCM.



## 2.1.2 Synthesis of DOTA-AHA conjugates

The **DOTA-AHA** pro-chelator was reacted with two dicarboxylic acids in order to obtain molecules with two **DOTA-AHA** units. Thus adipic acid and 1,3-phenyldiacetic acid were reacted with DO3A(*t*-Bu)-A(Alloc)HA(Be) in the presence HATU, HOBt and DIPEA to give the corresponding dimmers in 96% and 86 % yield (Scheme 2.4). Figure 2.3 shows the  $^1\text{H}$  NMR spectrum of compound **14**. The two  $\text{CH}_2$  protons from the linker appear as singlets at 3.49 ppm.



**Scheme 2.4:** Synthesis of DOTA-AHA dimers, **15** and **17**. **a)** 1,3-phenyldiacetic acid, DIPEA, HATU, HOBt, MeCN; **b)** adipic acid, DIPEA, HATU, HOBt, MeCN; **c)** TFA, DCM.

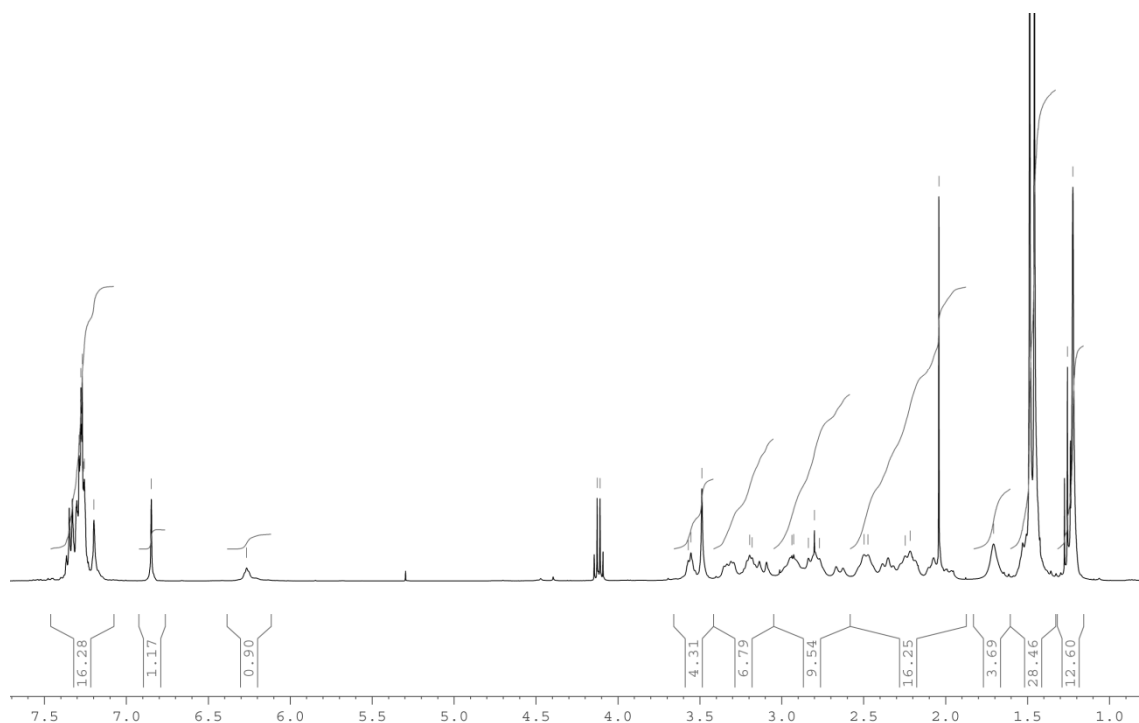
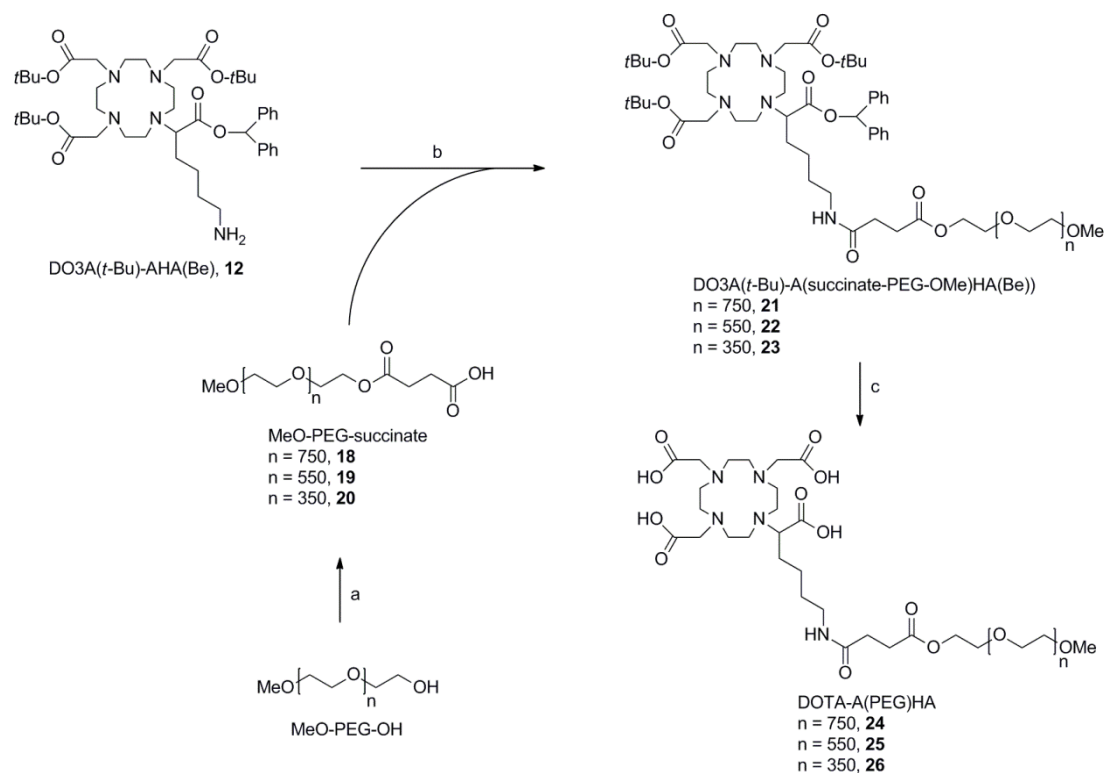


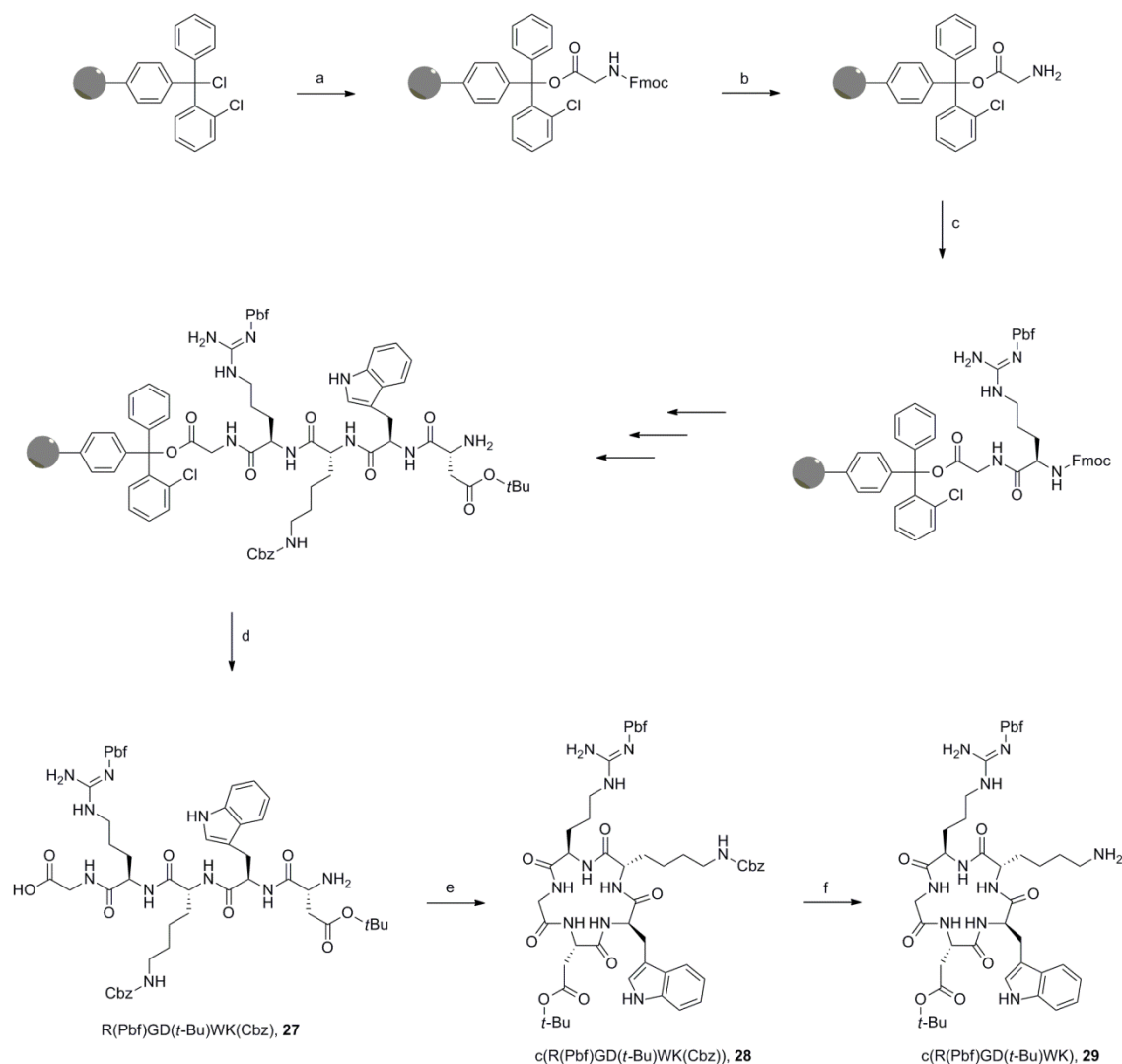
**Figure 2.3:**  $^1\text{H}$  NMR spectrum at 400 MHz of compound **14** in  $\text{CDCl}_3$ .

PEGylated **DOTA-AHA** conjugates were obtained by reacting **DO3A(*t*-Bu)-A(Alloc)HA(Be)** with PEG derivatives using HATU as coupling reagent (Scheme 2.5).



**Scheme 2.5:** Synthesis of **DOTA-AHA** PEGylated conjugates. **a)** succinic anhydride,  $\text{CHCl}_3$ ,  $\text{H}_2\text{SO}_4$  (95%); **b)** DIPEA, HATU, HOBT, MeCN; **c)** TFA, DCM.

**DOTA-AHA** pro-chelator was conjugated with a cyclic peptide with the sequence Arg-Gly-Asp-Trp-Lys (RGDWK). This peptide was prepared by solid phase using a 2-chlorotritylchloride resin and a fluorenylmethoxycarbonyl (Fmoc) strategy. The side-chain protecting groups of arginine, aspartic acid lysine were 2,2,4,6,7-pentamethyldihydrobenzofuran-5-sulfonyl (Pbf), *tert*-butyl ester (*t*-Bu) and carboxybenzyl (Cbz), respectively. Figure 2.4 shows the  $^1\text{H}$  NMR spectrum of compound **27**. The cyclization step was carried out in solution with HBTU as coupling reagent (Scheme 2.6).



**Scheme 2.6:** Synthesis of  $\text{c(R(Pbf)GD(t-Bu)WK)}$  peptide. **a)** Loading of the resin: Fmoc-Gly-OH, DIPEA, DCM; **b)** Deprotection: 20% Piperidine/DMF; **c)** Coupling: Fmoc-Arg(Pbf)-OH, DIC, HOBT, DMF; **d)** Cleavage from resin: AcOH, TFE, DCM; **e)** Cyclization: HBTU, DIPEA, DMF; **f)** Deprotection:  $\text{H}_2$ , Pd/C (10%), DCM/EtOH (7:3).

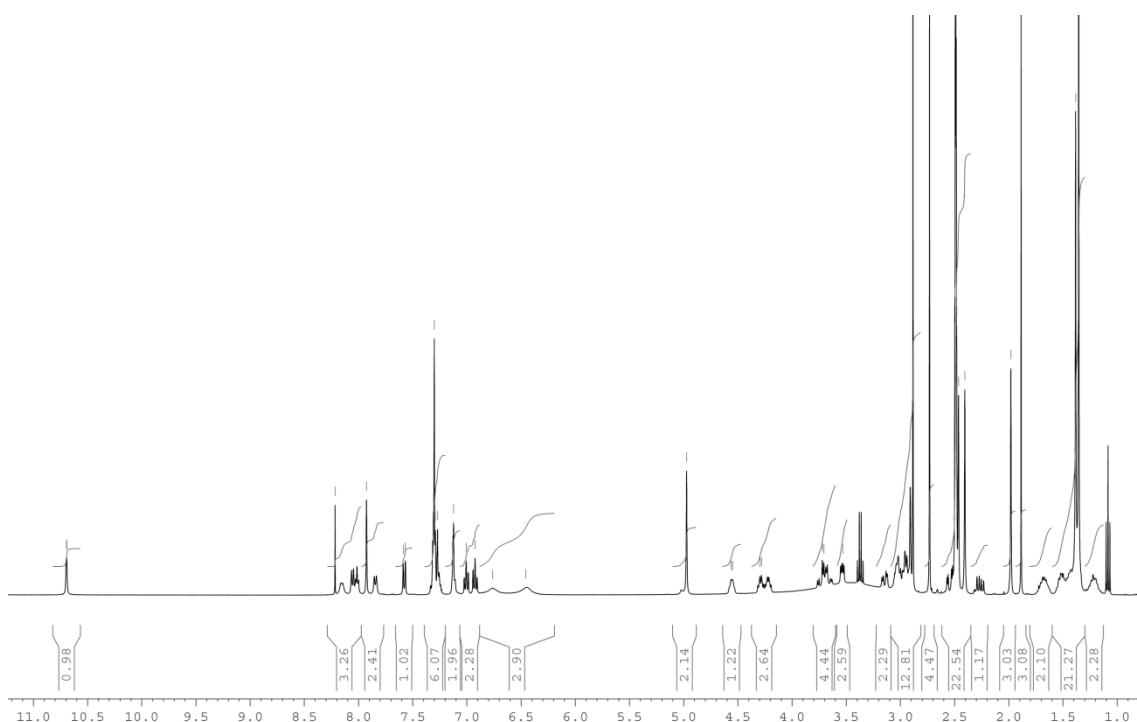
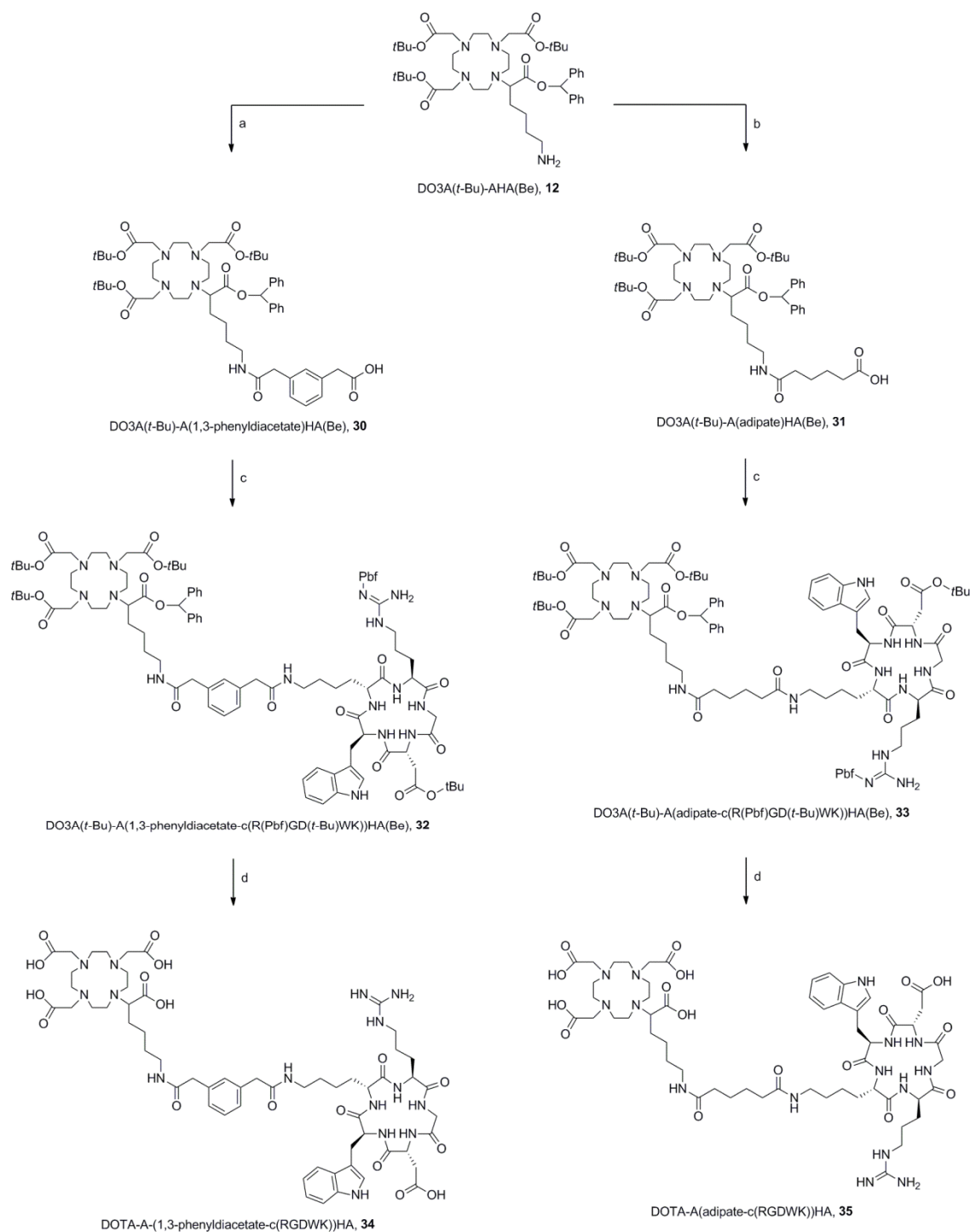


**Figure 2.4:** <sup>1</sup>H NMR spectrum at 400 MHz of compound 27 in DMSO.

Selective cleavage of the Cbz group allowed the coupling of the peptide with **DOTA-AHA** derivatives to give **DOTA-A(linker-c(RGDWK)HA)** conjugates. The **DOTA-AHA** derivatives were prepared from the pro-ligand **DO3A(*t*-Bu)-AHA(Be)** (Scheme 2.7).



**Scheme 2.7:** Synthesis of DOTA-AHA bioconjugates with c(RGDWK). **a**) 1,3-phenyldiacetic acid, DIPEA, HATU, HOBt, MeCN; **b**) adipic acid, DIPEA, HATU, HOBt, MeCN; **c**) c(R(Pbf)GD(*t*-Bu)WK), DIPEA, HATU, HOBt, DMF; **d**) TFA, DCM.

## 2.2 Temperature dependence and kinetic stability studies of Gd(DOTA-AHA) and [Gd(DOTA-A(PEG<sub>750</sub>)HA)]<sup>-</sup> chelates

The temperature dependence of the longitudinal proton relaxation rates of Gd(DOTA-AHA) and its PEG derivative [Gd(DOTA-A(PEG<sub>750</sub>)HA)]<sup>-</sup> was evaluated through relaxometric determinations at 20 MHz. A relaxometric study was also performed in order to evaluate the kinetic stability of both chelates.

The longitudinal proton relaxation rates were measured at eleven different temperatures (Figure 2.5). The results show that  $R_1$  is inversely proportional to the temperature, since longitudinal proton relaxation rates decrease with the temperature increasing. This result is consistent with a dominating effect of chelates' rotational correlation time over relaxivity at this Larmor frequency.

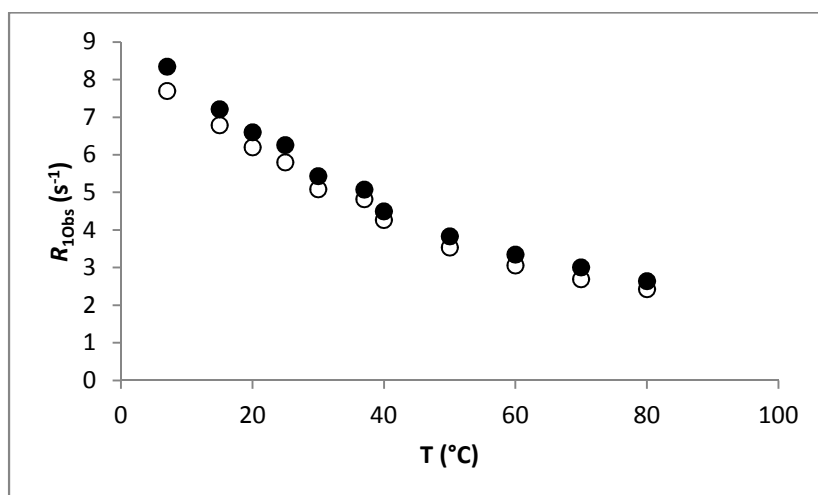


**Figure 2.5:** Dependency of longitudinal proton paramagnetic relaxation rate ( $R_{1\text{obs}}$ ) at 20 MHz and pH = 7.0 on the temperature for Gd(DOTA-AHA) (empty symbols) and [Gd(DOTA-A(PEG<sub>750</sub>)HA)]<sup>-</sup> (filled symbols) solutions.

As shown in Figure 2.6, the chelates present high stability against acid and base catalysed hydrolysis, according to the non-variance of the  $R_1$  values over a wide range of pH values.

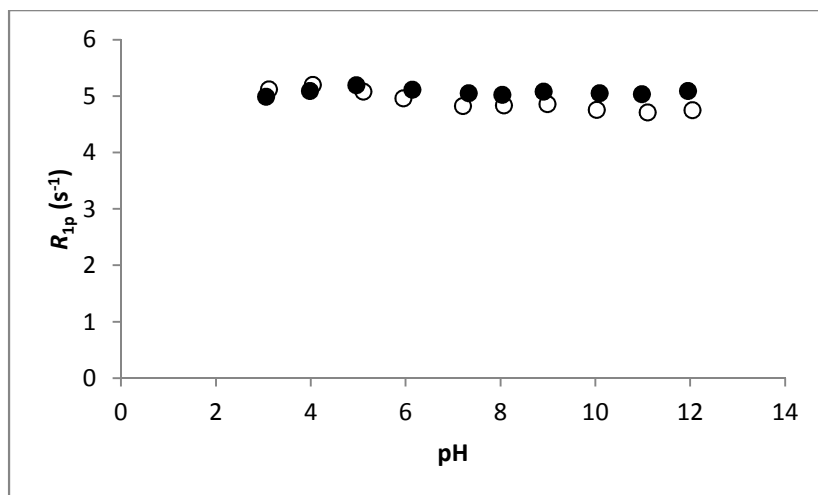


**Figure 2.6:** Dependency of longitudinal proton paramagnetic relaxation rate ( $R_{1p}$ ) at 20 MHz and 25 °C on the pH for Gd(DOTA-AHA) (empty symbols) and  $[Gd(DOTA-A(PEG_{750})HA)]^-$  (filled symbols) solutions.

**Gd(DOTA-AHA)** also shows to be kinetically inert to transmetalation. In the presence of one equimolar of Zn(II), no significant variation in the longitudinal proton relaxation rates was found over a period of 48 hours when compared to the relaxivity of chelator solution absent of zinc ion (Figure 2.7).

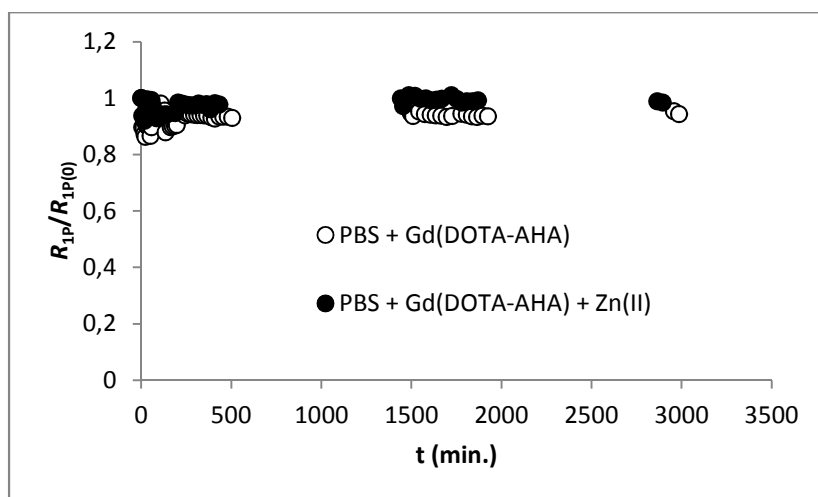


**Figure 2.7:** Time evolution of the relative longitudinal proton paramagnetic relaxation rate ( $R_{1p}(t)/R_{1p}(0)$ ) at 20 MHz and 37 °C for Gd(DOTA-AHA) + PBS solution (filled symbols) and Gd(DOTA-AHA) + PBS + Zn(II) solution (empty symbols).



## 2.3 $^1\text{H}$ NMRD and $^{17}\text{O}$ NMR relaxometric studies

In order to obtain parameters characterizing the efficiency of water relaxation enhancement of the chelates **Gd(DOTA-AHA)**, **[Gd<sub>2</sub>(Bis(DOTA-AHA)adipate)]<sup>2-</sup>**, **[Gd<sub>2</sub>(Bis(DOTA-AHA)1,3-phenyldiacetate)]<sup>2-</sup>** and **[Gd(DOTA-A(PEG<sub>750</sub>)HA)]<sup>-</sup>**,  $^1\text{H}$  NMRD profiles and  $^{17}\text{O}$  relaxation and chemical shift measurements have been performed. The simultaneous fitting of  $^1\text{H}$  NMR and  $^{17}\text{O}$  NMR data of those four Gd(III) chelates was performed using the Solomon-Bloembergen-Morgan model. Experimental results and fitted curves are shown in Figures 2.8, 2.11, 2.12 and 2.13. The fitted and the principal fixed parameters are given in Table 2.1 and 2.3.

### 2.3.1 DOTA-AHA and binuclear Gd(III) chelates

In order to obtain parameters characterizing the efficiency of water relaxation enhancement of the mononuclear compound **Gd(DOTA-AHA)**, as well as the binuclear compounds **[Gd<sub>2</sub>(Bis(DOTA-AHA)adipate)]<sup>2-</sup>** and **[Gd<sub>2</sub>(Bis(DOTA-AHA)1,3-phenyldiacetate)]<sup>2-</sup>**,  $^1\text{H}$  NMRD and  $^{17}\text{O}$  NMR studies have been performed (Figure 2.8). From the experimental NMRD data it can be seen that the two binuclear compounds clearly show a relaxivity hump between 20 and 120 MHz whereas the relaxivity profile of the mononuclear compound is rather flat (Figure 2.8c). The reduced transverse  $^{17}\text{O}$  relaxation,  $1/T_{2r}$ , is very similar for the three compounds over the whole temperature range studied (Figure 2.8a), indicating that water exchange should be similar. The reduced longitudinal  $^{17}\text{O}$  relaxation,  $1/T_{1r}$ , is also similar which would indicate that the rotational motion of the mononuclear and binuclear compounds do not differ significantly. Apparently this is in contradiction to the NMRD data.

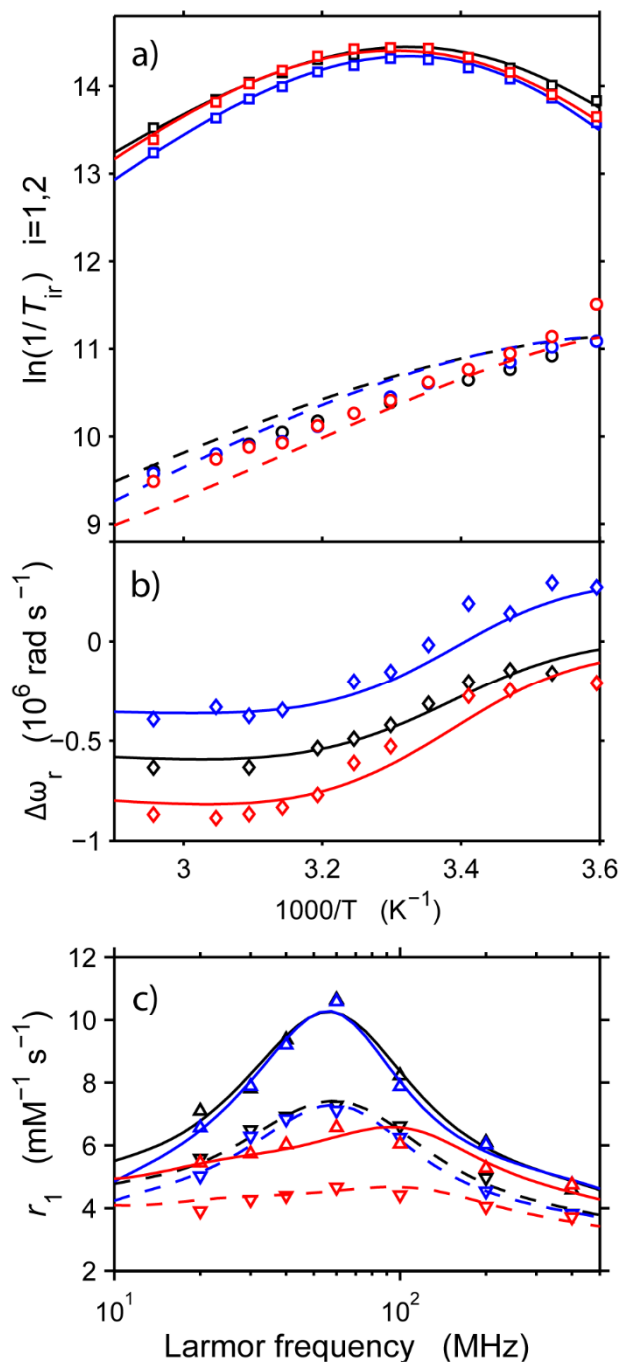


**Figure 2.8:** **a)** Reduced transverse (squares) and longitudinal (circles)  $^{17}O$  NMR relaxation rates for Gd(DOTA-AHA) (20 mM [Gd(III)] (red),  $[Gd_2(Bis(DOTA-AHA)adipate)]^{2-}$  (black) (12 mM [Gd(III)]) and  $[Gd_2(Bis(DOTA-AHA)1,3-phenyldiacetate)]^{2-}$  (blue) (12 mM [Gd(III)]); **b)** Reduced  $^{17}O$  chemical shifts for Gd(DOTA-AHA) ( $\diamond$ ),  $[Gd_2(Bis(DOTA-AHA)adipate)]^{2-}$  ( $\blacklozenge$ ) and  $[Gd_2(Bis(DOTA-AHA)1,3-phenyldiacetate)]^{2-}$  ( $\blacklozenge$ ); **c)**  $^1H$  NMRD profiles for Gd(DOTA-AHA) (red),  $[Gd_2(Bis(DOTA-AHA)adipate)]^{2-}$  (black) and  $[Gd_2(Bis(DOTA-AHA)1,3-phenyldiacetate)]^{2-}$  (blue) at 25 °C ( $\Delta$ ) and 37 °C ( $\nabla$ ). The lines represent the best fit of the data resulting from simultaneous fitting based on SBM equations.

It was assumed that standard Solomon-Bloembergen-Theory (SBM)<sup>86, 242</sup> is valid in our case (see references 289, 290 for a comparison of different theoretical approaches). The <sup>1</sup>H NMRD and <sup>17</sup>O NMR data have been evaluated using a simultaneous fitting procedure.<sup>143</sup> This procedure is the most efficient way to get reliable parameters characterizing the relaxation properties of gadolinium complexes in solution:

- Water exchange ( $k_{\text{ex}}$ ,  $\Delta H^\ddagger$ ) is best obtained from temperature dependent transverse <sup>17</sup>O relaxation ( $1/T_{2r}$ ); the scalar coupling constant ( $A/\hbar$ ) entering this data can be obtained from <sup>17</sup>O NMR chemical shift.
- Rotational correlation times ( $\tau_R$ ) are obtained from frequency dependent longitudinal <sup>1</sup>H relaxation ( $r_1$ , NMRD) and from temperature dependent longitudinal <sup>17</sup>O NMR relaxation ( $1/T_{1r}$ ).

The information on the dynamics of the paramagnetic complexes is obtained by relaxation enhancement measured on bulk water molecules to which it has been transmitted by chemical exchange. It is not known *per se* if there is only one exchanging species present or if there are several with different rotational behavior.

A first attempt showed that the <sup>1</sup>H NMRD and <sup>17</sup>O NMR data could not be fitted satisfactorily using a single rotational correlation time (see chapter 6.1). A satisfactory fit of the data could be obtained using two correlation times – a short one ( $\tau_R < 200$  ps) and a long one ( $\tau_R > 2000$  ps). In the case of Gd-complexes in solution there are two possible scenarios:

a) Most of the gadolinium complexes aggregate. The rotational diffusion of the Gd-H vectors can be described by the global reorientation of the aggregate (global correlation time  $\tau_g$ ) and by possible local motions (local correlation time  $\tau$ ). The theoretical description follows the Lipari-Szabo model developed for the dynamics of proteins.<sup>153, 154, 291</sup> The way the Gd-H vectors sense both motions is described by a model-free order parameter  $S$ .

b) Some gadolinium complexes aggregate but some are still present as single compounds. The rotational motion of the single compounds (monomers) is characterized by  $\tau_R^{\text{mono}}$  and the rotational motion of the aggregates by  $\tau_R^{\text{agg}}$ .

To check for aggregation of the compounds we measured <sup>1</sup>H relaxivity as a function of concentration. In absence of aggregation the relaxivity,  $r_1$ , should not depend on [Gd(III)]. The results show that for both binuclear chelates  $r_1$  increases by

more than 50% if the concentration of the paramagnetic ion is raised from 0.1 mM to about 12 mM (Figure 2.9). This increase is less than, for example, that observed for the trinuclear  $\text{Gd}_3\text{Ph}_4(\text{DTTA})_3$ <sup>292</sup> and it also starts at much higher concentration, 4 mM in contrast to 0.1 mM. The relaxivity of  $[\text{Gd}_2(\text{Bis}(\text{DOTA-AHA})\text{adipate})]^{2-}$  and  $[\text{Gd}_2(\text{Bis}(\text{DOTA-AHA})1,3\text{-phenyldiacetate})]^{2-}$  measured at low concentration is close to that of the mononuclear compound  $\text{Gd}(\text{DOTA-AHA})$ . These data suggest that the binuclear compounds weakly aggregate. This finding is remarkable, because first, there is no hydrophobic linker between the two chelates and second, the  $\text{Gd}(\text{DOTA})$ -chelates are charged and not neutral like the  $\text{Gd}(\text{DO3A})$ -type chelates.

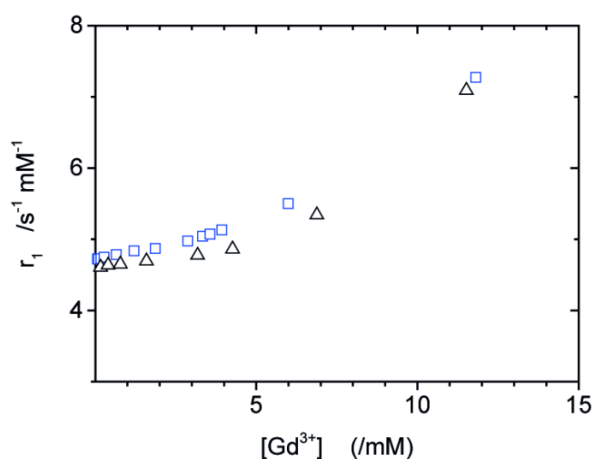
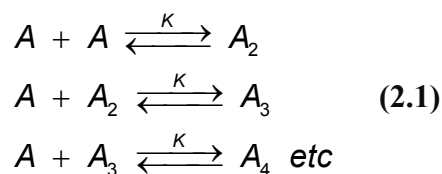


**Figure 2.9:** Concentration dependent relaxivity of the binuclear  $[\text{Gd}_2(\text{Bis}(\text{DOTA-AHA})\text{adipate})]^{2-}$  (□) and  $[\text{Gd}_2(\text{Bis}(\text{DOTA-AHA})1,3\text{-phenyldiacetate})]^{2-}$  (Δ) measured at 1.41 T (60 MHz) and 37 °C.

The Lipari-Szabo model has been used to describe rotational diffusion of different kinds of compounds like dendrimers, polymers, micelles and aggregates. As far as we know the second scenario with weakly self-aggregating monomers has not yet been applied in the context of paramagnetic compounds forming weakly bound aggregates and exchanging water molecules with the bulk. To be able to treat the data with a reasonable number of parameters some assumptions have to be made:

a) First, the water exchange between the first coordination sphere and bulk does not change when the compounds form aggregates. This assumption is very reasonable because it has been shown that water exchange does not change markedly if binuclear compounds are formed using the same chelator.<sup>293</sup>

b) The second assumption is that all equilibrium constants for forming dimers, trimers, tetramers, etc. from the same monomer are equal. If we name the monomer A we have<sup>294</sup>



and

$$\begin{aligned}
 [A_2] &= K[A]^2 \\
 [A_3] &= K^2[A]^3 \\
 &\dots \\
 [A_n] &= K^{n-1}[A]^n
 \end{aligned} \quad (2.2)$$

The total amount of compound A in solution is given by<sup>295</sup>

$$\begin{aligned}
 [A]_0 &= [A] + 2[A_2] + 3[A_3] + \dots + n[A_n] \\
 &= [A] + 2K[A]^2 + 3K^2[A]^3 + \dots + nK^{n-1}[A]^n \\
 &= \frac{[A]}{(1 - K[A])^2}
 \end{aligned} \quad (2.3)$$

The temperature dependence of the equilibrium constant is

$$K = e^{-\left(\frac{\Delta H^0}{RT} - \frac{\Delta S^0}{R}\right)} \quad (2.4)$$

If the binding between the aggregate forming monomers is relatively weak we can assume that the rates of formation and dissociation of the aggregates are fast compared to the rate of water exchange. In this case we can calculate the enhancement of longitudinal relaxation  $1/T_{1r}$  as

$$\frac{1}{T_{1r}} = \frac{1}{\langle T_{1m} \rangle + \tau_m} \quad (2.5)$$

$$\text{With } \left\langle \frac{1}{T_{1m}} \right\rangle = \sum_{i=1}^n \frac{x_i}{T_{1m,i}} \quad (2.6)$$

where  $x_i$  are the mole fractions of  $\text{Gd}^{3+}$  in the monomer (1), dimer (2), etc and  $\langle T_{1m} \rangle$  is the weighted mean of the longitudinal relaxation rate of bound water spins. The mole fractions can be calculated from the equilibrium constants via the roots of equation 2.3. The relaxation rates of bound water molecules,  $1/T_{1m,i}$  in the different aggregates differ only by the rotational correlation times. Clearly, we should have  $\tau_{R,1} < \tau_{R,2} < \tau_{R,3} < \text{etc.}$  To keep the number of fitted parameters reasonable we used only two correlation times, that for the rotation of the monomer,  $\tau_{R,1} = \tau_R^{\text{mono}}$ , and a mean correlation time for the rotation of aggregates  $\langle \tau_{R,i} \rangle = \tau_R^{\text{agg}}$ . As a test we fitted the data of the binuclear compound **[Gd<sub>2</sub>(Bis(DOTA-AHA)1,3-phenyldiacetate)]<sup>2-</sup>** with three correlations times. The quality of the fit did not increase markedly and besides the correlation times all other parameters of the fits were unchanged (see chapter 6.1).

Inspection of the equations resulting from the two scenarios described above shows that the theoretical descriptions are nearly equal with the main difference that the Lipari-Szabo order free parameter  $S^2$  is replaced by the mole fraction of Gd(III) present in the aggregates. In contrast to  $S^2$  the mole fraction depends on temperature leading to an increased quality of the fit (see chapter 6.1). Consequently we fitted the three data sets using the self-aggregation model (Figure 2.8).

As can be seen from the results in Table 1 water exchange rate constants at room temperature,  $^{298}k_{\text{ex}}$ , are equal within experimental error. This is not surprising because all compounds use the same chelating unit to bind Gd(III). The rate constants at 298 K are slightly higher than that of **[Gd(DOTA)]<sup>-</sup>** ( $^{298}k_{\text{ex}} = 4.1 \cdot 10^6 \text{ s}^{-1}$ ) but about four times faster than that of the DO3A-based dimers **(bisoxa[(Gd(DO3A))<sub>2</sub>])** and **(pip[(Gd(DO3A))<sub>2</sub>])** ( $^{298}k_{\text{ex}} = 1.4 \cdot 10^6 \text{ s}^{-1}$  and  $^{298}k_{\text{ex}} = 1.5 \cdot 10^6 \text{ s}^{-1}$ , respectively). The increase in lability is most probably due to the negative charge of the DOTA compounds.<sup>245</sup> From the positive entropies of activation,  $\Delta S^\ddagger$ , one can conclude that the mechanism has a more dissociative character than on DO3A-type complexes ( $\Delta S^\ddagger = +1.7$  and  $-11.7 \text{ J.K}^{-1}.\text{mol}^{-1}$ ).

**Table 2.1:** Water exchange parameters,  $^{298}k_{\text{ex}}$ ,  $\Delta H^\ddagger$ ,  $\Delta S^\ddagger$ , rotational correlation times,  $^{298}\tau_{\text{R}}^{\text{mono}}$ ,  $^{298}\tau_{\text{R}}^{\text{agg}}$ , and equilibrium constants,  $K^{298}$ ,  $\Delta H^0$ ,  $\Delta S^0$ , for aggregation Gd(DOTA-AHA),  $[\text{Gd}_2(\text{Bis}(\text{DOTA-AHA})\text{adipate})]^{2-}$  and  $[\text{Gd}_2(\text{Bis}(\text{DOTA-AHA})1,3\text{-phenyldiacetate})]^{2-}$ . The parameters were obtained from a simultaneous fit of  $^{17}\text{O}$  NMR and  $^1\text{H}$  NMRD data using SBM theory.

	$^{298}k_{\text{ex}}$ ( $10^6 \text{ s}^{-1}$ )	$\Delta H^\ddagger$ ( $\text{kJ}\cdot\text{mol}^{-1}$ )	$\Delta S^\ddagger$ ( $\text{J}\cdot\text{K}^{-1}\cdot\text{mol}^{-1}$ )	$^{298}\tau_{\text{R}}^{\text{mono}}$ (ps)	$^{298}\tau_{\text{R}}^{\text{agg}}$ (ps)	$\Delta H^0$ ( $\text{kJ}\cdot\text{mol}^{-1}$ )	$\Delta S^0$ ( $\text{kJ}\cdot\text{mol}^{-1}$ )	$K^{298}$ ( $\text{M}^{-1}$ )	$x_1^{\text{a}}$
Mononuclear									
<b>Gd(DOTA-AHA)</b>	$6.4 \pm 1.4$	$58 \pm 7$	$+81 \pm 23$	$103 \pm 13$	$2600 \pm 2100$	$-41 \pm 19$	$-129 \pm 63$	2.9	$0.90^{\text{b}}$
Binuclear									
<b><math>[\text{Gd}_2(\text{Bis}(\text{DOTA-AHA})\text{adipate})]^{2-}</math></b>	$6.8 \pm 3$	$54 \pm 8$	$+68 \pm 30$	$129 \pm 10$	$4000 \pm 1800$	$-32 \pm 9$	$-84 \pm 31$	15.6	$0.85^{\text{c}}$
<b><math>[\text{Gd}_2(\text{Bis}(\text{DOTA-AHA})1,3\text{-phenyldiacetate})]^{2-}</math></b>	$6.4 \pm 1.1$	$63 \pm 5$	$+95 \pm 18$	$134 \pm 7$	$4000 \pm 1200$	$-33 \pm 6$	$-89 \pm 20$	14.6	$0.86^{\text{c}}$

a) mole fraction of the monomer; b)  $[\text{Gd}(\text{DOTA-AHA})] = 20 \text{ mM}$ ; c)  $[\text{Gd}_2(\text{Bis}(\text{DOTA-AHA})\text{adipate})]^{2-}/[\text{Gd}_2(\text{Bis}(\text{DOTA-AHA})1,3\text{-phenyldiacetate})]^{2-} = 6 \text{ mM}$ .

**Table 2.2:** Distribution of gadolinium in monomers, dimers and trimers calculated from  $K^{298}$  and equation 2.3 at 298K.

	<b>[Gd(III)]</b>	<b><math>K^{298}</math> (<math>\text{M}^{-1}</math>)</b>	<b>monomer</b>	<b>dimer</b>	<b>trimer</b>
Mononuclear					
<b>Gd(DOTA-AHA)</b>	20 mM	2.9	89.9 %	9.4 %	0.7 %
Binuclear					
<b><math>[\text{Gd}_2(\text{Bis}(\text{DOTA-AHA})\text{adipate})]^{2-}</math></b>	12 mM	15.6	84.8 %	13.4 %	1.6
<b><math>[\text{Gd}_2(\text{Bis}(\text{DOTA-AHA})1,3\text{-phenyldiacetate})]^{2-}</math></b>	12 mM	14.6	85.6%	12.8 %	1.4

All complexes, the mononuclear **Gd(DOTA-AHA)** as well as the binuclear  $[\text{Gd}_2(\text{Bis}(\text{DOTA-AHA})\text{adipate})]^{2-}$  and  $[\text{Gd}_2(\text{Bis}(\text{DOTA-AHA})1,3\text{-phenyldiacetate})]^{2-}$  form aggregates in solution. For **Gd(DOTA-AHA)** the constant for complex formation  $K^{298}$  is 5 to 6 times smaller than for the binuclear complexes (Table 2.1). From the equilibrium constants we can calculate the relative amounts of Gd(III) ions as monomer, dimer or trimer (Table 2.2). For the mononuclear species dimers are present only in a small amount ( $\approx 10\%$ ). For both binuclear species the amount of Gd(III) present in an aggregate is  $\approx 15\%$  and the major aggregated form is again the dimer. The intermolecular interaction leading to aggregation is much weaker between our compounds if compared to DO3A-based binuclear compounds.<sup>296, 297</sup> The seven-coordinating **DO3A** chelator allows formation of carboxylate bridges and leads therefore to very stable aggregates.

From the point of view of water proton relaxivity the compounds in its monomeric or aggregated form are characterized by the rotational correlation times  $\tau_{\text{R}}^{\text{mono}}$  and  $\tau_{\text{R}}^{\text{agg}}$ , respectively. The values obtained by the fitting differ for all three compounds by more than one order of magnitude (Table 2.1). Surprisingly the  $^{298}\tau_{\text{R}}^{\text{mono}}$  value fitted for the mononuclear compound is only 25% shorter than the corresponding values of the binuclear compounds. A possible explanation could be a high degree of internal rotation in both binuclear compounds. The longer value of  $^{298}\tau_{\text{R}}^{\text{mono}}$  of **Gd(DOTA-AHA)** in respect to for example  $[\text{Gd}(\text{DOTA})]^-$  can be explained by the  $\text{C}_5\text{NH}_2$ -chain attached to the ligand. The  $^{298}\tau_{\text{R}}^{\text{mono}}$  of the binuclear  $[\text{Gd}_2(\text{Bis}(\text{DOTA-AHA})\text{adipate})]^{2-}$  and  $[\text{Gd}_2(\text{Bis}(\text{DOTA-AHA})1,3\text{-phenyldiacetate})]^{2-}$  are in the same order as those of other binuclear compounds ( $\text{Gd}_2(\text{bisoxa}(\text{DO3A})_2) = 106 \text{ ps}$ ;<sup>143</sup>  $\text{Gd}_2(\text{pip}(\text{DO3A})_2) = 171 \text{ ps}$ ;<sup>143</sup>  $\text{Gd}_2(\text{DOPTA}) = 200 \text{ ps}$ ;<sup>247</sup>  $\text{Gd}_2(\text{CS}(\text{DO3A-PNBn})_2) = 183 \text{ ps}$ ;<sup>249</sup> and  $\text{Gd}_2(\text{bipy}(\text{DO3A})_2) = 185 \text{ ps}$ <sup>297</sup>).

A rotational correlation time  $^{298}\tau_{\text{R}}^{\text{mono}}$  of “only”  $\approx 130 \text{ ps}$  can be explained by the rod-like shape of the binuclear compounds (Figures 2.10 and 2.14). The rotational motion sensed by the Gd-H vector is probably close to the rotation around the Gd-Gd axis (Figure 2.10); rotation around an axis perpendicular to the Gd-Gd axis would lead to much slower  $^{298}\tau_{\text{R}}^{\text{mono}}$ .



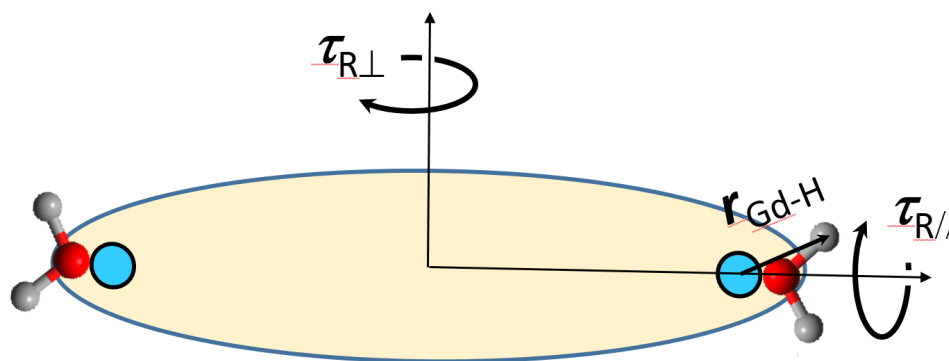
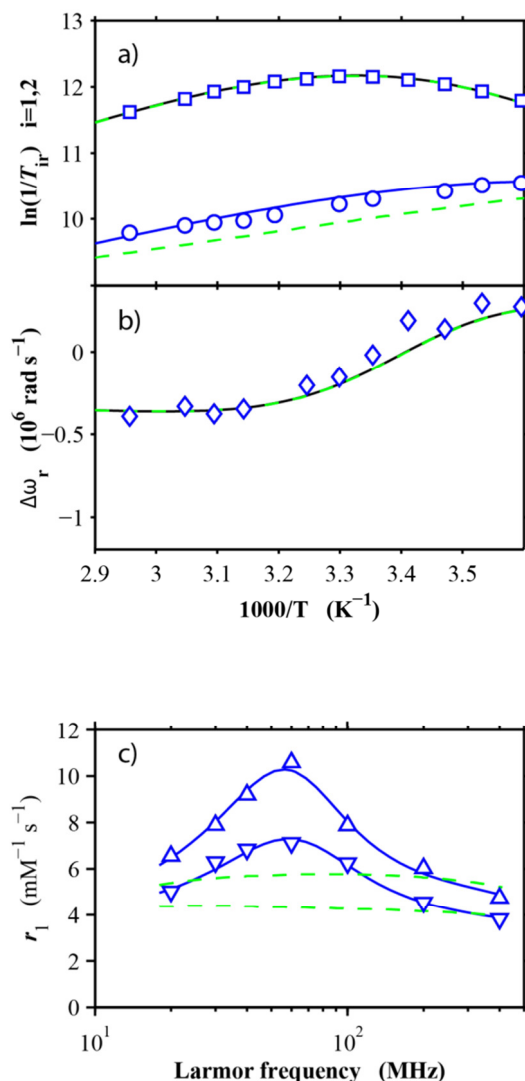


Figure 2.10: Anisotropic rotation of binuclear compounds.

The rotational correlation times for the aggregates are  $^{298}\tau_{\text{R}}^{\text{agg}} \approx 2.6$  ns for **Gd(DOTA-AHA)** and  $\approx 4.0$  ns for the binuclear compounds with relatively big statistical errors. The increase by more than a factor of twenty from a monomer to essentially a dimer seems to be quite substantial. An effective molecular radius of the aggregates can be estimated to  $r_{\text{eff}} \approx 1.5$  nm using the Debye-Stokes equation (equation 1.27). Such a radius is fully compatible with the elongated molecular mechanics structures (see chapter 2.4). The strong increase from  $^{298}\tau_{\text{R}}^{\text{mono}} \approx 0.13$  ns to  $^{298}\tau_{\text{R}}^{\text{agg}} \approx 4.0$  ns can therefore be explained by the anisotropic rotation of the monomer with  $r_{\text{GdH}}$  sensing the fast motion and the more isotropic rotation of the aggregates with  $r_{\text{GdH}}$  sensing the slow overall motion. This explanation implies the absence of fast internal motion in the aggregates (see chapter 6.1).

The NMR relaxation results clearly show that the binuclear but also the mononuclear compounds form weak aggregates in solution. Only 15 % in the binuclear compounds and 10 % in the mononuclear compound of the total amount of Gd(III) is present in aggregates. This is however enough to influence markedly the NMRD profiles (Figure 2.11c).



**Figure 2.11:** Influence of  $[\text{Gd}_2(\text{Bis}(\text{DOTA-AHA})1,3\text{-phenyldiacetate})]^{2-}$  aggregation on  $^{17}\text{O}$  NMR and  $^1\text{H}$  NMRD: blue full curves calculated with parameters in Table 2.1; green dashed curves calculated with 100% monomer. **a)**  $^{17}\text{O}$   $1/T_{2r}$  ( $\square$ ) and  $1/T_{1r}$  ( $\circ$ ); **b)**  $^{17}\text{O}$   $\Delta\omega_r$  ( $\diamond$ ); **c)**  $^1\text{H}$  NMRD at 25 °C ( $\triangle$ ) and 37 °C ( $\nabla$ ).

The relaxivities of the binuclear compounds  $[\text{Gd}_2(\text{Bis}(\text{DOTA-AHA})\text{adipate})]^{2-}$  and  $[\text{Gd}_2(\text{Bis}(\text{DOTA-AHA})1,3\text{-phenyldiacetate})]^{2-}$  are about 50% higher than that of the mononuclear  $\text{Gd}(\text{DOTA-AHA})$ : at 60 MHz and 37 °C the relaxivities of  $[\text{Gd}_2(\text{Bis}(\text{DOTA-AHA})\text{adipate})]^{2-}$  and  $[\text{Gd}_2(\text{Bis}(\text{DOTA-AHA})1,3\text{-phenyldiacetate})]^{2-}$  are  $r_1 = 7.3 \text{ mM}^{-1} \cdot \text{s}^{-1}$  and  $r_1 = 7.1 \text{ mM}^{-1} \cdot \text{s}^{-1}$  respectively, and  $\text{Gd}(\text{DOTA-AHA})$  has  $r_1 = 4.7 \text{ mM}^{-1} \cdot \text{s}^{-1}$ . The relaxivity of the mononuclear compound is slightly higher than that of  $\text{Gd}(\text{DOTA})$  ( $r_1 = 3.1 \text{ mM}^{-1} \cdot \text{s}^{-1}$  at 60 MHz, 37 °C)<sup>298</sup> which is mainly due to the 10 % of aggregates formed. Without aggregates one can calculate a relaxivity of  $3.7 \text{ mM}^{-1} \cdot \text{s}^{-1}$  at 60 MHz, 37 °C. The remaining small increase is due to the C4 chain attached to the chelate.

### 2.3.2 PEGylated Gd(III) chelates

All PEGylated Gd(III) chelates have been studied by  $^1\text{H}$  relaxometry (Figure 2.12). The chelate  $[\text{Gd}(\text{DOTA-A}(\text{PEG}_{550})\text{HA})]^-$  has also been studied by  $^{17}\text{O}$  NMR spectroscopy (Figure 2.13). Results of a combined analysis of this latter chelate study show that water exchange rate is not influenced by PEGylation. The values are slightly smaller than those obtained for the binuclear chelates, but almost identical to the values obtained for **Gd(DOTA-AHA)**. These results are in contrast with what was previously reported for the PEGylated hetero-tripodal hydroxypyridonate (**HOPO**) gadolinium complexes, since the coupling of PEG moieties lead to a decrease in the  $k_{\text{ex}}$  values in relation to HOPO complexes without PEG.<sup>299, 300</sup> PEG moieties are able to form hydrogen bonds with water molecules and induce a partial displacement of the inner sphere water molecules. The presence of PEG around the chelate can restrict the flow of the water molecules from the bulk to the inner sphere and vice-versa, leading to higher residence times of the water molecules in the inner sphere. The strength of these bonds is strong enough that the reduction of the number of water molecules in the inner sphere ( $q$ ) from 2 (non-PEGylated chelate) to 1 (PEGylated chelates) was noticed for the Gd(III)-HOPO chelates. Contrary to what happens to PEGylated HOPO gadolinium chelates, the oxygen donors of the PEG moieties seem not to influence the water molecules residence time in  $[\text{Gd}(\text{DOTA-A}(\text{PEG})\text{HA})]^-$  chelates. We therefore fixed the water exchange rate constants in the analysis of the relaxivity data to the values of  $[\text{Gd}(\text{DOTA-A}(\text{PEG}_{550})\text{HA})]^-$  (Table 2.3).

The  $^1\text{H}$  NMRD profiles of PEGylated compounds (Figure 2.12) have similar shapes to those previously presented (Figure 2.8), reaching their maximum relaxivity at 60 MHz. It is observable that PEGylation results in improved relaxivity values in relation to **Gd(DOTA-AHA)** at all applied frequencies. Through the analysis of the  $^1\text{H}$  NMRD profiles, it is also noticeable that the relaxivity is related to the PEG molecular weight.  $[\text{Gd}(\text{DOTA-A}(\text{PEG}_{750})\text{HA})]^-$  ( $r_1 = 6.5 \text{ mM}^{-1} \cdot \text{s}^{-1}$  at 37 °C and  $r_1 = 8.0 \text{ mM}^{-1} \cdot \text{s}^{-1}$  at 25 °C), which is the chelate with an heavier PEG moiety displays higher relaxivities in comparison to  $[\text{Gd}(\text{DOTA-A}(\text{PEG}_{550})\text{HA})]^-$  ( $r_1 = 5.9 \text{ mM}^{-1} \cdot \text{s}^{-1}$  at 37 °C and  $r_1 = 7.8 \text{ mM}^{-1} \cdot \text{s}^{-1}$  at 25 °C), which in turn demonstrate higher relaxivity than  $[\text{Gd}(\text{DOTA-A}(\text{PEG}_{350})\text{HA})]^-$  ( $r_1 = 5.1 \text{ mM}^{-1} \cdot \text{s}^{-1}$  at 37 °C and  $r_1 = 6.8 \text{ mM}^{-1} \cdot \text{s}^{-1}$  at 25 °C), the smaller PEGylated chelate. This trend is most perceptible at frequencies (between 40 and 100 MHz) where the rotational correlation time has more influence on the relaxivity values.

Surprisingly, the relaxivities observed for the PEGylated chelates are lower than those found for the binuclear chelates. This result was not predictable, since both binuclear and PEGylated chelates have similar water exchange rates and the rotational correlation times are higher than the binuclear chelates. It was expected that the PEG moiety would significantly slow the chelate rotational correlation time and thus, resulting in improved relaxivity values. However, the increase in relaxivity observed upon addition of the PEG chain is very modest considering the large increase in molecular weight.

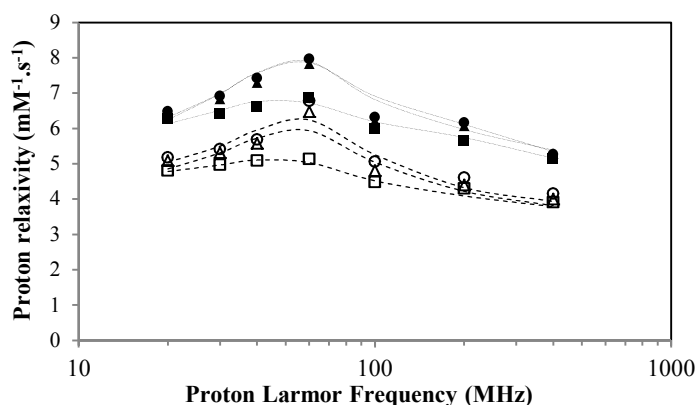


**Figure 2.12:**  $^1\text{H}$  NMRD profile of  $[\text{Gd}(\text{DOTA-A}(\text{PEG}_{350})\text{HA})]^-$  ( $\blacksquare$ ,  $\square$ ),  $[\text{Gd}(\text{DOTA-A}(\text{PEG}_{550})\text{HA})]^-$  ( $\blacktriangle$ ,  $\triangle$ ) and  $[\text{Gd}(\text{DOTA-A}(\text{PEG}_{750})\text{HA})]^-$  ( $\bullet$ ,  $\circ$ ) chelates at  $25^\circ\text{C}$  (filled symbols) and  $37^\circ\text{C}$  (empty symbols). The lines represent the best fit of the data resulted from simultaneous fitting based on SBM equation.

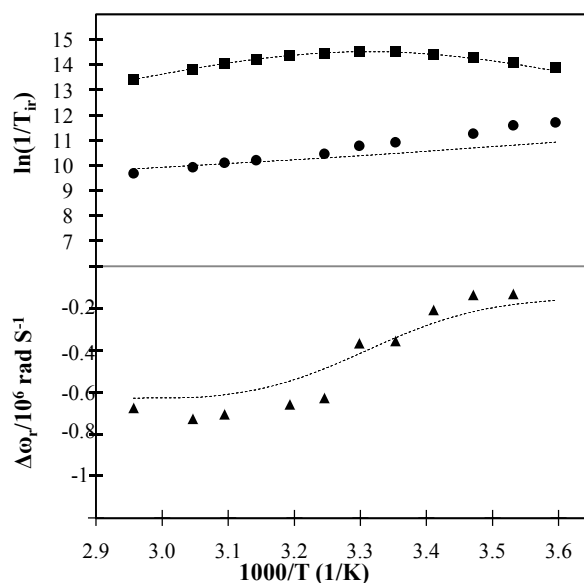


**Figure 2.13:** Reduced  $^{17}\text{O}$  transverse ( $\blacksquare$ ) and longitudinal ( $\bullet$ ) relaxation rates and reduced chemical shifts ( $\blacktriangle$ ) ( $B = 9.4 \text{ T}$ ) for the  $[\text{Gd}(\text{DOTA-A}(\text{PEG}_{550})\text{HA})]^-$  chelate. The lines represent the best simulation fit of experimental data.

To describe the rotational diffusion of the PEGylated chelates, two correlation times were also taken into account.  $[\text{Gd}(\text{DOTA-A}(\text{PEG}_{550})\text{HA})]^-$  chelate display elevated global rotational correlation time, while the local rotational correlation time is *circa* 25 times lower (Table 2.3). For certain polymers, the proton relaxivity may be independent of the molecular weight, since their relaxivity is limited by fast rotation.<sup>151, 152</sup> According to the Lipari and Szabo model free,<sup>153, 154</sup> the rotational correlation time of these polymers is dominated by segmental motions, which are independent of the molecular weight. PEG polymers are very flexible, leading to rapid isotropic internal motions and therefore low  $S^2$  values (equations 1.20 and 1.21), resulting in only a modest increase in the rotational motion.<sup>253</sup> The  $[\text{Gd}(\text{DOTA-A}(\text{PEG}_{550})\text{HA})]^-$  order parameter value is even lower than the ones calculated for the binuclear chelates and similar to the value found for  $\text{Gd}(\text{DOTA-AHA})$ . These low  $S^2$  values indicate that the rotational motion is mainly modulated by the local correlation time.

The results obtained for the PEGylated compounds on the rotational behavior are also surprising. Like in the case of binuclear chelates, the modest relaxivity hump observed in NMRD profiles is no characteristic of a chelate with slow rotation. However, the slow rotation must be taken into account to describe the increase in the PEGylated chelates relaxivity. Once again, the only way to explain such slow global rotation is the formation of aggregates of compounds in solution. Assembling of low weight PEG moieties ( $M_w = 400$  and  $600 \text{ g}\cdot\text{mol}^{-1}$ ) in aqueous solution is possible and has been previously reported.<sup>301, 302</sup> The chain of any PEG is alternately hydrophilic and hydrophobic, exhibiting specific interactions with water that lead to the development of a helical structure. Under certain conditions, this helix conformations adopted by PEG in water can generate aggregates with hydrophobic domains. It is possible that due to the presence of PEG moieties, large  $[\text{Gd}(\text{DOTA-A}(\text{PEG})\text{HA})]^-$  particles may have been formed at measurement concentration, which may explain the extremely elevated  $\tau_g$  value (almost 7 ns). However, this possibility was not checked and unlike the binuclear chelates, it cannot be ensured that the high global rotational rotation time is due to PEG assembling.

Despite having slow global rotational time, the fast local rotation of PEGylated chelates (also similar to similar to  $\text{Gd}(\text{DOTA-AHA})$ ) prevents a higher relaxivity improvement. Thus, covalent attachment of PEG polymers to a gadolinium chelate may not be suitable for tuning the rotation correlational time in order to obtain contrast agents with improved relaxivity.

**Table 2.3:** Relaxometric parameters for [Gd(DOTA-A(PEG<sub>350</sub>)HA)]<sup>-</sup>, [Gd(DOTA-A(PEG<sub>550</sub>)HA)]<sup>-</sup> and [Gd(DOTA-A(PEG<sub>750</sub>)HA)]<sup>-</sup>. The [Gd(DOTA-A(PEG<sub>550</sub>)HA)]<sup>-</sup> parameters were obtained from the simultaneous analysis of <sup>17</sup>O NMR and <sup>1</sup>H NMRD data, using the Solomon-Bloembergen-Morgan approach<sup>(a)(b)</sup>.

Parameter	[Gd(DOTA-A(PEG <sub>350</sub> )HA)] <sup>-</sup>	[Gd(DOTA-A(PEG <sub>550</sub> )HA)] <sup>-</sup>	[Gd(DOTA-A(PEG <sub>750</sub> )HA)] <sup>-</sup>
$\Delta H^\ddagger$ (kJ.mol <sup>-1</sup> )	<i>47</i>	47 ± 7	<i>47</i>
<sup>298</sup> <i>k</i> <sub>ex</sub> (10 <sup>6</sup> s <sup>-1</sup> )	<i>4.9</i>	4.9 ± 0.8	<i>4.9</i>
<i>A/h</i> (10 <sup>6</sup> rad.s <sup>-1</sup> )	<i>-2.7</i>	-2.7 ± 0.3	<i>-2.7</i>
<i>C</i> <sub>os</sub>	<i>0.22</i>	0.22 ± 0.16	<i>0.22</i>
<sup>298</sup> <i>τ</i> <sub>g</sub> (ps)	<i>6900</i>	6900 ± 2000	<i>6900</i>
<sup>298</sup> <i>τ</i> <sub>1</sub> (ps)	243 ± 5	275 ± 12	211 ± 9
<i>S</i> <sup>2</sup>	0.02 ± 0.00	0.05 ± 0.01	0.05 ± 0.01
<sup>298</sup> <i>τ</i> <sub>v</sub> (ps)	45 ± 1.5	26 ± 4	25 ± 4

(a) The italicized values of parameters in the table were calculated from <sup>17</sup>O NMR measurements of [Gd(DOTA-A(PEG<sub>550</sub>)HA)]<sup>-</sup> and kept as constant parameters for the NMRD fitting of the other two [Gd(DOTA-A(PEG<sub>350</sub>)HA)]<sup>-</sup> and [Gd(DOTA-A(PEG<sub>750</sub>)HA)]<sup>-</sup> compounds.

(b) Other parameters fixed in the fitting procedure are:  $\Delta^2/10^{20} = 1.0 \text{ s}^{-2}$ ,  $r_{\text{GdO}} = 2.5 \text{ \AA}$ ,  $r_{\text{GdH}} = 3.1 \text{ \AA}$ ,  $a_{\text{GdH}} = 3.6 \text{ \AA}$ ,  $E_{\text{GdH}} = 20 \text{ kJ.mol}^{-1}$  and  $q = 1$ .

## 2.4 DEER and modelling studies of Gd(III) binuclear chelates

Distributions of Gd-Gd distances for the binuclear chelates were measured with double electron-electron resonance (DEER) technique.<sup>303, 304</sup> This pulse EPR technique allows detecting static magnetic dipolar interaction in the pairs of paramagnetic centers, which is then recalculated into the distance distribution. Currently, most applications of DEER technique<sup>305, 306</sup> are found in the field of structural biology in combination with site-directed spin labeling,<sup>307</sup> but the technique is generally applicable to any large molecules possessing paramagnetic centers with nanometer-range distances between them. While most DEER experiments are done with pairs of nitroxide radicals, over the last seven years gadolinium chelates were proved to be a possible alternative type of spin centers for DEER measurements.<sup>308-311</sup>

Gd-Gd DEER measurements we performed on both [**Gd<sub>2</sub>(Bis(DOTA-AHA)adipate)]<sup>2-</sup>** and [**Gd<sub>2</sub>(Bis(DOTA-AHA)1,3-phenyldiacetate)]<sup>2-</sup>** chelates, in order to determine the distribution of distances between the two Gd(III) centers and try to understand if the distances may have influence on the binuclear compounds relaxivity. The DEER experiment is done in a frozen glassy state, and thus can be considered as a static snap-shot of the dynamic ensemble of conformations present in solution. The measured distance distribution is, however, limited to the inter-spin distances above approximately 1.3 nm due to the bandwidth limitation of the microwave pulses. The upper limit of the detectable distances is set by the transverse relaxation time of the paramagnetic centers, and this limit was well beyond the longest detected distances in our experiments.<sup>312</sup>

The longest Gd-Gd distances present in the samples were about 2.7 nm for [**Gd<sub>2</sub>(Bis(DOTA-AHA)adipate)]<sup>2-</sup>** and about 3 nm for [**Gd<sub>2</sub>(Bis(DOTA-AHA)1,3-phenyldiacetate)]<sup>2-</sup>** (see chapter 6.2). In both cases the fitted distance distributions appeared broad and covered the whole range of distances from the corresponding upper distance value down to the shortest detectable distance. Neither for [**Gd<sub>2</sub>(Bis(DOTA-AHA)adipate)]<sup>2-</sup>** nor for [**Gd<sub>2</sub>(Bis(DOTA-AHA)1,3-phenyldiacetate)]<sup>2-</sup>** could the intra-molecular DEER form factors be perfectly fitted by the standard routines of DeerAnalysis<sup>313</sup> package, suggesting the presence of some Gd-Gd distances below the detection limit. Such short distances are known to cause fitting deviations. Still, an estimate of the fraction of such short distances in the statistical ensemble is very

difficult in the present case. Typically the fraction of detected spin pairs is estimated from the depth of dipolar oscillations in the DEER time trace. For short Gd-Gd distances, however, other effects, such as interference with strong pseudo-secular term in the dipolar spin-Hamiltonian, were claimed to influence DEER modulation depth, example given by a bis-Gd compound, similar to the ones studied in this work.<sup>314</sup> We can thus conclude that DEER measurements are in line with the flexible molecular structure of the studied compounds, and that these measurements would not contradict the presence of shorter Gd-Gd distances, originating, for instance, from some degree of aggregation (as no molecular conformations with Gd-Gd distances below 1.3 nm were predicted by modeling, see below). The estimate of the possible degree of aggregation could not be unambiguously done from the given EPR data.

Molecular modelling using MM3 force field in vacuum afforded Gd-Gd distances for  $[\text{Gd}_2(\text{Bis}(\text{DOTA-AHA})\text{adipate})]^{2-}$  and  $[\text{Gd}_2(\text{Bis}(\text{DOTA-AHA})1,3\text{-phenyldiacetate})]^{2-}$  (Figure 2.14) which are in good agreement with the DEER results. The distances reported for each compound are the longest and the shortest distance from short molecular dynamics sampling. The linker is the only feature that distinguishes the two chelates. 1,3-phenyldiacetate is a lengthier linker than adipate so, the small difference found in the Gd-Gd distances for completely stretched conformation was predictable. The slightly longer rotational correlation time of the monomeric  $[\text{Gd}_2(\text{Bis}(\text{DOTA-AHA})1,3\text{-phenyldiacetate})]^{2-}$  also reflects its lengthier linker.

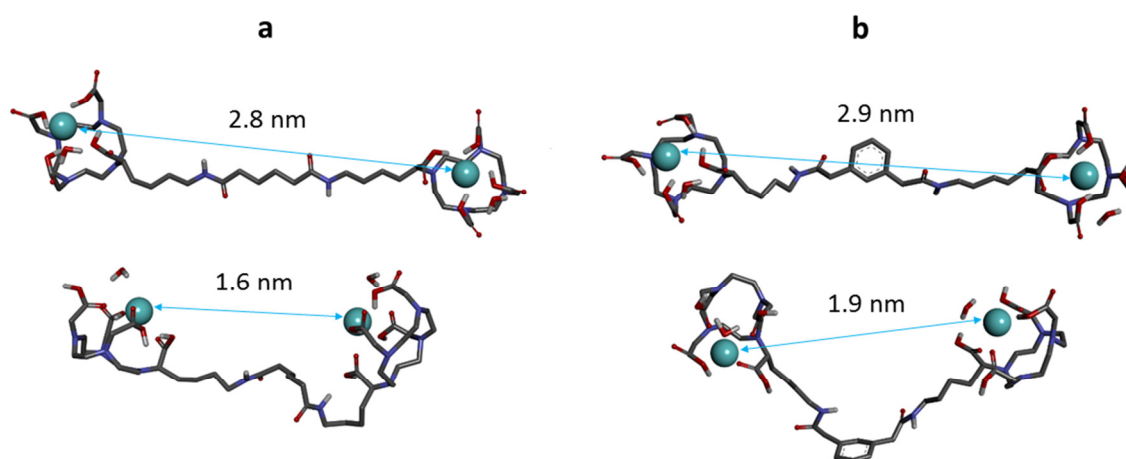


**Figure 2.14:** Molecular mechanics structures (MM3 force field) illustrating possible conformations of **a)**  $[\text{Gd}_2(\text{Bis}(\text{DOTA-AHA})\text{adipate})]^{2-}$  and **b)**  $[\text{Gd}_2(\text{Bis}(\text{DOTA-AHA})1,3\text{-phenyldiacetate})]^{2-}$  with Gd-Gd distances.



## 2.5 $^1\text{H}$ NMR studies of paramagnetic lanthanide DOTA-A(PEG<sub>750</sub>)HA chelates

The trivalent lanthanide complexes of DOTA-based ligands exhibit a variety of conformational and coordination isomers which may display dynamic behavior on the NMR timescale.<sup>315-317</sup> The isomers of their Gd(III) chelates have been found to have different relaxivity properties.<sup>318</sup> Considering this, some  $^1\text{H}$  NMR studies have been performed with some paramagnetic lanthanide DOTA-A(PEG<sub>750</sub>)HA chelates.

$^1\text{H}$  NMR is a valuable technique for the solution study of the isomers of the Ln(III) complexes of DOTA and its derivatives.<sup>315, 316</sup> The high symmetry of DOTA leads to the existence of two isomers of the  $[\text{Ln}(\text{DOTA})]^-$  chelates in solution, with square antiprismatic (*M*) and square twisted antiprismatic (*m*) geometries.<sup>319-322</sup> These isomers have the same [3.3.3.3] square conformation with fourfold symmetry of the tetraazacyclododecane ring, where all its ethylenic groups adopt a  $\delta$  or  $\lambda$  conformation, thus leading to conformations of clockwise or counterclockwise helicity,  $\lambda\lambda\lambda\lambda$  or  $\delta\delta\delta\delta$ . They only differ on the layout of the four acetate pendant arms, resulting from rotations around the N-CH<sub>2</sub>-CO<sub>2</sub> bonds, with either a clockwise ( $\Lambda$ ) or counterclockwise ( $\Delta$ ) helicity. These lead to the two diastereoisomers existing in solution (*m* and *M*), with separate NMR resonances, each of which is an enantiomer pair: the square antiprismatic (*M*) geometry results from the opposite helicity of the tetraaza ring and the acetate arms ( $\Delta(\lambda\lambda\lambda\lambda)$  or  $\Lambda(\delta\delta\delta\delta)$ ), while the twisted antiprismatic (*m*) geometry has the same ring and acetate helicity ( $\Lambda(\lambda\lambda\lambda\lambda)$  or  $\Delta(\delta\delta\delta\delta)$ ). Thus *M* and *m* differ in the value and sign of the twist angle  $\alpha$  between the diagonals of the parallel squares formed by four N-atoms and the four carboxylate O-atoms in the coordination polyhedron of the DOTA chelates (typical values of  $\alpha \approx +35^\circ$  and  $\alpha \approx -15^\circ$ , respectively, found from crystallographic structures).<sup>315</sup> The isomer *M* shows a wider paramagnetic shift range than *m* throughout the lanthanide series. The isomer *m* is dominant relative to *M* for the early Ln(III) chelates (Ln = La - Pr), but *M* becomes dominant for the smaller ions (Ln = Eu - Lu).<sup>317</sup>

Similarly to the ligand DOTASA,<sup>323</sup> DOTA-A(PEG<sub>750</sub>)HA is an asymmetrical derivative of DOTA, with one of the four acetate C( $\alpha$ ) atoms substituted. In the case of DOTA-A(PEG<sub>750</sub>)HA the asymmetry is introduced through the inclusion of a amide-PEG-bearing group, leading to the existence of a chiral center in the ligand and a site of asymmetry in the complexes which double the number of possible isomeric species. As

we have obtained the ligand **DOTA-A(PEG<sub>750</sub>)HA** as a racemic mixture of the ( $\alpha R$ ) and ( $\alpha S$ ) enantiomers, the complete identification of all possible stereoisomers requires identification of the configuration ( $\alpha R$ ) of the chiral C-atom of the ligand, together with the four arrangements of the ligand itself in the complex described above for **DOTA** complexes. Due to this, in solution there can be up to eight stereoisomers of **[Ln(DOTA-A(PEG<sub>750</sub>)HA)]<sup>-</sup>** of the type  $W-X$  ( $W = (R)$  or ( $S$ );  $X = M$  ( $\Delta(\lambda\lambda\lambda\lambda)$ ) or  $\Lambda(\delta\delta\delta\delta)$ ) or  $m$  ( $\Lambda(\lambda\lambda\lambda\lambda)$  or  $\Delta(\delta\delta\delta\delta)$ ), consistent with four enantiomer pairs: ( $R$ )- $M$ , ( $R$ )- $m$ , ( $S$ )- $M$  and ( $S$ )- $m$ . Considering this, up to four sets of <sup>1</sup>H NMR signals are to be expected from these enantiomer pairs. The lack of  $C_4$  symmetry removes the signal degeneracy found in the NMR spectra of **[Ln(DOTA)]<sup>-</sup>** complexes and leads to a large number of resonances for each isomer in the <sup>1</sup>H NMR spectra.

The special properties of the paramagnetic Pr(III), Nd(III), Sm(III), Eu(III) and Yb(III) chelates of **DOTA-A(PEG<sub>750</sub>)HA** were investigated by <sup>1</sup>H NMR at three different temperatures (25 °C, 40 °C and 60 °C), showing a large number of partially overlapping resonances covering paramagnetic shift ranges in accordance with those observed for the corresponding **DOTA** chelates.<sup>320, 322</sup> Previous <sup>1</sup>H NMR studies with the symmetrical **[Ln(DOTA)]<sup>-</sup>** chelates, and with a variety of lanthanide derivatives of **DOTA**,<sup>315</sup> have demonstrated that the two diastereoisomers  $m$  and  $M$  are present in solution, with a relative proportion that is a function of the lanthanide ion, temperature, solvent and the steric crowding of the chelate.<sup>315, 317</sup> They are characterized by different dipolar shifts, with complexes of the  $M$  form possessing the larger paramagnetic shift for a given ligand resonance.

Through the analysis of the obtained <sup>1</sup>H NMR spectra, the  $M/m$  isomer ratio could be determined for several complexes. For this purpose it is particularly useful to observe the resonance in the most-shifted axial ring proton,  $ax_1$ , which is well separated from the others.<sup>315, 317, 319-322</sup> For example, in the case of **[Ln(DOTA)]<sup>-</sup>** complexes this resonance is observed at *circa* +30-50 ppm and *circa* +150-160 ppm for the  $M$  isomers, while for the corresponding  $m$  forms, the axial ring protons  $ax_1$  has resonances at lower frequencies, at *circa* +10-30 ppm and *circa* +90-100 ppm for Eu(III) and Yb (III) complexes, respectively.<sup>315, 324-326</sup> Similarly to what has been previously found in asymmetric DOTA-based complexes, the  $ax_1$  protons of most of the studied Ln(III) complexes of **DOTA-A(PEG<sub>750</sub>)HA** originated two sets of well separated signals, which could be assigned to the isomers  $M$  and  $m$ , as shown in Figures 2.15 and 2.16.

Integration of those signals afforded the isomer ratios  $M/m$ , as shown in Table 2.4. As expected, isomer  $m$  is dominant for the early lanthanide chelate (praseodymium), decreasing its fraction along the lanthanide series, as the ionic radius of the Ln(III) ions decreases.<sup>315, 317</sup> It is known that  $m$  isomers of lanthanide macrocyclic DOTA-type chelates have about 50 times faster water exchange ( $k_{\text{ex}}$ ) than  $M$  isomers.<sup>327-329</sup> For  $[\text{Gd}(\text{DOTA})]^-$  an  $M/m$  isomer ratio of *circa* 6:1 was calculated by interpolation of the ratio for the Eu(III) and Tb(III) chelates, while for  $[\text{Gd}(\text{DOTASA})]^{2-}$  an isomer ratio of 1:1 was obtained, accounting for a 50% increase in the water exchange rate of the latter chelate.<sup>323</sup> The comparison of the observed  $M/m$  ratio for the present PEGylated chelate shows that despite the preservation of the trend in the  $M/m$  ratio just described, the dominance of the  $m$  isomer for the complexes of the early Ln(III) ions is not so significant as in other cases.<sup>323, 325</sup> By analogy with the ratio obtained for other Gd(III) chelates, which show to be close to that of the corresponding Eu(III) chelates, a value of *circa* 1:0.2 can be estimated for our Gd(III) chelate, very close to that of  $[\text{Gd}(\text{DOTA})]^-$ . This might be a consequence of the PEG moiety, which is a bulky substituent that does not favor the stabilization of the  $m$  form in sterically crowded systems,<sup>326</sup> as it happens in less bulky and flexible systems, such as in DOTASA chelates.<sup>147</sup> The predominance of the  $M$  isomer could be why  $[\text{Gd}(\text{DOTA-A}(\text{PEG}_{750})\text{HA})]^-$  has a similar water exchange rate to  $[\text{Gd}(\text{DOTA})]^-$ . Exchange between the  $m$  and  $M$  isomers is demonstrated by the broadening at 40 °C (Figure 2.16) and further signal collapse of the resonances of both isomers observed at 60 °C.<sup>321</sup>

**Table 2.4:**  $^1\text{H}$  NMR chemical shifts (ppm) of the  $\text{ax}_1$  protons of the paramagnetic lanthanide DOTA-A( $\text{PEG}_{750}$ )HA chelates in  $M$  and  $m$  isomeric forms at 25 °C and pH=7.

Metal Ion	$M$ Isomer	$m$ Isomer	$M/m$ Ratio
Pr	-47.16; -40.31	-31.55; -28.81; -24.81; -23.87	1 : 1.5
Nd	-24.38; -21.21	-11.99; -10.31; -8.24; -7.80	1 : 1
Sm	-3.53; -3.04; -2.49	Not Assigned	---
Eu	33.16; 36.83	13.34; 14.01; 16.77; 18.19	1 : 0.25
Yb	Not Assigned	Not Assigned	---

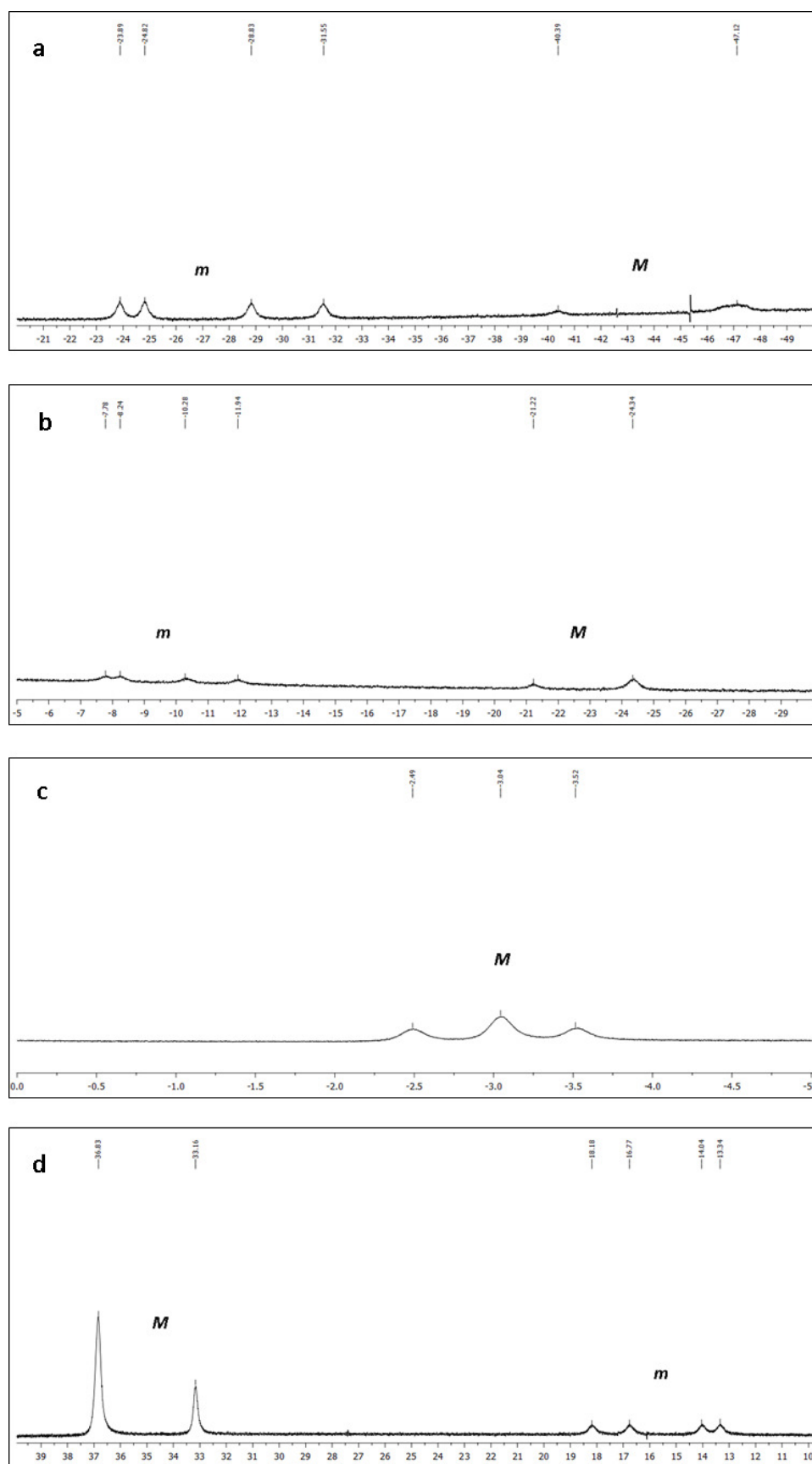


**Figure 2.15:**  $^1\text{H}$  NMR resonances of the  $ax_1$  protons of the  $M$  and  $m$  isomers of the paramagnetic lanthanide DOTA-A(PEG<sub>750</sub>)HA chelates at pH=7. 1 and 25 °C. **a)** Ln = Pr; **b)** Ln = Nd; **c)** Ln = Sm; **d)** Ln = Eu.

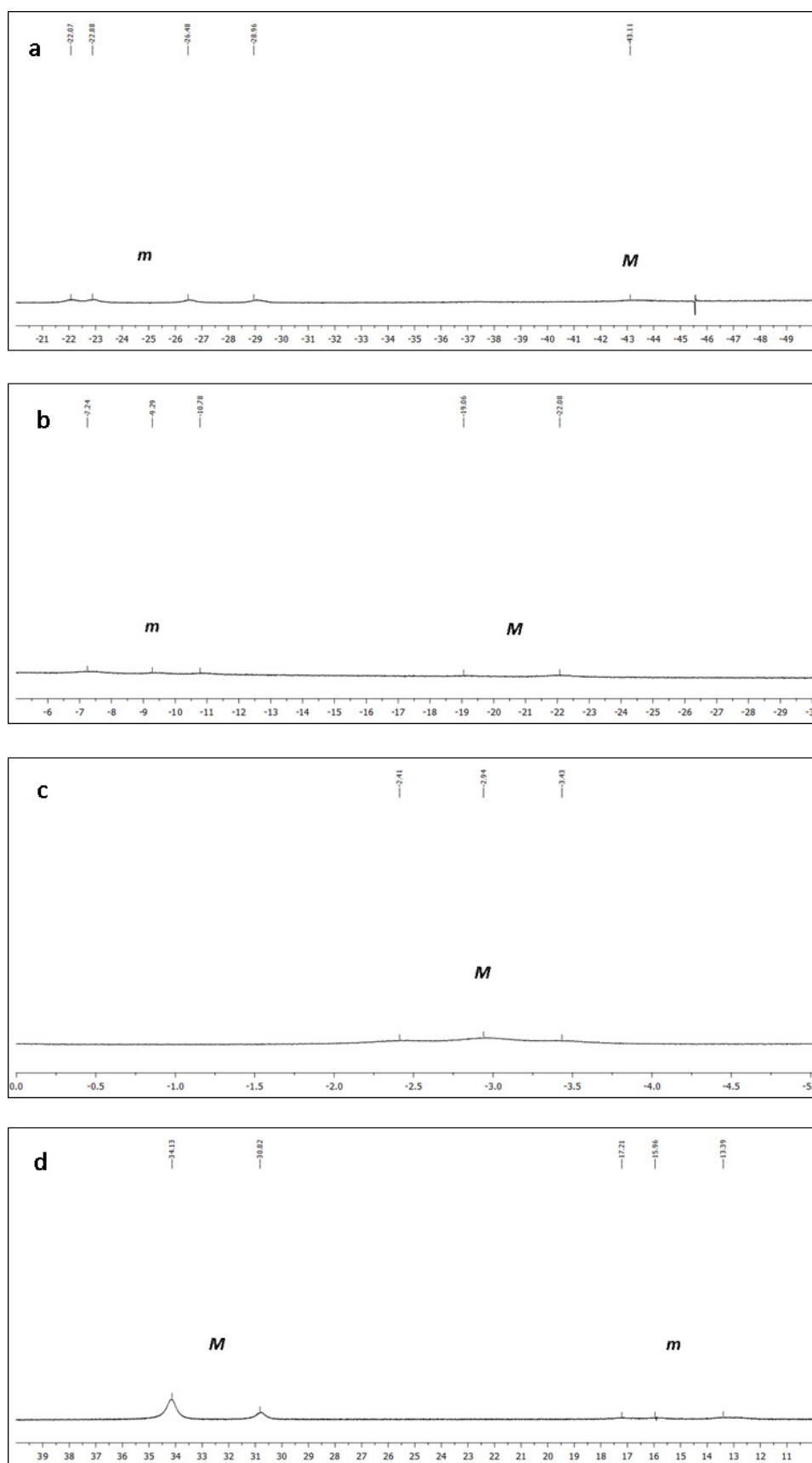


**Figure 2.16:**  $^1\text{H}$  NMR resonances of the  $ax_1$  protons of the  $M$  and  $m$  isomers of the paramagnetic lanthanide DOTA-A(PEG<sub>750</sub>)HA chelates at pH=7.1 and 40 °C. **a)** Ln = Pr; **b)** Ln = Nd; **c)** Ln = Sm; **d)** Ln = Eu.

## 2.6 *In vitro* and *in vivo* studies of $^{67}\text{Ga}(\text{DOTA-AHA})$ and $[\text{}^{67}\text{Ga}(\text{DOTA-A}(\text{PEG}_{750})\text{HA})]^-$

$^{67}\text{Ga}(\text{III})$ -radiolabelled chelates of **DOTA-AHA** and **DOTA-A(PEG<sub>750</sub>)HA** can be used to determinate physical-chemical parameters such as the octanol-water partition coefficient (LogP), and *in vitro* and *in vivo* studies are particularly useful to evaluate the chelate stability and biodistribution. Using the radioactive probe  $^{67}\text{Ga}(\text{III})$ , LogP values were determined for the gallium chelate of **DOTA-AHA** and **DOTA-A(PEG<sub>750</sub>)HA**. Biodistribution and blood clearance studies were also performed with these chelates on Wistar rats. The  $^{67}\text{Ga}$ -radiolabelled chelate  $[\text{}^{67}\text{Ga}(\text{DOTA-A}(\text{PEG}_{750})\text{HA})]^-$  was also employed for stability studies in blood serum, in order to evaluate if its interaction in terms of transmetalation.

LogP is a simple and fast way to evaluate the hydrophilicity/hydrophobicity of a certain compound, since its distribution between two immiscible solvents can be directly obtained from activity measurements. For medical purposes, it is very important to develop compounds with good hydrophilic/hydrophobic balance and avoid extreme cases. Most imaging agents need to be dissolved in saline solutions and prepared for intravenous injection, which requires a hydrophilic chelate. This is particularly crucial for MRI contrast agents, since the solution concentration used for patient administration is elevated and requires agents with elevated water miscibility. The chelate should also be hydrophilic enough not to accumulate on body fat tissues, avoiding long residence times, and preferably to be eliminated by the kidneys. When we compare the LogP values obtained for  $^{67}\text{Ga}(\text{DOTA-AHA})$  (LogP =  $-3.611 \pm 0.052$ ) and for  $[\text{}^{67}\text{Ga}(\text{DOTA-A}(\text{PEG}_{750})\text{HA})]^-$  (LogP =  $-3.606 \pm 0.060$ ), it is clear that both chelates are very hydrophilic compounds. It was expected that both chelates were hydrophilic, since the ligand structure is similar to DOTA, which is a ligand routinely used in MRI for Gd(III) chelation. Moreover, both chelates have two hydrophilic functional groups (carboxylic acids) that are not chelated with trivalent gallium, since its coordination number is six and all four nitrogen atoms in the tetraaza ring are used in the chelation.<sup>174</sup> Other factor that contributes to the hydrophilicity of these compounds is the fact that  $^{67}\text{Ga}(\text{DOTA-AHA})$  possess a free amine group on a pendant arm, whereas  $[\text{}^{67}\text{Ga}(\text{DOTA-A}(\text{PEG}_{750})\text{HA})]^-$  has a PEG moiety attached, which is very hydrophilic. It was expected

that the presence of the PEG moiety would result on a different LogP value. However, both chelates seem to have the same hydrophobic degree.

PEG moieties are commonly used as pharmacokinetic modifiers, able to increase the PEGylated compounds lifetime in living systems by reducing the protein adsorption. However, it is known that PEG is also able to weakly interact and bind non-covalently to human serum albumin, specially through hydrogen bonding.<sup>330</sup> The radiolabelled  $[^{67}\text{Ga}(\text{DOTA-A}(\text{PEG}_{750})\text{HA})]^-$  was checked for its association with serum proteins. Table 2.5 shows the values of the percentage of  $[^{67}\text{Ga}(\text{DOTA-A}(\text{PEG}_{750})\text{HA})]^-$  associated to human serum proteins 30, 60 and 180 minutes after incubation. It can be seen that the percentage of chelate bound to proteins almost triplicates between 30 and 180 minutes, from 11.7 to 30.8%. Despite not being an extravagant percentage, these results show that  $[^{67}\text{Ga}(\text{DOTA-A}(\text{PEG}_{750})\text{HA})]^-$  can associate with blood proteins in a significant percentage. This can be an advantageous feature for **DOTA-A(PEG<sub>750</sub>)HA** chelates with other metal ions, more specifically with trivalent gadolinium. The association may influence the  $[\text{Gd}(\text{DOTA-A}(\text{PEG}_{750})\text{HA})]^-$  relaxivity in human conditions compared to the aqueous solutions, since chelates associated with big biomolecules will have a slower tumbling velocity ( $\tau_R$ ), which may result in enhanced relaxivities. Non-covalent bounding to HSA has already been reported for Gd-DOTA-based chelates containing hydrophobic moieties.<sup>145, 277</sup> In those cases strong relaxation enhancements were observed, promoted by the formation of slowly tumbling paramagnetic adducts between gadolinium chelates and HSA. To prove that hypothesis, relaxometric measurements in the presence and absence of HSA must be made for the  $[\text{Gd}(\text{DOTA-A}(\text{PEG}_{750})\text{HA})]^-$ .

The activity of the supernatant 180 minutes after incubation was evaluated by TLC to check whether the chelate remained intact. The data obtained by TLC revealed that the chelate present in the supernatant remained intact, revealing a kinetic stability towards transmetalation. However, further research would be needed to confirm the chelate kinetic inertness, in particular studies in the presence of excess of a competitive ligand or in the presence of cold gallium, in order to determine the degree of metal exchange.

**Table 2.5:** Measured activity of [<sup>67</sup>Ga(DOTA-A(PEG<sub>750</sub>)HA)]<sup>-</sup> in aqueous and proteins phase of human serum solution.

Time (min)	Activity (Aqueous Phase)	Activity (Protein Phase)	% Associated With Proteins
30	28127	3301	11.7
60	14580	3527	24.2
180	12326	3793	30.8

Biodistribution studies of <sup>67</sup>Ga(DOTA-AHA) and [<sup>67</sup>Ga(DOTA-A(PEG<sub>750</sub>)HA)]<sup>-</sup> were performed on Wistar rats. The percentage of injected dose per gram of organ (%ID/g) was measured 1 hour (Figure 2.17) and 24 hours (Figure 2.18) after injection. At the same time, blood clearance studies were also performed for both chelators. The percentage of injected dose per gram of organ (%ID/g) was measured 5, 30, 60 and 1440 minutes after the injection (Figure 2.19), being the results the mean of four animals. The biodistribution profiles show that both chelates do not possess specific tissue uptake. This lack of biospecificity was expected, since these agents do not possess any biomolecule that can be used for tissue targeting or any moiety that may impose some tissue specificity, like hydrophobic groups.<sup>262</sup> Thus their biodistribution is determined entirely by their physical-chemical properties. 1 hour after injection both chelates have a strong uptake on kidneys, which reflects the renal excretion pathway of this kind of hydrophilic compounds. However, their uptake is also considerable in the majority of the remaining tissues, with a relatively elevated value on bone tissue. This uptake is a concerning result, since gallium may deposit on bone tissue, providing anabolic activity and block the bone formation.<sup>331, 332</sup> At this point, the introduction of the PEG moiety on the chelator structure seems to not influence the biodistribution profile, since both agents have similar accumulation profile for the different tissues.



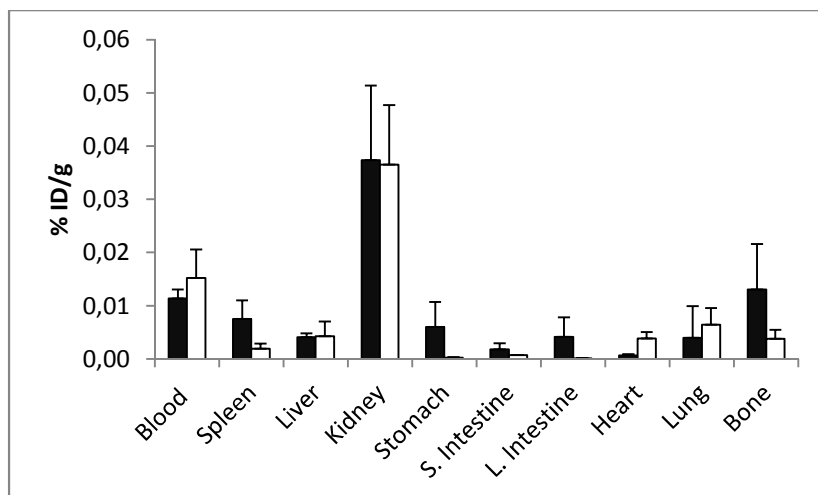


**Figure 2.17:** Biodistribution results of  $^{67}\text{Ga}(\text{DOTA-AHA})$  (filled bars) and  $[\text{}^{67}\text{Ga}(\text{DOTA-A}(\text{PEG}_{750})\text{HA})]^-$  (empty bars). Percentage of injected dose per gram of organ (%ID/g) 1 hour after injection on Wistar rats. Results are mean of four animals.

Despite having fast renal excretion, the chelates are still present in the majority of tissues 24 hours after injection. The uptake of  $^{67}\text{Ga}(\text{DOTA-AHA})$  was reduced over time, but it was still present in significant amounts.  $[\text{}^{67}\text{Ga}(\text{DOTA-A}(\text{PEG}_{750})\text{HA})]^-$  was also partially eliminated from the body over this time period. However, its presence increased on spleen, stomach and small intestine when compared to the results after 1 hour. It seems that the PEG moiety can slightly delay the agent excretion rate. In fact, the PEG containing chelate has higher activity for the majority of tissues than the non-containing PEG chelate 24 hours after injection.

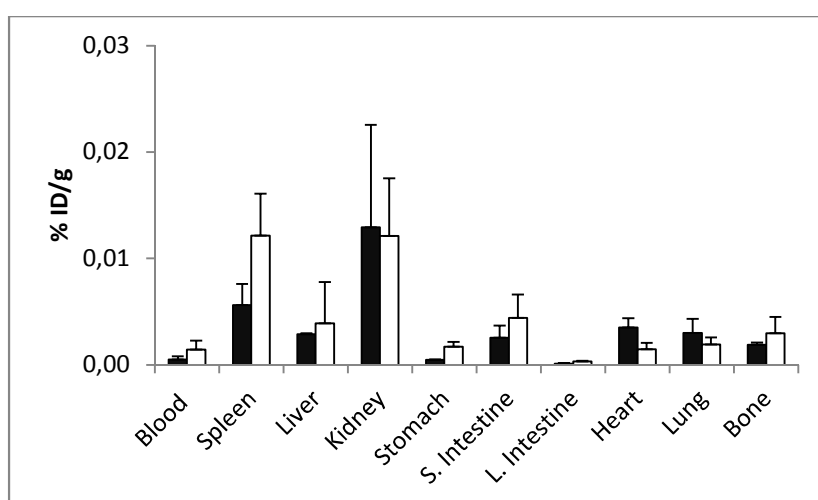


**Figure 2.18:** Biodistribution results of  $^{67}\text{Ga}(\text{DOTA-AHA})$  (filled bars) and  $[\text{}^{67}\text{Ga}(\text{DOTA-A}(\text{PEG}_{750})\text{HA})]^-$  (empty bars). Percentage of injected dose per gram of organ (%ID/g) 24 hours after injection on Wistar rats. Results are mean of four animals.

Blood clearance results show that both chelates concentration increases over the first half hour, and then they are practically eliminated after 24 hours. In this case, it is clear that [ $^{67}\text{Ga}(\text{DOTA-A}(\text{PEG}_{750})\text{HA})$ ] has higher blood retention than  $^{67}\text{Ga}(\text{DOTA-AHA})$ , since the activity of the PEG containing agent was always higher in every sample analyzed.

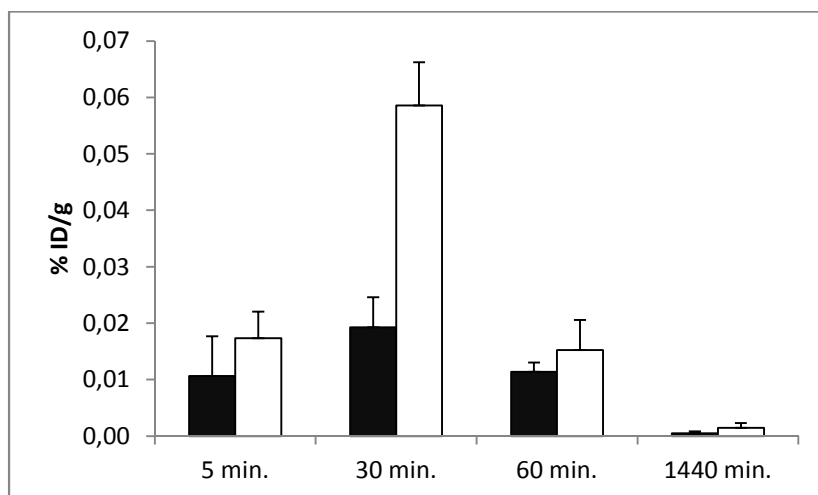


**Figure 2.19:** Blood clearance results of  $^{67}\text{Ga}(\text{DOTA-AHA})$  (filled bars) and [ $^{67}\text{Ga}(\text{DOTA-A}(\text{PEG}_{750})\text{HA})$ ] (empty bars). Percentage of injected dose per gram of organ (%ID/g) 5, 30, 60 and 1440 minutes after injection on Wistar rats. Results are mean of four animals.

# **3 Conclusion and Perspectives**



### 3.1 Conclusion

This thesis was focused on the development of new DOTA and DO3A-based chelates with potential application as imaging probes for MRI, PET and SPECT modalities.

With that in mind, the synthesis of three  $N_4O_4$  polyaminopolycarboxylate ligands, the **DOTA-APPA**, **DO3A- $\beta$ BABA** and **DOTA-AHA** was attempted. The synthesis of the first two ligands has proved to be challenging and demanding, and only **DOTA-AHA** was successfully synthesized and characterized. Due to the presence of the **DOTA** moiety, this bifunctional ligand is capable of efficiently chelate metal ions such as Gd(III) and Ga(III), while the extra amine group in one of the pendant arms enables its conjugation to different (bio)molecules through a variety of linkages. The **DOTA-AHA** pro-ligand was used as a building block for the development of three types of conjugates: a) dimeric ligands; b) PEGylated chelators; and c) bioconjugates with c(RGDWK) peptide for targeted  $\alpha_v\beta_3$  integrin receptor mediated imaging. Dimeric **bis(DOTA-AHA)adipate** and **bis(DOTA-AHA)1,3-phenyldiacetate** ligands were specially designed to prepare Gd(III) chelates, in order to be used as contrast agents. These molecules may enhance the relaxivity due to a long rotational correlation time provided by their increased molecular weight. The same relaxivity enhancement strategy was applied to the PEGylated ligands **DOTA-A(PEG<sub>350</sub>)HA**, **DOTA-A(PEG<sub>550</sub>)HA** and **DOTA-A(PEG<sub>750</sub>)HA**. Besides increasing the molecular weight, the PEG moieties may also act as pharmacokinetic modifiers, improving the chelates biodistribution profiles.

Relaxometric studies were performed with trivalent gadolinium chelates of **DOTA-AHA** and their binuclear and PEGylated conjugates. Measurements made at 20 MHz revealed that **Gd(DOTA-AHA)** present high stability against acid and base catalysed hydrolysis, also showing to be kinetically inert to transmetalation in the presence of Zn(II) in solution.  $^1\text{H}$  NMRD and  $^{17}\text{O}$  NMR studies performed with these chelates allowed the determination of the parameters that govern their relaxivities. The chelate **Gd(DOTA-AHA)** has a slightly faster water exchange than **Gd(DOTA)** but its higher relaxivity is due to the existence of *circa* 10% of Gd(III) in the aggregated form, besides to the lateral pendant C4-NH<sub>2</sub> chain.

The binuclear derivatives  $[\text{Gd}_2(\text{Bis}(\text{DOTA-AHA})\text{adipate})]^{2-}$  and  $[\text{Gd}_2(\text{Bis}(\text{DOTA-AHA})\text{1,3-phenyldiacetate})]^{2-}$  do not show a considerable relaxivity improvement in comparison to other existing DO3A-based binuclear Gd(III) chelates for lower frequencies (20 MHz), despite the higher water exchange rates on DOTA based chelates in comparison to DO3A based chelates. However, these binuclear chelates show a considerable augment in relaxivity as the frequency increases, surpassing other Gd(III) binuclear constructs at the frequencies with relevance for MRI scans (between 50 and 100 MHz). This augment in relaxivity has also been attributed to aggregation of the chelates (with approximately 15% of Gd(III) in the aggregated form).

All PEGylated Gd(III) chelates were studied by  $^1\text{H}$  relaxometry, but  $^{17}\text{O}$  NMR measurements were only recorded for  $[\text{Gd}(\text{DOTA-A}(\text{PEG}_{550})\text{HA})]^-$ . The PEGylation of **Gd(DOTA-AHA)** only resulted in a modest relaxivity increase, giving chelates with relaxivity values even lower than those found for the binuclear chelates. This result was not predictable for two reasons: a) The PEGylation did not affect the water exchange rate; b) the PEG chain attachment resulted in chelates with elevated global rotational correlation times. Despite this elevated  $\tau_g$  value also suggesting an aggregation of the PEGylated chelates in solution, that possibility was not evaluated. The elevated PEG flexibility gave rise to faster local correlation time ( $\approx 250$  ps) and the extremely low  $S^2$  values ( $\approx 0.05$ ), which prevented higher relaxivity improvements.

For the binuclear chelates, DEER and modelling studies afforded the distances of maximum and minimum approach of the two Gd(III) centers in a very reasonable agreement, consistent with the assumption that chelates of such dimensions by themselves, without aggregation, would not present such high relaxivities.

$^1\text{H}$  NMR studies were performed with **DOTA-A(PEG<sub>750</sub>)HA** paramagnetic lanthanide chelates. The presence of both square antiprismatic (*M*) and square twisted antiprismatic isomers (*m*) in solution was observed for the majority of lanthanide chelates. The presence of a chiral center at one of the DOTA acetate arms did not result in change of the predictable isomer proportions, since the *M/m* ratio for the  $[\text{Ln}(\text{DOTA-A}(\text{PEG}_{750})\text{HA})]^-$  series is similar to the  $[\text{Ln}(\text{DOTA})]^-$  chelates,<sup>317</sup> where the *M/m* isomer ratio increases along the lanthanide series.

Different studies using  $^{67}\text{Ga}$ (III) were performed with **DOTA-AHA** and **DOTA-A(PEG<sub>750</sub>)HA**.  $^{67}\text{Ga}(\text{DOTA-AHA})$  and  $[\text{Gd}(\text{DOTA-A}(\text{PEG}_{750})\text{HA})]^-$  present very negative LogP values, showing that both chelates are extremely hydrophilic. Although it was expected that PEGylation would increase the  $[\text{Gd}(\text{DOTA-A}(\text{PEG}_{750})\text{HA})]^-$

hydrophilicity, both chelates seem to have the same hydrophobic degree. Stability studies in blood serum revealed that  $[^{67}\text{Ga}(\text{DOTA-A}(\text{PEG}_{750})\text{HA})]^-$  can associate with blood serum proteins with a considerable degree. This association seems not to affect the chelate integrity at least for 180 minutes, since no radiolysis breakdown products were identified. The lack of *in vivo* biospecificity of  $^{67}\text{Ga}(\text{DOTA-AHA})$  and  $[^{67}\text{Ga}(\text{DOTA-A}(\text{PEG}_{750})\text{HA})]^-$  suggest that their biodistribution profiles are entirely determined by their physical-chemical properties. Despite suffering fast renal excretion, these chelates showed considerable uptake at the majority of tissues. The PEGylation only result in a small delay of the chelate excretion rate, which is more evident for the spleen, stomach and small intestine.

### 3.2 Perspectives

The work developed during this thesis gave some encourage results and further studies and improvements are necessary to complement the obtained results. The general strategy for the synthesis of DOTA-based bifunctional chelators needs to be adjusted, since only **DOTA-AHA** was successfully obtained. The synthetic strategy for the **DOTA-AHA** conjugation containing RGD peptide moieties also needs to be optimized in order to obtain different conjugates with high yields and elevated purity. Despite the fact that no studies were performed with these biomolecules, several *in vitro* and *in vivo* studies with  $^{67/68}\text{Ga}$ -radiolabeled chelates can be conducted as part of their characterization, such as: determination of partition coefficient (LogP); affinity studies with cell lines overexpressing  $\alpha\text{v}\beta\text{3}$  integrin receptor; competition studies for the  $\alpha\text{v}\beta\text{3}$  integrin receptor using an irreversible blocker; biodistribution with animal models bearing tumors with overexpressed  $\alpha\text{v}\beta\text{3}$  integrin receptor or PET imaging experiments in normal and tumour animal models. The characterization of Gd(III) conjugates by  $^1\text{H}$  NMRD and  $^{17}\text{O}$  NMR can also be performed to evaluate the efficiency of these compounds as contrast agents, although these studies require large chelate amounts.

The aggregation process displayed by the binuclear Gd(III) chelates should also be process of further reflection. This is a surprising and unexpected aspect of the work and it can be studied in more detail. In order to understand how and why aggregation occurs, NMRD profiles at different concentrations, relaxivity measurements as function of temperature and pH and dynamic light scattering measurements must be conducted.





# 4 Experimental Part



## 4.1 Chemicals and materials

Analytical grade solvents were used and dried by the usual methods when was needed. Analytical grade reagents were purchased from Sigma-Aldrich, Acros, Bachem, Merck, Chematech and used without further purification.  $^{17}\text{O}$ -enriched water was purchased from IsoTrade GmbH (Mönchengladbach, Germany).  $^{67}\text{Ga}$ -citrate was purchased from CIS-BIO (Gif-sur-Yvette, France) and ITLC-SC stripes (instant thin layer chromatography) were from Gelman Sciences Inc (Ann Arbor, United States of America).

The reactions were monitored by thin layer chromatography (TLC) on glass plates coated with silica gel 60 F<sub>254</sub> (Whatman) and detection was made by examination under UV light (240 nm), by adsorption of iodine vapor and/or by spraying with ninhydrin. Chromatographic separations were performed on silica gel 60 (Whatman 230-240 Mesh). The radiochemical purity of the [ $^{67}\text{GaL}$ ] solutions was monitored by ITLC-SC stripes.

## 4.2 Instruments

The  $^1\text{H}$  and  $^{13}\text{C}$  NMR spectra (assigned by DEPT, HSQC and HMBC techniques) were recorded on a Bruker Avance III 400 spectrometer, operating at 400.13 MHz and 100.62 MHz, for  $^1\text{H}$  and  $^{13}\text{C}$  NMR respectively. The  $^1\text{H}$  NMR spectra of DO3A- $\alpha$ AHA<sub>PEG750</sub> paramagnetic lanthanide complexes were recorded on a Varian Unity Plus 300, operating at 299.938 MHz. The chemical shifts ( $\delta$ ) are reported in ppm, relative to TMS (tetramethylsilane) for  $\text{CDCl}_3$  solvent ( $^1\text{H}$ ,  $\delta=7.26$ ;  $^{13}\text{C}$ ,  $\delta=77.16$ ) or DMSO solvent ( $^1\text{H}$ ,  $\delta=2.50$ ;  $^{13}\text{C}$ ,  $\delta=39.52$ ), and relative to TSP (3-(trimethylsilyl)propionic-2,2,3,3-d<sub>4</sub> acid sodium salt) for  $\text{D}_2\text{O}$  solvent ( $^1\text{H}$ ,  $\delta=4.79$ ).<sup>333</sup> The high resolution mass spectra (HRMS) were recorded on a VG Autospec M spectrometer and the low resolution mass spectra (LRMS) were recorded on a Finnigan LXQ MS DETECTOR spectrometer. The pH measurements were performed on a pH meter Crison micro TT 2050 with an electrode Mettler Toledo InLab 422. The purity degree of peptide moieties was determined by HPLC analysis and performed on a system comprised by a Rheodyne 7725i injector, a Jasco PU-980 pump, a Lichospher<sup>®</sup>

100, RP-18 (5  $\mu$ M) column, a Jasco UV-975 wavelength UV/Vis detector and a Shimadzu C-R6A chromatopac register.

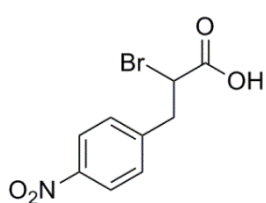
For the relaxometric experiments at 20 MHz, the water proton longitudinal relaxation rates ( $1/T_1$ ) were measured on a Bruker Minispec mq20, equipped with a temperature control unit. The proton longitudinal relaxation rates ( $1/T_1$ ) for the water nuclear magnetic relaxation dispersion profiles (NMRD) were measured using the following equipment: Bruker minispecs mq20 0.47 T ( $^1\text{H}$  Larmor frequency: 20 MHz); mq30 0.70 T (30 MHz); mq40 0.94 T (40 MHz); and mq60 1.41 T (60 MHz); Bruker Avance console connected to 2.35 T (100 MHz) and 4.7 T (200 MHz) cryomagnets and Bruker Avance II 9.4 T (400 MHz). The temperature was controlled either by a thermostated gas flow (cryomagnets) or by pumping a thermostated liquid through the probe (minispecs). All temperatures were measured by substitution technique.<sup>334</sup> The variable-temperature  $^{17}\text{O}$  measurements were performed on a Bruker Avance II 9.4 T ( $^{17}\text{O}$  Larmor frequency: 54.3 MHz) spectrometer, equipped with a Bruker BVT3000 temperature control unit and a Bruker BCU05 cooling unit. The susceptibility measurements were performed on a Bruker Avance 400 spectrometer, also equipped with a BVT-3000 temperature control unit.

For the EPR experiments, the Gd(III)-Gd(III) distance measurements were performed with the 4 pulse double electron-electron resonance experiment,<sup>304, 308</sup> at Q band on a home-built high microwave power spectrometer<sup>335</sup> equipped with a rectangular resonator accommodating for 3 mm outer diameter samples.<sup>336, 337</sup> The temperature was set and stabilized with a He-flow cryostat Oxford Instruments ER 4118 CF.

For the assays with  $^{67}\text{Ga(III)}$ , the activity measurements were performed with a DPC-C<sub>12</sub>  $\gamma$ -counter, coupled with a Compaq DeskPro computer.

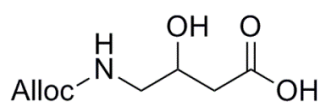
### 4.3 Synthesis

#### 2-Bromo-3-(4-nitrophenyl)-propionic acid, **2**



4-Nitrophenylalanine (908 mg, 4.3 mmol) and sodium bromide (1.5 g, 14.7 mmol) were dissolved in HBr 1M (8.6 mL) and the solution cooled in an ice bath. Sodium nitrite (526 mg, 7.6 mmol) was added in small portions and the mixture was stirred for 2 hours at 0 °C. Water (30 mL) and ethyl ether (60 mL) were added to the reaction mixture. The organic phase was separated and the aqueous phase was extracted with ethyl ether (3 x 60 mL). The organic phases were combined, washed with brine (3 x 60 mL), dried with anhydrous MgSO<sub>4</sub> and concentrated under reduced pressure to give yellow oil. The oil was purified by column chromatography over silica gel 60 (ethyl acetate/EtOH 2:1) to afford (868.9 mg, 73 %) of a yellow oil. <sup>1</sup>H NMR (400 MHz, DMSO, TMS) δ: 2.28 (1H, dd, *J*<sub>1</sub>=20.0 Hz, *J*<sub>2</sub>=10.0 Hz, β-CH<sub>2</sub>), 3.54 (1H, dd, *J*<sub>1</sub>=20.0 Hz, *J*<sub>2</sub>=8.0 Hz, β-CH<sub>2</sub>), 4.76 (1H, m, α-CH), 7.59 (2H, d, *J*=12.0 Hz, ArH), 8.17 (2H, d, *J*=12.0 Hz, ArH) ppm. <sup>13</sup>C NMR (100 MHz, DMSO, TMS) δ: 46.43 (β-CH<sub>2</sub>), 70.31 (α-CH), 123.27 (CH), 130.43 (CH), 145.47 (C), 146.55 (C), 170.09 (C=O) ppm. LRMS (ESI) calculated for C<sub>9</sub>H<sub>8</sub>BrNO<sub>4</sub> (MH<sup>+</sup>) 273.97, 275.97; found 273.96, 275.96 (MH<sup>+</sup>).

#### 4-Allyloxycarbonylamino-3-hydroxy-butyric acid



GABOB (18.0 g, 151.1 mmol) was dissolved in Na<sub>2</sub>CO<sub>3</sub> (10% w/w) (430 mL) and 1,4-dioxane (260 mL). The solution was cooled in an ice bath and allyl chloroformate (16.6 mL, 156.2 mmol) were added dropwise. The reaction mixture was stirred for 4 hours at 0 °C and overnight at room temperature. Water (800 mL) was added and the mixture was washed with ethyl ether (2 x 700 mL). The aqueous phase was acidified to pH = 2 with HCl and extracted with ethyl acetate (3 x 700 mL). The organic phases were combined, dried with anhydrous MgSO<sub>4</sub> and concentrated under reduced pressure to afford (29.4 g, 97 %) of a colorless oil. <sup>1</sup>H NMR (400 MHz, DMSO, TMS) δ: 2.13-2.35 (2H, m, α-CH<sub>2</sub>), 2.96-3.00 (2H, m, γ-CH<sub>2</sub>), 3.83-3.89 (1H, m, β-CH), 4.45 (2H, dd, *J*<sub>1</sub>=5.1 Hz, *J*<sub>2</sub>=1.6 Hz, OCH<sub>2</sub> Alloc), 5.15 (1H, dd, *J*<sub>1</sub>=10.6 Hz, *J*<sub>2</sub>=1.8 Hz, CH-cis Alloc), 5.26 (1H, dd, *J*<sub>1</sub>=17.2 Hz, *J*<sub>2</sub>=1.8 Hz, CH-trans Alloc), 5.84-5.94 (1H, m, CH Alloc), 7.14 (1H, t, *J*=5.8 Hz, NH) ppm. <sup>13</sup>C NMR (100 MHz, DMSO, TMS) δ: 40.02 (α-CH<sub>2</sub>), 46.31 (γ-CH<sub>2</sub>), 64.24

(OCH<sub>2</sub> Alloc), 66.62 (β-CH<sub>2</sub>), 116.87 (CH<sub>2</sub> Alloc), 133.77 (CH Alloc), 156.10 (C=O Alloc), 172.77 (C=O) ppm.

#### 4-Allyloxycarbonylamino-3-hydroxy-butyric acid methyl ester, **5**

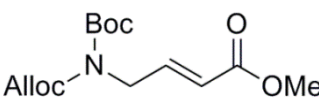
Methanol (330 mL) was cooled in an ice bath and thionyl chloride (51.6 mL, 710.4 mmol) was added dropwise. The 4-Allyloxycarbonylamino-3-hydroxy-butyric acid (28.9 g, 142.26 mmol) was dissolved in MeOH (330 mL) and added dropwise. The reaction mixture was stirred for 5 hours at reflux, concentrated under reduced pressure and triturated with petroleum ether (2 x 100 mL). Compound **5** was obtained as a yellow oil (27.8 g, 90%) of a yellow oil. <sup>1</sup>H NMR (400 MHz, DMSO, TMS) δ: 2.21 (1H, dd, *J*<sub>1</sub>=15.0 Hz, *J*<sub>2</sub>=3.9 Hz, α-CH<sub>2</sub>), 2.45 (1H, dd, *J*<sub>1</sub>=15.0 Hz, *J*<sub>2</sub>=3.8 Hz, α-CH<sub>2</sub>), 2.92-3.04 (2H, m, γ-CH<sub>2</sub>), 3.57 (3H, s, OCH<sub>3</sub>), 3.85-3.91 (1H, m, β-CH), 4.45 (2H, dd, *J*<sub>1</sub>=5.4 Hz, *J*<sub>2</sub>=1.4 Hz, OCH<sub>2</sub> Alloc), 5.15 (1H, dd, *J*<sub>1</sub>=10.4 Hz, *J*<sub>2</sub>=1.8 Hz, CH-cis Alloc), 5.26 (1H, dd, *J*<sub>1</sub>=17.2 Hz, *J*<sub>2</sub>=1.8 Hz, CH-trans Alloc), 5.84-5.94 (1H, m, CH Alloc), 7.17 (1H, t, *J*=5.8 Hz, NH) ppm. <sup>13</sup>C NMR (100 MHz, DMSO, TMS) δ: 39.75 (α-CH<sub>2</sub>), 46.24 (γ-CH<sub>2</sub>), 51.20 OCH<sub>3</sub>), 64.24 (OCH<sub>2</sub> Alloc), 66.56 (β-CH<sub>2</sub>), 116.88 (CH<sub>2</sub> Alloc), 133.74 (CH Alloc), 156.09 (C=O Alloc), 171.60 (C=O) ppm. HRMS (ESI): calculated for C<sub>9</sub>H<sub>15</sub>NO<sub>5</sub> (MH<sup>+</sup>) 218.10285, (MNa<sup>+</sup>) 240.08479; found 218.10230 (MH<sup>+</sup>), 240.08424 (MNa<sup>+</sup>).

#### 4-Allyloxycarbonylamino-but-2-enoic acid methyl ester, **6**

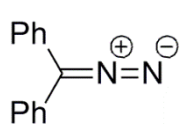
2 Compound **5** (2.2 g, 10.0 mmol) was dissolved dry MeCN (20 mL) and *tert*-butyl dicarbonate (Boc<sub>2</sub>O) (2.6 g, 12.0 mmol) and 4-dimethylaminopyridine (DMAP) (122 mg, 1.0 mmol) were added. The solution was stirred for 72 hours at room temperature and the formation of the carbonate intermediate was monitored by <sup>1</sup>H NMR spectroscopy. 1,1,3,3-Tetramethylguanidine (TMG) (832 μL) was added and the solution was stirred at room temperature for 24 hours. The solvent was removed under reduced pressure, the residue dissolved in ethyl acetate (130 mL) and washed with KHSO<sub>4</sub> 1 M (2 x 100 mL), NaHCO<sub>3</sub> 1 M (2 x 100 mL) and brine (2 x 100 mL). The organic phase was dried with anhydrous MgSO<sub>4</sub> and concentrated under reduced pressure to give a yellow oil. The oil was purified by column chromatography over silica gel 60 (cyclohexane/ethyl ether 1:1) to afford compound **6** as a colorless oil (1.0 g, 54 %). <sup>1</sup>H NMR (400 MHz, CDCl<sub>3</sub>,

TMS)  $\delta$ : 3.73 (3H, s, OCH<sub>3</sub>), 3.94-4.01 (2H, m,  $\gamma$ -CH<sub>2</sub>), 4.59 (2H, d,  $J$ =9.2 Hz, OCH<sub>2</sub> Alloc), 4.98-5.07 (1H, m, NH), 5.22 (1H, dd,  $J_1$ =10.8 Hz,  $J_2$ =1.6 Hz, CH-cis Alloc), 5.31 (1H, dd,  $J_1$ =17.2 Hz,  $J_2$ =1.6 Hz, CH-trans Alloc), 5.87-5.97 (1H, m, CH Alloc), 5.92-5.99 (1H, m,  $\alpha$ -CH), 6.91 (1H, dt,  $J_1$ =15.6 Hz,  $J_2$ =4.8 Hz,  $\beta$ -CH) ppm. <sup>13</sup>C NMR (100 MHz, CDCl<sub>3</sub>, TMS)  $\delta$ : 41.66 ( $\gamma$ -CH<sub>2</sub>), 51.62 (OCH<sub>3</sub>), 65.85 (OCH<sub>2</sub> Alloc), 117.91 (CH<sub>2</sub> Alloc), 121.14 ( $\alpha$ -CH), 132.58 (CH Alloc), 144.46 ( $\beta$ -CH), 156.02 (C=O Alloc), 166.40 (C=O) ppm. HRMS (ESI<sup>+</sup>): calculated for C<sub>9</sub>H<sub>13</sub>NO<sub>4</sub> (MH<sup>+</sup>) 200.09228; found 200.09173.

#### 4-Amino(Alloc, Boc)but-2(*E*)-enoate methyl ester

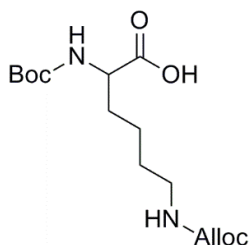
 Compound **5** (434 mg, 2.0 mmol) was dissolved in dry MeCN (4 mL). Boc<sub>2</sub>O (1.3 g, 6.0 mmol) and DMAP (73 mg, 0.6 mmol) were added. The solution was stirred for 72 hours at room temperature and the formation of the carbonate intermediate was monitored by <sup>1</sup>H NMR spectroscopy. TMG (82  $\mu$ L) was added and the solution was stirred for 24 hours at room temperature. The reaction mixture was concentrated under reduced pressure, the residue was dissolved in ethyl acetate (30 mL) and the washed with KHSO<sub>4</sub> 1 M (2 x 15 mL), NaHCO<sub>3</sub> 1 M (2 x 15 mL) and brine (2 x 15 mL). The organic phase was dried with anhydrous MgSO<sub>4</sub> and concentrated under reduced pressure to afford a yellow oil (544.5 mg, 91 %). <sup>1</sup>H NMR (400 MHz, CDCl<sub>3</sub>, TMS)  $\delta$ : 1.51 (9H, s, CH<sub>3</sub> Boc), 3.74 (3H, s, OCH<sub>3</sub>), 4.42 (2H, dd,  $J_1$ =5.2 Hz,  $J_2$ =1.6 Hz,  $\gamma$ -CH<sub>2</sub>), 4.70 (2H, dt,  $J_1$ =6.0 Hz,  $J_2$ =1.4 Hz, OCH<sub>2</sub> Alloc), 5.28 (1H, dd,  $J_1$ =10.4 Hz,  $J_2$ =1.6 Hz, CH-cis Alloc), 5.38 (1H, dd,  $J_1$ =17.4 Hz,  $J_2$ =1.6 Hz, CH-trans Alloc), 5.87-5.99 (1H, m, CH Alloc), 5.89-5.94 (1H, m,  $\alpha$ -CH), 6.91 (1H, dt,  $J_1$ =16.0 Hz,  $J_2$ =5.2 Hz,  $\beta$ -CH) ppm. <sup>13</sup>C NMR (100 MHz, CDCl<sub>3</sub>, TMS)  $\delta$ : 27.94 (CH<sub>3</sub> Boc), 46.82 ( $\gamma$ -CH<sub>2</sub>), 51.63 (OCH<sub>3</sub>), 67.62 (OCH<sub>2</sub> Alloc), 83.53 (C Boc), 118.96 (CH<sub>2</sub> Alloc), 121.71 ( $\alpha$ -CH), 131.50 (CH Alloc), 143.23 ( $\beta$ -CH), 151.33 (C=O Boc), 153.27 (C=O Alloc), 166.41 (C=O OMe) ppm. HRMS (ESI): calculated for C<sub>14</sub>H<sub>21</sub>NO<sub>6</sub> (MH<sup>+</sup>) 300.14471; found 300.14495 (MH<sup>+</sup>).

### Diphenyldiazomethane (DDM)



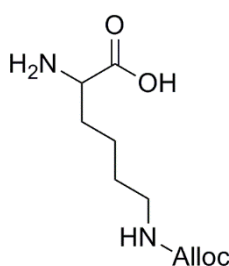
DDM was prepared according to the method of Miller.<sup>338</sup> To benzophenonehydrazone (10.0 g, 51.1 mmol) anhydrous sodium sulfate (11.5 g), yellow mercury(II) oxide (26.9 g, 124.2 mmol), a solution of ethanol saturated with potassium oxide (3.8 mL) and ethyl ether (160 mL) were added. The mixture was stirred for 75 minutes at room temperature, filtered and concentrated under reduced pressure to give a dark red oil. This oil was dissolved in petroleum ether 40-60 °C and filtered. The filtrate was concentrated under reduced pressure to give a dark red oil. The oil was left to freeze over 3 hours and heated to room temperature to afford (9.9 g, 99 %) of dark red crystals.

### Boc-Lys(Alloc)-OH

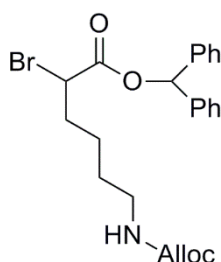


Boc-Lys-OH (9.0 g, 36.5 mmol) was dissolved in Na<sub>2</sub>CO<sub>3</sub> (10% w/w) (150 mL) and 1,4-dioxane (90 mL). The solution was cooled in an ice bath and allyl chloroformate (3.9 mL, 36.7 mmol) of was added dropwise. The reaction mixture was stirred for 4 hours at 0 °C and overnight at room temperature. Water (1.5 L) was added and the aqueous phase was washed with ethyl ether (2 x 600 mL). The aqueous phase was acidified to pH = 2 with HCl conc. and extracted with ethyl acetate (3 x 900 mL). The organic phases were combined, dried with anhydrous MgSO<sub>4</sub> and concentrated under reduced pressure to afford Boc-Lys(Alloc)-OH (11.9 g, 98 %) as a colorless oil. <sup>1</sup>H NMR (400 MHz, CDCl<sub>3</sub>, TMS) δ: 1.44 (9H, s, CH<sub>3</sub> Boc), 1.48-1.60 (2H, m, γ-CH<sub>2</sub>), 1.60-1.93 (4H, m, β-CH<sub>2</sub> + δ-CH<sub>2</sub>), 3.14-3.25 (2H, m, ε-CH<sub>2</sub>), 4.22-4.38 (1H, m, α-CH), 4.56 (2H, d, *J*=5.2 Hz, OCH<sub>2</sub> Alloc), 5.20 (1H, d, *J*=10.4 Hz, CH-cis Alloc), 5.30 (1H, d, *J*=16.4 Hz, CH-trans Alloc), 5.86-5.96 (1H, m, CH Alloc) ppm. <sup>13</sup>C NMR (100 MHz, CDCl<sub>3</sub>, TMS) δ: 22.29 (γ-CH<sub>2</sub>), 28.29 (CH<sub>3</sub> Boc), 29.32 (δ-CH<sub>2</sub>), 31.87 (β-CH<sub>2</sub>), 40.47 (ε-CH<sub>2</sub>), 53.12 (α-CH), 65.55 (OCH<sub>2</sub> Alloc), 80.11 (C Boc), 117.68 (CH<sub>2</sub> Alloc), 132.87 (CH Alloc), 155.83 (C=O), 156.80 (C=O), 176.08 (C=O CO<sub>2</sub>H) ppm.



**H-Lys(Alloc)-OH**

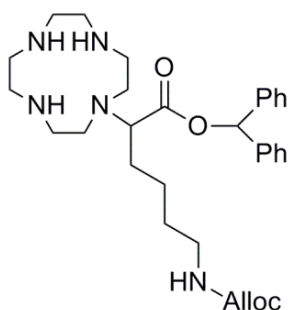
Boc-Lys(Alloc)-OH (11.8 g, 35.7 mmol) was dissolved in TFA (170 mL). The solution was stirred for 4 hours at room temperature and concentrated under reduced pressure to give a brown oil. The oil was dissolved in MeOH and ethyl ether was added to the solution. The solid was filtered washed with cold ethyl ether to give H-Lys(Alloc)-OH (7.5 g, 61 %).  $^1\text{H}$  NMR (400 MHz, DMSO, TMS)  $\delta$ : 1.28-1.44 (4H, m,  $\gamma$ -CH<sub>2</sub> +  $\delta$ -CH<sub>2</sub>), 1.72-1.76 (2H, m,  $\beta$ -CH<sub>2</sub>), 2.94-2.98 (2H, m,  $\epsilon$ -CH<sub>2</sub>), 3.84-3.87 (1H, m,  $\alpha$ -CH), 4.45 (2H, d,  $J$ =5.2 Hz, OCH<sub>2</sub> Alloc), 5.15 (1H, dd,  $J_1$ =10.4 Hz,  $J_2$ =3.2 Hz, CH-cis Alloc), 5.25 (1H, dd,  $J_1$ =20.0 Hz,  $J_2$ =3.2 Hz, CH-trans Alloc), 5.83-5.92 (1H, m, CH Alloc), 7.16 (1H, t,  $J$ =5.4 Hz, NH), 8.11-8.32 (3H, m, NH<sub>3</sub><sup>+</sup>) ppm.  $^{13}\text{C}$  NMR (100 MHz, DMSO, TMS)  $\delta$ : 21.64 ( $\gamma$ -CH<sub>2</sub>), 28.90 ( $\delta$ -CH<sub>2</sub>), 29.72 ( $\beta$ -CH<sub>2</sub>), 39.90 ( $\epsilon$ -CH<sub>2</sub>), 51.94 ( $\alpha$ -CH), 64.19 (OCH<sub>2</sub> Alloc), 116.92 (CH<sub>2</sub> Alloc), 133.86 (CH Alloc), 155.98 (C=O Alloc), 171.11 (C=O CO<sub>2</sub>H) ppm.

**6-Amino(Alloc)-2-bromohexanoate benzhydryl ester, 9**

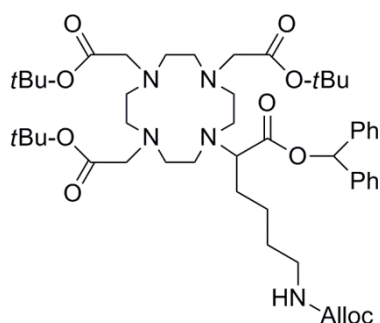
H-Lys(Alloc)-OH (4.0 g, 11.6 mmol) and sodium bromide (4.2 g, 40.3 mmol) were dissolved in hydrobromic acid 1M (23 mL). The solution was cooled in an ice bath and sodium nitrite (1.6 g, 23.0 mmol) was added in small portions. The reaction mixture was stirred for 2 hours at 0 °C. Water (45 mL) and ethyl ether (105 mL) were added to the mixture. The organic phase was collected, and the aqueous phase was extracted with ethyl ether (3 x 35 mL). The organic phases were combined, washed with brine (3 x 35 mL), dried with anhydrous MgSO<sub>4</sub> and concentrated under reduced pressure to give a yellow oil. The oil was dissolved in acetone (90 mL), stirred at 0 °C and DDM (2.7 g, 13.9 mmol) in acetone (150 mL) were added dropwise over a period of 1 hour. The mixture was stirred for 4 hours at 0 °C and over 2 days at room temperature. The solution was concentrated under reduced pressure to give a yellow oil. The oil was purified by column chromatography over silica gel 60 (cyclohexane/ethyl acetate 4:1) to afford compound **8** (5.3 g, 52 %).  $^1\text{H}$  NMR (400 MHz, DMSO, TMS)  $\delta$ : 1.16-1.47 (4H, m,  $\gamma$ -CH<sub>2</sub> +  $\delta$ -CH<sub>2</sub>), 1.85-2.08 (2H, m,  $\beta$ -CH<sub>2</sub>), 2.92 (2H, q,  $J$ =6.3 Hz,  $\epsilon$ -CH<sub>2</sub>), 4.43 (2H, d,  $J$ =5.6 Hz, OCH<sub>2</sub> Alloc), 4.69 (1H, t,  $J$ =7.2 Hz,  $\alpha$ -CH), 5.14 (1H, dd,  $J_1$ =10.4 Hz,  $J_2$ =1.6 Hz, CH-cis Alloc), 5.25 (1H, dd,  $J_1$ =17.2 Hz,  $J_2$ =2.0 Hz, CH-trans Alloc)

Alloc), 5.83-5.91 (1H, m, CH Alloc), 6.83 (1H, s, CH Benzhydryl), 7.16 (1H, t,  $J=5.8$  Hz, NH), 7.26-7.43 (10H, m, ArH) ppm.  $^{13}\text{C}$  NMR (100 MHz, DMSO, TMS)  $\delta$ : 23.28 ( $\gamma\text{-CH}_2$ ), 28.58 ( $\delta\text{-CH}_2$ ), 33.90 ( $\beta\text{-CH}_2$ ), 39.86 ( $\epsilon\text{-CH}_2$ ), 46.71 ( $\alpha\text{-CH}$ ), 64.09 (OCH<sub>2</sub> Alloc), 77.68 (CH Benzhydryl), 116.81 (CH<sub>2</sub> Alloc), 126.47 (CH), 127.96 (CH), 128.55 (CH), 133.84 (CH Alloc), 139.80 (C), 155.88 (C=O Alloc), 168.15 (C=O) ppm. HRMS (ESI): calculated for C<sub>23</sub>H<sub>26</sub>BrNO<sub>4</sub> (MH<sup>+</sup>) 460.11235, 462.11030, (MNa<sup>+</sup>) 482.09429, 484.09224; found 460.11168, 462.10987 (MH<sup>+</sup>), 482.09549, 484.09181 (MNa<sup>+</sup>).

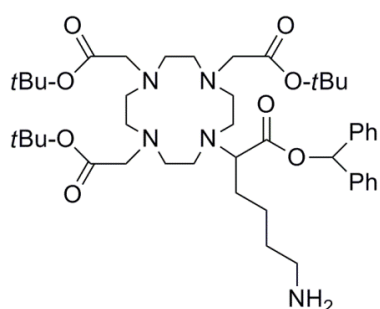
### DO0A-A(Alloc)HA(Be), 10



To a solution of cyclen (726 mg, 4.4 mmol) in MeCN (70 mL) potassium carbonate (432 mg, 3.1 mmol) and a solution of 6-amino(Alloc)-2-bromohexanoate benzhydryl ester, **9** (1.4 g, 3.1 mmol) in MeCN (40 mL) were added. The reaction mixture was stirred overnight at room temperature, filtered under vacuum and concentrated under reduced pressure to give a yellow oil. The oil was purified by column chromatography over silica gel 60 (DCM/EtOH 7:3) to afford compound **10** (1.6 g, 94 %) as a yellow oil.  $^1\text{H}$  NMR (400 MHz, DMSO, TMS)  $\delta$ : 1.17-1.32 (2H, m,  $\gamma\text{-CH}_2$ ), 1.33-1.51 (2H, m,  $\delta\text{-CH}_2$ ), 1.52-1.74 (2H, m,  $\beta\text{-CH}_2$ ), 2.52-2.82 (16H, m, 8xCH<sub>2</sub> cyclen), 2.92-3.02 (2H, m,  $\epsilon\text{-CH}_2$ ), 3.45-3.51 (1H, m,  $\alpha\text{-CH}$ ), 4.43 (2H, d,  $J=5.2$  Hz, OCH<sub>2</sub> Alloc), 5.15 (1H, dd,  $J_1=9.6$  Hz,  $J_2=2.8$  Hz, CH-cis Alloc), 5.25 (1H, dd,  $J_1=17.6$  Hz,  $J_2=2.8$  Hz, CH-trans Alloc), 5.83-5.93 (1H, m, CH Alloc), 6.82 (1H, s, CH Benzhydryl), 7.16 (1H, t,  $J=5.4$  Hz, NH), 7.25-7.45 (10H, m, ArH) ppm.  $^{13}\text{C}$  NMR (100 MHz, DMSO, TMS)  $\delta$ : 23.20 ( $\gamma\text{-CH}_2$ ), 28.90 ( $\delta\text{-CH}_2$ ), 29.12 ( $\beta\text{-CH}_2$ ), 40.24 ( $\epsilon\text{-CH}_2$ ), 44.88, 46.36, 47.92, 48.44 (CH<sub>2</sub> cyclen), 64.10 (OCH<sub>2</sub> Alloc), 64.46 ( $\alpha\text{-CH}$ ), 76.70 (CH Benzhydryl), 116.86 (CH<sub>2</sub> Alloc), 126.70 (CH), 127.80 (CH), 128.54 (CH), 133.83 (CH Alloc), 140.46 (C), 155.90 (C=O Alloc), 171.81 (C=O) ppm. HRMS (ESI): calculated for C<sub>31</sub>H<sub>45</sub>N<sub>5</sub>O<sub>4</sub> (MH<sup>+</sup>) 552.35498; found 552.35443 (MH<sup>+</sup>).

**DO3A(*t*-Bu)-A(Alloc)HA(Be), 11**

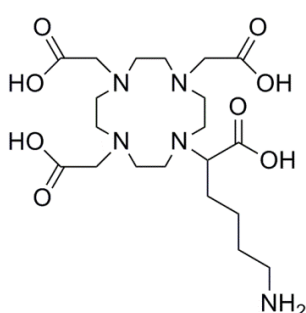
To a solution of compound **10** (1.6 g, 2.9 mmol) in MeCN (150 mL) potassium carbonate (2.4 g, 17.3 mmol) and *tert*-butyl bromoacetate (1.4 mL, 9.2 mmol) were added. The mixture was stirred overnight at room temperature, filtered under vacuum and concentrated under reduced pressure to give an oil. The oil was purified by column chromatography over silica gel 60 (DCM/EtOH 9:1) to afford compound **11** (2.0 g, 78 %) as a yellow solid.  $^1\text{H}$  NMR (400 MHz,  $\text{CDCl}_3$ , TMS)  $\delta$ : 1.35-1.65 (31H, m,  $\gamma$ - $\text{CH}_2$  +  $\delta$ - $\text{CH}_2$  +  $\text{CH}_3$  *t*-Bu), 1.66-1.84 (2H, m,  $\beta$ - $\text{CH}_2$ ), 2.05-3.59 (24H, m,  $\text{CH}_2$  cyclen +  $\epsilon$ - $\text{CH}_2$  +  $3\text{xCH}_2\text{COR}$ ), 3.49-3.61 (1H, m,  $\alpha$ -CH), 4.52 (2H, d,  $J=5.6$  Hz,  $\text{OCH}_2$  Alloc), 5.17 (1H, dd,  $J_1=10.4$  Hz,  $J_2=1.2$  Hz, CH-cis Alloc), 5.28 (1H, dd,  $J_1=17.2$  Hz,  $J_2=1.6$  Hz, CH-trans Alloc), 5.84-5.91 (1H, m, CH Alloc), 6.87 (1H, s, CH Benzhydryl), 7.23-7.40 (10H, m, ArH) ppm.  $^{13}\text{C}$  NMR (100 MHz,  $\text{CDCl}_3$ , TMS)  $\delta$ : 23.76 ( $\gamma$ - $\text{CH}_2$ ), 27.86 ( $\text{CH}_3$  *t*-Bu), 29.62 ( $\delta$ - $\text{CH}_2$ ), 30.00 ( $\beta$ - $\text{CH}_2$ ), 40.52 ( $\epsilon$ - $\text{CH}_2$ ), 44.77, 47.46, 48.16, 48.53 ( $\text{CH}_2$  cyclen), 55.56, 55.75 ( $\text{CH}_2\text{COR}$ ), 61.49 ( $\alpha$ -CH), 65.30 ( $\text{OCH}_2$  Alloc), 78.10 (CH Benzhydryl), 81.73, 81.88 (C *t*-Bu), 117.41 ( $\text{CH}_2$  Alloc), 126.97 (CH), 127.21 (CH), 128.66 (CH), 133.02 (CH Alloc), 139.17 (C), 156.36 (C=O Alloc), 172.78 (C=O *t*-Bu), 175.09 (C=O Benzhydryl) ppm. HRMS (ESI): calculated for  $\text{C}_{49}\text{H}_{75}\text{N}_5\text{O}_{10}$  ( $\text{MH}^+$ ) 894.55922; found 894.55867 ( $\text{MH}^+$ ).

**DO3A(*t*-Bu)-AHA(Be), 12**

To a solution of compound **11** (965 mg, 1.1 mmol) in DCM (50 mL) a borane dimethylamine complex (635 mg, 10.8 mmol) and tetrakis(triphenylphosphine)palladium(0) (1.4 mg, 110  $\mu\text{mol}$ ) were added. The solution was stirred for 2 hours at room temperature and silica gel 60 was added. The mixture was stirred for 30 minutes at room temperature, concentrated under reduced pressure to give a brown powder. The powder was purified by column chromatography over silica gel 60 (DCM/EtOH 8:2 followed by DCM/EtOH 7:3) to afford compound **12** (672 mg, 77 %) as a brown solid,  $^1\text{H}$  NMR (400 MHz, DMSO, TMS)  $\delta$ : 1.32-1.85 (33H,  $m_b$ ,  $\beta$ - $\text{CH}_2$  +  $\gamma$ - $\text{CH}_2$  +  $\delta$ - $\text{CH}_2$  +  $\text{CH}_3$  *t*-Bu), 1.90-3.62 (25H,  $m_b$ ,  $\text{CH}_2$  cyclen +  $\alpha$ -

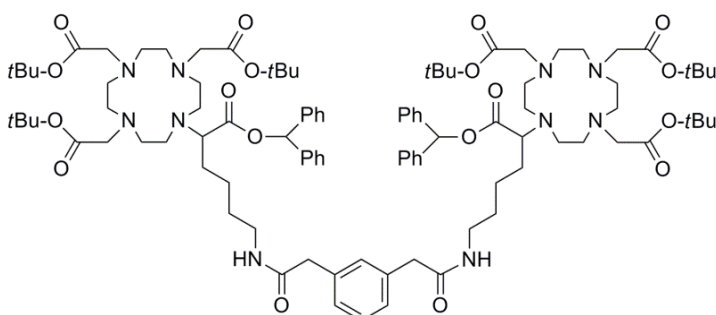
CH +  $\epsilon$ -CH<sub>2</sub> + CH<sub>2</sub>COR), 6.81 (1H, s, CH Benzhydryl), 7.25-7.45 (10H, m, ArH) ppm. <sup>13</sup>C NMR (100 MHz, DMSO, TMS)  $\delta$ : 23.61 ( $\gamma$ -CH<sub>2</sub>), 25.74 ( $\delta$ -CH<sub>2</sub>), 27.31 ( $\beta$ -CH<sub>2</sub>), 27.53 (CH<sub>3</sub> *t*-Bu), 38.58 ( $\epsilon$ -CH<sub>2</sub>), 44.18, 47.22, 47.78, 52.27 (CH<sub>2</sub> cyclen), 55.23 (CH<sub>2</sub>COR), 60.96 ( $\alpha$ -CH), 77.56 (CH Benzhydryl), 81.31 (C *t*-Bu), 126.64 (CH), 128.06 (CH), 128.76 (CH), 140.47 (C), 172.67 (C=O *t*-Bu), 174.47 (C=O Benzhydryl) ppm. HRMS (ESI): calculated for C<sub>45</sub>H<sub>71</sub>N<sub>5</sub>O<sub>8</sub> (MH<sup>+</sup>) 810.53809; found 810.53754 (MH<sup>+</sup>).

### DOTA-AHA, 13



To a solution of compound 12 (150 mg, 0.2 mmol) in DCM (3 mL) TFA was added (3 mL). The solution was stirred overnight at room temperature, concentrated under reduced pressure to give an oil. The oil was washed twice with *n*-hexane and twice with water. Compound 13 was obtained as a yellow solid in trifluoroacetate salt (106 mg). <sup>1</sup>H NMR (400 MHz, D<sub>2</sub>O, TSP)  $\delta$ : 1.37-1.95 (6H, m<sub>b</sub>,  $\beta$ -CH<sub>2</sub> +  $\gamma$ -CH<sub>2</sub> +  $\delta$ -CH<sub>2</sub>), 2.75-4.35 (25H, m<sub>b</sub>, CH<sub>2</sub> cyclen +  $\alpha$ -CH +  $\epsilon$ -CH<sub>2</sub> + CH<sub>2</sub>COR) ppm. <sup>13</sup>C NMR (100 MHz, D<sub>2</sub>O, TSP)  $\delta$ : 22.78 ( $\gamma$ -CH<sub>2</sub>), 26.35 ( $\delta$ -CH<sub>2</sub>), 28.52 ( $\beta$ -CH<sub>2</sub>), 38.77 ( $\epsilon$ -CH<sub>2</sub>), 50.03, 51.12, 53.21, 55.14 (CH<sub>2</sub> cyclen), 59.81 ( $\alpha$ -CH), 63.57 (CH<sub>2</sub>CO<sub>2</sub>H), 169.51 (C=O), 174.53 (C=O) ppm. HRMS (ESI): calculated for C<sub>20</sub>H<sub>37</sub>N<sub>5</sub>O<sub>8</sub> (MH<sup>+</sup>) 476.27204; found 476.27149 (MH<sup>+</sup>).

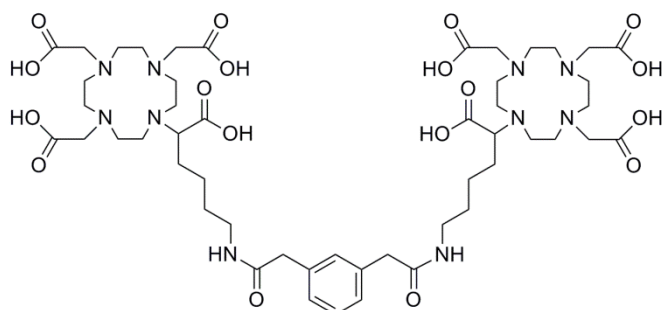
### Bis(DO3A(*t*-Bu)-AHA(Be))1,3-phenyldiacetate, 14



DO3A(*t*-Bu)-AHA(Be), 12, (425 mg, 525  $\mu$ mol) were dissolved in dry MeCN (20 mL) and to this solution 1,3-phenyldiacetic acid (43 mg, 219  $\mu$ mol), DIPEA (92  $\mu$ L, 525  $\mu$ mol), HOBt (71 mg, 525  $\mu$ mol) and HATU (200 mg, 525  $\mu$ mol) were added. The solution was stirred for 72 hours at room temperature and more HOBt (71 mg, 525  $\mu$ mol) and HATU (200 mg, 525  $\mu$ mol) were added. The solution was stirred for 48 hours at room temperature and more HOBt (71 mg, 525  $\mu$ mol) and HATU (200 mg, 525  $\mu$ mol) were added. The solution was stirred for more 48 hours at room temperature and

concentrated under reduced pressure to give a yellow solid. The solid was dissolved in ethyl acetate (100 mL), and the organic phase was washed with  $\text{KHSO}_4$  1M (3 x 50 mL),  $\text{NaHCO}_3$  1M (3 x 50 mL) and brine (3 x 50 mL). The organic phases were combined, dried with anhydrous  $\text{MgSO}_4$  and concentrated under reduced pressure to afford compound **14** (335 mg, 86 %) as a yellow solid.  $^1\text{H}$  NMR (400 MHz,  $\text{CDCl}_3$ , TMS)  $\delta$ : 1.17-1.58 (62H,  $m_b$ ,  $\gamma\text{-CH}_2 + \delta\text{-CH}_2 + \text{CH}_3$  *t*-Bu), 1.63-1.77 (4H,  $m$ ,  $\beta\text{-CH}_2$ ), 1.94-3.39 (48H,  $m_b$ ,  $\text{CH}_2$  cyclen) +  $\epsilon\text{-CH}_2 + \text{CH}_2\text{COR}$ ), 3.49 (4H,  $s$ ,  $2\times\text{CH}_2$  linker), 3.51-3.59 (2H,  $m$ ,  $2\times\alpha\text{-CH}_2$ ), 6.27 (2H,  $m$ , NH), 6.85 (2H,  $s$ , CH Benzhydryl), 7.14-7.40 (24H,  $m_b$ , ArH + CH linker) ppm.  $^{13}\text{C}$  NMR (100 MHz,  $\text{CDCl}_3$ , TMS)  $\delta$ : 24.14 ( $\gamma\text{-CH}_2$ ), 26.38 ( $\delta\text{-CH}_2$ ), 27.85 ( $\text{CH}_3$  *t*-Bu), 29.19 ( $\beta\text{-CH}_2$ ), 39.11 ( $\epsilon\text{-CH}_2$ ), 43.51 ( $\text{CH}_2$  linker), 44.34, 47.31, 47.81, 48.19 ( $\text{CH}_2$  cyclen), 55.68 ( $\text{CH}_2\text{COR}$ ), 61.26 ( $\alpha\text{-CH}$ ), 78.10 (CH Benzhydryl), 81.91 (C *t*-Bu), 126.92 (CH), 127.66 (CH), 128.13 (CH), 128.65 (CH), 128.80 (CH), 130.48 (CH), 136.02 (C), 139.22 (C), 171.38 (RCOR'), 172.85 (C=O *t*-Bu), 175.18 (C=O Benzhydryl) ppm. HRMS (ESI): calculated for  $\text{C}_{100}\text{H}_{148}\text{N}_{10}\text{O}_{18}$  ( $\text{MH}_2^{2+}$ ) 890.05816; found 890.05753 ( $\text{MH}_2^{2+}$ ).

### Bis(DOTA-AHA)1,3-phenyldiacetate, **15**

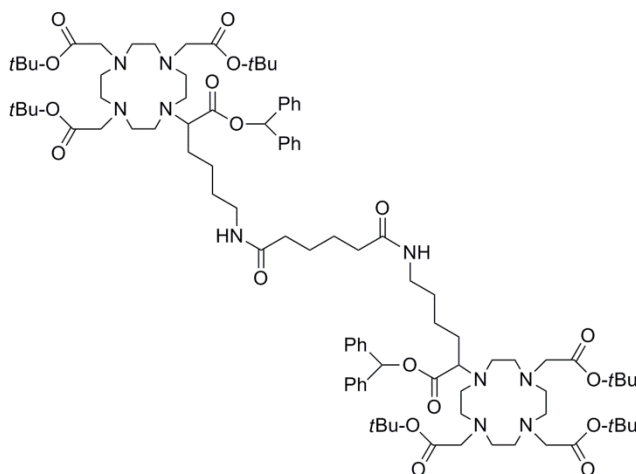


Bis(DO3A(*t*-Bu)-AHA(Be))1,3-phenyldiacetate, **14** (334 mg, 188  $\mu\text{mol}$ ) were dissolved in DCM (5 mL) and TFA (5 mL). The solution was stirred overnight at room temperature and

concentrated under reduced pressure to give a purple oil. The oil was washed with *n*-hexane (2x) and with water (2x) to give a yellow oil. The oil was dissolved in water (60 mL) and the aqueous solution was washed with DCM (4 x 30 mL), concentrated under reduced pressure to give a white solid. The solid was purified by ion change column chromatography over dowex® resin (HO<sup>-</sup> form) to afford compound **15** (281 mg) as a white solid in hydrochloride salt form.  $^1\text{H}$  NMR (400 MHz,  $\text{D}_2\text{O}$ , TSP)  $\delta$ : 1.34-1.87 (16H,  $m_b$ ,  $\beta\text{-CH}_2 + \gamma\text{-CH}_2 + \delta\text{-CH}_2$ ), 2.75-4.29 (54H,  $m_b$ ,  $\text{CH}_2$  cyclen +  $\alpha\text{-CH} + \epsilon\text{-CH}_2 + \text{CH}_2\text{CO}_2\text{H}$ ), 3.55 (4H,  $s$ ,  $\text{CH}_2$  linker), 7.11-7.26 (3H,  $m$ , CH linker + CH linker), 7.31-7.38 (1H,  $m$ , CH linker) ppm.  $^{13}\text{C}$  NMR (100 MHz,  $\text{D}_2\text{O}$ , TSP)  $\delta$ : 23.64 ( $\gamma\text{-CH}_2$ ), 26.43 ( $\delta\text{-CH}_2$ ), 28.11 ( $\delta\text{-CH}_2$ ), 38.72 ( $\epsilon\text{-CH}_2$ ), 42.32 ( $\text{CH}_2$  linker), 48.85, 50.55, 53.36, 54.20

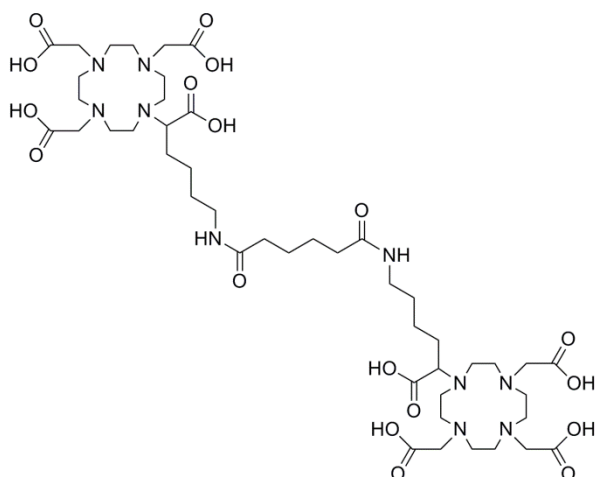
(CH<sub>2</sub> cyclen), 60.21 (α-CH), 63.36 (CH<sub>2</sub>CO<sub>2</sub>H), 127.84 (CH), 129.76 (CH), 129.81 (CH), 135.74 (C), 168.79 (C=O), 174.16 (C=O), 174.28 (C=O) ppm. HRMS (ESI): calculated for C<sub>50</sub>H<sub>80</sub>N<sub>10</sub>O<sub>18</sub> (MH<sup>+</sup>) 1109.57303, (MH<sub>2</sub><sup>2+</sup>) 555.29043; found 1109.57248 (MH<sup>+</sup>), 555.28988 (MH<sub>2</sub><sup>2+</sup>).

### Bis(DO3A(*t*-Bu)-AHA(Be))adipate, **16**



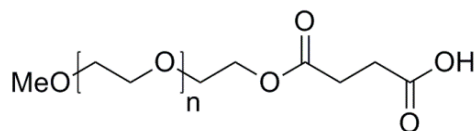
DO3A(*t*-Bu)-AHA(Be), **12** (335 mg, 414 μmol) were dissolved in dry MeCN (15 mL) and to this solution, adipic acid (25 mg, 172 μmol), DIPEA (72 μL, 370 μmol), HOBt (56 mg, 414 μmol) and HATU (157 mg, 414 μmol) were added. The solution was stirred for 72 hours at room temperature and more HOBt

(56 mg, 414 μmol) and HATU (157 mg, 414 μmol) were added. The solution was stirred for 48 hours at room temperature and more HOBt (60 mg, 414 μmol) and HATU (157 mg, 414 μmol) were added. The solution was stirred for more 48 hours at room temperature and concentrated under reduced pressure to give a white solid. The solid was dissolved in ethyl acetate (80 mL), and the organic phase was washed with KHSO<sub>4</sub> 1M (3 x 40 mL), NaHCO<sub>3</sub> 1M (3 x 40 mL) and brine (3 x 40 mL). The organic phases were combined, dried with anhydrous MgSO<sub>4</sub> and concentrated under reduced pressure to afford compound **16** (286 mg, 96 %) as a white solid. <sup>1</sup>H NMR (400 MHz, CDCl<sub>3</sub>, TMS) δ: 1.41-1.66 (66H, m<sub>b</sub>, γ-CH<sub>2</sub> + δ-CH<sub>2</sub> + CH<sub>3</sub> *t*-Bu + CH<sub>2</sub> linker), 1.67-1.83 (4H, m, β-CH<sub>2</sub>), 1.97-3.40 (52H, m<sub>b</sub>, CH<sub>2</sub> cyclen + ε-CH<sub>2</sub> + CH<sub>2</sub>COR + COCH<sub>2</sub> linker), 3.58-3.65 (2H, m, α-CH<sub>2</sub>), 6.35 (2H, m, NH), 6.88 (2H, s, CH Benzhydryl), 7.23-7.38 (20H, m, ArH) ppm. <sup>13</sup>C NMR (100 MHz, CDCl<sub>3</sub>, TMS) δ: 24.63 (γ-CH<sub>2</sub>), 26.43 (CH<sub>2</sub> linker), 27.86 (CH<sub>3</sub> *t*-Bu), 29.21 (δ-CH<sub>2</sub>), 29.65 (β-CH<sub>2</sub>), 35.27 (COCH<sub>2</sub> linker), 38.91 (ε-CH<sub>2</sub>), 44.38, 47.36, 47.84, 48.21 (CH<sub>2</sub> cyclen), 55.59 (CH<sub>2</sub>COR), 61.29 (α-CH), 78.14 (CH Benzhydryl), 81.93 (C *t*-Bu), 126.95 (CH), 128.12 (CH), 128.63 (CH), 139.24 (C), 172.87 (C=O *t*-Bu), 173.57 (C=O), 175.26 (C=O Benzhydryl) ppm. HRMS (ESI) z: calculated for C<sub>96</sub>H<sub>148</sub>N<sub>10</sub>O<sub>18</sub> (MH<sup>+</sup>) 1731.10849, (MH<sub>2</sub><sup>2+</sup>) 866.05816; found 1731.10778 (MH<sup>+</sup>), 866.05753 (MH<sub>2</sub><sup>2+</sup>).

**Bis(DOTA-AHA)adipate, 17**

Bis(DO3A(*t*-Bu)-AHA(Be))adipate, **16** (279 mg, 161  $\mu\text{mol}$ ) were dissolved in DCM (5 mL) and TFA (5 mL). The solution was stirred overnight at room temperature and concentrated under reduced pressure to give a purple oil. The oil was washed with *n*-hexane (2x) and with water (2x) to give a yellow oil. The oil was dissolved in water (60 mL)

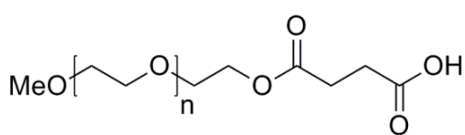
and the aqueous solution was washed with DCM (4 x 30 mL) and concentrated under reduced pressure to give a white solid. The solid was purified by ion change column chromatography over dowex<sup>®</sup> resin (HO<sup>-</sup> form) to afford compound **17** (245 mg) as a white solid in hydrochloride salt form. <sup>1</sup>H NMR (400 MHz, D<sub>2</sub>O, TSP)  $\delta$ : 1.35-2.00 (16H, m<sub>b</sub>,  $\beta$ -CH<sub>2</sub> +  $\gamma$ -CH<sub>2</sub> +  $\delta$ -CH<sub>2</sub> + CH<sub>2</sub> linker), 2.15-2.35 (4H, m, COCH<sub>2</sub> linker), 2.72-4.45 (54H, m<sub>b</sub>, CH<sub>2</sub> cyclen +  $\alpha$ -CH +  $\epsilon$ -CH<sub>2</sub> + CH<sub>2</sub>CO<sub>2</sub>H) ppm. <sup>13</sup>C NMR (100 MHz, D<sub>2</sub>O, TSP)  $\delta$ : 23.61 ( $\gamma$ -CH<sub>2</sub>), 24.81 (CH<sub>2</sub> linker), 26.48 ( $\delta$ -CH<sub>2</sub>), 28.14 ( $\beta$ -CH<sub>2</sub>), 35.39 (COCH<sub>2</sub> linker), 38.15 ( $\epsilon$ -CH<sub>2</sub>), 49.12, 50.57, 53.42, 54.32 (CH<sub>2</sub> cyclen), 60.28 ( $\alpha$ -CH), 63.41 (CH<sub>2</sub>CO<sub>2</sub>H), 168.99 (C=O), 174.22 (C=O), 176.41 (C=O) ppm. HRMS (ESI): calculated for C<sub>46</sub>H<sub>80</sub>N<sub>10</sub>O<sub>18</sub> (MH<sup>+</sup>) 1061.57303, (MNa<sup>+</sup>), 1083.55498 (MH<sub>2</sub><sup>2+</sup>) 531.29043, (MH<sub>3</sub><sup>3+</sup>) 354.52956; found 1061.57249 (MH<sup>+</sup>), 1083.55443 (MNa<sup>+</sup>), 531.29143 (MH<sub>2</sub><sup>2+</sup>), 354.53011 (MH<sub>3</sub><sup>3+</sup>).

**MeO-PEG<sub>750</sub>-succinate, 18**

MeO-PEG<sub>750</sub> (4.2 g, 5.4 mmol) were dissolved in dry CHCl<sub>3</sub> (20 mL) and to this solution succinic anhydride (554 mg, 5.3 mmol) and 3 drops of sulfuric acid (95%) were added. The solution was stirred for 6 hours at reflux temperature and concentrated under reduced to afford compound **18** (4.7 g) as a colorless oil. The product was carried through without further purification. <sup>1</sup>H NMR (400 MHz, CDCl<sub>3</sub>, TMS)  $\delta$ : 2.61-2.71 (4H, m,  $\alpha$ -CH<sub>2</sub> succinate +  $\beta$ -CH<sub>2</sub> succinate), 3.38 (3H, s, OMe), 3.54-3.56 (2H, m, o-CH<sub>2</sub> PEG), 3.59-3.72 (nH, m,  $\beta$ -CH<sub>2</sub> PEG) + nPEG), 4.24-4.27 (2H, m,  $\alpha$ -CH<sub>2</sub> PEG) ppm. <sup>13</sup>C NMR (100 MHz, CDCl<sub>3</sub>, TMS)  $\delta$ :

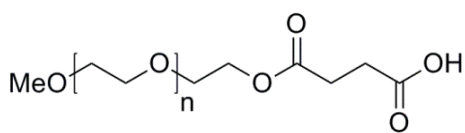
28.95 ( $\alpha$ -CH<sub>2</sub> succinate), 29.41 ( $\beta$ -CH<sub>2</sub> succinate), 58.98 (OMe), 63.80 ( $\alpha$ -CH<sub>2</sub> PEG), 68.93 ( $\beta$ -CH<sub>2</sub> PEG), 70.46, 70.48, 70.50 (nPEG), 71.88 (o-CH<sub>2</sub> PEG), 172.02 (C=O), 174.36 (C=O) ppm. LRMS (ESI<sup>+</sup>) – m/z: calculated for: n = 17 – C<sub>41</sub>H<sub>80</sub>O<sub>22</sub> (MH<sup>+</sup>) 925.52; found 925.75 (MH<sup>+</sup>); n = 16 – C<sub>39</sub>H<sub>76</sub>O<sub>21</sub> (MH<sup>+</sup>) 881.50; found 881.75, (MH<sup>+</sup>); n = 15 – C<sub>37</sub>H<sub>72</sub>O<sub>20</sub> (MH<sup>+</sup>) 837.47; found 837.67, (MH<sup>+</sup>); n = 14 – C<sub>35</sub>H<sub>68</sub>O<sub>19</sub> (MH<sup>+</sup>) 793.44; found 793.69, (MH<sup>+</sup>); n = 13 – C<sub>33</sub>H<sub>64</sub>O<sub>18</sub> (MH<sup>+</sup>) 749.42; found 749.70 (MH<sup>+</sup>).

### MeO-PEG<sub>550</sub>-succinate, 19



Using a similar procedure to that previously described for compound **18**, but using OMe-PEG<sub>550</sub>-OH (2.2 g, 3.7 mmol) it was possible to obtain compound **19** (4.7 g) as a colorless oil. The product was carried through without further purification. <sup>1</sup>H NMR (400 MHz, DMSO, TMS)  $\delta$ : 2.43-2.58 (4H, m,  $\alpha$ -CH<sub>2</sub> succinate +  $\beta$ -CH<sub>2</sub> succinate), 3.23 (3H, s, OMe), 3.39-3.43 (2H, m, o-CH<sub>2</sub> PEG), 3.46-3.54 (nH, m, nPEG), 3.58 (2H, t, *J*=4.8 Hz,  $\beta$ -CH<sub>2</sub> PEG), 4.11 (2H, t, *J*=4.6 Hz,  $\alpha$ -CH<sub>2</sub> PEG) ppm. <sup>13</sup>C NMR (100 MHz, DMSO, TMS)  $\delta$ : 28.61, 28.64 ( $\alpha$ -CH<sub>2</sub> succinate +  $\beta$ -CH<sub>2</sub> succinate), 58.03 (OMe), 63.44 ( $\alpha$ -CH<sub>2</sub> PEG), 68.22 ( $\beta$ -CH<sub>2</sub> PEG), 69.57, 69.72, 69.77 (nPEG), 71.27 (o-CH<sub>2</sub> PEG), 171.94 (C=O'), 173.35 (C=O) ppm. LRMS (ESI<sup>+</sup>) – m/z: calculated for: n = 13 – C<sub>33</sub>H<sub>64</sub>O<sub>18</sub> (MH<sup>+</sup>) 749.42; found 749.83, (MH<sup>+</sup>); n = 12 – C<sub>31</sub>H<sub>60</sub>O<sub>17</sub> (MH<sup>+</sup>) 705.39; found 705.50, (MH<sup>+</sup>); n = 11 – C<sub>29</sub>H<sub>56</sub>O<sub>16</sub> (MH<sup>+</sup>) 661.36; found 661.42, (MH<sup>+</sup>); n = 10 – C<sub>27</sub>H<sub>52</sub>O<sub>15</sub> (MH<sup>+</sup>) 617.34; found 317.42, (MH<sup>+</sup>); n = 9 – C<sub>25</sub>H<sub>48</sub>O<sub>14</sub> (MH<sup>+</sup>) 573.31; found 573.52 (MH<sup>+</sup>).

### MeO-PEG<sub>350</sub>-succinate, 20

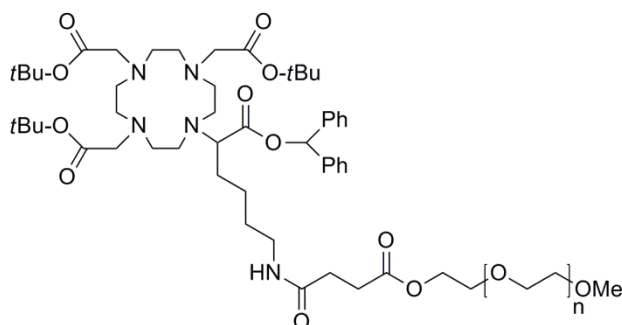


Using a similar procedure to the previously described, but with OMe-PEG<sub>350</sub>-OH (4.3 g, 12.2 mmol) it was possible to obtain compound **20** (5.4 g) as a colorless oil. The product was carried through without further purification. <sup>1</sup>H NMR (400 MHz, DMSO, TMS)  $\delta$ : 2.43-2.59 (4H, m,  $\alpha$ -CH<sub>2</sub> succinate +  $\beta$ -CH<sub>2</sub> succinate), 3.23 (3H, s, OMe), 3.39-3.44 (2H, m, o-CH<sub>2</sub> PEG), 3.48-3.55 (nH, m, nPEG), 3.59 (2H, t, *J*=4.8 Hz,  $\beta$ -CH<sub>2</sub> PEG), 4.11 (2H, t, *J*=4.6 Hz,  $\alpha$ -CH<sub>2</sub> PEG) ppm. <sup>13</sup>C NMR (100 MHz, DMSO, TMS)  $\delta$ : 28.57, 28.64 ( $\alpha$ -CH<sub>2</sub> succinate) + ( $\beta$ -CH<sub>2</sub> succinate), 58.02 (OMe), 63.44 ( $\alpha$ -CH<sub>2</sub> PEG), 68.23 ( $\beta$ -CH<sub>2</sub> PEG), 69.56, 69.72, 69.77



(nPEG), 71.27 (o-CH<sub>2</sub> PEG), 171.89 (C=O), 173.34 (C=O) ppm. LRMS (ESI<sup>+</sup>): calculated for: n = 9 – C<sub>25</sub>H<sub>48</sub>O<sub>14</sub> (MH<sup>+</sup>) 573.31; found 573.70 (MH<sup>+</sup>); n = 8 – C<sub>23</sub>H<sub>44</sub>O<sub>13</sub> (MH<sup>+</sup>) 529.29; found 529.36, (MH<sup>+</sup>); n = 7 – C<sub>21</sub>H<sub>40</sub>O<sub>12</sub> (MH<sup>+</sup>) 485.26; found 485.63, (MH<sup>+</sup>); n = 6 – C<sub>19</sub>H<sub>36</sub>O<sub>11</sub> (MH<sup>+</sup>) 441.23; found 441.92, (MH<sup>+</sup>); n = 5 – C<sub>17</sub>H<sub>32</sub>O<sub>10</sub> (MH<sup>+</sup>) 397.21; found 397.83 (MH<sup>+</sup>).

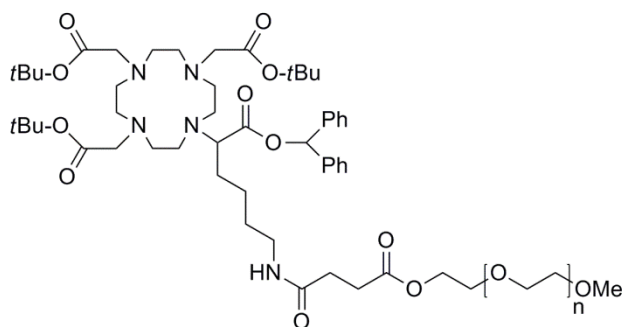
### DO3A(*t*-Bu)-A(succinate-PEG<sub>750</sub>-OMe)HA(Be), **21**



DO3A(*t*-Bu)-AHA(Be), **12** (370 mg, 457 μmol) were dissolved in dry MeCN (30 mL) and to this solution, MeO-PEG<sub>750</sub>-succinate (544 mg, 640 μmol), DIPEA (80 μL, 457 μmol), HOBt (104 mg, 767 μmol) HATU

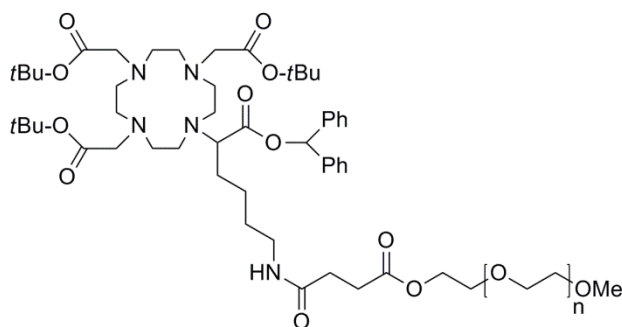
(292 mg, 767 μmol) were added. The solution was stirred for 48 hours at room temperature and more HOBt (104 mg, 767 μmol), HATU (292 mg, 767 μmol) were added. The solution was stirred for more 48 hours at room temperature and concentrated under reduced to give a yellow oil. The oil was dissolved in ethyl acetate (75 mL), and the organic phase was washed with KHSO<sub>4</sub> 1M (2 x 45 mL), NaHCO<sub>3</sub> 1M (2 x 45 mL) and brine (2 x 45 mL). The organic phases were combined, dried with anhydrous MgSO<sub>4</sub> and concentrated under reduced pressure to afford compound **21** (485 mg, 65 %) as a yellow solid. <sup>1</sup>H NMR (400 MHz, CDCl<sub>3</sub>, TMS) δ: 1.15-1.50 (31H, m<sub>b</sub>, γ-CH<sub>2</sub> + δ-CH<sub>2</sub> + CH<sub>3</sub> *t*-Bu), 1.62-1.81 (2H, m, β-CH<sub>2</sub>), 1.97-3.34 (28H, m, CH<sub>2</sub> cyclen + ε-CH<sub>2</sub> + CH<sub>2</sub>COR + α-CH<sub>2</sub> succinate + β-CH<sub>2</sub> succinate), 3.36 (3H, s, OMe), 3.50-3.65 (nH, m<sub>b</sub>, nPEG + α-CH), 3.65-3.73 (2H, m, β-CH<sub>2</sub> PEG), 4.13-4.22 (2H, m, α-CH<sub>2</sub> PEG), 6.86 (1H, s, CH Benzhydryl), 7.20-7.44 (10H, m, ArH) ppm. <sup>13</sup>C NMR (100 MHz, CDCl<sub>3</sub>, TMS) δ: 26.43 (γ-CH<sub>2</sub>), 27.78 (CH<sub>3</sub> *t*-Bu), 28.91, 29.33, 29.60 (β-CH<sub>2</sub> + δ-CH<sub>2</sub> + α-CH<sub>2</sub> succinate), 30.62 (β-CH<sub>2</sub> succinate), 39.00 (ε-CH<sub>2</sub>), 44.38, 47.36, 47.80, 48.15 (CH<sub>2</sub> cyclen), 55.53 (CH<sub>2</sub>COR), 58.83 (OMe), 61.35 (α-CH), 63.46 (α-CH<sub>2</sub> PEG), 68.68 (β-CH<sub>2</sub> PEG), 70.13, 70.27, 70.37 (nPEG), 71.69 (o-CH<sub>2</sub> PEG), 78.09 (CH Benzhydryl), 81.91 (C *t*-Bu), 126.41 (ArH), 128.15 (ArH), 128.54 (ArH), 139.98 (C ArH), 171.65 (C=O), 172.12 (C=O), 172.54 (C=O *t*-Bu), 175.10 (C=O Benzhydryl) ppm.

**DO3A(*t*-Bu)-A(succinate-PEG<sub>550</sub>-OMe)HA(Be), 22**



Using a similar procedure to the previously described, but with OMe-PEG<sub>550</sub>-succinate (324 mg, 498  $\mu$ mol) it was possible to obtain compound **22** (347 mg, 68 %) as a yellow solid. <sup>1</sup>H NMR (400 MHz, CDCl<sub>3</sub>, TMS)  $\delta$ : 1.18-1.57 (31H, m<sub>b</sub>,  $\gamma$ -CH<sub>2</sub> +  $\delta$ -CH<sub>2</sub> + CH<sub>3</sub> *t*-Bu), 1.61-1.79 (2H, m,  $\beta$ -CH<sub>2</sub>), 1.97-3.31 (28H, m<sub>b</sub>, CH<sub>2</sub> cyclen +  $\epsilon$ -CH<sub>2</sub> + CH<sub>2</sub>COR +  $\alpha$ -CH<sub>2</sub> succinate +  $\beta$ -CH<sub>2</sub> succinate), 3.34 (3H, s, OMe), 3.49-3.65 (nH, m, nPEG +  $\alpha$ -CH), 3.66-3.69 (2H, m,  $\beta$ -CH<sub>2</sub> PEG), 4.17-4.24 (2H, m,  $\alpha$ -CH<sub>2</sub> PEG), 6.86 (1H, s, CH Benzhydryl), 7.22-7.39 (10H, m, ArH) ppm. <sup>13</sup>C NMR (100 MHz, CDCl<sub>3</sub>, TMS)  $\delta$ : 26.39 ( $\gamma$ -CH<sub>2</sub>), 27.77 (CH<sub>3</sub> *t*-Bu), 28.90, 29.07, 29.63 ( $\beta$ -CH<sub>2</sub> +  $\delta$ -CH<sub>2</sub> +  $\alpha$ -CH<sub>2</sub> succinate), 30.62 ( $\beta$ -CH<sub>2</sub> succinate), 39.00 ( $\epsilon$ -CH<sub>2</sub>), 44.29, 47.27, 47.75, 48.10 (CH<sub>2</sub> cyclen), 55.39 (CH<sub>2</sub>COR), 58.68 (OMe), 61.31 ( $\alpha$ -CH), 63.59 ( $\alpha$ -CH<sub>2</sub> PEG), 68.88 ( $\beta$ -CH<sub>2</sub> PEG), 69.71, 69.92, 70.19 (nPEG), 71.37 (o-CH<sub>2</sub> PEG), 78.06 (CH Benzhydryl), 81.92 (C *t*-Bu), 126.38 (CH), 128.11 (CH), 128.55 (CH), 140.01 (C), 171.71 (C=O), 172.20 (C=O), 172.84 (C=O *t*-Bu), 175.11 (C=O Benzhydryl) ppm.

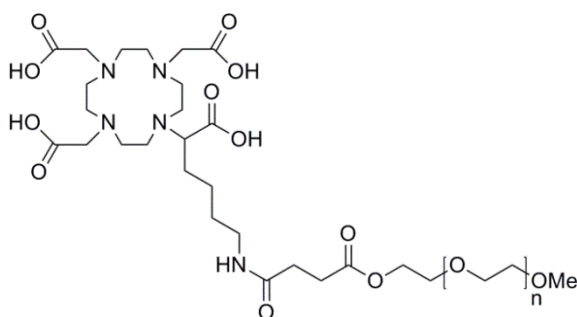
**DO3A(*t*-Bu)-A(succinate-PEG<sub>350</sub>-OMe)HA(Be), 23**



Using a similar procedure to the previously described, but with OMe-PEG<sub>350</sub>-succinate (178 mg, 396  $\mu$ mol) it was possible to obtain compound **23** (194 mg, 79 %) as a yellow solid. <sup>1</sup>H NMR (400 MHz, CDCl<sub>3</sub>, TMS)  $\delta$ : 1.18-1.55 (31H, m<sub>b</sub>,  $\gamma$ -CH<sub>2</sub> +  $\delta$ -CH<sub>2</sub> + CH<sub>3</sub> *t*-Bu), 1.64-1.82 (2H, m,  $\beta$ -CH<sub>2</sub>), 1.96-3.32 (28H, m<sub>b</sub>, CH<sub>2</sub> cyclen +  $\epsilon$ -CH<sub>2</sub> + CH<sub>2</sub>COR +  $\alpha$ -CH<sub>2</sub> succinate +  $\beta$ -CH<sub>2</sub> succinate), 3.35 (3H, s, OMe), 3.51-3.65 (nH, m, nPEG +  $\alpha$ -CH), 3.65-3.71 (2H, m,  $\beta$ -CH<sub>2</sub> PEG), 4.16-4.25 (2H, m,  $\alpha$ -CH<sub>2</sub> PEG), 6.85 (1H, s, CH Benzhydryl), 7.22-7.43 (10H, m, ArH) ppm. <sup>13</sup>C NMR (100 MHz, CDCl<sub>3</sub>, TMS)  $\delta$ : 26.45 ( $\gamma$ -CH<sub>2</sub>), 27.77 (CH<sub>3</sub> *t*-Bu), 28.95, 29.34, 29.62 ( $\beta$ -CH<sub>2</sub> +  $\delta$ -CH<sub>2</sub> +  $\alpha$ -CH<sub>2</sub> succinate), 30.60 ( $\beta$ -CH<sub>2</sub> succinate), 38.99 ( $\epsilon$ -CH<sub>2</sub>), 44.30, 47.28,

47.75, 48.13 (CH<sub>2</sub> cyclen), 55.52 (CH<sub>2</sub>COR), 58.83 (OMe), 61.30 (α-CH), 63.45 (α-CH<sub>2</sub> PEG), 68.68 (β-CH<sub>2</sub> PEG), 70.09, 70.26, 70.35 (nPEG), 71.68 (o-CH<sub>2</sub> PEG), 78.06 (CH Benzhydryl), 81.90 (C *t*-Bu), 126.39 (CH), 128.12 (CH), 128.55 (CH), 139.96 (C), 171.65 (C=O), 172.11 (C=O), 172.56 (C=O *t*-Bu), 175.08 (C=O Benzhydryl) ppm.

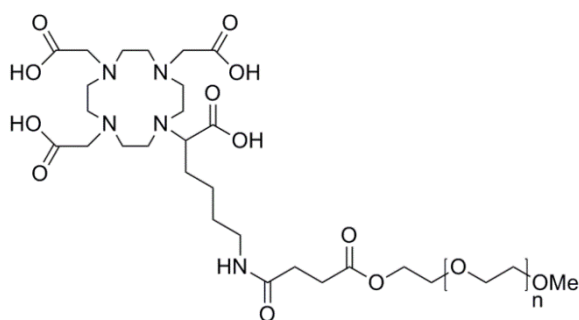
#### DOTA-A(PEG<sub>750</sub>)HA, **24**



DO3A(*t*-Bu)-A(succinate-PEG<sub>750</sub>-OMe)HA(Be), **21** (480 mg, 292 μmol) were dissolved in DCM (7 mL) and in TFA (7 mL). The solution was stirred overnight at room temperature and concentrated under reduced pressure to

give a purple oil. The oil was washed with *n*-hexane (2x) and with water (2x) to give a yellow oil. The oil was dissolved in water (70 mL) and the aqueous solution was washed with DCM (4 x 35 mL) and concentrated under reduced pressure to afford compound **24** (400 mg) as a yellow solid in trifluoroacetate salt form. <sup>1</sup>H NMR (400 MHz, D<sub>2</sub>O, TSP) δ: 1.35-1.93 (6H, m<sub>b</sub>, β-CH<sub>2</sub> + γ-CH<sub>2</sub> + δ-CH<sub>2</sub>), 2.50-2.59 (2H, m, β-CH<sub>2</sub> succinate), 2.67-2.73 (2H, m, α-CH<sub>2</sub> succinate), 2.88-4.23 (25H, m<sub>b</sub>, CH<sub>2</sub> cyclen + α-CH + ε-CH<sub>2</sub> + CH<sub>2</sub>CO<sub>2</sub>H), 3.39 (3H, s, OMe), 3.51-3.73 (nH, m<sub>b</sub>, nPEG), 3.77-3.81 (2H, m, β-CH<sub>2</sub> PEG), 4.25-4.29 (2H, m, α-CH<sub>2</sub> PEG) ppm. <sup>13</sup>C NMR (100 MHz, D<sub>2</sub>O, TSP) δ: 23.63 (γ-CH<sub>2</sub>), 28.00 (β-CH<sub>2</sub>), 28.17 (δ-CH<sub>2</sub>), 29.43 (α-CH<sub>2</sub> succinate), 30.27 (β-CH<sub>2</sub> succinate), 38.71 (ε-CH<sub>2</sub>), 50.47, 51.19, 53.46, 54.35 (CH<sub>2</sub> cyclen), 58.63 (OMe), 60.35 (CH<sub>2</sub>CO<sub>2</sub>H), 61.17 (α-CH), 64.01 (α-CH<sub>2</sub> PEG), 68.42 (β-CH<sub>2</sub> PEG), 68.42, 69.56, 69.62 (nPEG), 70.97 (o-CH<sub>2</sub> PEG), 168.49 (C=O), 174.41 (C=O), 174.70 (C=O), 176.79 (C=O) ppm. LRMS (ESI<sup>+</sup>): calculated for: n = 18 - C<sub>63</sub>H<sub>119</sub>N<sub>5</sub>O<sub>30</sub> (MH<sup>+</sup>) 1426.80, (MH<sub>2</sub><sup>2+</sup>) 713.90; found 1426.80, (MH<sup>+</sup>), 713.87 (MH<sub>2</sub><sup>2+</sup>); n = 17 - C<sub>61</sub>H<sub>115</sub>N<sub>5</sub>O<sub>29</sub> (MH<sup>+</sup>) 1382.78, (MH<sub>2</sub><sup>2+</sup>) 691.89; found 1382.78, (MH<sup>+</sup>), 691.86 (MH<sub>2</sub><sup>2+</sup>); n = 16 - C<sub>59</sub>H<sub>111</sub>N<sub>5</sub>O<sub>28</sub> (MH<sup>+</sup>) 1338.75, (MH<sub>2</sub><sup>2+</sup>) 669.88; found 1338.75, (MH<sup>+</sup>), 669.85 (MH<sub>2</sub><sup>2+</sup>); n = 15 - C<sub>57</sub>H<sub>107</sub>N<sub>5</sub>O<sub>27</sub> (MH<sup>+</sup>) 1294.72, (MH<sub>2</sub><sup>2+</sup>) 647.86; found 1294.72, (MH<sup>+</sup>), 647.83 (MH<sub>2</sub><sup>2+</sup>); n = 14 - C<sub>55</sub>H<sub>103</sub>N<sub>5</sub>O<sub>26</sub> (MH<sup>+</sup>) 1250.70, (MH<sub>2</sub><sup>2+</sup>) 625.85; found 1250.70, (MH<sup>+</sup>), 625.82 (MH<sub>2</sub><sup>2+</sup>).

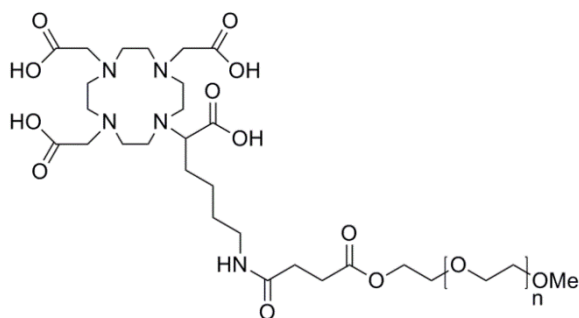
**DOTA-A(PEG<sub>550</sub>)HA, 25**



Using a similar procedure to the previously described, but using DO3A(*t*-Bu)-A(succinate-PEG<sub>550</sub>-OMe)HA(Be), **22** (347 mg, 241 μmol) it was possible to obtain compound **25** (313 mg) as a yellow solid in trifluoroacetate salt form.

<sup>1</sup>H NMR (400 MHz, D<sub>2</sub>O, TSP) δ: 1.31-1.86 (6H, m<sub>b</sub>, β-CH<sub>2</sub> + γ-CH<sub>2</sub> + δ-CH<sub>2</sub>), 2.43 (2H, t, J=6.6Hz, β-CH<sub>2</sub> succinate), 2.56 (2H, t, J=6.4Hz, α-CH<sub>2</sub> succinate), 2.72-4.25 (25H, m<sub>b</sub>, CH<sub>2</sub> cyclen) + α-CH + ε-CH<sub>2</sub> + CH<sub>2</sub>CO<sub>2</sub>H), 3.28 (3H, s, OMe), 3.50-3.70 (nH, m<sub>b</sub>, nPEG + β-CH<sub>2</sub> PEG), 4.12-4.17 (2H, m, α-CH<sub>2</sub> PEG) ppm. <sup>13</sup>C NMR (100 MHz, D<sub>2</sub>O, TSP, δ): 23.64 (γ-CH<sub>2</sub>), 28.08 (β-CH<sub>2</sub>), 28.65 (δ-CH<sub>2</sub>), 29.32 (α-CH<sub>2</sub> succinate), 30.24 (β-CH<sub>2</sub> succinate), 38.89 (ε-CH<sub>2</sub>), 45.48, 50.65, 53.19, 54.05 (CH<sub>2</sub> cyclen), 57.96 (OMe), 60.29 (CH<sub>2</sub>CO<sub>2</sub>H), 61.07 (α-CH), 63.94 (α-CH<sub>2</sub> PEG), 68.34 (β-CH<sub>2</sub> PEG), 69.32, 69.34, 69.56 (nPEG), 70.89 (o-CH<sub>2</sub> PEG), 168.72 (C=O), 174.36 (C=O), 174.54 (C=O), 176.79 (C=O) ppm. LRMS (ESI<sup>+</sup>): calculated for: n = 14 – C<sub>55</sub>H<sub>103</sub>N<sub>5</sub>O<sub>26</sub> (MNa<sup>+</sup>) 1272.78, (MNaH<sup>2+</sup>) 636.84; found 1272.79, (MNa<sup>+</sup>), 638.89 (MNaH<sup>2+</sup>); n = 13 – C<sub>53</sub>H<sub>99</sub>N<sub>5</sub>O<sub>25</sub> (MNa<sup>+</sup>) 1228.65, (MNaH<sup>2+</sup>) 614.83; found 1382.76, (MNa<sup>+</sup>), 614.88 (MNaH<sup>2+</sup>); n = 12 – C<sub>51</sub>H<sub>95</sub>N<sub>5</sub>O<sub>24</sub> (MNa<sup>+</sup>) 1184.63, (MNaH<sup>2+</sup>) 592.81; found 1184.73, (MNa<sup>+</sup>), 592.87 (MNaH<sup>2+</sup>); n = 11 – C<sub>49</sub>H<sub>91</sub>N<sub>5</sub>O<sub>23</sub> (MNa<sup>+</sup>) 1140.60, (MNaH<sup>2+</sup>) 570.80; found 1140.71, (MNa<sup>+</sup>), 570.85 (MNaH<sup>2+</sup>).

**DOTA-A(PEG<sub>350</sub>)HA, 26**

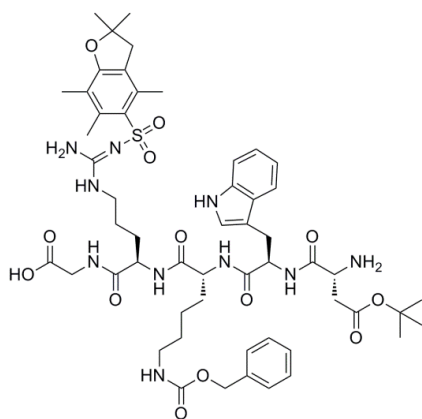


Using a similar procedure to the previously described, but using DO3A(*t*-Bu)-A(succinate-PEG<sub>350</sub>-OMe)HA(Be), **23** (277 mg, 223 μmol) it was possible to obtain compound **26** (252 mg) as a yellow solid in trifluoroacetate salt form.

<sup>1</sup>H NMR (400 MHz, D<sub>2</sub>O, TSP) δ: 1.29-1.83 (6H, m<sub>b</sub>, β-CH<sub>2</sub> + γ-CH<sub>2</sub> + δ-CH<sub>2</sub>), 2.37-2.47 (2H, m, β-CH<sub>2</sub> succinate), 2.48-2.62 (2H, m, α-CH<sub>2</sub> succinate), 2.75-4.12 (25H, m<sub>b</sub>, CH<sub>2</sub> cyclen + α-CH + ε-CH<sub>2</sub> + CH<sub>2</sub>CO<sub>2</sub>H), 3.34 (3H, s, OMe), 3.46-3.63 (nH, m<sub>b</sub>, nPEG), 3.63-3.67 (2H, m, β-CH<sub>2</sub> PEG), 4.10-4.14 (2H, m, α-CH<sub>2</sub> PEG) ppm. <sup>13</sup>C NMR

(100 MHz, D<sub>2</sub>O, TSP)  $\delta$ : 23.66 ( $\gamma$ -CH<sub>2</sub>), 28.06 ( $\beta$ -CH<sub>2</sub>), 29.30 ( $\delta$ -CH<sub>2</sub>), 29.37 ( $\alpha$ -CH<sub>2</sub> succinate), 30.22 ( $\beta$ -CH<sub>2</sub> succinate), 38.62 ( $\epsilon$ -CH<sub>2</sub>), 45.36, 50.71, 53.25, 53.95 (CH<sub>2</sub> cyclen), 57.93 (OMe), 60.26 (CH<sub>2</sub>CO<sub>2</sub>H), 61.08 ( $\alpha$ -CH), 63.92 ( $\alpha$ -CH<sub>2</sub> PEG), 68.30 ( $\beta$ -CH<sub>2</sub> PEG), 69.29, 69.31, 69.45 (nPEG), 70.86 (o-CH<sub>2</sub>PEG), 168.35 (C=O), 174.47 (C=O), 174.64 (C=O), 176.73 (C=O) ppm. LRMS (ESI<sup>+</sup>): calculated for: n = 10 – C<sub>47</sub>H<sub>87</sub>N<sub>5</sub>O<sub>22</sub> (MH<sub>2</sub><sup>2+</sup>) 537.80; found 537.56, (MH<sub>2</sub><sup>2+</sup>); n = 9 – C<sub>45</sub>H<sub>83</sub>N<sub>5</sub>O<sub>21</sub> (MH<sub>2</sub><sup>2+</sup>) 515.78; found 515.34, (MH<sub>2</sub><sup>2+</sup>); n = 8 – C<sub>43</sub>H<sub>79</sub>N<sub>5</sub>O<sub>20</sub> (MH<sub>2</sub><sup>2+</sup>) 493.77; found 493.28, (MH<sub>2</sub><sup>2+</sup>); n = 7 – C<sub>41</sub>H<sub>75</sub>N<sub>5</sub>O<sub>19</sub> (MH<sub>2</sub><sup>2+</sup>) 471.76; found 471.30 (MH<sub>2</sub><sup>2+</sup>); n = 6 – C<sub>39</sub>H<sub>71</sub>N<sub>5</sub>O<sub>18</sub> (MH<sub>2</sub><sup>2+</sup>) 449.75; found 449.25 (MH<sub>2</sub><sup>2+</sup>).

### R(Pbf)GD(*t*-Bu)WK(Cbz), **27**



The full protected linear peptide, **27** was obtained by solid phase peptide synthesis using a 2-chlorotritylchloride resin and a Fmoc strategy. The synthetic process has 6 steps: **I**-loading of the resin, **II**- evaluation of the resin loading, **III**- Fmoc cleavage, **IV**- TNBS test, **V**- Fmoc-protected amino acids coupling and **VI**- peptide cleavage from the resin.

#### I. Loading of the resin.

- 1) Approximately 1.0 g of 2-chlorotritylchloride resin (2-Cl-(Trt)-Cl, 1.0 mmol.g<sup>-1</sup>) was placed together with the glass material in the desiccator containing KOH pallets for 24 hours;
- 2) 2 equivalents of Fmoc-Gly-OH (604 mg) were dissolved in dry DCM (10 mL) and to this solution, 8 equivalents of DIPEA (1.4 mL) were added;
- 3) The dry resin was added to the previously solution and the mixture was stirred for 6 hours at room temperature;
- 4) The mixture was transferred to a reaction vessel, filtered under vacuum and washed with a DCM/MeOH/DIPEA solution (17:2:1) (3 x 10 mL), DCM (3 x 10 mL), DMF (2 x 10 mL) and DCM (2 x 10 mL). The resin was dried in the desiccator overnight.

**II. Estimation of resin loading.** The method used was based on the Novabiochem protocol (Method 6P: Estimation of the level of first residue attachment).

- 1) 25 mL of a piperidine in DMF 20% (v/v) freshly solution of was prepared;
- 2) 3 mL of this solution was placed into a quartz cuvette and the absorbance was measured at 290 nm in the UV spectrophotometer (use as a blank);
- 3) Approximately 1.0  $\mu\text{mol}$  (1 mg) of the dry resin was weighed, 3 mL of the piperidine solution were added to the resin and the mixture was stirred for 3 minutes at room temperature;
- 4) The absorbance was read at 290 nm using the piperidine solution as a blank, after the resin was settled on the bottom of the cuvette;
- 5) The first residue attachment was estimated from equation 4.1.

$$\text{Amino acid loading (mmol. g}^{-1}\text{)} = \frac{\text{Absorbance}_{\text{sample}}}{1.65 \times \text{mg (resin)}} \quad (4.1)$$

- 6) It was obtained a 0.57 mmol.g<sup>-1</sup> loading.

**III. Fmoc protecting group cleavage.**

- 1) The resin was washed with DMF (2 x 10 mL) for 2 minutes;
- 2) The resin was stirred with a solution of 20% (v/v) piperidine in DMF (10 mL) for 3 hours;
- 3) The resin was washed with DMF (2 x 10 mL) for 2 minutes;
- 4) The resin was washed with 2-propanol (2 x 10 mL) for 2 minutes;
- 5) Steps 3) and 4) were repeated once each.

**IV. TNBS (2,4,6-Trinitrobenzenesulfonic acid) test.**

The TNBS test was made to assess the presence or not of free amino groups on the resin. This test was performed according to method 14 of the Novabiochem catalogue (p S43).

- 1) A few resin beads were withdrawn and washed 3 times with DMF;
- 2) The beads were suspended in DMF and 2 drops of a DIPEA in DMF 10% (v/v) and 2 drops of a TNBS in DMF 1% (v/v) were added;
- 3) After 5 minutes the beads were washed with DMF and the DMF removed. A positive test is indicated by red beads.

**V. Fmoc-protected amino acids coupling.**

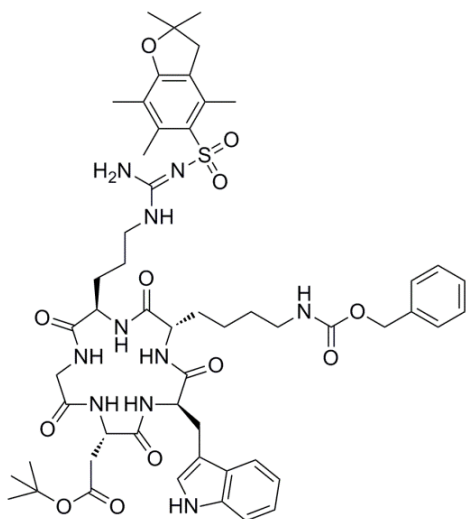
- 1) In a round bottom flask, 4 equivalents of Fmoc-aa-OH (Fmoc-Arg(Pbf)-OH: 1.5 g; Fmoc-Lys(Cbz)-OH: 1.15 g; Fmoc-Trp-OH: 972 mg; Fmoc-Asp(*t*-Bu)-OH: 938 mg) were dissolved in DMF (10 mL) and to this solution, 4 equivalents of HOBt (308 mg) and 4 equivalents of DIC (353  $\mu$ L) were added. The equivalents are relative to the loading level of the resin determined in **II**;
- 2) The solution was transferred to the reaction vessel containing the resin and the mixture was allowed to react (under shaking) overnight at room temperature;
- 3) The solution was drained and the resin was washed with DMF (3 x 10 mL) and DCM (3 x 10 mL) (all washes must have a minimum of 2 minutes);
- 4) The coupling reaction was assessed by the TNBS test. In all coupling reactions made, the resin was always yellow.
- 5) Steps **III**, **IV** and **V** were repeated until the desire peptide was synthesized.

**VI. Peptide cleavage from the resin.**

- 1) The resin was stirred with a AcOH/TFE/DCM (1:1:3) solution (20 mL) for 3 hours at room temperature;
- 2) The solution was drained to a round bottom flask;
- 3) The resin was washed with AcOH/TFE/DCM (1:1:3) solution (3 x 10 mL) for 2 minutes and the washing solutions were combined in the round bottom flask;
- 4) The filtrate was concentrated under reduced pressure to give a yellow oil;
- 5) Ethyl ether was added to the oil and the mixture was placed on the freezer overnight;
- 6) The suspension was filtered under reduced pressure, triturated with cold ethyl ether to afford peptide **27** (331 mg, 50 %) as a slightly yellow solid.  $^1\text{H}$  NMR (400 MHz, DMSO, TMS)  $\delta$ : 1.13-1.29 (2H, m,  $\gamma$ -CH<sub>2</sub> Lys), 1.36 (9H, s, CH<sub>3</sub>*t*-Bu), 1.38 (6H, s, CH<sub>3</sub> Pbf), 1.38-1.57 (4H, m<sub>b</sub>,  $\gamma$ -CH<sub>2</sub> Arg +  $\delta$ -CH<sub>2</sub> Lys), 1.61-1.74 (4H, m<sub>b</sub>,  $\beta$ -CH<sub>2</sub> Arg +  $\beta$ -CH<sub>2</sub> Lys), 1.98 (3H, s, 7-CH<sub>3</sub> Pbf), 2.26 (1H, dd,  $J_1=16.4$  Hz,  $J_2=8.4$  Hz,  $\beta$ -CH<sub>2</sub>Asp), 2.41 (3H, s, 4-CH<sub>3</sub> Pbf), 2.47 (3H, s, 6-CH<sub>3</sub> Pbf), 2.54 (1H, dd,  $J_1=16.4$  Hz,  $J_2=4.4$  Hz,  $\beta$ -CH<sub>2</sub> Asp), 2.91 (2H, s, 3-CH<sub>2</sub> Pbf), 2.92-3.09 (4H, m<sub>b</sub>,  $\delta$ -CH<sub>2</sub> Arg +  $\epsilon$ -CH<sub>2</sub> Lys), 3.15 (1H, dd,  $J_1=14.6$  Hz,  $J_2=4.6$  Hz,  $\beta$ -CH<sub>2</sub> Trp), 3.35-3.55 (1H, m,  $\alpha$ -CH Asp), 3.66 (1H, dd,  $J_1=17.4$  Hz,  $J_2=5.4$  Hz,  $\beta$ -CH<sub>2</sub>Trp), 3.71-3.77 (2H, m, CH<sub>2</sub> Gly), 4.20-4.32 (2H, m<sub>b</sub>,  $\alpha$ -CH Arg +  $\alpha$ -

CH Lys), 4.52-4.58 (1H, m,  $\alpha$ -CH Trp), 4.97 (2H, s, CH<sub>2</sub> Cbz), 6.46 (2H, s<sub>b</sub>, RNH<sub>2</sub>), 6.76 (2H, s<sub>b</sub>, RNH<sub>2</sub>), 6.93 (1H, t,  $J$ =7.4 Hz, 5-CH Trp), 7.01 (1H, t,  $J$ =7.2 Hz, 6-CH Trp), 7.08-7.15 (2H, m, 4-CH Trp + NH), 7.23-7.34 (6H, m, 7-CH Trp + ArH Cbz), 7.58 (1H, d,  $J$ =7.6 Hz, 2-CH Trp), 7.85 (1H, d,  $J$ =8.0 Hz, NH), 8.02 (1H, t,  $J$ =5.6 Hz, NH), 8.06 (1H, d,  $J$ =7.6 Hz, NH), 8.16 (1H, d,  $J$ =6.0 Hz, NH'), 10.70 (1H, s, NH Trp) ppm. <sup>13</sup>C NMR (100 MHz, DMSO, TMS)  $\delta$ : 12.13 (7-CH<sub>3</sub> Pbf), 17.48 (6-CH<sub>3</sub> Pbf), 18.83 (4-CH<sub>3</sub> Pbf), 22.53 ( $\gamma$ -CH<sub>2</sub> Lys), 24.97 ( $\gamma$ -CH<sub>2</sub> Arg), 27.56 ( $\beta$ -CH<sub>2</sub> Trp), 27.63 (CH<sub>3</sub> *t*-Bu), 28.20 (CH<sub>3</sub> Pbf), 29.04 ( $\delta$ -CH<sub>2</sub> Lys), 29.30 ( $\beta$ -CH<sub>2</sub> Arg), 31.15 ( $\beta$ -CH<sub>2</sub> Lys), 40.17 ( $\epsilon$ -CH<sub>2</sub> Lys), 40.99 ( $\beta$ -CH<sub>2</sub> Asp), 41.05 ( $\delta$ -CH<sub>2</sub> Arg), 42.45 (CH<sub>2</sub> Gly), 42.56 (CH<sub>2</sub> Pbf) 51.10 ( $\alpha$ -CH<sub>2</sub> Asp), 51.85 ( $\alpha$ -CH<sub>2</sub> Lys), 52.68 ( $\alpha$ -CH<sub>2</sub> Arg), 53.16 ( $\alpha$ -CH<sub>2</sub> Trp), 65.03 (CH<sub>2</sub> Cbz), 80.01 (C *t*-Bu), 85.98 (2-C Pbf), 109.55 (3-C Trp), 111.08 (7-CH Trp), 116.17 (7-C Pbf), 118.00 (5-CH Trp), 118.40 (2-CH Trp), 120.65 (6-CH Trp), 123.61 (4-CH Trp), 124.06 (3a-C Pbf), 127.34 (3a-C Trp), 127.51 (p-CH Cbz), 127.57 (m-CH Cbz), 128.12 (o-CH Cbz), 131.35 (4-C Pbf), 133.99 (5-C Pbf), 135.94 (1a-C Trp), 137.11 (6-C Pbf), 137.20 (CR<sub>4</sub> Cbz), 155.95 (C=O Cbz), 156.04 (C-N Arg), 157.40 (1a-C Pbf), 171.01, 171.15, 171.26, 171.32, 171.81 (C=O), 172.29 (C=O Gly) ppm. HRMS (ESI): calculated for C<sub>54</sub>H<sub>74</sub>N<sub>10</sub>O<sub>13</sub>S (MH<sup>+</sup>) 1103.52358; Found 1103.52286 (MH<sup>+</sup>). Analytical HPLC (retention time): 1.669 min (MeCN/H<sub>2</sub>O (3:1), 0.8 mL.min<sup>-1</sup>).

**c(R(Pbf)GD(*t*-Bu)WK(Cbz)), 28**

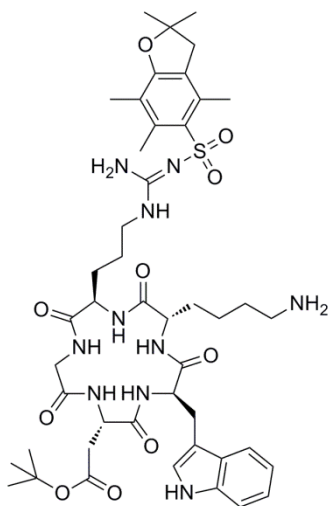


HBTU (107 mg, 281.9  $\mu$ mol) were dissolved in DMF (2.2 mL) and to this solution R(Pbf)GD(*t*-Bu)WK(Cbz), **27** (327 mg, 281.1  $\mu$ mol) and DIPEA (79  $\mu$ L, 460  $\mu$ mol) dissolved in DMF (2.7 mL) were added dropwise over a period of 6 hours. The mixture was stirred overnight at room temperature and concentrated under reduced pressure to give a yellow oil. Ethyl ether was added and the mixture was placed in the freezer overnight. The suspension was filtered under reduced pressure and triturated with cold ethyl ether to afford compound **28** (284 mg, 93



%) as a yellow solid. HRMS (ESI<sup>+</sup>): calculated for C<sub>54</sub>H<sub>72</sub>N<sub>10</sub>O<sub>12</sub>S (MH<sup>+</sup>) 1085.51301; found 1085.51246 (MH<sup>+</sup>). Analytical HPLC (retention time): 1.819 min (MeCN/H<sub>2</sub>O (3:1), 0.8 mL.min<sup>-1</sup>).

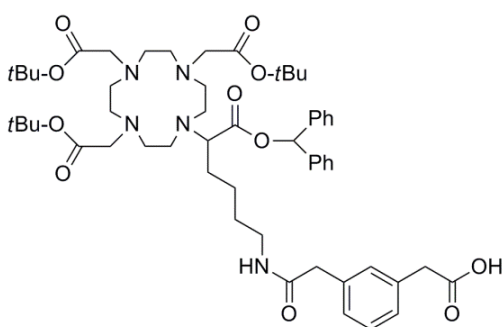
### c(R(Pbf)GD(*t*-Bu)WK), **29**



c(R(Pbf)GD(*t*-Bu)WK(Cbz)), **28** (228 mg, 210.1 μmol) were dissolved in DCM/EtOH (7:3) (25 mL) and to this solution Pd/C (10%) (228 mg) was added. The mixture was stirred under hydrogen atmosphere for 24 hours at room temperature and filtered through celite. The celite was washed with DCM/EtOH (7:3) (100 mL) and the filtrate was concentrated under reduced pressure to give a brown oil. Ethyl ether was added and the mixture was placed in the freezer overnight. The suspension was filtered under reduced pressure and triturated with cold ethyl ether to

afford peptide **29** (129 mg, 65 %) as a yellow solid. HRMS (ESI<sup>+</sup>): calculated for C<sub>46</sub>H<sub>66</sub>N<sub>10</sub>O<sub>10</sub>S (MH<sup>+</sup>) 951.47623; found 951.47569 (MH<sup>+</sup>). Analytical HPLC (retention time): 2.803 min (MeCN/H<sub>2</sub>O (3:1), 0.8 mL.min<sup>-1</sup>).

### DO3A(*t*-Bu)-A(1,3-phenyldiacetate)HA(Be), **30**

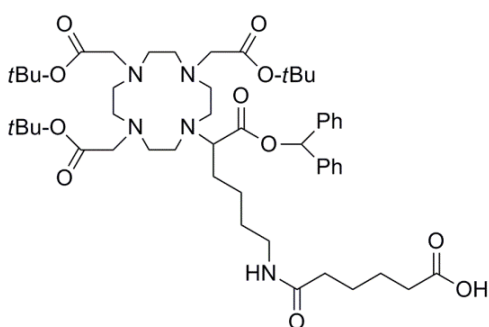


DO3A(*t*-Bu)-AHA(Be), **12** (230 mg, 284 μmol) were dissolved in dry MeCN (20 mL) and to this solution 1,3-phenyldiacetic acid (441 mg, 2.3 mmol) DIPEA (50 μL, 284 μmol), HOBt (56 mg, 426 μmol) and HBTU (162 mg, 426 μmol) were added. The solution was

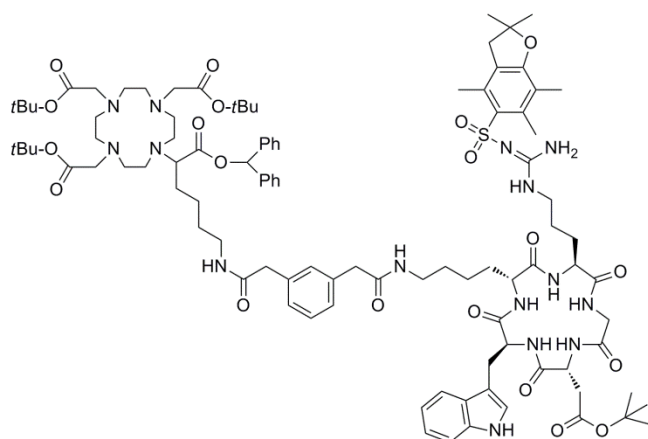
stirred for 72 hours at room temperature and concentrated under reduced pressure to give grey solid. The solid was dissolved in ethyl acetate (40 mL), and the organic phase was washed with 1 M KHSO<sub>4</sub> (3 x 20 mL), 1 M NaHCO<sub>3</sub> (3 x 20 mL) and brine (3 x 20 mL). The organic phases were combined, dried with anhydrous MgSO<sub>4</sub> and concentrated under reduced pressure to afford compound **30** (189 mg, 67 %) as a slightly grey solid. <sup>1</sup>H NMR (400 MHz, CDCl<sub>3</sub>, TMS) δ: 1.18-1.55 (31H, m<sub>b</sub>, γ-CH<sub>2</sub> + δ-CH<sub>2</sub> + CH<sub>3</sub> *t*-Bu), 1.61-1.77 (2H, m<sub>b</sub>, β-CH<sub>2</sub>), 1.93-3.37 (23H, m<sub>b</sub>, CH<sub>2</sub> cyclen + ε-

CH<sub>2</sub> + CH<sub>2</sub>COR), 3.50 (2H, s, RNH-CH<sub>2</sub> linker), 3.51-3.59 (1H, m, α-CH<sub>2</sub>), 3.57 (2H, s, RO-CH<sub>2</sub> linker), 6.34 (1H, m, NH), 6.85 (1H, s, CH Benzhydryl), 7.15-7.38 (14H, m<sub>b</sub>, ArH + ArH linker) ppm. <sup>13</sup>C NMR (100 MHz, CDCl<sub>3</sub>, TMS δ: 24.09 (γ-CH<sub>2</sub>), 26.39 (δ-CH<sub>2</sub>), 27.94 (CH<sub>3</sub> *t*-Bu), 29.19 (β-CH<sub>2</sub>), 39.19 (ε-CH<sub>2</sub>), 41.23 (RO-CH<sub>2</sub> linker), 43.17 (CH<sub>2</sub> linker), 44.34, 47.29, 47.83, 48.18 (CH<sub>2</sub> cyclen), 55.59 (CH<sub>2</sub>COR), 61.30 (α-CH), 78.10 (CH Benzhydryl), 81.91 (C *t*-Bu), 126.95 (CH), 127.91 (CH), 128.13 (CH-Ph), 128.63 (CH), 128.70 (CH), 128.75 (CH), 130.48 (CH), 134.68 (C), 135.64 (C), 139.23 (C), 171.70 (C=O), 172.89 (C=O *t*-Bu), 174.74 (C=O Benzhydryl), 175.20 (C=O) ppm. HRMS (ESI<sup>+</sup>): calculated for C<sub>55</sub>H<sub>79</sub>N<sub>5</sub>O<sub>11</sub> (MH<sup>+</sup>) 986.58543; found 986.58506 (MH<sup>+</sup>).

### DO3A(*t*-Bu)-A(adipate)HA(Be), **31**

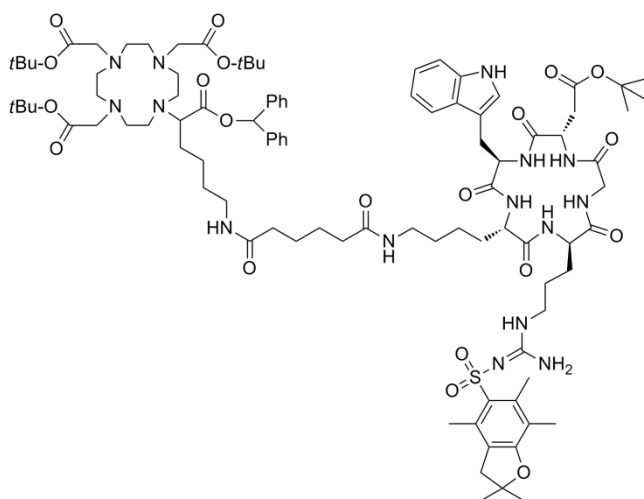


DO3A(*t*-Bu)-AHA(Be), **12** (154 mg, 190 μmol) were dissolved in dry MeCN (15 mL) and to this solution adipic acid (222 mg, 1.5 mmol), DIPEA (33 μL, 190 μmol), HOBT (39 mg, 285 μmol) and HBTU (108 mg, 285 μmol) were added. The solution was stirred for 72 hours at room temperature and concentrated under reduced pressure to give a grey solid. The solid was dissolved in ethyl acetate (30 mL), and the organic phase was washed with KHSO<sub>4</sub> 1M (3 x 15 mL), NaHCO<sub>3</sub> 1M (3 x 15 mL) and of brine (3 x 15 mL). The organic phases were combined, dried with anhydrous MgSO<sub>4</sub> and concentrated under reduced pressure to afford compound **31** (178 mg, 62 %) as a slightly grey solid. <sup>1</sup>H NMR (400 MHz, CDCl<sub>3</sub>, TMS) δ) 1.19-1.77 (37H, m<sub>b</sub>, β-CH<sub>2</sub> + γ-CH<sub>2</sub> + δ-CH<sub>2</sub> + CH<sub>3</sub> *t*-Bu + CH<sub>2</sub> linker), 1.96-3.36 (28H, m<sub>b</sub>, CH<sub>2</sub> cyclen + ε-CH<sub>2</sub> + CH<sub>2</sub>COR + COCH<sub>2</sub> linker), 3.56-3.63 (1H, m, α-CH<sub>2</sub>), 6.55-6.62 (1H, m, NH), 6.86 (1H, s, CH Benzhydryl), 7.24-7.39 (10H, m, ArH) ppm. <sup>13</sup>C NMR (100 MHz, CDCl<sub>3</sub>, TMS) δ: 24.16 (γ-CH<sub>2</sub>), 24.99, 26.44 (CH<sub>2</sub> linker), 27.83 (CH<sub>3</sub> *t*-Bu), 27.95 (δ-CH<sub>2</sub>), 29.25 (β-CH<sub>2</sub>), 34.00, 35.71 (COCH<sub>2</sub> linker), 38.97 (ε-CH<sub>2</sub>), 44.40, 47.33, 47.82, 48.19 (CH<sub>2</sub> cyclen), 55.61 (CH<sub>2</sub>COR), 61.29 (α-CH), 78.11 (CH Benzhydryl), 81.93 (C *t*-Bu), 126.92 (CH), 128.14 (CH), 128.66 (CH), 139.19 (C), 172.84 (C=O *t*-Bu), 173.77 (C=O), 177.17 (C=O Benzhydryl), 177.02 (C=O) ppm. HRMS (ESI<sup>+</sup>): calculated for C<sub>51</sub>H<sub>79</sub>N<sub>5</sub>O<sub>11</sub> (MH<sup>+</sup>) 938.58543; found 938.58488 (MH<sup>+</sup>).

**DO3A(*t*-Bu)-A(1,3-phenyldiacetate-*c*(R(Pbf)GD(*t*-Bu)WK))HA(Be), 32**

DO3A(*t*-Bu)-A(1,3-phenyldiacetate)HA(Be), **30** (36 mg, 37  $\mu$ mol) was dissolved in DMF (5 mL) and to this solution, HOBt (6 mg, 44  $\mu$ mol), HATU (17 mg, 44  $\mu$ mol), DIPEA (15  $\mu$ L, 110  $\mu$ mol) and *c*(R(Pbf)GD(*t*-Bu)WK) (35 mg, 37  $\mu$ mol) of were added.

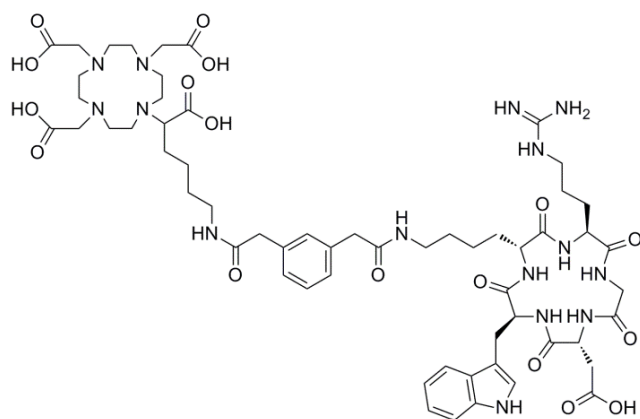
The addition of the reagents was performed at intervals of 10 minutes. The solution was stirred for 72 hours at room temperature and concentrated under reduced pressure to give a yellow oil. Water was added and the mixture was placed in the fridge overnight. The suspension was filtered under reduced pressure and triturated with cold water to afford compound **32** (53 mg, 76 %) a slightly yellow solid. HRMS (ESI<sup>+</sup>): calculated for C<sub>101</sub>H<sub>143</sub>N<sub>15</sub>O<sub>20</sub>S (MH) 1920.04608, (MH<sub>2</sub><sup>2+</sup>) 960.52668; found 1920.04563 (MH), 960.52603 (MH<sub>2</sub><sup>2+</sup>).

**DO3A(*t*-Bu)-A(adipate-*c*(R(Pbf)GD(*t*-Bu)WK))HA(Be), 33**

DO3A(*t*-Bu)-A(adipate)HA(Be), **31** (35 mg, 37  $\mu$ mol) of was dissolved in DMF (5 mL) and to this solution HOBt (6 mg, 44  $\mu$ mol), HATU (17 mg, 44  $\mu$ mol), DIPEA (15  $\mu$ L, 110  $\mu$ mol) and *c*(R(Pbf)GD(*t*-Bu)WK) (35 mg, 37  $\mu$ mol) were added. The addition of the reagents was performed at

intervals of 10 minutes. The solution was stirred for 72 hours at room temperature and concentrated under reduced pressure to give a yellow oil. Water was added and the mixture was placed in the fridge overnight. The suspension was filtered under reduced pressure and triturated with cold water to afford **33** (55 mg, 79 %) as a slightly yellow solid. HRMS (ESI<sup>+</sup>): calculated for C<sub>97</sub>H<sub>143</sub>N<sub>15</sub>O<sub>20</sub>S (MH<sub>2</sub><sup>2+</sup>) 936.52668; found 936.52654 (MH<sub>2</sub><sup>2+</sup>).

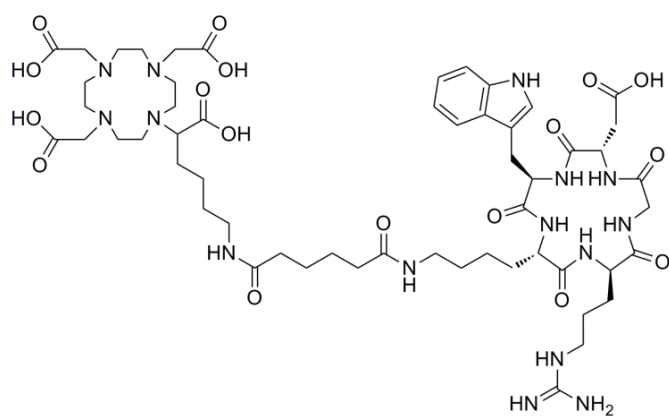
**DOTA-A-(1,3-phenyldiacetate-c(RGDWK))HA, 34**



DO3A(*t*-Bu)-A(1,3-phenyldiacetate-c(R(Pbf)GD(*t*-Bu)WK))HA(Be), **32** (50 mg, 26  $\mu$ mol) was dissolved in DCM (4 mL) and TFA (1 ML). The solution was stirred overnight at room temperature and concentrated under reduced pressure to give a purple oil. The oil was washed with

*n*-hexane (2x) to give a yellow oil. The oil was dissolved in MeOH, ethyl ether was added and the mixture was placed in the freezer overnight. The suspension was filtered under reduced pressure and triturated with cold ethyl ether to afford compound **34** (36 mg) as a slightly yellow solid in trifluoroacetate salt form. HRMS (ESI<sup>+</sup>): calculated for C<sub>59</sub>H<sub>85</sub>N<sub>15</sub>O<sub>17</sub> (MH<sub>2</sub><sup>2+</sup>) 638.81967; found 631.82019 (MH<sub>2</sub><sup>2+</sup>).

**DOTA-A(adipate-c(RGDWK))HA, 35**



DO3A(*t*-Bu)-A(adipate-c(R(Pbf)GD(*t*-Bu)WK))HA(Be), **33** (50 mg, 27  $\mu$ mol) was dissolved in DCM (4 mL) and in TFA (1mL). The solution was stirred overnight at room temperature and concentrated under reduced pressure to give a

purple oil. The oil was washed with *n*-hexane (2x) to give a yellow oil. The oil was dissolved in MeOH, ethyl ether was added and the mixture was placed in the freezer overnight. The suspension was filtered under reduced pressure and triturated with cold ethyl ether to afford compound **35** (30 mg) as a slightly yellow solid in trifluoroacetate salt form. HRMS (ESI<sup>+</sup>): calculated for C<sub>55</sub>H<sub>85</sub>N<sub>15</sub>O<sub>17</sub> (MH<sub>2</sub><sup>2+</sup>) 614.81967; found 614.81999 (MH<sub>2</sub><sup>2+</sup>).

## 4.4 Temperature dependence and kinetic stability studies of Gd(DOTA-AHA) and [Gd(DOTA-A(PEG<sub>750</sub>)HA)]<sup>-</sup> chelates

### 4.4.1 Samples preparation

To an aqueous solution of the ligand, a GdCl<sub>3</sub> solution in 1:1 mole ratio was added dropwise (a slight excess of ligand was used: 5%). The pH was adjusted to around 4 with the addition of a 0.01 M NaOH solution and the solution was stirred for 1 hour at 60 °C. The pH was adjusted to pH 5 with the addition of a 0.01 M NaOH solution and the solution was stirred overnight. The pH was then adjusted to 7 and the solution was concentrated under reduced pressure.

For relaxometric measurements, the solutions were prepared by dissolving the respective chelate in H<sub>2</sub>O or PBS buffer solution (pH = 7). The absence of free metal was checked in each sample with xylenol orange.<sup>339</sup> The water proton longitudinal relaxation rates were measured at 20 MHz.

### 4.4.2 Measurements

Relaxometric measurements for both chelate solutions (1.25 mM) were performed at variable temperatures (pH = 7.0) and variable pH values (T = 25 °C). The kinetic stability study of **Gd(DOTA-AHA)** was performed with transmetalation experiments at 37 °C. The time evolution of proton longitudinal relaxation rates of two chelate solutions (1.0 mM) in PBS buffer (10 mM), wherein one of them containing equimolar of Zn(II), were recorded and monitored through a period of 48 hours. Acidified water (pH = 3.0) was used as an external reference.

## 4.5 $^1\text{H}$ NMRD and $^{17}\text{O}$ NMR relaxometric studies

### 4.5.1 Samples preparation

To an aqueous solution of the ligand, a  $\text{GdCl}_3$  solution in 1:1 mole ratio (for mononuclear chelates) or in 1:2 mole ratio (for binuclear chelates) was added dropwise (a slight excess of ligand was used: 5%). The pH was adjusted to around 4 with the addition of a 0.01 M NaOH solution and the solution was stirred for 1 hour at 60 °C. The pH was adjusted to pH 5 with the addition of a 0.01 M NaOH solution and the solution was stirred overnight. The pH was then adjusted to 5.7 and the solution was concentrated under reduced pressure.

In all cases, the final solutions were obtained by the addition of  $\text{H}_2^{17}\text{O}$  ( $^{17}\text{O} = 20.2\%$ ) and  $\text{H}_2\text{O}$ . The  $^{17}\text{O}$ -enriched water was added to the solutions to obtain a final 2%  $^{17}\text{O}$  enrichment and improve the  $^{17}\text{O}$  NMR measurements sensibility. The absence of free metal was checked in each sample with xylenol orange.<sup>339</sup> The final solutions concentration was determined by susceptibility measurements in the presence of *t*-butanol.<sup>340</sup> The Gd(III) concentration in the samples were: mononuclear chelate  $\approx 20$  mM, binuclear chelates  $\approx 12$  mM and PEGylated chelates  $\approx 8$  mM.

### 4.5.2 $^1\text{H}$ NMRD

Sample tubes with an outer diameter of 5 mm were used for measurements. The proton longitudinal relaxation rates ( $1/T_1$ ) for the water nuclear magnetic relaxation dispersion profiles (NMRD) were measured at 0.47 T ( $^1\text{H}$  Larmor frequency: 20 MHz), 0.70 T (30 MHz), 0.94 T (40 MHz), 1.41 T (60 MHz), 2.35 T (100 MHz), 4.7 T (200 MHz) and 9.4 T (400 MHz). The longitudinal relaxation rates of six chelates with known concentration were measured at two different temperatures (25 and 37 °C). Acidified water (pH = 3.0) was used as an external reference. The relaxivities  $r_1$  ( $\text{mM}^{-1}\cdot\text{s}^{-1}$ ) were calculated using equation 4.2 using diamagnetic relaxation contributions  $1/T_{1(d)}$  of  $0.31\text{ s}^{-1}$  (400 MHz) /  $0.40\text{ s}^{-1}$  (20 MHz) for 25 °C and  $0.25\text{ s}^{-1}$  (400 MHz) /  $0.29\text{ s}^{-1}$  (20 MHz) for 37 °C, respectively. For full equations see chapter 6.1.2.

$$r_1 = \frac{1}{[\text{Gd(III)}]} \left( \frac{1}{T_1} - \frac{1}{T_{1,d}} \right), \text{ with } [\text{Gd(III)}] \text{ in mM} \quad (4.2)$$

### 4.5.3 $^{17}\text{O}$ NMR

The samples were sealed in glass spheres adapted for 10 mm NMR tubes, in order to avoid susceptibility corrections to the chemical shifts.<sup>341, 342</sup> Variable-temperature  $^{17}\text{O}$  measurements were performed at 9.4 T ( $^{17}\text{O}$  Larmor frequency: 54.3 MHz). The longitudinal ( $1/T_1$ ) and transverse ( $1/T_2$ ) relaxation rates were measured using the inversion-recovery<sup>343</sup> and the Carr–Purcell–Meiboom–Gill<sup>344</sup> pulse sequences, respectively, and chemical shifts ( $\Delta\omega$ ) were measured at 12 different temperatures in the range from 5 to 65 °C. The reduced relaxation rates  $T_{1r}$  and  $T_{2r}$  and the reduced chemical shift differences  $\Delta\omega_r$ , with respect to a pH 3.0 water reference (2%  $^{17}\text{O}$  enrichment), were calculated using equations 4.3 to 4.5. The number of water molecules in the inner sphere of the complex  $q$  was fixed to one. For full equations see chapter 6.1.3.

$$\frac{1}{T_{i,r}} = \frac{1}{P_M} \left( \frac{1}{T_i} - \frac{1}{T_i^{\text{ref}}} \right), \text{ where } i = 1, 2 \quad (4.3)$$

$$\Delta\omega_r = \frac{1}{P_M} (\omega - \omega^{\text{ref}}) \quad (4.4)$$

$$P_M = \frac{q[\text{M}^{n+}]}{55.56} \quad (4.5)$$

### 4.5.4 Data analysis

For fits of the  $^1\text{H}$  NMRD and  $^{17}\text{O}$  NMR data, a Solomon–Bloembergen-based theory was used<sup>342, 345, 346</sup> supplemented with the Lipari–Szabo free-model approach for the internal rotation.<sup>153, 154</sup> The simultaneous fits were performed using Visualiseur/Optimiseur<sup>347</sup> running on a MATLAB<sup>®</sup> 8.0 (R2012b) platform.

## **4.6 DEER and modelling studies of Gd(III) binuclear chelates**

### **4.6.1 Samples preparation**

To an aqueous solution of the ligand, a GdCl<sub>3</sub> solution in 1:2 mole ratio was added dropwise (a slight excess of ligand was used: 5%). The pH was adjusted to around 4 with the addition of a 0.01 M NaOH solution and the solution was stirred for 1 hour at 60 °C. The pH was adjusted to pH 5 with the addition of a 0.01 M NaOH solution and the solution was stirred overnight. The pH was then adjusted to 5.7 and the solution was concentrated under reduced pressure to give a white solid. The absence of free metal was checked in each sample with xylenol orange.<sup>339</sup>

For the measurements, solutions were prepared by dissolving 600 μmol of the chelate in 2 ml of H<sub>2</sub>O and then the mixture was centrifuged. A 200 μL aliquot of supernatant was collected and mixed with a 200 μL aliquot of glycerol to obtain the final solution.

### **4.6.2 Measurements**

The Gd(III)-Gd(III) distance measurements were performed with the 4 pulse double electron-electron resonance experiment<sup>304, 308</sup> at Q band on a home-built high microwave power spectrometer<sup>335</sup> equipped with a rectangular resonator accommodating for 3 mm outer diameter samples.<sup>336, 337</sup> The measurements were performed at 10 K and the temperature was set and stabilized with a He-flow cryostat Oxford Instruments ER 4118 CF.

In the DEER pulse sequence all microwave pulses were set to duration of 12 ns, first inter-pulse interval of 400 ns and the length of the DEER time trace of 3 μs was set. The frequency difference between pump and detection pulses was set to 300 MHz.

### **4.6.3 Data analysis**

The DEER time traces were analyzed with the DeerAnalysis software.<sup>313</sup> A model free fit with Tikhonov regularization was performed in each case.



#### **4.6.4 Molecular modelling**

The molecular modelling has been performed Scigress (Fujitsu) Version 3.1.0. Structures are taken from MD conformational searches and energy minimized both in vacuum. The force-field used is MM3; Gd(III) has been replaced by Y(III) which has approximately the same ionic radius.

### **4.7 <sup>1</sup>H NMR studies of paramagnetic lanthanide DOTA-A(PEG<sub>750</sub>)HA chelates**

#### **4.7.1 Samples preparation**

To an aqueous solution of the ligand, the corresponding LnCl<sub>3</sub> solution in 1:1 mole ratio was added dropwise (a slight excess of ligand was used: 5%). The pH was adjusted to around 4 with the addition of a 0.01 M NaOH solution and the solution was stirred for 1 hour at 60 °C. The pH was adjusted to pH 5 with the addition of a 0.01 M NaOH solution and the solution was stirred overnight. The pH was then adjusted to 7 and the solution was concentrated under reduced pressure.

#### **4.7.2 Measurements**

The solutions were prepared by dissolving the respective chelate in D<sub>2</sub>O (700 μL). The proton spectra of the Pr(III), Nd(III), Sm(III), Eu(III) and Yb(III) chelates were obtained at 7, 25, 40 and 60 °C. The <sup>1</sup>H NMR spectra were recorded on a Varian Unity Plus 300 spectrometer, operating at 299.938 MHz.

## 4.8 *In vitro* and *in vivo* studies of $^{67}\text{Ga}(\text{DOTA-AHA})$ and $[\text{}^{67}\text{Ga}(\text{DOTA-A}(\text{PEG}_{750})\text{HA})]^-$

### 4.8.1 Samples preparation

The  $^{67}\text{Ga}$  chelates for *in vivo* and *in vitro* experiments were prepared by adding 1 mCi of  $^{67}\text{Ga}(\text{citrate})$  to a solution of 1 mg of chelator dissolved in HEPES buffer solution (0.150 mL, 0.1 M, pH 5). The solution was stirred for 1 hour at 80 °C. The radiochemical purity of the  $^{67}\text{GaL}$  solutions was determined either by TLC eluting with methanol or using ITLC stripes eluting with a saline/acetic acid (9:1) mixture. In the first case the  $^{67}\text{Ga}(\text{III})$  ion remains in the origin and  $^{67}\text{GaL}$  migrates ( $R_f = 0.6$ ) while in the second case  $^{67}\text{GaL}$  remains in the origin and the  $^{67}\text{Ga}(\text{III})$  ion migrates ( $R_f = 0.8$ ). The percentage of bound metal averaged 96%.

### 4.8.2 Determination of LogP

The octanol/water partition coefficients (LogP) of  $^{67}\text{Ga}(\text{DOTA-AHA})$  and  $[\text{}^{67}\text{Ga}(\text{DOTA-AHA}_{\text{PEG}_{750}})]^-$  were calculated using the *shake-flask* method. For the measurements, 25  $\mu\text{L}$  of chelate solution were added to a tube containing 1 mL of saline solution and 1 mL of 1-octanol. The resulting mixture was shaken at room temperature for 1 h and then centrifuged for 3 min at 3000 rpm. After the centrifugation, 100  $\mu\text{L}$  of each phase were collected and the activity was measured. The partition coefficient was calculated as a ratio of the counts in the octanol fraction to the counts in the water fraction, being this the result of the average of 5 determinations.

### **4.8.3 Stability studies in blood serum**

For the blood serum stability studies, 5  $\mu\text{Ci}$  of [ $^{67}\text{Ga}(\text{DOTA-AHA}_{\text{PEG750}})]^-$  standard solution were added to 5 mL of fresh human serum, previously equilibrated in 5%  $\text{CO}_2$  (95% air) environment at 37 °C. The mixture was stored in the same environment conditions, and aliquots of 100  $\mu\text{L}$  (in triplicate) were taken at appropriate periods of time (30 min, 60 min and 180 min). The aliquots were treated with 200  $\mu\text{L}$  of ethanol, cooled (4 °C) and centrifuged for 15 min at 4000 rpm, in order to precipitate the serum proteins. A 100  $\mu\text{L}$  aliquot of supernatant were collected for activity counting with a  $\gamma$  well-counter. The sediment was washed twice with 1 mL of ethanol and its activity was also measured. The activity of the supernatant was compared with the activity measured for the sediment, in order to acquire the percentage of chelate associated with proteins. The activity of the supernatant at  $t = 180$  minutes was also measured after a TLC assay to check whether the chelate remained intact.

### **4.8.4 Biodistribution and blood clearance studies**

Groups of four animals (Wistar male rat weighting about 200 g) were anaesthetized with ketamine (50.0  $\text{mg}\cdot\text{mL}^{-1}$ )/chlorpromazine (2.5%) (10:3), injected in the tail vein with 100  $\mu\text{Ci}$  of the radiotracer and sacrificed 1 hour and 24 hours later. Blood samples and the major organs were removed, weighted and the activity was measured with a  $\gamma$  well-counter.

## 4.9 Ligand titrations

Every ligand used on previous studies was titrated, because the obtained compounds were in salt form due to the protecting groups' removal in acidic conditions. In order to identify the actual amount (mol) of chelating agent per mass unit (mg) titrations were made for each of the chelators.

The chelates were prepared by mixing an aqueous solution of the ligand and a  $\text{GdCl}_3$  solution in 1:1 mole ratio (for mononuclear chelates) or in 1:2 mole ratio (for binuclear chelates). In this case, the ligand solution was prepared using the theoretical molar mass of the ligand, which provided final chelate solutions with free Gd(III). The pH was adjusted to 4 with the addition of a 0.01 M NaOH solution and the solution was stirred for 1 hour at 60 °C. The pH was adjusted to pH 5 with the addition of a 0.01 M NaOH solution and the solution was stirred overnight. The pH was then adjusted to 5.7 and the solution was concentrated under reduced pressure.

For titrations, 500  $\mu\text{l}$  of chelate solution, 200  $\mu\text{l}$  of xylenol orange solution (0.5 %) and 1 ml of urotropin buffer solution (20 %, pH = 5.7) were combined to give a yellow solution. This mixture was titrated with 0.15 mM **EDTA** solution until the solution turned pink. This procedure was repeated three times for each chelate solution. The number of moles of each ligand in solution was calculated through the subtraction of the amount of **EDTA** used to chelate the free Gd(III) relatively to the total amount of Gd(III) used in the preparation of the samples. The exact molar mass of each ligand was then calculated using the obtained number of moles and the used mass in each sample.

# 5 Bibliography



1. Ronconi, L.; Sadler, P. J. *Coord. Chem. Rev.* **2008**, *252*, 2239.
2. Fraústo da Silva, J. J. R.; Williams, R. J. P. *The Biological Chemistry of the Elements: The Inorganic Chemistry of Life*; Oxford: Oxford University Press, 2001.
3. Linn, S. M.; Roberts, R. J. *Nucleases*; New York: Cold Spring Harbor Laboratory Press, 1993.
4. Lake, J. A. *Annu. Rev. Biochem.* **1985**, *54*, 507.
5. Roat-Malone, R. M. *Bioinorganic Chemistry: A short course*; New York: John Wiley & Sons, Inc, 2002.
6. Burton, J. D.; Culkin, F.; Riley, J. P. *Geochim. Cosmochim. Acta* **1959**, *16*, 151.
7. Clausen, J.; Edeling, C. J.; Fogh, J. *Cancer Res.* **1974**, *34*, 1931.
8. Camargo, E. E.; Wagner, H. N.; Tsan, M. F. *Nuklearmedizin* **1979**, *18*, 147.
9. Hayes, R. L. *Handbook of Toxicity of Inorganic Compounds*; New York: Marcel Dekker, 1988.
10. Baes, C. F.; Mesmer, R. E. *The Hydrolysis of Cations*; New York: John Wiley & Sons, Inc, 1976.
11. Pearson, R. G. *Chem. Br.* **1967**, *3*, 103.
12. Miller, M. J. *Chem. Rev.* **1989**, *89*, 1563.
13. Yokoyama, A.; Ohmomo, Y.; Horiuchi, K.; Saji, H.; Tanaka, H.; Yamamoto, K.; Ishii, Y.; Torizuka, K. *J. Nucl. Med.* **1982**, *23*, 909.
14. Caraco, C.; Aloj, L.; Eckelman, W. C. *Appl. Radiat. Isot.* **1998**, *49*, 1477.
15. Martell, A. E.; Smith, R. M. *Critical Stability Constants*; New York: Plenum Press, 1974.
16. Harris, W. R.; Martell, A. E. *Inorg. Chem.* **1976**, *15*, 713.
17. Motekaitis, R. J.; Sun, Y. Z.; Martell, A. E. *Inorg. Chem.* **1991**, *30*, 1554.
18. Wong, E.; Caravan, P.; Liu, S.; Rettig, S. J.; Orvig, C. *Inorg. Chem.* **1996**, *35*, 715.
19. Martell, A. E.; Motekaitis, R. J.; Clarke, E. T.; Delgado, R.; Sun, Y. Z.; Ma, R. *Supramol. Chem.* **1996**, *6*, 353.
20. Andre, J. P.; Maecke, H. R.; Zehnder, M.; Macko, L.; Akyel, K. G. *Chem. Commun.* **1998**, 1301.
21. Wadas, T. J.; Wong, E. H.; Weisman, G. R.; Anderson, C. J. *Chem. Rev.* **2010**, *110*, 2858.
22. Bandoli, G.; Dolmella, A.; Tisato, F.; Porchia, M.; Refosco, F. *Coord. Chem. Rev.* **2009**, *253*, 56.

23. Sun, Y. Z.; Anderson, C. J.; Pajeau, T. S.; Reichert, D. E.; Hancock, R. D.; Motekaitis, R. J.; Martell, A. E.; Welch, M. J. *J. Med. Chem.* **1996**, *39*, 458.
24. Harris, W. R.; Pecoraro, V. L. *Biochemistry* **1983**, *22*, 292.
25. Collery, P.; Millart, H.; Lamiable, D.; Vistelle, R.; Rinjard, P.; Tran, G.; Gourdier, B.; Cossart, C.; Bouana, J. C.; Pechery, C.; Etienne, J. C.; Choisy, H.; Demontreynaud, J. M. D. *Anticancer Res.* **1989**, *9*, 353.
26. Bernstein, L. R. *Pharmacol. Rev.* **1998**, *50*, 665.
27. Shannon, R. D. *Acta Crystallogr. Sect. A* **1976**, *32*, 751.
28. Pearson, R. G. *Inorg. Chem.* **1988**, *27*, 734.
29. Huheey, J. E.; Keiter, E. A.; Keiter, R. L. *Inorganic Chemistry: Principles of Structure and Reactivity*; New York: Harper Collins, 1993.
30. Kerr, J. A. In *CRC Handbook of Chemistry and Physics*; CRC Press: Boca Raton, 1996.
31. Hancock, R. D.; Marsicano, F. *Inorg. Chem.* **1980**, *19*, 2709.
32. Logan, K. J.; Ng, P. K.; Turner, C. J.; Schmidt, R. P.; Terner, U. K.; Scott, J. R.; Lentle, B. C.; Noujaim, A. A. *International Journal of Nuclear Medicine & Biology* **1981**, *8*, 271.
33. Weiner, R. E. *Nuclear Medicine and Biology* **1996**, *23*, 745.
34. Dudley, H. C.; Maddox, G. E. *J. Pharmacol. Exp. Ther.* **1949**, *96*, 224.
35. Nelson, B.; Andrews, G. A.; Hayes, R. L.; Kniseley, R. M.; Edwards, C. L. *J. Nucl. Med.* **1972**, *13*, 92.
36. Hoffer, P. *J. Nucl. Med.* **1980**, *21*, 484.
37. Tsan, M. F. *J. Nucl. Med.* **1985**, *26*, 88.
38. Crichton, R. R.; Charloteauxwauters, M. *Eur. J. Biochem.* **1987**, *164*, 485.
39. Brittenham, G. M. In *Hematology, Basic Principles and Practice*; Churchill Livingstone: New York, 1991.
40. Huebers, H. A.; Finch, C. A. *Physiol. Rev.* **1987**, *67*, 520.
41. Gatter, K. C.; Brown, G.; Trowbridge, I. S.; Woolston, R. E.; Mason, D. Y. *J. Clin. Pathol.* **1983**, *36*, 539.
42. Kubal, G.; Mason, A. B.; Patel, S. U.; Sadler, P. J.; Woodworth, R. C. *Biochemistry* **1993**, *32*, 3387.
43. Levay, P. F.; Viljoen, M. *Haematologica* **1995**, *80*, 252.
44. Sanchez, L.; Calvo, M.; Brock, J. H. *Arch. Dis. Child.* **1992**, *67*, 657.
45. Bennett, R. M.; Kokocinski, T. *Br. J. Haematol.* **1978**, *39*, 509.



46. Masson, P. L.; Heremans, J. F.; Schonke, E. *J. Exp. Med.* **1969**, *130*, 643.
47. Theil, E. C. *Annu. Rev. Biochem.* **1987**, *56*, 289.
48. Chitambar, C. R.; Zivkovic, Z. *Cancer Res.* **1987**, *47*, 3929.
49. Feremans, W.; Bujan, W.; Neve, P.; Delville, J. P.; Schandene, L. *Am. J. Hematol.* **1991**, *36*, 215.
50. Tsuchiya, Y.; Nakao, A.; Komatsu, T.; Yamamoto, M.; Shimokata, K. *Chest* **1992**, *102*, 530.
51. Lentle, B. C.; Penney, H.; Ensslen, R. *Semin. Nucl. Med.* **1984**, *14*, 143.
52. Engelstad, B.; Luk, S. S.; Hattner, R. S. *Am. J. Roentgenol.* **1982**, *139*, 755.
53. Audi, G.; Bersillon, O.; Blachot, J.; Wapstra, A. H. *Nucl. Phys. A* **2003**, *729*, 3.
54. Firestone, R. B.; Chu, S. Y. F.; Baglin, C. M. *Table of isotopes*; New York: John Wiley & Sons, Inc., 1999.
55. Levaditi, C.; Bardet, J.; Tchakirian, A.; Vaisman, A. *C. R. Hebd. Seances Acad. Sci.* **1931**, *193*, 117.
56. Warrell, R. P.; Bockman, R. S. *Important Advances in Oncology*; Philadelphia: J.B. Lippincott, 1989.
57. Warrell, R. P.; Bockman, R. S.; Bosco, B.; Levine, B.; Lane, J. *Clin. Res.* **1989**, *37*, A463.
58. Warrell, R. P.; Alcock, N. W.; Bockman, R. S. *J. Clin. Oncol.* **1987**, *5*, 292.
59. Warrell, R. P. *Handbook of Metal-Ligand Interactions in Biological Fluids*; New York: Marcel Dekker, 1995.
60. Brucer, M.; Andrews, G. A.; Bruner, H. D. *Radiology* **1953**, *61*, 534.
61. Edwards, C. L.; Hayes, R. L. *J. Nucl. Med.* **1969**, *10*, 103.
62. Bruner, H. D.; Hayes, R. L.; Perkinson, J. D. *Radiology* **1953**, *61*, 602.
63. Anderson, C. J.; Welch, M. J. *Chem. Rev.* **1999**, *99*, 2219.
64. Fani, M.; Andre, J. P.; Maecke, H. R. *Contrast Media Mol. Imaging* **2008**, *3*, 53.
65. Rösch, F.; Knapp, R. In *Radiochemistry and Radiopharmaceutical Chemistry in Life Sciences*; Kluwer Academic Publishers: Dordrecht/Boston/London, 2003.
66. Greene, M. W.; Tucker, W. D. *International Journal of Applied Radiation and Isotopes* **1961**, *12*, 62.
67. Arino, H.; Skraba, W. J.; Kramer, H. H. *International Journal of Applied Radiation and Isotopes* **1978**, *29*, 117.
68. Kopecky, P.; Mudrova, B. *International Journal of Applied Radiation and Isotopes* **1974**, *25*, 263.

69. Neirinckx, R. D.; Davis, M. A. *J. Nucl. Med.* **1979**, *20*, 1075.
70. Loch, C.; Maziere, B.; Comar, D. *J. Nucl. Med.* **1980**, *21*, 171.
71. Bao, B.; Song, M. *J. Radioanal. Nucl. Chem.-Lett.* **1996**, *213*, 233.
72. Schuhmacher, J.; Maierborst, W. *International Journal of Applied Radiation and Isotopes* **1981**, *32*, 31.
73. Nakayama, M.; Haratake, M.; Koiso, T.; Ishibashi, O.; Harada, K.; Nakayama, H.; Sugii, A.; Yahara, S.; Arano, Y. *Anal. Chim. Acta* **2002**, *453*, 135.
74. O'Brien, P.; Salacinski, H.; Motevalli, M. *Journal of the American Chemical Society* **1997**, *119*, 12695.
75. Edwards, C. L.; Hayes, R. L.; Ahumada, J.; Kniseley, R. M. *J. Nucl. Med.* **1966**, *7*, 363.
76. Vanheerd, P. D.; Klopper, J. F.; Schoone, R.; Vakilita, A.; Baard, W. S. *Afr. Med. J.* **1973**, *47*, 2449.
77. Bailey, T. B.; Pinsky, S. M.; Mitemey.Bt; Borski, A. A.; Johnson, M. *J. Urol.* **1973**, *110*, 307.
78. Palumbo, R.; Tonato, M.; Martelli, M. F.; Corso, S.; Grignani, F. *Journal of Nuclear Biology and Medicine* **1973**, *17*, 100.
79. Motekaitis, R. J.; Sun, Y. Z.; Martell, A. E. *Inorg. Chim. Acta* **1989**, *159*, 29.
80. Wang, X. Y.; Jin, T. Z.; Comblin, V.; Lopezmut, A.; Merciny, E.; Desreux, J. F. *Inorg. Chem.* **1992**, *31*, 1095.
81. Kubicek, V.; Havlickova, J.; Kotek, J.; Gyula, T.; Hermann, P.; Toth, E.; Lukes, I. *Inorg. Chem.* **2010**, *49*, 10960.
82. Cotton, F. A.; G., W. *Advanced Inorganic Chemistry: A Comprehensive Text*; New York: John Wiley & Sons, 1988.
83. Aspinall, H. C. *Chemistry of the f-Block Elements*: CRC Press, 2001.
84. Aime, S.; Botta, M.; Fasano, M.; Terreno, E. *Chem. Soc. Rev.* **1998**, *27*, 19.
85. Caravan, P.; Ellison, J. J.; McMurry, T. J.; Lauffer, R. B. *Chem. Rev.* **1999**, *99*, 2293.
86. Toth, E.; Helm, L.; Merbach, A. E. *Contrast Agents I* **2002**, *221*, 61.
87. Chan, K. W. Y.; Wong, W. T. *Coord. Chem. Rev.* **2007**, *251*, 2428.
88. Accardo, A.; Tesauro, D.; Aloj, L.; Pedone, C.; Morelli, G. *Coord. Chem. Rev.* **2009**, *253*, 2193.
89. Caravan, P. *Accounts Chem. Res.* **2009**, *42*, 851.
90. Shibasaki, M.; Yoshikawa, N. *Chem. Rev.* **2002**, *102*, 2187.

91. Inanaga, J.; Furuno, H.; Hayano, T. *Chem. Rev.* **2002**, *102*, 2211.
92. Edelmann, F. T. In *Molecular Catalysis of Rare-Earth Elements*; Roesky, P. W., Ed.; Springer-Verlag Berlin: Berlin, 2010; Vol. 137, pp. 109.
93. Kido, J.; Okamoto, Y. *Chem. Rev.* **2002**, *102*, 2357.
94. Sessoli, R.; Powell, A. K. *Coord. Chem. Rev.* **2009**, *253*, 2328.
95. Huang, Y. G.; Jiang, F. L.; Hong, M. C. *Coord. Chem. Rev.* **2009**, *253*, 2814.
96. Carlos, L. D.; Ferreira, R. A. S.; Bermudez, V. D.; Julian-Lopez, B.; Escribano, P. *Chem. Soc. Rev.* **2011**, *40*, 536.
97. Yuan, J. L.; Wang, G. L. *Trac-Trends Anal. Chem.* **2006**, *25*, 490.
98. Vetrone, F.; Capobianco, J. A. *Int. J. Nanotechnol.* **2008**, *5*, 1306.
99. Montgomery, C. P.; Murray, B. S.; New, E. J.; Pal, R.; Parker, D. *Accounts Chem. Res.* **2009**, *42*, 925.
100. Hagan, A. K.; Zuchner, T. *Anal. Bioanal. Chem.* **2011**, *400*, 2847.
101. Choppin, G. R. *Journal of the Less-Common Metals* **1984**, *100*, 141.
102. Kowall, T.; Foglia, F.; Helm, L.; Merbach, A. E. *Journal of the American Chemical Society* **1995**, *117*, 3790.
103. Shannon, R. D.; Prewitt, C. T. *Acta Crystallographica Section B-Structural Crystallography and Crystal Chemistry* **1970**, *B 26*, 1046.
104. Williams, R. J. P. *Quarterly Reviews* **1970**, *24*, 331.
105. Darnall, D. W.; Birnbaum, E. R. *Biochemistry* **1973**, *12*, 3489.
106. Nayak, D.; Lahiri, S. *J. Radioanal. Nucl. Chem.* **1999**, *242*, 423.
107. Cutler, C. S.; Smith, C. J.; Ehrhardt, G. J.; Tyler, T. T.; Jurisson, S. S.; Deutsch, E. *Cancer Biother. Radiopharm.* **2000**, *15*, 531.
108. Anderson, P. *Expert Opin. Pharmacother.* **2006**, *7*, 1475.
109. Stimmel, J. B.; Kull, F. C. *Nuclear Medicine and Biology* **1998**, *25*, 117.
110. Dejong, M.; Breeman, W. A. P.; Bernard, B. F.; Rolleman, E. J.; Hofland, L. J.; Visser, T. J.; Setyonohan, B.; Bakker, W. H.; Vanderpluijm, M. E.; Krenning, E. P. *Eur. J. Nucl. Med.* **1995**, *22*, 608.
111. Komyei, J.; Szentesi, M.; Foldes, I.; Antalffy, M.; Torko, J. *Eur. J. Nucl. Med.* **2000**, *27*, S96.
112. Vuorela, J.; Kauppinen, T.; Sokka, T. *Cancer Biother. Radiopharm.* **2005**, *20*, 333.
113. Hong, Y. D.; Park, K. B.; Jang, B. S.; Choi, S. J.; Choi, S. M.; Kim, Y. M. *Nuclear Medicine and Biology* **2002**, *29*, 833.

114. Breitz, H. B.; Wendt, R. E.; Stabin, M. S.; Shen, S.; Erwin, W. D.; Rajendran, J. G.; Eary, J. F.; Durack, L.; Delpassand, E.; Martin, W.; Meredith, R. F. *J. Nucl. Med.* **2006**, *47*, 534.
115. Gobel, D.; Gratz, S.; vonRothkirch, T.; Becker, W. *Z. Rheumatol.* **1997**, *56*, 207.
116. Meredith, R. F.; Partridge, E. E.; Alvarez, R. D.; Khazaeli, M. B.; Plott, G.; Russell, C. D.; Wheeler, R. H.; Liu, T. P.; Grizzle, W. E.; Schlom, J.; LoBuglio, A. F. *J. Nucl. Med.* **1996**, *37*, 1491.
117. Hemmila, I.; Laitala, V. *J. Fluoresc.* **2005**, *15*, 529.
118. Binnemans, K. *Chem. Rev.* **2009**, *109*, 4283.
119. Sabbatini, N.; Guardigli, M.; Lehn, J. M. *Coord. Chem. Rev.* **1993**, *123*, 201.
120. Richardson, F. S. *Chem. Rev.* **1982**, *82*, 541.
121. Cotton, S. *Lanthanide and Actinide Chemistry*; Chichester: John Wiley & Sons, Inc, 2006.
122. Peters, J. A.; Huskens, J.; Raber, D. J. *Prog. Nucl. Magn. Reson. Spectrosc.* **1996**, *28*, 283.
123. Sinha, S. P. *Systematics and the Properties of the Lanthanides*; Dordrecht: Reidel, 1983.
124. La Mar, G. N.; Horrocks, W. D.; Holm, R. H. *NMR of paramagnetic molecules; principles and applications*; New York: Academic Press, 1973.
125. Keevil, S. F. *Physics Education* **2001**, *36*, 476.
126. Gil, V. M. S.; Geraldes, C. F. G. C. *Ressonância Magnética Nuclear: Fundamentos, Métodos e Aplicações*; Lisboa: Fundação Calouste Gulbenkian, 1987.
127. Birn, R. M.; Donahue, K. M.; Bandentinni, P. A. In *Biomedical Uses of Radiation*; John Wiley and Sons: New York, 1999; Vol. 1.
128. Lauffer, R. B. *Chem. Rev.* **1987**, *87*, 901.
129. Botta, M. *Eur. J. Inorg. Chem.* **2000**, 399.
130. Aime, S.; Caravan, P. *J. Magn. Reson. Imaging* **2009**, *30*, 1259.
131. Horrocks, W. D.; Sudnick, D. R. *Journal of the American Chemical Society* **1979**, *101*, 334.
132. Alpoim, M. C.; Urbano, A. M.; Geraldes, C.; Peters, J. A. *J. Chem. Soc.-Dalton Trans.* **1992**, 463.
133. Toth, E.; Ni Dhubhghaill, O. M.; Besson, G.; Helm, L.; Merbach, A. E. *Magn. Reson. Chem.* **1999**, *37*, 701.

134. Yerly, F.; Dunand, F. A.; Toth, E.; Figueirinha, A.; Kovacs, Z.; Sherry, A. D.; Geraldes, C.; Merbach, A. E. *Eur. J. Inorg. Chem.* **2000**, 1001.
135. Helm, L.; Merbach, A. E. *Eur. J. Solid State Inorg. Chem.* **1991**, 28, 245.
136. Cossy, C.; Helm, L.; Powell, D. H.; Merbach, A. E. *New J. Chem.* **1995**, 19, 27.
137. Clarkson, R. B.; Hwang, J. H.; Belford, R. L. *Magn. Reson. Med.* **1993**, 29, 521.
138. Benazeth, S.; Purans, J.; Chalbot, M. C.; Nguyen-van-Duong, M. K.; Nicolas, L.; Keller, F.; Gaudemer, A. *Inorg. Chem.* **1998**, 37, 3667.
139. Steele, M. L.; Wertz, D. L. *Journal of the American Chemical Society* **1976**, 98, 4424.
140. Aime, S.; Barge, A.; Botta, M.; Parker, D.; DeSousa, A. S. *Journal of the American Chemical Society* **1997**, 119, 4767.
141. Aime, S.; Botta, M.; Fasano, M.; Paoletti, S.; Terreno, E. *Chem.-Eur. J.* **1997**, 3, 1499.
142. Micskei, K.; Helm, L.; Brucher, E.; Merbach, A. E. *Inorg. Chem.* **1993**, 32, 3844.
143. Powell, D. H.; NiDhubghaill, O. M.; Pubanz, D.; Helm, L.; Lebedev, Y. S.; Schlaepfer, W.; Merbach, A. E. *Journal of the American Chemical Society* **1996**, 118, 9333.
144. Toth, E.; Vauthey, S.; Pubanz, D.; Merbach, A. E. *Inorg. Chem.* **1996**, 35, 3375.
145. Aime, S.; Botta, M.; Crich, S. G.; Giovenzana, G. B.; Pagliarin, R.; Piccinini, M.; Sisti, M.; Terreno, E. *J. Biol. Inorg. Chem.* **1997**, 2, 470.
146. Aime, S.; Chiaussa, M.; Digilio, G.; Gianolio, E.; Terreno, E. *J. Biol. Inorg. Chem.* **1999**, 4, 766.
147. Andre, J. P.; Maecke, H. R.; Toth, E.; Merbach, A. A. *J. Biol. Inorg. Chem.* **1999**, 4, 341.
148. Ferreira, M. F.; Martins, A. F.; Martins, J. A.; Ferreira, P. M.; Toth, E.; Geraldes, C. F. G. C. *Chem. Commun.* **2009**, 6475.
149. Laus, S.; Ruloff, R.; Toth, E.; Merbach, A. E. *Chem.-Eur. J.* **2003**, 9, 3555.
150. Caravan, P. *Chem. Soc. Rev.* **2006**, 35, 512.
151. Vexler, V. S.; Clement, O.; Schmittwillich, H.; Brasch, R. C. *JMRI-J. Magn. Reson. Imaging* **1994**, 4, 381.
152. Desser, T. S.; Rubin, D. L.; Muller, H. H.; Qing, F.; Khodor, S.; Zanazzi, G.; Young, S. W.; Ladd, D. L.; Wellons, J. A.; Kellar, K. E.; Toner, J. L.; Snow, R. A. *JMRI-J. Magn. Reson. Imaging* **1994**, 4, 467.

153. Lipari, G.; Szabo, A. *Journal of the American Chemical Society* **1982**, *104*, 4546.
154. Lipari, G.; Szabo, A. *Journal of the American Chemical Society* **1982**, *104*, 4559.
155. Aime, S.; Botta, M.; Terreno, E.; Anelli, P. L.; Uggeri, F. *Magn.Reson.Med.* **1993**, *30*, 583.
156. Albrand, J. P.; Taieb, M. C.; Fries, P. H.; Belorizky, E. *J. Chem. Phys.* **1983**, *78*, 5809.
157. Hwang, L. P.; Freed, J. H. *J. Chem. Phys.* **1975**, *63*, 4017.
158. Freed, J. H. *J. Chem. Phys.* **1978**, *68*, 4034.
159. Geraldes, C. F. G. C.; Sherry, A. D.; Cacheris, W. P.; Kuan, K. T.; Brown, R. D.; Koenig, S. H.; Spiller, M. *Magn.Reson.Med.* **1988**, *8*, 191.
160. Geraldes, C. F. G. C.; Urbano, A. M.; Alpoim, M. C.; Sherry, A. D.; Kuan, K. T.; Rajagopalan, R.; Maton, F.; Muller, R. N. *Magn. Reson. Imaging* **1995**, *13*, 401.
161. Melson, G. A. *Coordination Chemistry of Macrocyclic Compounds*; New York: Plenum Press, 1979.
162. Cabiness, D. K.; Margerum, D. W. *Journal of the American Chemical Society* **1969**, *91*, 6540.
163. Hancock, R. D. *J. Chem. Educ.* **1992**, *69*, 615.
164. Zeglis, B. M.; Lewis, J. S. *Dalton Trans.* **2011**, *40*, 6168.
165. Drahos, B.; Lukes, I.; Toth, E. *Eur. J. Inorg. Chem.* **2012**, 1975.
166. Kumar, S. *Chem. Soc. Rev.* **2006**, *35*, 83.
167. Park, J. K.; Lee, H. R.; Chen, J. P.; Shinokubo, H.; Osuka, A.; Kim, D. *J. Phys. Chem. C* **2008**, *112*, 16691.
168. Yordanov, A. T.; Roundhill, D. M. *Coord. Chem. Rev.* **1998**, *170*, 93.
169. Cacheris, W. P.; Nickle, S. K.; Sherry, A. D. *Inorg. Chem.* **1987**, *26*, 958.
170. Clarke, E. T.; Martell, A. E. *Inorg. Chim. Acta* **1991**, *190*, 37.
171. Clarke, E. T.; Martell, A. E. *Inorg. Chim. Acta* **1991**, *190*, 27.
172. Chang, C. A.; Francesconi, L. C.; Malley, M. F.; Kumar, K.; Gougoutas, J. Z.; Tweedle, M. F.; Lee, D. W.; Wilson, L. J. *Inorg. Chem.* **1993**, *32*, 3501.
173. Benetollo, F.; Bombieri, G.; Calabi, L.; Aime, S.; Botta, M. *Inorg. Chem.* **2003**, *42*, 148.
174. Viola, N. A.; Rarig, R. S.; Ouellette, W.; Doyle, R. P. *Polyhedron* **2006**, *25*, 3457.

175. Chaves, S.; Delgado, R.; Dasilva, J. J. R. F. *Talanta* **1992**, *39*, 249.
176. Volkert, W. A.; Hoffman, T. J. *Chem. Rev.* **1999**, *99*, 2269.
177. Liu, S.; Edwards, D. S. *Contrast Agents Ii* **2002**, *222*, 259.
178. Liu, S. *Chem. Soc. Rev.* **2004**, *33*, 445.
179. Liu, S.; Edwards, D. S. *Chem. Rev.* **1999**, *99*, 2235.
180. Li, L.; Yazaki, P. J.; Anderson, A. L.; Crow, D.; Colcher, D.; Wu, A. M.; Williams, L. E.; Wong, J. Y. C.; Raubitschek, A.; Shively, J. E. *Bioconjugate Chem.* **2006**, *17*, 68.
181. Dijkgraaf, I.; Liu, S. A.; Kruijtzter, J. A. W.; Soede, A. C.; Oyen, W. J. G.; Liskamp, R. M. J.; Corstens, F. H. M.; Boerman, O. C. *Nuclear Medicine and Biology* **2007**, *34*, 29.
182. Parry, J. J.; Kelly, T. S.; Andrews, R.; Rogers, B. E. *Bioconjugate Chem.* **2007**, *18*, 1110.
183. Basu, A.; Yang, K.; Wang, M. L.; Liu, S.; Chintala, R.; Palm, T.; Zhao, H.; Peng, P.; Wu, D. C.; Zhang, Z. F.; Hua, J.; Hsieh, M. C.; Zhou, J.; Petti, G.; Li, X. G.; Janjua, A.; Mendez, M.; Liu, J.; Longley, C.; Zhang, Z.; Mehlig, M.; Borowski, V.; Viswanathan, M.; Filpula, D. *Bioconjugate Chem.* **2006**, *17*, 618.
184. Rajan, R. S.; Li, T. S.; Aras, M.; Sloey, C.; Sutherland, W.; Arai, H.; Briddell, R.; Kinstler, O.; Lueras, A. M. K.; Zhang, Y.; Yeghnazar, H.; Treuheit, M.; Brems, D. N. *Protein Sci.* **2006**, *15*, 1063.
185. Shi, J. Y.; Kim, Y. S.; Zhai, S. Z.; Liu, Z. F.; Chen, X. Y.; Liu, S. *Bioconjugate Chem.* **2009**, *20*, 750.
186. Shi, J. Y.; Wang, L. J.; Kim, Y. S.; Zhai, S. Z.; Liu, Z. F.; Chen, X. Y.; Liu, S. *J. Med. Chem.* **2008**, *51*, 7980.
187. Wang, L. J.; Shi, J. Y.; Kim, Y. S.; Zhai, S. Z.; Jia, B.; Zhao, H. Y.; Liu, Z. F.; Wang, F.; Chen, X. Y.; Liu, S. *Mol. Pharm.* **2009**, *6*, 231.
188. Lewis, M. R.; Shively, J. E. *Bioconjugate Chem.* **1998**, *9*, 72.
189. McMurry, T. J.; Brechbiel, M.; Kumar, K.; Gansow, O. A. *Bioconjugate Chem.* **1992**, *3*, 108.
190. Renn, O.; Meares, C. F. *Bioconjugate Chem.* **1992**, *3*, 563.
191. Cooper, M. S.; Sabbah, E.; Mather, S. J. *Nat. Protoc.* **2006**, *1*, 314.
192. Grunberg, J.; Novak-Hofer, I.; Honer, M.; Zimmermann, K.; Knogler, K.; Blauenstein, P.; Ametamey, S.; Maecke, H. R.; Schubiger, P. A. *Clin. Cancer Res.* **2005**, *11*, 5112.

193. Mohsin, H.; Fitzsimmons, J.; Shelton, T.; Hoffman, T. J.; Cutler, C. S.; Lewis, M. R.; Atheye, P. S.; Gulyas, G.; Kiefer, G. E.; Frank, R. K.; Simon, J.; Lever, S. Z.; Jurisson, S. S. *Nuclear Medicine and Biology* **2007**, *34*, 493.
194. Chappell, L. L.; Rogers, B. E.; Khazaeli, M. B.; Mayo, M. S.; Buchsbaum, D. J.; Brechbiel, M. W. *Bioorg. Med. Chem.* **1999**, *7*, 2313.
195. Chappell, L. L.; Ma, D.; Milenic, D. E.; Garmestani, K.; Venditto, V.; Beitzel, M. P.; Brechbiel, M. W. *Nuclear Medicine and Biology* **2003**, *30*, 581.
196. Eisenwiener, K. P.; Powell, P.; Macke, H. R. *Bioorg. Med. Chem. Lett.* **2000**, *10*, 2133.
197. Yoo, B.; Pagel, M. D. *Tetrahedron Lett.* **2006**, *47*, 7327.
198. Yoo, B.; Pagel, M. D. *Bioconjugate Chem.* **2007**, *18*, 903.
199. Knor, S.; Modlinger, A.; Poethko, T.; Schottelius, M.; Wester, H. J.; Kessler, H. *Chem.-Eur. J.* **2007**, *13*, 6082.
200. Liu, S. *Mol. Pharm.* **2006**, *3*, 472.
201. Beer, A. J.; Schwaiger, M. *Cancer Metastasis Rev.* **2008**, *27*, 631.
202. Ruoslahti, E. *Annu. Rev. Cell Dev. Biol.* **1996**, *12*, 697.
203. Hood, J. D.; Cheresch, D. A. *Nat. Rev. Cancer* **2002**, *2*, 91.
204. Folkman, J.; Klagsbrun, M. *Science* **1987**, *235*, 442.
205. Risau, W. *Nature* **1997**, *386*, 671.
206. Hynes, R. O. *Nat. Med.* **2002**, *8*, 918.
207. Schottelius, M.; Laufer, B.; Kessler, H.; Wester, H. J. *Accounts Chem. Res.* **2009**, *42*, 969.
208. Cai, W.; Chen, X. *Anti-cancer agents in medicinal chemistry* **2006**, *6*, 407.
209. Hynes, R. O. *Cell* **2002**, *110*, 673.
210. Humphries, M. J.; McEwan, P. A.; Barton, S. J.; Buckley, P. A.; Bella, J.; Mould, A. P. *Trends Biochem.Sci.* **2003**, *28*, 313.
211. Xiong, J. P.; Stehle, T.; Diefenbach, B.; Zhang, R. G.; Dunker, R.; Scott, D. L.; Joachimiak, A.; Goodman, S. L.; Arnaout, M. A. *Science* **2001**, *294*, 339.
212. Craig, W. S.; Cheng, S.; Mullen, D. G.; Blevitt, J.; Pierschbacher, M. D. *Biopolymers* **1995**, *37*, 157.
213. Gurrath, M.; Muller, G.; Kessler, H.; Aumailley, M.; Timpl, R. *Eur. J. Biochem.* **1992**, *210*, 911.
214. Dechantsreiter, M. A.; Planker, E.; Matha, B.; Lohof, E.; Holzemann, G.; Jonczyk, A.; Goodman, S. L.; Kessler, H. *J. Med. Chem.* **1999**, *42*, 3033.



215. Haubner, R.; Wester, H. J.; Reuning, U.; Senekowitsch-Schmidtke, R.; Diefenbach, B.; Kessler, H.; Stocklin, G.; Schwaiger, M. *J. Nucl. Med.* **1999**, *40*, 1061.
216. Haubner, R.; Gratiyas, R.; Diefenbach, B.; Goodman, S. L.; Jonczyk, A.; Kessler, H. *Journal of the American Chemical Society* **1996**, *118*, 7461.
217. Haubner, R.; Wester, H. J.; Burkhart, F.; Senekowitsch-Schmidtke, R.; Weber, W.; Goodman, S. L.; Kessler, H.; Schwaiger, M. *J. Nucl. Med.* **2001**, *42*, 326.
218. Haubner, R.; Wester, H. J.; Weber, W. A.; Mang, C.; Ziegler, S. I.; Goodman, S. L.; Senekowitsch-Schmidtke, R.; Kessler, H.; Schwaiger, M. *Cancer Res.* **2001**, *61*, 1781.
219. Chen, X. Y.; Hou, Y. P.; Tohme, M.; Park, R.; Khankaldyyan, V.; Gonzales-Gomez, I.; Bading, J. R.; Laug, W. E.; Conti, P. S. *J. Nucl. Med.* **2004**, *45*, 1776.
220. Thumshirn, G.; Hersel, U.; Goodman, S. L.; Kessler, H. *Chem.-Eur. J.* **2003**, *9*, 2717.
221. Sancey, L.; Ardisson, V.; Riou, L. M.; Ahmadi, M.; Marti-Batlle, D.; Boturyn, D.; Dumy, P.; Fagret, D.; Ghezzi, C.; Vuillez, J. P. *Eur. J. Nucl. Med. Mol. Imaging* **2007**, *34*, 2037.
222. Shi, J. Y.; Zhou, Y.; Chakraborty, S.; Kim, Y. S.; Jia, B.; Wang, F.; Liu, S. *Theranostics* **2011**, *1*, 322.
223. Cai, H.; Conti, P. S. *Journal of Labelled Compounds and Radiopharmaceuticals* **2013**, *56*, 264.
224. Decristoforo, C.; Gonzalez, I. H.; Carlsen, J.; Rupprich, M.; Huisman, M.; Virgolini, I.; Wester, H. J.; Haubner, R. *Eur. J. Nucl. Med. Mol. Imaging* **2008**, *35*, 1507.
225. Tanaka, K.; Fukase, K. *Org. Biomol. Chem.* **2008**, *6*, 815.
226. Chen, X. Y.; Park, R.; Tohme, M.; Shahinian, A. H.; Bading, J. R.; Conti, P. S. *Bioconjugate Chem.* **2004**, *15*, 41.
227. Harris, J. M.; Martin, N. E.; Modi, M. *Clin. Pharmacokinet.* **2001**, *40*, 539.
228. Chen, X. Y.; Park, R.; Shahinian, A. H.; Bading, J. R.; Conti, P. S. *Nuclear Medicine and Biology* **2004**, *31*, 11.
229. Chen, X. Y.; Liu, S.; Hou, Y. P.; Tohme, M.; Park, R.; Bading, J. R.; Conti, P. S. *Mol. Imaging. Biol.* **2004**, *6*, 350.
230. Liu, S. *Bioconjugate Chem.* **2009**, *20*, 2199.
231. Chen, X. Y.; Sievers, E.; Hou, Y. P.; Park, R.; Tohme, M.; Bart, R.; Bremner, R.; Bading, J. R.; Conti, P. S. *Neoplasia* **2005**, *7*, 271.

232. Boturnyn, D.; Coll, J. L.; Garanger, E.; Favrot, M. C.; Dumy, P. *Journal of the American Chemical Society* **2004**, *126*, 5730.
233. Wu, Y.; Zhang, X. Z.; Xiong, Z. M.; Cheng, Z.; Fisher, D. R.; Liu, S.; Gambhir, S. S.; Chen, X. Y. *J. Nucl. Med.* **2005**, *46*, 1707.
234. Mammen, M.; Choi, S. K.; Whitesides, G. M. *Angew. Chem.-Int. Edit.* **1998**, *37*, 2755.
235. Liu, Y. J.; Welch, M. J. *Bioconjugate Chem.* **2012**, *23*, 671.
236. Coyne, K.; Magnet Lab: Los Alamos.
237. Wehrli, F. W.; Macfall, J. R.; Shutts, D.; Breger, R.; Herfkens, R. J. *J. Comput. Assist. Tomogr.* **1984**, *8*, 369.
238. El Saghir, N. S.; Elhajj, II; Geara, F. B.; Hourani, M. H. *BMC Cancer* **2005**, *5*.
239. Brasch, R. C. *Radiology* **1992**, *183*, 1.
240. Weisman, G. R.; Reed, D. P. *J. Org. Chem.* **1996**, *61*, 5186.
241. Herve, G.; Bernard, H.; Le Bris, N.; Yaouanc, J. J.; Handel, H.; Toupet, L. *Tetrahedron Lett.* **1998**, *39*, 6861.
242. Geraldese, C. F. G. C.; Laurent, S. *Contrast Media Mol. Imaging* **2009**, *4*, 1.
243. Vanwagoner, M.; Worah, D. *Invest. Radiol.* **1993**, *28*, S44.
244. Oksendal, A. N.; Hals, P. A. *JMRI-J. Magn. Reson. Imaging* **1993**, *3*, 157.
245. Hermann, P.; Kotek, J.; Kubicek, V.; Lukes, I. *Dalton Trans.* **2008**, 3027.
246. Siriwardena-Mahanama, B. N.; Allen, M. J. *Molecules* **2013**, *18*, 9352.
247. Li, W.-h.; Parigi, G.; Fragai, M.; Luchinat, C.; Meade, T. J. *Inorg. Chem.* **2002**, *41*, 4018.
248. Jebasingh, B.; Alexander, V. *Inorg. Chem.* **2005**, *44*, 9434.
249. Rudovsky, J.; Botta, M.; Hermann, P.; Koridze, A.; Aime, S. *Dalton Trans.* **2006**, 2323.
250. Song, Y.; Kohlmeir, E. K.; Meade, T. J. *Journal of the American Chemical Society* **2008**, *130*, 6662.
251. Mastarone, D. J.; Harrison, V. S. R.; Eckermann, A. L.; Parigi, G.; Luchinat, C.; Meade, T. J. *Journal of the American Chemical Society* **2011**, *133*, 5329.
252. Tanwar, J.; Datta, A.; Tiwari, A. K.; Chaturvedi, S.; Ojha, H.; Allard, M.; Chaudary, N. K.; Thirumal, M.; Mishra, A. K. *Dalton Trans.* **2011**, *40*, 3346.
253. Toth, E.; van Uffelen, I.; Helm, L.; Merbach, A. E.; Ladd, D.; Briley-Saebo, K.; Kellar, K. E. *Magn. Reson. Chem.* **1998**, *36*, S125.

254. Zarabi, B.; Nan, A.; Zhuo, J.; Gullapalli, R.; Ghandehari, H. *Mol. Pharm.* **2006**, *3*, 550.
255. Lee, H. Y.; Jee, H. W.; Seo, S. M.; Kwak, B. K.; Khang, G.; Cho, S. H. *Bioconjugate Chem.* **2006**, *17*, 700.
256. Venditto, V. J.; Regino, C. A. S.; Brechbiel, M. W. *Mol. Pharm.* **2005**, *2*, 302.
257. Kobayashi, H.; Brechbiel, M. W. *Adv. Drug Deliv. Rev.* **2005**, *57*, 2271.
258. Langereis, S.; Dirksen, A.; Hackeng, T. M.; van Genderen, M. H. P.; Meijer, E. W. *New J. Chem.* **2007**, *31*, 1152.
259. Andre, J. P.; Toth, E.; Fischer, H.; Seelig, A.; Macke, H. R.; Merbach, A. E. *Chem.-Eur. J.* **1999**, *5*, 2977.
260. Nicolle, G. M.; Toth, E.; Eisenwiener, K. P.; Macke, H. R.; Merbach, A. E. *J. Biol. Inorg. Chem.* **2002**, *7*, 757.
261. Mulder, W. J. M.; Strijkers, G. J.; van Tilborg, G. A. F.; Griffioen, A. W.; Nicolay, K. *NMR Biomed.* **2006**, *19*, 142.
262. Fontes, A.; Prata, M. I. M.; Geraldes, C. F. G. C.; Andre, J. P. *Nuclear Medicine and Biology* **2011**, *38*, 363.
263. Aime, S.; Castelli, D. D.; Lawson, D.; Terreno, E. *Journal of the American Chemical Society* **2007**, *129*, 2430.
264. Kamaly, N.; Kalber, T.; Ahmad, A.; Oliver, M. H.; So, P. W.; Herlihy, A. H.; Bell, J. D.; Jorgensen, M. R.; Miller, A. D. *Bioconjugate Chem.* **2008**, *19*, 118.
265. Laurent, S.; Elst, L. V.; Thirifays, C.; Muller, R. N. *Eur. Biophys. J. Biophys. Lett.* **2008**, *37*, 1007.
266. Livramento, J. B.; Sour, A.; Borel, A.; Merbach, A. E.; Tóth, E. *Chemistry – A European Journal* **2006**, *12*, 989.
267. Ranganathan, R. S.; Fernandez, M. E.; Kang, S. I.; Nunn, A. D.; Ratsep, P. C.; Pillai, K. M. R.; Zhang, X.; Tweedle, M. F. *Invest. Radiol.* **1998**, *33*, 779.
268. Dong, Q.; Hurst, D. R.; Weinmann, H. J.; Chenevert, T. L.; Lundy, F. J.; Prince, M. R. *Invest. Radiol.* **1998**, *33*, 699.
269. Martin, V. V.; Ralston, W. H.; Hynes, M. R.; Keana, J. F. W. *Bioconjugate Chem.* **1995**, *6*, 616.
270. Boros, E.; Polasek, M.; Zhang, Z. D.; Caravan, P. *Journal of the American Chemical Society* **2012**, *134*, 19858.
271. Aime, S.; Anelli, P. L.; Botta, M.; Fedeli, F.; Grandi, M.; Paoli, P.; Uggeri, F. *Inorg. Chem.* **1992**, *31*, 2422.

272. Pope, S. J. A.; Kenwright, A. M.; Boote, V. A.; Faulkner, S. *Dalton Trans.* **2003**, 3780.
273. Hill, L. R.; Sorensen, T. J.; Blackburn, O. A.; Brown, A.; Beer, P. D.; Faulkner, S. *Dalton Trans.* **2013**, 42, 67.
274. Carmeliet, P. *Nat. Med.* **2003**, 9, 653.
275. Jacques, V.; Desreux, J. F. In *Contrast Agents I: Magnetic Resonance Imaging*; Krause, W., Ed.; Springer-Verlag Berlin: Berlin, 2002; Vol. 221, pp. 123.
276. Knopp, M. V.; von Tengg-Kobligk, H.; Floemer, F.; Schoenberg, S. O. *JMRI-J. Magn. Reson. Imaging* **1999**, 10, 314.
277. Aime, S.; Botta, M.; Fasano, M.; Crich, S. G.; Terreno, E. *J. Biol. Inorg. Chem.* **1996**, 1, 312.
278. Weissleder, R.; Elizondo, G.; Wittenberg, J.; Rabito, C. A.; Bengele, H. H.; Josephson, L. *Radiology* **1990**, 175, 489.
279. Mornet, S.; Vasseur, S.; Grasset, F.; Duguet, E. *J. Mater. Chem.* **2004**, 14, 2161.
280. Misselwitz, B.; Platzek, J.; Raduchel, B.; Oellinger, J. J.; Weinmann, H. J. *Magn. Reson. Mat. Phys. Biol. Med.* **1999**, 8, 190.
281. Poduslo, J. F.; Wengenack, T. M.; Curran, G. L.; Wisniewski, T.; Sigurdsson, E. M.; Macura, S. I.; Borowski, B. J.; Jack, C. R. *Neurobiol. Dis.* **2002**, 11, 315.
282. Wadghiri, Y. Z.; Sigurdsson, E. M.; Sadowski, M.; Elliott, J. I.; Li, Y. S.; Scholtzova, H.; Tang, C. Y.; Aguinaldo, G.; Pappolla, M.; Duff, K.; Wisniewski, T.; Turnbull, D. H. *Magn. Reson. Med.* **2003**, 50, 293.
283. Sipkins, D. A.; Cheresch, D. A.; Kazemi, M. R.; Nevin, L. M.; Bednarski, M. D.; Li, K. C. P. *Nat. Med.* **1998**, 4, 623.
284. Brownell, G. L.; Sweet, W. H. *Nucleonics* **1953**, 11, 40.
285. Semmler, W.; Schwaiger, M. *Molecular Imaging I*; Berlin: Springer, 2008.
286. <http://www.drugs.com/cg/positron-emission-tomography-scan-inpatient-care.html>. Drugs.com - Drug Information Online, 2013.
287. Liu, S. *Adv. Drug Deliv. Rev.* **2008**, 60, 1347.
288. Ferreira, P. M. T.; Monteiro, L. S.; Pereira, G.; Ribeiro, L.; Sacramento, J.; Silva, L. *Eur. J. Org. Chem.* **2007**, 5934.
289. Helm, L. *Prog. Nucl. Magn. Reson. Spectrosc.* **2006**, 49, 45.
290. Kowalewski, J.; Kruk, D.; Parigi, G. *Advances in Inorganic Chemistry - Including Bioinorganic Studies, Vol 57* **2005**, 57, 41.

291. Dunand, F. A.; Toth, E.; Hollister, R.; Merbach, A. E. *J. Biol. Inorg. Chem.* **2001**, *6*, 247.
292. Jaccard, H.; Mieville, P.; Cannizzo, C.; Mayer, C. R.; Helm, L. *J. Biol. Inorg. Chem.* **2014**, *19*, 145.
293. Toth, E.; Helm, L.; Merbach, A. A. In *The Chemistry of Contrast Agents in Medical Magnetic Resonance Imaging*; John Wiley & Sons: Chichester, 2013, pp. 25.
294. Adams, E. T.; Lewis, M. S. *Biochemistry* **1968**, *7*, 1044.
295. Tso, P. O. P.; Melvin, I. S.; Olson, A. C. *Journal of the American Chemical Society* **1963**, *85*, 1289.
296. Costa, J.; Balogh, E.; Turcry, V.; Tripier, R.; Le Baccon, M.; Chuburu, F.; Handel, H.; Helm, L.; Tóth, E.; Merbach, A. E. *Chemistry – A European Journal* **2006**, *12*, 6841.
297. Regueiro-Figueroa, M.; Nonat, A.; Rolla, G. A.; Esteban-Gómez, D.; de Blas, A.; Rodríguez-Blas, T.; Charbonnière, L. J.; Botta, M.; Platas-Iglesias, C. *Chemistry – A European Journal* **2013**, *19*, 11696.
298. Laurent, S.; Elst, L. V.; Muller, R. N. *Contrast Media Mol. Imaging* **2006**, *1*, 128.
299. Doble, D. M. J.; Botta, M.; Wang, J.; Aime, S.; Barge, A.; Raymond, K. N. *Journal of the American Chemical Society* **2001**, *123*, 10758.
300. Thompson, M. K.; Doble, D. M. J.; Tso, L. S.; Barra, S.; Botta, M.; Aime, S.; Raymond, K. N. *Inorg. Chem.* **2004**, *43*, 8577.
301. Derkaoui, N.; Said, S.; Grohens, Y.; Olier, R.; Privat, M. *J. Colloid Interface Sci.* **2007**, *305*, 330.
302. Azri, A.; Giamarchi, P.; Grohens, Y.; Olier, R.; Privat, M. *J. Colloid Interface Sci.* **2012**, *379*, 14.
303. Milov, A. D.; Ponomarev, A. B.; Tsvetkov, Y. D. *Chem. Phys. Lett.* **1984**, *110*, 67.
304. Pannier, M.; Veit, S.; Godt, A.; Jeschke, G.; Spiess, H. W. *J. Magn. Reson.* **2000**, *142*, 331.
305. Jeschke, G.; Polyhach, Y. *Phys. Chem. Chem. Phys.* **2007**, *9*, 1895.
306. Schiemann, O.; Prisner, T. F. *Q. Rev. Biophys.* **2007**, *40*, 1.
307. Farrens, D. L.; Altenbach, C.; Yang, K.; Hubbell, W. L.; Khorana, H. G. *Science* **1996**, *274*, 768.

308. Raitsimring, A. M.; Gunanathan, C.; Potapov, A.; Efremenko, I.; Martin, J. M. L.; Milstein, D.; Goldfarb, D. *Journal of the American Chemical Society* **2007**, *129*, 14138.
309. Lueders, P.; Jeschke, G.; Yulikov, M. *J. Phys. Chem. Lett.* **2011**, *2*, 604.
310. Goldfarb, D. *Phys. Chem. Chem. Phys.* **2014**, *16*, 9685.
311. Yulikov, M. In *Electron Paramagnetic Resonance: Volume 24*; The Royal Society of Chemistry, 2015; Vol. 24, pp. 1.
312. Jeschke, G. In *Structural Information from Spin-Labels and Intrinsic Paramagnetic Centres in the Biosciences*; Timmel, C. R., Harmer, J. R., Eds.; Springer Berlin Heidelberg, 2013; Vol. 152, pp. 83.
313. Jeschke, G.; Chechik, V.; Ionita, P.; Godt, A.; Zimmermann, H.; Banham, J.; Timmel, C. R.; Hilger, D.; Jung, H. *Appl. Magn. Reson.* **2006**, *30*, 473.
314. Potapov, A.; Song, Y.; Meade, T. J.; Goldfarb, D.; Astashkin, A. V.; Raitsimring, A. *J. Magn. Reson.* **2010**, *205*, 38.
315. Peters, J. A.; Zitha-Bovens, E.; Corsi, E.; Geraldes, C. F. G. C. In *The Chemistry of Contrast Agents in Medical Magnetic Resonance Imaging*; Toth, E., Merbach, A. E., Eds.; Wiley: Chichester, 2001.
316. Frullano, L.; Rohovec, J.; Peters, J. A.; Geraldes, C. In *Contrast Agents I: Magnetic Resonance Imaging*; Krause, W., Ed.; Springer-Verlag Berlin: Berlin, 2002; Vol. 221, pp. 25.
317. Aime, S.; Botta, M.; Fasano, M.; Marques, M. P. M.; Geraldes, C. F. G. C.; Pubanz, D.; Merbach, A. E. *Inorg. Chem.* **1997**, *36*, 2059.
318. Aime, S.; Botta, M.; Garino, E.; Crich, S. G.; Giovenzana, G.; Pagliarin, R.; Palmisano, G.; Sisti, M. *Chem.-Eur. J.* **2000**, *6*, 2609.
319. Desreux, J. F. *Inorg. Chem.* **1980**, *19*, 1319.
320. Aime, S.; Botta, M.; Ermondi, G. *Inorg. Chem.* **1992**, *31*, 4291.
321. Jacques, V.; Desreux, J. F. *Inorg. Chem.* **1994**, *33*, 4048.
322. Marques, M. P. M.; Geraldes, C. F. G. C.; Sherry, A. D.; Merbach, A. E.; Powell, H.; Pubanz, D.; Aime, S.; Botta, M. *J. Alloy. Compd.* **1995**, *225*, 303.
323. Andre, J. P.; Brucher, E.; Kiraly, R.; Carvalho, R. A.; Macke, H.; Geraldes, C. *Helvetica Chimica Acta* **2005**, *88*, 633.
324. Howard, J. A. K.; Kenwright, A. M.; Moloney, J. M.; Parker, D.; Port, M.; Navet, M.; Rousseau, O.; Woods, M. *Chem. Commun.* **1998**, 1381.

325. Woods, M.; Aime, S.; Botta, M.; Howard, J. A. K.; Moloney, J. M.; Navet, M.; Parker, D.; Port, M.; Rousseaux, O. *Journal of the American Chemical Society* **2000**, *122*, 9781.
326. Aime, S.; Botta, M.; Ermondi, G.; Terreno, E.; Anelli, P. L.; Fedeli, F.; Uggeri, F. *Inorg. Chem.* **1996**, *35*, 2726.
327. Aime, S.; Barge, A.; Botta, M.; De Sousa, A. S.; Parker, D. *Angew. Chem.-Int. Edit.* **1998**, *37*, 2673.
328. Aime, S.; Barge, A.; Bruce, J. I.; Botta, M.; Howard, J. A. K.; Moloney, J. M.; Parker, D.; de Sousa, A. S.; Woods, M. *Journal of the American Chemical Society* **1999**, *121*, 5762.
329. Dunand, F. A.; Aime, S.; Merbach, A. E. *Journal of the American Chemical Society* **2000**, *122*, 1506.
330. Azegami, S.; Tsuboi, A.; Izumi, T.; Hirata, M.; Dubin, P. L.; Wang, B. L.; Kokufuta, E. *Langmuir* **1999**, *15*, 940.
331. Bockman, R. S.; Guidon, P. T.; Pan, L. C.; Salvatori, R.; Kawaguchi, A. *J. Cell. Biochem.* **1993**, *52*, 396.
332. Guidon, P. T.; Salvatori, R.; Bockman, R. S. *J. Bone Miner. Res.* **1993**, *8*, 103.
333. Gottlieb, H. E.; Kotlyar, V.; Nudelman, A. *J. Org. Chem.* **1997**, *62*, 7512.
334. Ammann, C.; Meier, P.; Merbach, A. E. *J. Magn. Reson.* **1982**, *46*, 319.
335. Gromov, I.; Shane, J.; Forrer, J.; Rakhmatoullin, R.; Rozentzwaig, Y.; Schweiger, A. *J. Magn. Reson.* **2001**, *149*, 196.
336. Tschaggelar, R.; Kasumaj, B.; Santangelo, M. G.; Forrer, J.; Leger, P.; Dube, H.; Diederich, F.; Harmer, J.; Schuhmann, R.; Garcia-Rubio, I.; Jeschke, G. *J. Magn. Reson.* **2009**, *200*, 81.
337. Polyhach, Y.; Bordignon, E.; Tschaggelar, R.; Gandra, S.; Godt, A.; Jeschke, G. *Phys. Chem. Chem. Phys.* **2012**, *14*, 10762.
338. Miller, J. B. *J. Org. Chem.* **1959**, *24*, 560.
339. Brunisholz, G.; Randin, M. *Helvetica Chimica Acta* **1959**, *42*, 1927.
340. Corsi, D. M.; Platas-Iglesias, C.; Bekkum, H. v.; Peters, J. A. *Magn. Reson. Chem.* **2001**, *39*, 723.
341. Hugi, A. D.; Helm, L.; Merbach, A. E. *Helvetica Chimica Acta* **1985**, *68*, 508.
342. Solomon, I. *Physical Review* **1955**, *99*, 559.
343. Vold, R. L.; Waugh, J. S.; Klein, M. P.; Phelps, D. E. *The Journal of Chemical Physics* **1968**, *48*, 3831.

344. Meiboom, S.; Gill, D. *Review of Scientific Instruments* **1958**, *29*, 688.
345. Bloembergen, N. *The Journal of Chemical Physics* **1957**, *27*, 572.
346. Bloembergen, N.; Morgan, L. O. *The Journal of Chemical Physics* **1961**, *34*, 842.
347. Yerly, F.: EPFL, Lausanne, 2003.
348. Zimmerman, J. R.; Brittin, W. E. *The Journal of Physical Chemistry* **1957**, *61*, 1328.
349. Luz, Z.; Meiboom, S. *The Journal of Chemical Physics* **1964**, *40*, 2686.
350. Swift, T. J.; Connick, R. E. *The Journal of Chemical Physics* **1962**, *37*, 307.
351. Powell, D. H.; Merbach, A. E.; Gonzalez, G.; Brucher, E.; Micskei, K.; Ottaviani, M. F.; Kohler, K.; Vonzelewsky, A.; Grinberg, O. Y.; Lebedev, Y. S. *Helvetica Chimica Acta* **1993**, *76*, 2129.
352. Ayant, Y.; Belorizky, E.; Alizon, J.; Gallice, J. *Journal De Physique* **1975**, *36*, 991.
353. Gonzalez, G.; Powell, D. H.; Tissieres, V.; Merbach, A. E. *The Journal of Physical Chemistry* **1994**, *98*, 53.
354. Fries, P. H. *Eur. J. Inorg. Chem.* **2012**, 2156.
355. Yazyev, O. V.; Helm, L. *J. Chem. Phys.* **2007**, *127*.
356. Yazyev, O. V.; Helm, L. *Eur. J. Inorg. Chem.* **2008**, 201.
357. de la Torre, J. G.; Huertas, M. L.; Carrasco, B. *J. Magn. Reson.* **2000**, *147*, 138.



# 6 Appendix



## 6.1 General equations for the analysis of $^1\text{H}$ NMRD and $^{17}\text{O}$ NMR experimental data<sup>293</sup>

The normalized relaxation enhancement of  $^1\text{H}$  and  $^{17}\text{O}$  nuclear spins due to water exchanging between bulk and paramagnetic compounds is given by<sup>348-350</sup>

$$\frac{1}{T_{1r}} = \frac{1}{P_m} \left[ \frac{1}{T_1} - \frac{1}{T_{1A}} \right] = \frac{1}{T_{1m} + \tau_m} + \frac{1}{T_1^{OS}} \quad (6.1)$$

$$\frac{1}{T_{2r}} = \frac{1}{P_m} \left[ \frac{1}{T_2} - \frac{1}{T_{2A}} \right] = \frac{1}{\tau_m} \frac{T_{2m}^{-2} + \tau_m^{-1} T_{2m}^{-1} + \Delta\omega_m^2}{(\tau_m^{-1} + T_{2m}^{-1})^2 + \Delta\omega_m^2} + \frac{1}{T_2^{OS}} \quad (6.2)$$

$$P_m = \frac{q[\text{Gd(III)}]}{55.56} \quad (6.3)$$

where  $m$  refers to the metal bound state,  $A$  to the bulk state and  $q$  to the number of bound water molecules.  $P_m$  is the mole fraction of bound water. The relaxivity,  $r_1$ , which refers to  $^1\text{H}$  relaxation enhancement induced by 1 mM concentration of the paramagnetic metal ion is given by

$$\frac{1}{T_1} = \frac{1}{T_{1A}} + [\text{Gd(III)}]r_1 \quad (6.4)$$

$$r_1 = r_1^{IS} + r_1^{OS} \quad (6.5)$$

The relaxivity is usually split into an inner-sphere,  $r_1^{IS}$ , and an outer-sphere,  $r_1^{OS}$ , term. The inner-sphere term can be related to the inner-sphere relaxation enhancement by

$$r_1^{IS} = \frac{1}{1000} \times \frac{q}{55.55} \times \frac{1}{T_{1m} + \tau_m} \quad (6.6)$$

In case of water exchange between bulk and fast forming and dissociating aggregates in equations 6.1 and 6.2 one can approximate the relaxation of  $^1\text{H}$  and  $^{17}\text{O}$  spins of bound water molecules by

$$\left\langle \frac{1}{T_{jm}} \right\rangle = \sum_{i=1}^n \frac{x_i}{T_{jm}}, \text{ with } \sum_{i=1}^n x_n = 1 \text{ and } j=1,2 \quad (6.7)$$

$x_i$  are the mole fractions of Gd(III) in the different aggregates: monomer (1), dimer (2), etc. It is assumed that the water exchange rate constant  $k_{\text{ex}} = 1/\tau_m$  is the same for monomers and aggregates. In case of  $^1\text{H}$  NMRD the outer-sphere contribution  $r_1^{\text{OS}}$  is the same for monomers and aggregates.

The relaxation rates of water nuclei in the inner-sphere and in the outer sphere can be calculated using the equations from Solomon-Bloembergen-Morgan (SBM) theory.<sup>289, 290</sup> In the following we repeat the SBM equations for  $^1\text{H}$  and  $^{17}\text{O}$  relaxation starting with electron spin relaxation.

### 6.1.1 Electron spin relaxation<sup>351</sup>

In SBM theory the longitudinal and transverse electronic relaxation rates ( $1/T_{1e}$  and  $1/T_{2e}$ ) are expressed by equations 6.8 and 6.9, where  $\tau_v$  is the correlation time for the modulation of the zero-field-splitting interaction,  $E_v$  is the corresponding activation energy and  $\Delta^2$  is the mean squared amplitude of the zero-field-splitting. For the temperature dependence of  $\tau_v$  we assume an Arrhenius equation (equation 6.10).

$$\left( \frac{1}{T_{1e}} \right)^{\text{ZFS}} = \frac{1}{25} \Delta^2 \tau_v \{4S(S+1) - 3\} \left( \frac{1}{1+\omega_S^2 \tau_v^2} + \frac{4}{1+4\omega_S^2 \tau_v^2} \right) \quad (6.8)$$

$$\left( \frac{1}{T_{2e}} \right)^{\text{ZFS}} = \frac{1}{25} \Delta^2 \tau_v \{4S(S+1) - 3\} \left( \frac{1}{1+\omega_S^2 \tau_v^2} + \frac{4}{1+4\omega_S^2 \tau_v^2} \right) \quad (6.9)$$

$$\tau_v = \tau_v^{298} \exp \left\{ \frac{E_v}{R} \left( \frac{1}{T} - \frac{1}{298.15} \right) \right\} \quad (6.10)$$

### 6.1.2 $^1\text{H}$ NMRD

The longitudinal relaxation rate of inner sphere protons ( $1/T_{1m}^H$ ) is expressed by equation 6.11, where  $r_{GdH}$  is the effective distance between the electron charge and the  $^1\text{H}$  nucleus,  $\omega_I$  is the proton resonance angular frequency and  $\omega_S$  is the Larmor frequency of the Gd(III) electron spin.

$$\frac{1}{T_{1m}^H} = \frac{2}{15} \left( \frac{\mu_0}{4\pi} \right) \frac{\hbar^2 \gamma_I^2 \gamma_S^2}{r_{GdH}^6} S(S+1) \times [3J(\omega_I; \tau_{d1}) + 7J(\omega_S; \tau_{d2})] \quad (6.11)$$

$$\text{with } J(\omega; \tau) = \left( \frac{\tau}{1+\omega^2\tau^2} \right), \text{ and } \frac{1}{\tau_{di}} = \frac{1}{\tau_m} + \frac{1}{\tau_R} + \frac{1}{T_{ie}} \quad (6.12)$$

In case of aggregate forming compounds the inner sphere proton relaxation rates differ only by the rotational correlation times  $\tau_R$  which we named  $\tau_R^{\text{mono}}$  for the monomers and  $\tau_R^{\text{agg}}$  for the aggregates. Because aggregates are mainly dimers and a small amount ( $\approx 10\%$  of the aggregates) of trimers we used only one correlation time to describe the rotation of the aggregates.

The outer sphere contribution can be described by equation 6.13, where  $N_A$  is the Avogadro constant and  $J^{OS}$  is its associated spectral density function.<sup>157, 158, 352</sup>

$$r_1^{OS} = \frac{32N_A\pi}{405} \left( \frac{\mu_0}{4\pi} \right)^2 \frac{\hbar^2 \gamma_I^2 \gamma_S^2}{a_{GdH} D_{GdH}} S(S+1) [3J^{OS}(\omega_I; T_{1e}) + 7J^{OS}(\omega_S; T_{2e})] \quad (6.13)$$

$$J^{OS}(\omega; T_{je}) = \text{Re} \left[ \frac{1 + 1/4 \left( i\omega\tau_{GdH} + \frac{\tau_{GdH}}{T_{je}} \right)^2}{1 + \left( i\omega\tau_{GdH} + \frac{\tau_{GdH}}{T_{je}} \right)^{1/2} + 4/9 \left( i\omega\tau_{GdH} + \frac{\tau_{GdH}}{T_{je}} \right) + 1/9 \left( i\omega\tau_{GdH} + \frac{\tau_{GdH}}{T_{je}} \right)^{3/2}} \right], \text{ where } j = 1, 2 \quad (6.13)$$

The temperature dependence of the coefficient for the mutual diffusion a water molecule and the Gd(III) complex ( $D_{GdH}$ ) is assumed to follow Arrhenius's law with an activation energy  $E_{GdH}$  (equation 6.15).

$$D_{GdH} = D_{GdH}^{298} \exp \left\{ \frac{E_{GdH}}{R} \left( \frac{1}{298.15} - \frac{1}{T} \right) \right\} \quad (6.15)$$

### 6.1.3 $^{17}\text{O}$ NMR

For the measured  $^{17}\text{O}$  NMR relaxation rates and angular resonance frequencies of the paramagnetic solutions ( $1/T_1$ ,  $1/T_2$  and  $\omega$ ) and from the acidified water reference ( $1/T_{1A}$ ,  $1/T_{2A}$  and  $\omega_A$ ), it is possible to calculate the reduced relaxation rates and chemical shifts ( $1/T_{1r}$ ,  $1/T_{2r}$  and  $\Delta\omega_r$ ) (equations 6.1, 6.2 and 6.16), where  $1/T_{1m}$  and  $1/T_{2m}$  are the longitudinal and transverse relaxation rates, respectively, of the bound water and  $\Delta\omega_m$  is the chemical shift difference between bound and bulk water in absence of exchange,  $\tau_m$  is the mean residence time or the inverse of the water exchange rate constant ( $k_{\text{ex}} = 1/\tau_m$ ) and  $P_m$  is the mole fraction of the bound water.<sup>348, 350</sup> The outer sphere contributions to the  $^{17}\text{O}$  relaxation rates ( $1/T_1^{\text{OS}}$  and  $1/T_2^{\text{OS}}$ ) can be neglected according to previous studies.<sup>142</sup>

$$\Delta\omega_r = \frac{1}{P_m} (\omega - \omega_A) = \frac{\Delta\omega_m}{(1 + \tau_m T_{2m}^{-1})^2 + \tau_m^2 \Delta\omega_m^2} + \Delta\omega^{\text{OS}} \quad (6.16)$$

The exchange rate constant is assumed to be described by Eyring's equation (equation 6.17), where  $\Delta S^\ddagger$  and  $\Delta H^\ddagger$  are the entropy and enthalpy of activation for the water exchange process, and  $k_{\text{ex}}^{298}$  is the exchange rate constant 298.15 K.  $R$  is the gas constant, and  $h$  and  $k_B$  are the Planck and Boltzmann constants, respectively.

$$\frac{1}{\tau_m} = k_{\text{ex}} = \frac{k_B T}{h} \exp\left\{\frac{\Delta S^\ddagger}{R} - \frac{\Delta H^\ddagger}{RT}\right\} = \frac{k_{\text{ex}}^{298} T}{298.15} \exp\left\{\frac{\Delta H^\ddagger}{R} \left(\frac{1}{298.15} - \frac{1}{T}\right)\right\} \quad (6.17)$$

The scalar relaxation contribution ( $1/T_{2SC}$ ) is dominating  $1/T_{2m}$ . In equation 6.18,  $1/\tau_{s1}$  is the sum of the exchange rate constant  $k_{\text{ex}}$  and the electron spin relaxation rate  $1/T_{ie}$ . This relaxation is independent on formation of aggregates

$$\frac{1}{T_{2m}} \cong \frac{1}{T_{2SC}} = \frac{S(S+1)}{3} \left(\frac{A}{h}\right)^2 \left(\tau_{S1} + \frac{\tau_{S2}}{1 + \omega_S^2 \tau_{S2}^2}\right) \quad (6.18)$$

The longitudinal relaxation of bound water is given as a sum of a dipolar  $1/T_{1dd}$  (equation 6.19) and a quadrupolar  $1/T_{1q}$  (equation 6.20) term.

$$\frac{1}{T_{1dd}^O} = \frac{2}{15} \left( \frac{\mu_0}{4\pi} \right) \frac{\hbar^2 \gamma_I^2 \gamma_S^2}{r_{GdO}^6} S(S+1) \times [3J(\omega_I; \tau_{d1}) + 7J(\omega_S; \tau_{d2})] \quad (6.19)$$

$$\text{With } J(\omega; \tau) = \left( \frac{\tau}{1+\omega^2\tau^2} \right) \quad \text{and} \quad \frac{1}{\tau_{di}} = \frac{1}{\tau_m} + \frac{1}{\tau_R} + \frac{1}{T_{ie}}$$

$$\frac{1}{T_{1q}^O} = \frac{3\pi}{10} \left( \frac{2I+3}{I^2(2I-1)} \right) \chi^2 (1 + \eta^2/3) [0.2J_1(\omega_I; \tau_R) + 0.8J_2(\omega_I; \tau_R)] \quad (6.20)$$

$$\text{with } J_n(\omega; \tau) = \left( \frac{\tau}{1+n^2\omega^2\tau^2} \right)$$

Both relaxation rates depend on the rotational motion of the compounds and  $\tau_R^{\text{mono}}$  for the monomers and  $\tau_R^{\text{agg}}$  for the aggregates are used.

In equation 6.16, the chemical shift of the bound water molecule ( $\Delta\omega_m$ ) depends on the hyperfine interaction between the Gd(III) electron spin and the  $^{17}\text{O}$  nucleus and is directly proportional to the scalar coupling constant ( $A/\hbar$ ) expressed in equation 6.21. The isotopic Landé  $g$  factor is equal to 2.0 for the Gd(III),  $B_0$  represents the magnetic field and  $k_B$  is the Boltzmann constant.

$$\Delta\omega_m = \frac{g\mu_{B_0} S(S+1) B_0 A}{3k_B T} \frac{1}{\hbar} \quad (6.21)$$

The outer sphere term of the chemical shift was found proportional to  $\Delta\omega_m$ , through an empirical constant ( $C_{OS}$ ).<sup>353</sup>

$$\Delta\omega^{OS} = C_{OS} \Delta\omega_m \quad (6.22)$$

#### 6.1.4 Simultaneous fits of $^{17}\text{O}$ NMR and $^1\text{H}$ NMRD experiments

We performed several preliminary fits using the experimental data of the mononuclear **Gd(DOTA-AHA)** and the binuclear **[Gd<sub>2</sub>(Bis(DOTA-AHA)1,3-phenyldiacetate)]<sup>2-</sup>** compound. In none of the different scenarios tested we could fit  $^1\text{H}$  NMRD relaxivities and  $^{17}\text{O}$  NMR data using the same parameters for electron spin relaxation. These parameters,  $^{298}\tau_v$ ,  $E_v$  and  $\Delta^2$ , have to be considered as fitting parameters without any deep physical meaning. We therefore decided to use different parameters for  $^1\text{H}$  NMRD (measured at variable magnetic field from 0.47 T to 9.4 T) and for  $^{17}\text{O}$  NMR (measured at the high field 9.4 T only). This choice has no marked influence on water exchange rate constant, rotational correlation times and order parameter.

a) Fit with one (standard SBM) or two rotational correlation times (Lipari-Szapo or self-aggregation): From the results in Figure 6.1 it can be seen that using only one rotational correlation time  $\tau_R$  does not allow a good fit of NMRD ( $^1\text{H}$ ) and  $1/T_{1r}$  ( $^{17}\text{O}$ ).



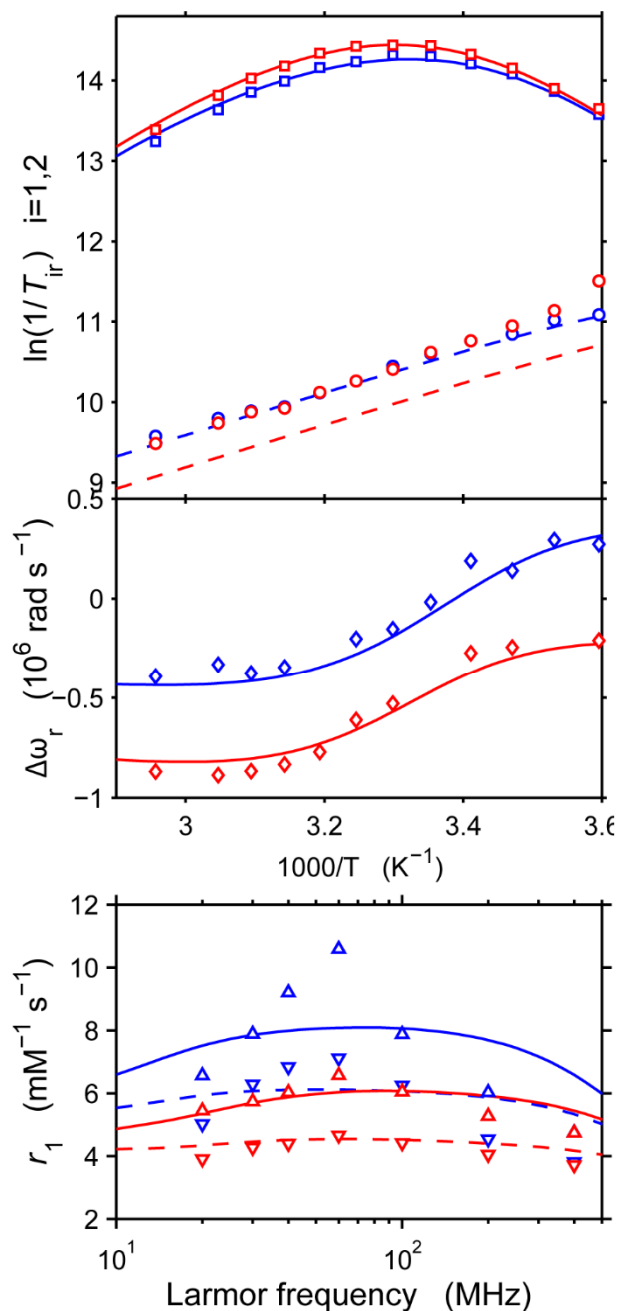


**Figure 6.1:** **a)** Reduced transverse (squares) and longitudinal (circles) <sup>17</sup>O NMR relaxation rates for Gd(DOTA-AHA) (20 mM [Gd(III)] (red) and [Gd<sub>2</sub>(Bis(DOTA-AHA)1,3-phenyldiacetate)]<sup>2-</sup> (blue) (12 mM [Gd(III)]). **b)** Reduced <sup>17</sup>O chemical shifts for Gd(DOTA-AHA) (◊) and [Gd<sub>2</sub>(Bis(DOTA-AHA)1,3-phenyldiacetate)]<sup>2-</sup> (◊). **c)** <sup>1</sup>H NMRD profiles for Gd(DOTA-AHA) (red) and [Gd<sub>2</sub>(Bis(DOTA-AHA)1,3-phenyldiacetate)]<sup>2-</sup> (blue) at 25 °C (△) and 37 °C (▽). The lines represent the best fit of the data resulting from simultaneous fitting based on SBM equations and using only a single rotational correlation time  $\tau_R$ . The sums of squares of errors (standard SBM) are  $R^2 = 4.8$  (Gd(DOTA-AHA)) and  $R^2 = 19.7$  ([Gd<sub>2</sub>(Bis(DOTA-AHA)1,3-phenyldiacetate)]<sup>2-</sup>).

b) Fit with SBM theory with Lipari-Szabo (two rotational correlation times):  
From the results of the fit of  $[\text{Gd}_2(\text{Bis}(\text{DOTA-AHA})\text{1,3-phenyldiacetate})]^{2-}$  in Figure 6.2 it can be seen that using Lipari-Szabo leads to a less good fit than using self-aggregation of the binuclear compound. The better fit is also expressed by a much lower sum of error squares  $\Sigma R^2$  (Table 6.1). The main difference in the equations used for the fitting comes from the temperature dependence of the equilibrium constant  $K$  ( $\Delta H^0$ ,  $\Delta S^0$ ) in respect to the Lipari-Szabo  $S^2$  which is independent on temperature. Comparison of the fitted parameters in Table 6.1 shows that the rotational correlation times obtained are very similar.

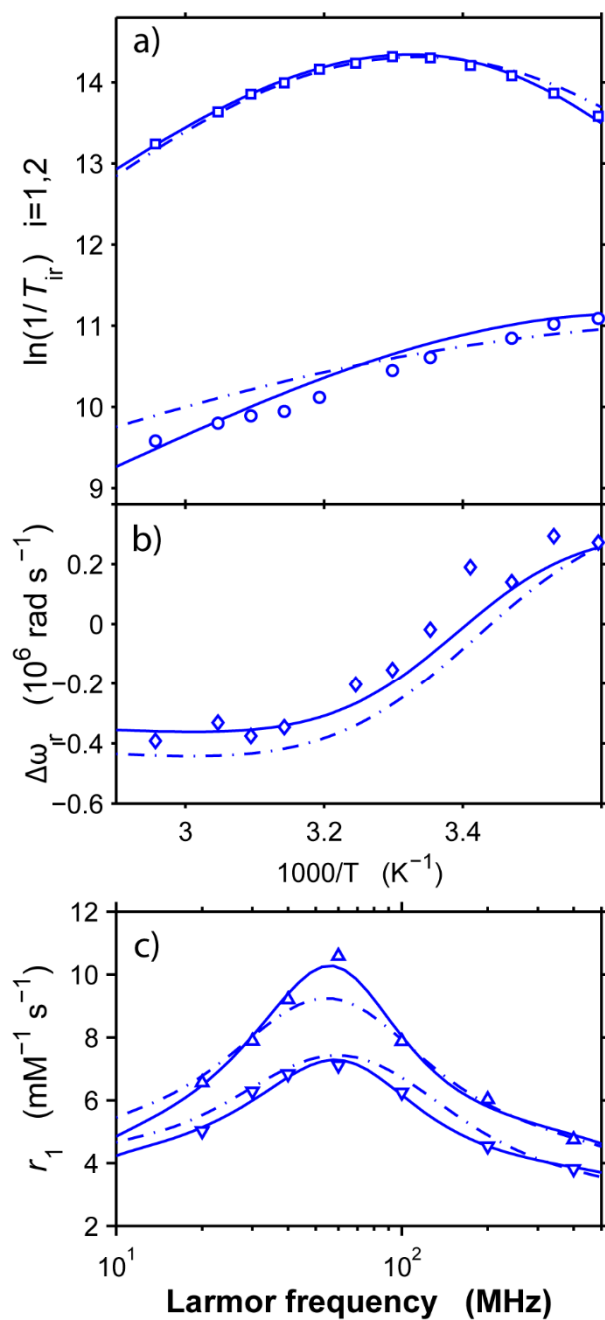


**Figure 6.2:** Simultaneous fits of  $[\text{Gd}_2(\text{Bis}(\text{DOTA-AHA})1,3\text{-phenyldiacetate})]^{2-}$  NMR data using Lipari-Szabo approach (dash-dotted lines) and formation of weak aggregates (full lines). **a)** Reduced transverse ( $\square$ ) and longitudinal ( $\circ$ )  $^{17}\text{O}$  NMR relaxation rates. **b)** Reduced  $^{17}\text{O}$  chemical shifts  $[\text{Gd}_2(\text{Bis}(\text{DOTA-AHA})1,3\text{-phenyldiacetate})]^{2-}$  ( $\diamond$ ). **c)**  $^1\text{H}$  NMRD profiles for  $[\text{Gd}_2(\text{Bis}(\text{DOTA-AHA})1,3\text{-phenyldiacetate})]^{2-}$  (blue) at  $25^\circ\text{C}$  ( $\triangle$ ) and  $37^\circ\text{C}$  ( $\nabla$ ). The sums of squares of errors are  $R^2 = 3.7$  (Lipari-Szabo) and  $R^2 = 0.74$  (aggregates).

**Table 6.1:** Comparison of parameters from simultaneous fits of  $[\text{Gd}_2(\text{Bis}(\text{DOTA-AHA})1,3\text{-phenyldiacetate})]^{2-}$   $^{17}\text{O}$  NMR and  $^1\text{H}$  NMRD using SBM theory with Lipari-Szabo and self-aggregation of compounds.

	Lipari-Szabo	Self-aggregation up to dimer	Self-aggregation up to trimer
$\Sigma R^2$	3.7	0.74	0.70
$^{298}k_{\text{ex}} (10^6 \text{ s}^{-1})$	6.4	$6.4 \pm 1.1$	6.4
$\Delta H^\ddagger (\text{kJ}\cdot\text{mol}^{-1})$	63	$63 \pm 5$	63
$^{298}\tau_{\text{R}}^{\text{local/mono}} (\text{ps})$	$128 \pm 39$	$134 \pm 6.4$	$135 \pm 6.7$
$^{298}\tau_{\text{R}}^{\text{global/agg}} (\text{ps})$	$2300 \pm 550$	$4000 \pm 1150$	$4000 \pm 1500$
$^{298}\tau_{\text{R}}^{\text{trimer}} (\text{ps})$	-	-	$10000 \pm 31000$
$E_a (\text{kJ}\cdot\text{mol}^{-1})$	<u>22</u>	<u>22</u>	<u>22</u>
$^{298}\tau_v (\text{ps}) ^1\text{H}$	$60 \pm 1300$	$50 \pm 300$	$50 \pm 300$
$\Delta^2 (10^{20} \text{ s}^{-2}) ^1\text{H}$	$1.6 \pm 34$	$1.8 \pm 11$	$1.9 \pm 11$
$^{298}\tau_v (\text{ps}) ^{17}\text{O}$	$60 \pm 3500$	$23 \pm 37$	$18 \pm 48$
$\Delta^2 (10^{20} \text{ s}^{-2}) ^{17}\text{O}$	$9 \pm 530$	$4.1 \pm 6$	$3.1 \pm 6$
$E_v (\text{kJ}\cdot\text{mol}^{-1})$	<u>6</u>	<u>1</u>	<u>1</u>
$A/\hbar (10^6 \text{ rad}\cdot\text{s}^{-1})$	$-3.8 \pm 0.8$	$-3.1 \pm 0.6$	$-3.1 \pm 0.6$
$C_{\text{OS}}$	$-0.4 \pm 0.12$	$-0.4 \pm 0.09$	$-0.4 \pm 0.09$
$K^{298}$		14.6	14.6
$S^2$	$0.13 \pm 0.02$	-	-
$\Delta H^0 (\text{kJ}\cdot\text{mol}^{-1})$	-	$-33.3 \pm 6.1$	$-34.1 \pm 6.8$
$\Delta S^0 (\text{J}\cdot\text{K}^{-1}\cdot\text{mol}^{-1})$	-	$-89.3 \pm 20$	$-92.1 \pm 23$

The following parameters were fixed to the same values for all systems:  $r_{\text{GdH}} = 3.1 \text{ \AA}$ ,  $a_{\text{GdH}} = 3.6 \text{ \AA}$ ,  $r_{\text{GdO}} = 2.5 \text{ \AA}$ ,  $^{298}D_{\text{GdH}} = 2.5 \cdot 10^{-9} \text{ m}^2\cdot\text{s}^{-1}$ ,  $E_{\text{GdH}} = 22 \text{ kJ}\cdot\text{mol}^{-1}$ ,  $\chi = 7.58 \text{ MHz}$ . In both cases different parameters ( $^{298}\tau_v$ ,  $\Delta^2$ ) had to be used to describe electron spin relaxation for  $^1\text{H}$  NMRD and  $^{17}\text{O}$  NMR relaxation.

c) Fit with self-aggregation up to formation of trimers  $(\text{Gd}_2\text{S}_3)_3$ : To test for higher self-aggregation of  $[\text{Gd}_2(\text{Bis}(\text{DOTA-AHA})\mathbf{1,3\text{-phenyldiacetate}})]^{2-}$  we fitted  $^1\text{H}$  NMRD and  $^{17}\text{O}$  NMR data using aggregation up to trimers. The quality of the fits with formation of dimers and trimers is essentially the same as for formation of only dimers (see the sums of error squares  $\Sigma R^2$  in Table 6.1). From the equilibrium constant we can calculate the following mole fractions for  $[\text{Gd}_2(\text{Bis}(\text{DOTA-AHA})\mathbf{1,3\text{-phenyldiacetate}})]^{2-}$  at 298K:  $x_{\text{monomer}} = 0.857$ ,  $x_{\text{dimer}} = 0.129$ ,  $x_{\text{trimer}} = 0.014$ . Only 1.4% of all  $[\text{Gd}_2(\text{Bis}(\text{DOTA-AHA})\mathbf{1,3\text{-phenyldiacetate}})]^{2-}$  binuclear compounds are present in trimers. We therefore conclude that we can neglect formation of higher aggregates and consider only monomers and dimers. Comparison of the fitted parameters in Table 6.1 shows that the correlation times obtained are very similar.

From all test-fits it can be seen that  $^{17}\text{O}$   $1/T_{2r}$  is not affected by the fitting procedure chosen. It is therefore not surprising that parameters characterizing water exchange are identical (within statistical errors) for all fits.

In the Solomon-Bloembergen-Morgan model electron spin relaxation is assumed to be due to transient zero-field splitting (ZFS, equations 6.8 to 6.10). This approximation is rather limited as it has been shown by Fries (reference 354 and references therein). Especially for slowly rotating complexes a contribution due to static ZFS cannot be neglected. An analysis using more sophisticated models is possible but rather complex. As it has been shown recently on similar aggregating compounds<sup>292</sup> the choice of a more sophisticated model does not change the results for the interesting parameters fitted namely water exchange rate constant, rotational correlation times and the order parameter).

All parameters used in the final fits of the three systems are given in Table 6.2. The amplitudes of the transient ZFS ( $\Delta^2$ ) are rather high leading to relatively fast electron spin relaxation. One reason for this could be intramolecular dipolar interaction between the two Gd(III) electron spins as for example described by Powell *et al.*<sup>143</sup>

The fitted values of  $C_{\text{OS}}$  for the dimers  $[\text{Gd}_2(\text{Bis}(\text{DOTA-AHA})\mathbf{adipate})]^{2-}$  and  $[\text{Gd}_2(\text{Bis}(\text{DOTA-AHA})\mathbf{1,3\text{-phenyldiacetate}})]^{2-}$  are negative indicating that resonances of outer-sphere water are shifted to the opposite direction as inner-sphere water (Table 6.2). This can be explained by a change in the isotropic hyperfine coupling constant as it has been found from quantum mechanical calculations on  $[\text{Gd}(\text{H}_2\text{O})_8]^{3+}$ .<sup>355, 356</sup>

**Table 6.2:** Parameters from simultaneous fits of  $^{17}\text{O}$  NMR and  $^1\text{H}$  NMRD using SBM theory and self-aggregation of compounds.

	<b>Gd(DOTA-AHA)</b>	<b>[Gd<sub>2</sub>(Bis(DOTA-AHA)adipate)]<sup>2-</sup></b>	<b>[Gd<sub>2</sub>(Bis(DOTA-AHA)1,3-phenyldiacetate)]<sup>2-</sup></b>
$^{298}k_{\text{ex}} (10^6 \text{ s}^{-1})$	$6.4 \pm 1.4$	$6.8 \pm 2.2$	$6.4 \pm 1.1$
$\Delta H^\ddagger (\text{kJ.mol}^{-1})$	$58.2 \pm 6.6$	$54.3 \pm 8.4$	$62.5 \pm 5.2$
$^{298}\tau_{\text{R}}^{\text{mono}} (\text{ps})$	$103 \pm 13$	$129 \pm 9.4$	$134 \pm 6.4$
$^{298}\tau_{\text{R}}^{\text{agg}} (\text{ps})$	$2560 \pm 2100$	$4000 \pm 1800$	$4000 \pm 1150$
$E_{\text{a}} (\text{kJ.mol}^{-1})$	<u>22</u>	<u>22</u>	<u>22</u>
$^{298}\tau_{\text{v}} (\text{ps}) ^1\text{H}$	$3 \pm 2$	$50 \pm 424$	$50 \pm 300$
$\Delta^2 (10^{20} \text{ s}^{-2}) ^1\text{H}$	$0.7 \pm 0.4$	$1.6 \pm 13$	$1.8 \pm 11$
$^{298}\tau_{\text{v}} (\text{ps}) ^{17}\text{O}$	$50 \pm 75$	$15 \pm 48$	$23 \pm 37$
$\Delta^2 (10^{20} \text{ s}^{-2}) ^{17}\text{O}$	$10 \pm 13$	$2.1 \pm 6$	$4.1 \pm 6$
$E_{\text{v}} (\text{kJ.mol}^{-1})$	<u>1</u>	<u>1</u>	<u>1</u>
$A/\hbar (10^6 \text{ rad.s}^{-1})$	$-4 \pm 0.9$	$-3.1 \pm 1.2$	$-3.1 \pm 0.6$
$C_{\text{OS}}$	$0.05 \pm 0.21$	$-0.02 \pm 0.3$	$-0.4 \pm 0.09$
$K^{298}$	2.9	15.6	14.6
$\Delta H^0 (\text{kJ.mol}^{-1})$	$-41.0 \pm 19$	$-31.8 \pm 9.4$	$-33.3 \pm 6.1$
$\Delta S^0 (\text{J.K}^{-1}.\text{mol}^{-1})$	$-129 \pm 63$	$-83.8 \pm 31$	$-89.3 \pm 20$

The following parameters were fixed to the same values for all systems:  $r_{\text{GdH}} = 3.1 \text{ \AA}$ ,  $a_{\text{GdH}} = 3.6 \text{ \AA}$ ,  $r_{\text{GdO}} = 2.5 \text{ \AA}$ ,  $^{298}D_{\text{GdH}} = 2.5 \cdot 10^{-9} \text{ m}^2.\text{s}^{-1}$ ,  $E_{\text{GdH}} = 22 \text{ kJ.mol}^{-1}$ ,  $\chi = 7.58 \text{ MHz}$ . Different parameters ( $^{298}\tau_{\text{v}}$ ,  $\Delta^2$ ) had to be used to describe electron spin relaxation for  $^1\text{H}$  NMRD and  $^{17}\text{O}$  NMR relaxation.

### 6.1.5 Rotational correlation time of dimers

To estimate the rotational diffusion behavior of the binuclear aggregates the program HYDRONMR<sup>357</sup> was used. As input a simple molecular mechanics model for a  $[\text{Gd}_2(\text{Bis}(\text{DOTA-AHA})\text{adipate})]^{2-}$  dimer was used (Figure 6.3).

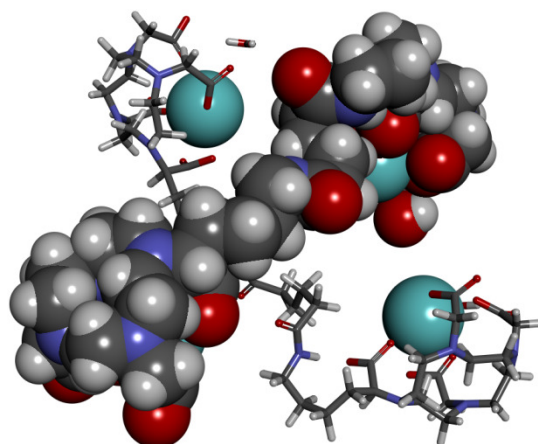


**Figure 6.3:** Simple molecular mechanics model of a  $[\text{Gd}_2(\text{Bis}(\text{DOTA-AHA})\text{adipate})]^{2-}$  dimer.

The results depend on the value of the “radius of atomic elements” as the input. Choosing 2.2 Å or 3.2 Å leads to isotropic rotational correlation times of 1.4 ns and 1.8 ns respectively. If an anisotropic rotation is considered we get  $\tau_{\parallel} \sim 1.3$  ns and  $\tau_{\perp} \sim 1.5$  ns (using 2.2 Å as “radius of atomic elements”, Figure 6.4). Keeping in mind that HYDRONMR has been intended for the calculation of hydrodynamic behavior of macromolecules; the calculated rotational correlation time is in reasonable agreement with  $^{298}\tau^{\text{agg}}$  from water relaxation.

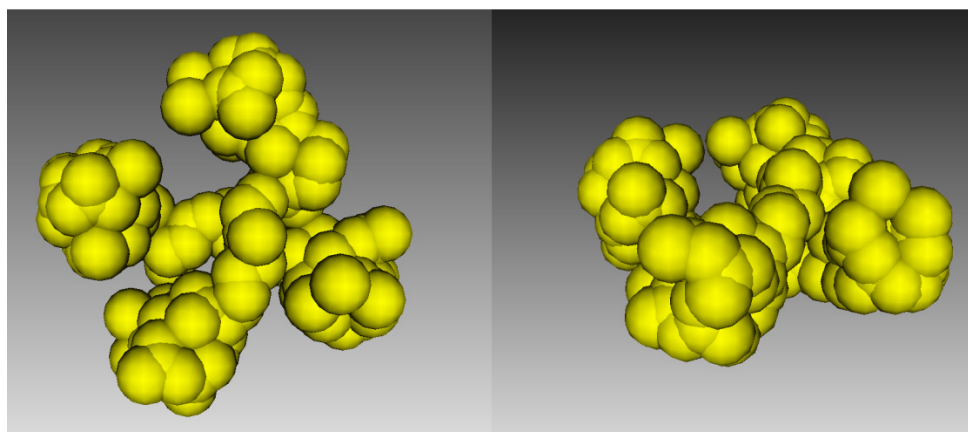


**Figure 6.4:** Hydrodynamic model of  $[\text{Gd}_2(\text{Bis}(\text{DOTA-AHA})\text{adipate})]^{2-}$  dimer created by HYDRONMR using 2.2 Å as effective radius of the atomic elements.

### 6.1.6 Experimental data of temperature dependence and kinetic stability studies.

**Table 6.3:** Longitudinal proton paramagnetic relaxation rate ( $R_{1\text{Obs}}$ ) of Gd(DOTA-AHA) (1.25 mM) and  $[\text{Gd}(\text{DOTA-A}(\text{PEG}_{750})\text{HA})]^-$  (1.25 mM) at 20 MHz and pH = 7.

Temperature (°C)	$R_{1\text{Obs}}$ Gd(DOTA-AHA) ( $\text{s}^{-1}$ )	$R_{1\text{p}}$ $[\text{Gd}(\text{DOTA-A}(\text{PEG}_{750})\text{HA})]^-$ ( $\text{s}^{-1}$ )
7	7.70	8.35
15	6.79	7.21
20	6.20	6.60
25	5.80	6.26
30	5.09	5.43
37	4.82	5.08
40	4.27	4.50
50	3.53	3.84
60	3.06	3.34
70	2.69	3.01
80	2.43	2.64

**Table 6.4:** Longitudinal proton paramagnetic relaxation rates ( $R_{1\text{p}}$ ) of Gd(DOTA-AHA) (1.25 mM) and  $[\text{Gd}(\text{DOTA-A}(\text{PEG}_{750})\text{HA})]^-$  (1.25 mM) at 20 MHz and 25 °C.

pH	$R_{1\text{p}}$ Gd(DOTA-AHA) ( $\text{s}^{-1}$ )	pH	$R_{1\text{p}}$ $[\text{Gd}(\text{DOTA-A}(\text{PEG}_{750})\text{HA})]^-$ ( $\text{s}^{-1}$ )
3.12	5.12	3.06	4.99
4.04	5.20	3.98	5.09
5.11	5.08	4.96	5.20
5.95	4.96	6.14	5.12
7.21	4.83	7.33	5.05
8.07	4.84	8.04	5.03
8.99	4.86	8.91	5.08
10.03	4.76	10.09	5.05
11.10	4.71	10.98	5.04
12.05	4.75	11.95	5.09



## 6.2 Experimental data of DEER studies

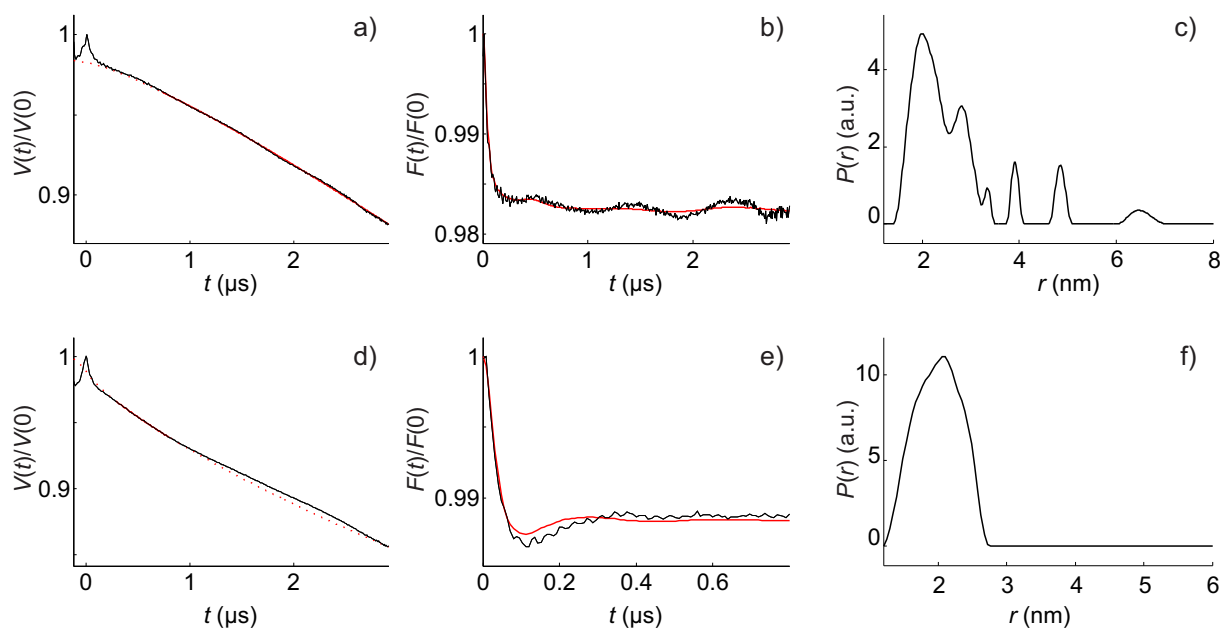


**Figure 6.5:** DEER measurements of  $[\text{Gd}_2(\text{Bis}(\text{DOTA-AHA})1,3\text{-phenyldiacetate})]^{2-}$  (a-c) and  $[\text{Gd}_2(\text{Bis}(\text{DOTA-AHA})\text{adipate})]^{2-}$  (d-f) samples: (a, d) normalized primary DEER time trace (black) and the background function (red); (b, e) normalized intramolecular form factor time trace (black) and its best fit with Deer Analysis,<sup>313</sup> model free fit with Tikhonov regularization (red); (c, f) resulting distance distribution.

### 6.3 Experimental data of *in vitro* and *in vivo* studies

**Table 6.5:** Biodistribution results of  $^{67}\text{Ga}(\text{DOTA-AHA})$  and  $[^{67}\text{Ga}(\text{DOTA-A}(\text{PEG}_{750})\text{HA})]^-$ . Percentage of injected dose per gram of organ (%ID/g) 1 hour and 24 hours after injection on Wistar rats. Results are mean of four animals.

Organ	%ID/g $^{67}\text{Ga}(\text{DOTA-AHA})$		%ID/g $[^{67}\text{Ga}(\text{DOTA-A}(\text{PEG}_{750})\text{HA})]^-$	
	1 Hour	24 Hour	1 Hour	24 Hour
Blood	0.0114 ± 0.0017	0.0005 ± 0.0003	0.0152 ± 0.0053	0.0014 ± 0.0009
Spleen	0.0075 ± 0.0035	0.0056 ± 0.0020	0.0019 ± 0.0009	0.0122 ± 0.0039
Liver	0.0041 ± 0.0007	0.0029 ± 0.0001	0.0043 ± 0.0028	0.0039 ± 0.0039
Kidney	0.0374 ± 0.0140	0.0129 ± 0.0096	0.0365 ± 0.0112	0.0121 ± 0.0054
Stomach	0.0060 ± 0.0047	0.0005 ± 0.0001	0.0002 ± 0.0001	0.0017 ± 0.0004
S. Intestine	0.0018 ± 0.0011	0.0025 ± 0.0012	0.0007 ± 0.0001	0.0044 ± 0.0022
L. Intestine	0.0042 ± 0.0036	0.0001 ± 0.0001	0.0001 ± 0.0001	0.0003 ± 0.0001
Heart	0.0006 ± 0.0002	0.0035 ± 0.0009	0.0039 ± 0.0012	0.0015 ± 0.0006
Lung	0.0040 ± 0.0059	0.0030 ± 0.0013	0.0064 ± 0.0031	0.0019 ± 0.0007
Bone	0.0130 ± 0.0085	0.0019 ± 0.0002	0.0038 ± 0.0017	0.0030 ± 0.0015

**Table 6.6:** Blood clearance results of  $^{67}\text{Ga}(\text{DOTA-AHA})$  and  $[^{67}\text{Ga}(\text{DOTA-A}(\text{PEG}_{750})\text{HA})]^-$ . Percentage of injected dose per gram of organ (%ID/g) 5, 30, 60 and 1440 minutes after injection on Wistar rats. Results are mean of four animals.

Time (min)	%ID/g $^{67}\text{Ga}(\text{DOTA-AHA})$	%ID/g $[^{67}\text{Ga}(\text{DOTA-A}(\text{PEG}_{750})\text{HA})]^-$
5	0.0107 ± 0.0070	0.0173 ± 0.0047
30	0.0193 ± 0.0053	0.0586 ± 0.0076
60	0.0114 ± 0.0017	0.0152 ± 0.0053
1440	0.0005 ± 0.0003	0.0014 ± 0.0009

**Table 6.7:** Activities of 1-octanol and water phases of the  $^{67}\text{Ga}(\text{DOTA-AHA})$  and  $[^{67}\text{Ga}(\text{DOTA-A}(\text{PEG}_{750})\text{HA})]^-$  solutions.

$^{67}\text{Ga}(\text{DOTA-AHA})$			$[^{67}\text{Ga}(\text{DOTA-A}(\text{PEG}_{750})\text{HA})]^-$		
Octanol	Water	LogP	Octanol	Water	LogP
1264	4522318	-3.554	1264	4254430	-3.527
1143	4547702	-3.600	1143	4547702	-3.600
907	4488042	-3.694	907	4488042	-3.694
1073	4468270	-3.620	1073	4468270	-3.620
806	3123966	-3.588	806	3123966	-3.588